THESE

PRESENTEE

A L'UNIVERSITE PIERRE ET MARIE CURIE

PARIS 6

POUR OBTENIR

LE GRADE DE DOCTEUR ES SCIENCES PHYSIQUES

par

Gilbert ZALCZER

ETUDE PAR DES METHODES OPTIQUES DES PROPRIETES DES MELANGES BINAIRES CRITIQUES ET DES FLUIDES SIMPLES HORS D'EQUILIBRE

Soutenue le 3 juin 1982, devant le jury composé de :

MM.	G.	MAYER	Président
	P.	BERGÉ	
	D.	BEYSENS	
	P.	LALLEMAND	Examinateurs
	J.C.	LE GUILLOU	
	B.	VOLOCHINE	

DUKE
CAPTAIN
1882

THESE

PRESENTEE

A L'UNIVERSITE PIERRE ET MARIE CURIE

PARIS 6

POUR OBTENIR

LE GRADE DE DOCTEUR ES SCIENCES PHYSIQUES

par

Gilbert ZALCZER

ETUDE PAR DES METHODES OPTIQUES DES PROPRIETES DES MELANGES BINAIRES CRITIQUES ET DES FLUIDES SIMPLES HORS D'EQUILIBRE

Soutenue le 3 juin 1982, devant le jury composé de :

MM.	G.	MAYER	Président
	P.	BERGÉ	
	D.	BEYSENS	
	P.	LALLEMAND	Examinateurs
	J.C.	LE GUILLOU	
	B.	VOLOCHINE	

Digitized by the Internet Archive
in 2026

https://archive.org/details/IA41543515_0016

A mes parents.

Les travaux faisant l'objet de cette thèse ont été effectués dans le Service de Physique du Solide et de Résonance Magnétique du Commissariant à l'Energie Atomique grâce à l'hospitalité que m'a accordée M. Bergé dans son laboratoire.

Cette thèse a pu être présentée grâce à l'amitié que m'a faite M. Lallemand d'accepter d'en assumer la direction.

Je suis très sensible à l'honneur que m'ont fait MM les professeurs Le Guillou, Mayer et Volochine en acceptant de participer au jury.

Ces travaux n'auraient sans doute pu être menés à bien sans l'aide constante de M. Beysens.

Certaines des publications présentées dans cette thèse sont le résultat d'une collaboration aussi agréable que fructueuse avec MM. Le Meindre, Tufeu, Garrabos et Bourgov.

J'ai également profité de discussions très enrichissantes avec mes collègues du laboratoire M^{me} Dubois et MM. Calmettes, Gbadamassi et Croquette.

Enfin je tiens à signaler l'efficacité de l'aide technique apportée par M^{elle} Poitou et MM Ozenda et Labouise.
Que tous veuillent trouver ici l'expression de mes remerciements les plus sincères et les plus chaleureux.

INTRODUCTION

Ce travail fait suite à ma thèse de IIIème cycle, soutenue en juin 1977. Celle-ci portait sur l'étude de la diffusion dépolarisée dans le mélange binaire critique de nitrobenzène et n-hexane. Elle avait mis en évidence l'existence de deux mécanismes différents : la diffusion multiple et celle due à l'anisotropie des molécules. Le premier de ces mécanismes avait été assez largement étudié et le bon accord entre les mesures et les modèles théoriques rendait inutiles de nouveaux développements. Sur le second, par contre, les résultats obtenus étaient seulement qualitatifs car, du fait de la rusticité des instruments employés, la première contribution masquait partiellement la seconde.

La première phase de ce travail a donc été la mise au point d'un système d'analyse plus performant. Grâce à ce nouveau montage, l'étude sur le nitrobenzène + n-hexane a été menée à bien. L'étape suivante a été de confronter ces résultats avec ceux obtenus dans d'autres systèmes, le mélange de nitroéthane et isooctane d'abord, le dioxyde de carbone ensuite. La variété des résultats obtenus pouvait inciter à multiplier les expériences semblables, avec l'espoir d'arriver à identifier les raisons de ces résultats. Cependant le manque de développement théorique dans ce domaine avait réduit une telle démarche à une sorte de "zoologie" qui ne justifiait pas la difficulté des expériences.

Deux directions de diversification ont été successivement explorées : la première vers des propriétés plus générales des points critiques, utilisant partiellement des résultats annexes des études précédentes, l'autre utilisant les mêmes techniques ou des techniques voisines vers des problèmes physiques différents tels que les phénomènes hors d'équilibre.

L'essentiel des résultats présentés ici est (ou sera) publié. Pour des raisons de simplicité, cette thèse sera centrée sur ces publications, qui seront reproduites et commentées, après une introduction générale succincte. (Les figures et les références désignées par des nombres sont celles des articles correspondants, celles désignées par des lettres sont dans le texte principal).

C H A P I T R E I

La diffusion de lumière

I.1 - Aspect moléculaire de la diffusion de lumière

Lorsqu'une molécule est soumise à un champ électrique $|E\rangle$, elle acquiert un moment dipolaire $|P\rangle$. Ce moment dipolaire est une fonction linéaire du champ incident. Si la molécule est isotrope, $|P\rangle$ et $|E\rangle$ sont parallèles :

$$|P\rangle = \alpha\,|E\rangle$$

où α est un scalaire. Si la molécule est anisotrope, nous avons

$$|P\rangle = [\alpha]\,|E\rangle \quad ,$$

où $[\alpha]$ est un tenseur. Ce tenseur peut se décomposer en deux parties :

$$[\alpha] = \bar{\alpha}\,\mathbb{1} + \Delta\alpha$$

où $\mathrm{Tr}\,\Delta\alpha = 0$ et $\bar{\alpha} = \frac{1}{3}\,\mathrm{Tr}\,\alpha$. $\mathbb{1}$ désigne le tenseur unité. Le premier terme est formellement équivalent au cas précédent. Enfin, une molécule étant généralement animée de mouvement vibratoires, il faut également considérer le cas où les composantes de $[\alpha]$ comportent une partie dépendant explicitement du temps.

Le champ diffusé par le dipole $|P\rangle$ au point $|r\rangle$ est une autre fonction linéaire de $|P\rangle$:

$$|E_d\rangle = T\,(|r\rangle)\,|P\rangle$$

avec

$$T(|r\rangle) = \frac{1}{4\pi\varepsilon_o}\left\{\frac{1}{r^3}\left(\frac{3|r\rangle\langle r|}{r^2}\right) - \mathbb{1}\right) + \frac{1}{cr^2}\left(\frac{2|r\rangle\langle r|}{r^2} - \mathbb{1}\right)\frac{\partial}{\partial t} + \frac{1}{c^2 r}\left(\frac{|r\rangle\langle r|}{r^2} - \mathbb{1}\right)\frac{\partial^2}{\partial t^2}\right\}$$

les dérivées étant prises au temps $t_o = t - \frac{r}{c}$

Lorsque plusieurs dipoles sont présents, chacun est également sensible au champ rayonné par les autres :

$$|P_i\rangle = [\alpha_i]\,(\,|E_o\rangle + \Sigma\ Tij\ |P_j\rangle\,)$$

soit en itérant :

$$|Pi\rangle = [\alpha_i]\ \ (1 + \Sigma Tij\ [\alpha j] + \Sigma\ Tij\ [\alpha j]\ Tjk\ \ [\alpha k] + \ldots)\ \ |E_o\rangle$$

Cette formule est très générale, elle contient par exemple les lois de la réfraction, d'une façon peu évidente, il est vrai. En se limitant au cas où les α sont des scalaires, on obtient une polarisabilité moyenne $\tilde{\alpha}$ faisant intervenir les densités simultanées [a] :

$$\tilde{\alpha} = \alpha\,(1 + \alpha \int \rho_{12}\ T_{12}\ \ |dr_2\rangle + \alpha^2 \iint \rho_{123}\ T_{12}\ T_{23}\ \ |dr_2\rangle|dr_3\rangle + \ldots\ )$$

Si le milieu est uniforme les quantités telles que ρ_{12} sont bien définies. Si par contre on s'intéresse à des fluctuations, ces grandeurs sont susceptibles de varier d'un point à un autre et le problème n'est pas encore résolu de manière universellement admise.

Si la molécule est soumise à un champ sinusoïdal de pulsation ω et qu'on l'observe à une distance r très supérieure à la longueur d'onde $\lambda = \frac{2\pi c}{\omega} = \frac{2\pi}{k_o}$ le tenseur T se simplifie en :

$$T(|r\rangle) = \frac{1}{4\pi\varepsilon_o}\ \ \frac{k^2}{r}\ (\frac{|r\rangle\langle r|}{r^2} - 1)\ e^{ik_o r}$$

Si une collection de molécules se trouve dans un petit volume, de dimension ρ telle que $\lambda < \rho << r$, seule l'exponentielle variera de façon significative dans ce volume. De plus on pourra la réécrire $e^{i\langle k_1|r\rangle}$ où $|k_1\rangle = \frac{k_o}{r}\ |r\rangle$

L'onde incidente a également un facteur de phase $e^{-i\langle k_o|r\rangle}$ d'où l'expression du champ diffusé :

$$|E_d\rangle = \frac{1}{4\pi\varepsilon_o}\ \ \frac{k^2}{r}\ (\frac{|r\rangle\langle r|}{r^2} - 1)\ \ \sum_j\ e^{i\langle k_D|r_j\rangle}\ \ \tilde{\alpha}_j\ |E_o\rangle$$

avec $|k_D\rangle = |k_1\rangle - |k_o\rangle$

On reconnaît dans cette formule la transformée de Fourier de la quantité $[\tilde{\alpha}(r)]$. L'angle entre le faisceau incident et le faisceau diffusé définit la composante (k_D) observée. Lorsque $[\tilde{\alpha}]$ est scalaire (molécules isotropes), le champ diffusé est proportionnel à la TF de la densité.

Une conséquence immédiate est qu'une densité constante ne donnera lieu à aucune diffusion. Toute diffusion proviendra donc de fluctuations.

Déterminer l'amplitude de la diffusion se heurte au problème du calcul de $\tilde{\alpha}$. Si on admet que les intégrales sont à courte portée, c'est-à-dire que chaque molécule est sensible uniquement à son environnement immédiat, on aboutit à la conclusion que tout se passe, pour cette molécule, comme si la fluctuation s'étendait à l'ensemble du milieu (modèle d'Einstein). On sait cependant que des termes à longue portée doivent intervenir puisqu'ils sont responsables de la réfraction. Si on admet qu'ils sont dominants, $\tilde{\alpha}$ va rester constant, puisque sur un grand volume la moyenne des fluctuations va s'annuler (modèle de Rocard). D'autres modèles (Yvon, Vuks) considèrent des cas intermédiaires où les deux termes contribuent.A l'heure actuelle, le modèle d'Einstein semble en contradiction avec l'expérience, les résultats se situant en général entre le modèle de Rocard et celui de Yvon-Vuks [b].

On peut également calculer directement l'intensité diffusée :

$$I = \langle E_d | E_d \rangle = \left(\frac{1}{4\pi\varepsilon_o}\right)^2 \frac{k^4}{r^2} \langle E_o | \left(\mathbb{1} - \frac{|r\rangle\langle r|}{r^2}\right) | E_o \rangle \sum_i \sum_j e^{i\langle k | r_i - r_j \rangle} \tilde{\alpha}_i \tilde{\alpha}_j$$

dont la valeur moyenne est à un facteur géométrique près la transformée de Fourier de la fonction de corrélation de la densité.

I .2 - Aspect hydrodynamique de la diffusion de lumière

Si on compare la longueur d'onde de la lumière ($\lambda \simeq 5.10^{-7}$ m) à la distance moyenne intermoléculaire ($\lambda \simeq 5.10^{-10}$m) il est évident que l'on peut considérer le milieu comme continu. Les fluctuations seront alors celles des grandeurs hydrodynamiques telles que la densité, la pression, etc. Cependant seules les fluctuations de densité entraîneront une diffusion de lumière.

On écrit donc les équations de l'hydrodynamique que l'on développe au premier ordre des fluctuations et l'on obtient ainsi un système d'équations différentielles linéaires que l'on résout par les méthodes algébriques traditionnelles [c] (diagonalisation de matrice). Les vecteurs propres obtenus correspondent à des modes hydrodynamiques qui évoluent indépendamment les uns des autres. Le système étant linéaire on obtient deux sortes de modes, les modes diffusifs et les modes propagatifs. Les modes propagatifs sont bien connus sous le nom d'ondes sonores qui se propagent en s'amortissant (fluctuations de pression à entropie constante). La concentration correspond à un mode diffusif, c'est-à-dire qu'il s'atténue sur place. Le dernier mode peut s'exprimer comme les fluctuations de température, à l'exception de celles dues aux ondes sonores et est également diffusif. Ces diverses fluctuations couplant avec la densité (ou les densités dans le cas de mélanges) ont donné lieu à une diffusion de lumière.

Les fluctuations déterminant l'amplitude du champ diffusé, celui-ci sera modulé en amplitude. Son analyse en fréquence permettra d'accéder à l'évolution temporelle des fluctuations de vecteur d'onde k. Un spectre typique est représenté par la figure a.

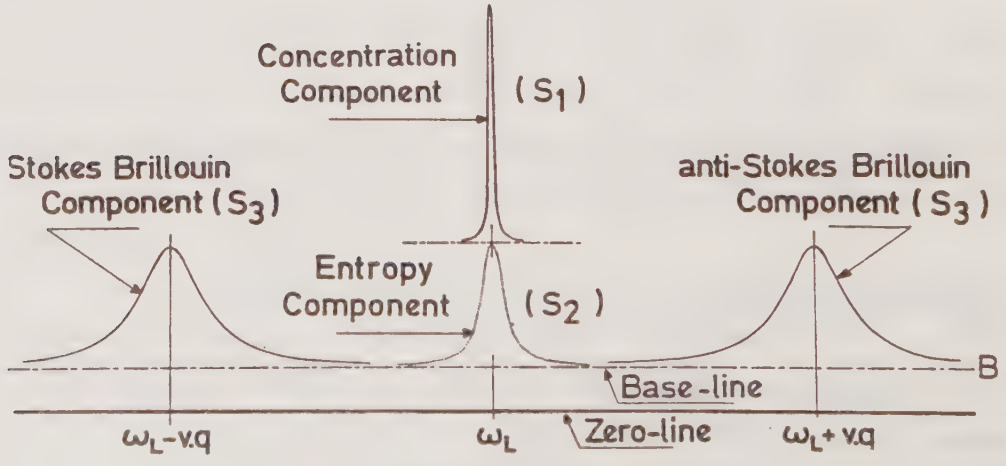

Figure a

Amplitude des fluctuations

La valeur quadratique moyenne d'une fluctuation peut être calculée facilement par la thermodynamique : la probabilité pour qu'un sous-système d'un système isolé ait une fluctuation est liée à l'accroissement de l'entropie du système total :

$$\omega \sim \exp \frac{\Delta S}{k_B}$$

Cet accroissement peut s'écrire, en fonction de variables fluctuantes :

$$\Delta S_{TOT} = \frac{1}{T} (\delta S\ \delta T - \delta p\ \delta V + \delta \mu\ \delta c \ \ldots) \equiv \frac{1}{T} \Sigma\ \delta X_1\ \delta Y_1$$

que nous pouvons transformer en utilisant les variables indépendantes P,C et $T - (\frac{To\ \alpha_T}{\rho_o\ Cp})P = \varphi$

$$kT \ln \omega = \frac{Cp}{To}\ \delta\varphi^2 + V\ \beta_s\ \delta p^2 + \left(\frac{\partial \mu}{\partial c}\right)_{Tp}\ \delta c^2$$

La loi de probabilité des variables $\delta\varphi$, δp , δc est donc gaussienne et l'on obtient les valeurs quadratiques moyennes :

$$\langle \delta\varphi^2 \rangle = k_B \frac{T^2}{Cp} \qquad \langle \delta p^2 \rangle = k_B \frac{T}{V\beta_s} \qquad \langle \delta c^2 \rangle = k_B \frac{T}{\left(\frac{\partial \mu}{\partial c}\right)_{Tp}}$$

I.3 - Diffusion anisotrope

a) Introduction

Lorsque nous considérons la partie anisotrope de la polarisabilité, les calculs ci-dessus restent formellement vrais, si l'on remplace le scalaire $\tilde{\alpha}$ par le tenseur $[\mathfrak{A}]$. Cependant comme les corrélations d'orientation sont à courte portée la diffusion sera insensible au vecteur d'onde. De plus il n'existe pas de couplage avec un paramètre macroscopique. Il nous faut donc revoir la théorie d'une façon plus détaillée.

L'intensité de la diffusion étant cette fois-ci liée à la corrélation des orientations, la question importante est de connaître la portée

de ces corrélations. Deux hypothèses principales peuvent être faites. La première est que les orientations des molécules sont indépendantes, donc que la diffusion est monomoléculaire. L'intensité correspondante est proportionnelle au nombre de particules et le comportement temporel observé correspond au mouvement d'une seule molécule. La seconde hypothèse est que ces corrélations bien qu'à courte portée ne sont pas négligeables.

Il est raisonnable de penser que des molécules anisotropes interagissent avec des potentiels anisotropes, au moins dans la partie répulsive à courte portée, surtout dans un liquide où les molécules sont presque dans un état d'empilement compact. Cependant il n'existe pas à l'heure actuelle de modèle théorique satisfaisant de ces corrélations, aussi en resterons nous là sur ce point. Notons cependant l'ordre de grandeur des deux termes que nous avons distingués : Si n est le nombre moyen de molécules corrélées angulairement le terme de corrélation est proportionnel à n^2 alors que le terme monomoléculaire donne pour ces n molécules une contribution proportionnelle à n. Le terme de corrélation peut donc devenir plus grand que l'autre dès que la portée de ces corrélations atteint quelques distances intermoléculaires.

La moyenne dynamique peut bien évidemment être découpée de la même façon : nous obtenons un terme provenant de la rotation individuelle des molécules et un terme provenant du comportement temporel des corrélations.

b) Diffusion monomoléculaire

Comme nous venons de le voir, l'intensité de cette diffusion varie comme le nombre des molécules anisotropes dans le volume observé : $N/V \sim N\rho$ où ρ est la densité, ce qui peut se généraliser pour un mélange : $I \sim \rho c$ où c est la concentration molaire. Le comportement temporel de cette diffusion est donné par une moyenne sur les mouvements de chaque molécule. Voyons donc quelques modèles de la rotation d'une molécule.

i) Rotation gouvernée par une équation de diffusion :

Considérons d'abord le cas où les rotations élémentaires sont suffisamment petites pour que toute rotation observable en soit composée

d'un grand nombre. On peut alors écrire une équation de type diffusion pour la probabilité P (Ω,t) de trouver la molécule dans l'angle solide $d\Omega$ centré sur la direction Ω au temps t :

$$\frac{\partial}{\partial t} P(\Omega,t) = - D \Delta_{\Omega} P(\Omega,t)$$

où l'opérateur Δ_{Ω} désigne le laplacien sur la sphère de rayon unité et D un coefficient phénoménologique. La fonction P (Ω,t) peut se décomposer en harmoniques sphériques, et comme le facteur électromagnétique qui la multiplie est lui-même un harmonique sphérique d'ordre 2, seul l'ordre 2 est à considérer. C'est par ailleurs une fonction propre de l'opérateur Δ_{Ω} avec la valeur propre 6. D'où :

$$\frac{\partial}{\partial t} P_2(\Omega,t) = - 6 D P_2(\Omega,t)$$

la fonction d'autocorrélation du champ varie comme :

$$F \sim \exp - 6 D|t|$$

Ce modèle ne permet pas d'expliciter le coefficient D.

Notons au passage que dans le cas de l'absorption diélectrique le raisonnement ci-dessus s'applique mais c'est l'harmonique sphérique d'ordre 1 qui intervient. La fonction d'autocorrélation temporelle correspondante sera : exp $(-2 D|t|)$. D'après ce modèle, le rapport des temps caractéristiques de diffusion dépolarisée et d'absorption diélectrique doit être de 1/3.

ii) Mouvement brownien de rotation

On peut essayer de justifier le modèle précédent en appliquant à la rotation d'une molécule la théorie du mouvement brownien de rotation d'un solide macroscopique. Pour celà, on part d'une équation de Langevin :

$$\frac{\partial \sigma}{\partial t} + a\sigma = A(t)$$

où σ désigne la vitesse angulaire de la particule, a un coefficient de frottement visqueux et A(t) un couple aléatoire exercé par le milieu.

Mais cette décomposition même, en deux parties, du couple exercé par le milieu implique la séparation des temps caractéristiques de A(t) et de la rotation. Nous sommes donc ramenés au cas précédent. Nous pouvons cependant calculer D à partir de a :

$$D = a/6$$

a est lui-même déterminé par l'hydrodynamique : un solide tournant de rayon r_o entraîne le fluide qui l'entoure ; ce mouvement est freiné par frottement visqueux. Le calcul de la distribution de vitesse conduit à :

$$D = \frac{1}{6} \cdot \frac{k_B T}{8\pi\eta r_o^3} \qquad \text{d'où} \qquad F \sim \exp - \frac{k_B T}{8\pi\eta r_o^3} |t|$$

où η est la viscosité du fluide.

Ce calcul qui met en jeu les conditions aux limites à la surface d'un solide, la distribution de vitesse, la viscosité est purement macroscopique et son extension au niveau de la molécule est assez hasardeuse. Certains raffinements ont été apportés à ce modèle, par exemple, la modification des conditions aux limites [d]. Ils diminuent assez peu l'arbitraire de la théorie. L'avantage de ces modèles est qu'ils donnent une valeur de D, qui est toujours proportionnelle à $1/\eta$.

iii) Marche au hasard

Une façon peut-être plus microscopique de décrire la rotation des molécules d'un liquide est la marche au hasard sur une sphère : la molécule "saute" brusquement d'une orientation à une autre. L'angle de rotation entre deux positions successives n'est pas nécessairement petit. S'il l'est, nous avons encore une diffusion de rotation. La théorie de la marche au hasard permet de déterminer à partir de quel angle de rotation la diffusion de rotation cesse de décrire le phénomène. Ivanov [e] a montré que cet angle doit être au minimum de 120°. Au-delà de cette valeur la variation temporelle reste exponentielle mais les temps de relaxation du premier harmonique sphérique (observé en relaxation diélectrique) et du second cessent d'être dans le rapport 3, et tendent à devenir identiques. Cette théorie ne permet pas de calculer D.

c) Approche expérimentale de la diffusion anisotrope

Nous venons d'exposer très succinctement les problèmes théoriques

liés à la diffusion anisotrope. Les quelques résultats obtenus ne l'ont été que grâce à des hypothèses très restrictives. Il nous faut maintenant comparer ces résultats aux données expérimentales pour pouvoir évaluer leur validité.

i) Diffusion monomoléculaire

La conclusion la plus directe que nous avons tirée de l'hypothèse de diffusion monomoléculaire est la relation entre l'intensité diffusée, la densité et la concentration. Des mesures d'intensité effectuées par Pinnow, Candau et Litovitz [f] dans plusieurs corps purs (bromoalcanes et polyalcools) ont montré une proportionnalité entre l'intensité et la densité. Dans les mélanges, les mesures de Coumou, Hijmans et Mackor [g] ont conduit à des résultats différents selon la nature du constituant anisotrope. (cf. fig. b).

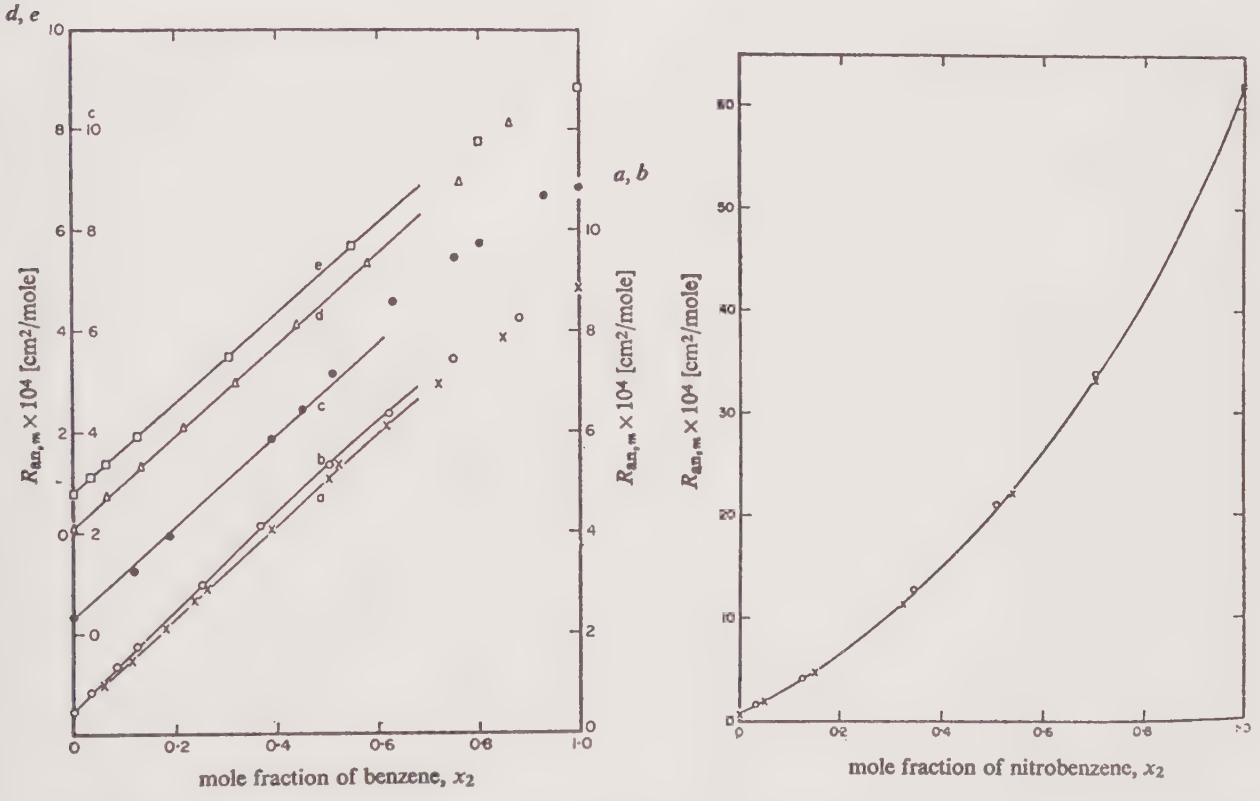

Fig. b : Intensité de la raie anisotrope dans des solutions

	de benzène	de nitrobenzène
dans	a) CCl_4	x CCl_4
	b) cyclohexane	o cyclohexane
	c) neopentane	
	d) méthanol	
	e) iso-octane	

Dans le cas du benzène la variation est linéaire jusqu'à une concentration voisine de 0,8, ce qui confirmerait l'hypothèse. Pour le nitrobenzène en revanche la courbe est indiscutablement non linéaire, même si l'on ne considère que la région de faible concentration. La forme parabolique de la courbe suggère la formation de paires parallèles, processus favorisé par le moment dipolaire de la molécule de nitrobenzène. Il semble donc que la validité de l'hypothèse de diffusion monomoléculaire dépende de la nature du constituant anisotrope (mais pas du solvant) et qu'en particulier elle ne soit pas vérifiée pour le nitrobenzène.

ii) Comparaison avec les résultats d'absorption diélectrique

Nous avons vu plus haut que le rapport des temps caractéristiques de relaxation diélectrique τ_D et de diffusion anisotrope τ_{OR} devait être : $\tau_D/\tau_{OR} = 1/3$ si la réorientation avait un caractère diffusif et qu'il pouvait atteindre 1 si elle avait lieu sous forme de sauts de grande amplitude. La table IV.1 montre les résultats obtenus par Pinnow, Candau et Litovitz qui s'échelonnent de 0,5 à 12,2, infirmant ainsi nos modèles de la rotation moléculaire.

Liquide	τ_{OR} (sec x 10^{12})	τ_D (sec x 10^{12})	τ_{OR}/τ_D
Ethyl bromide	2,0	3,8	0,53
1-butyl bromide	5,8	8,5	0,68
1-hexyl bromide	20	16	1,2
1-octyl bromide	49	22	2,2
1-decyl bromide	135	36	3,8
1-dodecyl bromide	210	50	4,2
1-tetradecyl bromide	420	54	8,0
1-hexadecyl bromide	840	69	12,2
Ethyleneglycol	58	110	0,5
Diethyleneglycol	210	220	0,96
Triethyleneglycol	600	190	3,2
Tetraethyleneglycol	850	190	4,5

Table IV.1

iii) Relation avec la viscosité macroscopique

Les mesures les plus précises dont nous disposons sur ce point sont dues à Alms, Bauer, Brauman et Pecora [h] . Pour faire varier la viscosité ces auteurs dissolvaient le soluté anisotrope (nitrobenzène) dans différents solvants isotropes. A température et concentration molaire constante le temps de réorientation est bien décrit par une loi de la forme :

$$\tau = a\eta + \tau_o$$

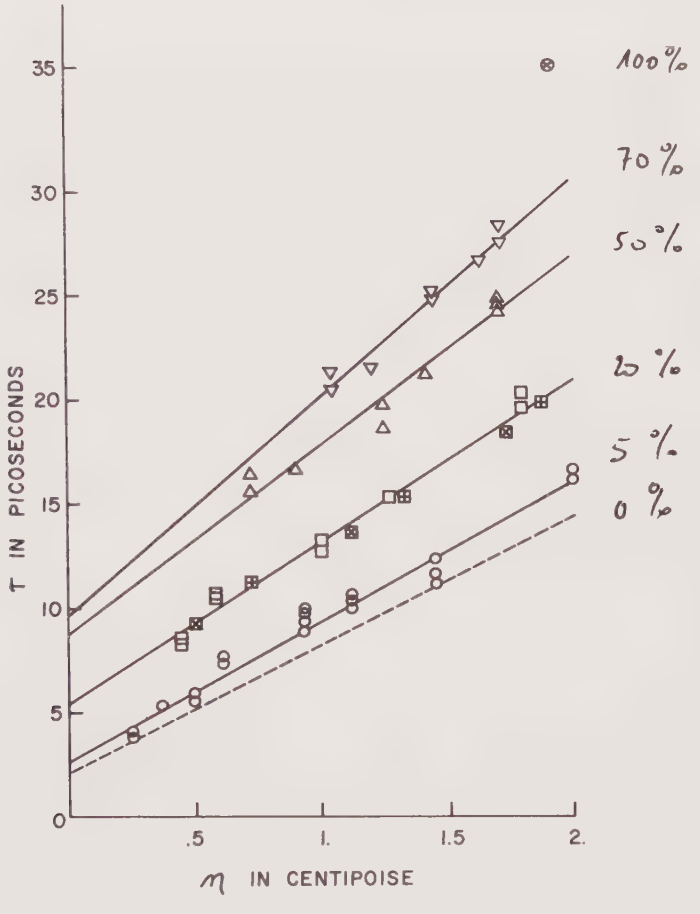

Fig. c : temps de réorientation et viscosité pour différentes concentrations de nitrobenzène

a et τ_o croissant avec la concentration.

De plus, Alms et coll. ont observé une loi de la même forme pour les temps de réorientation mesurés par résonance magnétique nucléaire,

à la différence que les variations en fonction de la concentration des coefficients a et τ_o sont respectivement nulle et très faible. Tous ces résultats n'ont malheureusement été obtenus que pour la seule température de 24°C.

Changer la viscosité en changeant le solvant peut apporter d'autres modifications. C'est pourquoi Bertucci et coll [i] ont étudié l'influence de la pression sur des solutions de molécules anisotropes, avec essentiellement le même type de variation :

$$\tau = a\eta + \tau_o$$

Dans le même article sont comparés les taux de corrélations statiques de diverses molécules de formes très voisines (dérivés monosubstitués du benzène) mais de moments dipolaires variant entre 0 et 4D, avec la conclusion que le moment dipolaire et les corrélations d'orientation sont tout-à-fait corrélés. Le mécanisme dominant provient donc plus de l'interaction électrostatique que des effets stériques.

L'effet de la température sur un mélange non critique a été étudié par Bourgou [j] . La variation avec la viscosité (divisée par la température) est encore linéaire mais la valeur de τ_o obtenue n'est pas significativement différente de zéro.

d) Conclusion

Le phénomène de diffusion anisotrope est, on le voit, très complexe. Ainsi on ne peut comparer ni les résultats obtenus sur systèmes différents avec la même méthode, ni ceux obtenus sur le même système avec des méthodes différentes. Un point cependant semble assuré : la relation étroite entre le temps de réorientation et la viscosité macroscopique. A la lumière de ce qui précède, la forte diminution de la largeur de la raie anisotrope près du point critique vue par Fabelinskii et coll. est incompréhensible, la viscosité ne présentant qu'une divergence faible. Il était donc nécessaire de vérifier ce point et éventuellement de déterminer avec précision l'exposant critique impliqué. En effet près du point critique la variation de certains paramètres devient plus franche et plus aisément reconnaissable que loin du point critique. On peut donc espérer par ce moyen reconnaître

leur variation dans celle d'autres paramètres. Il était donc de toute façon intéressant d'étudier le comportement de cette raie près d'un point critique.

I.4 - Diffusion Raman

La théorie classique de l'effet Raman consiste à introduire dans le tenseur de polarisabilité des termes dépendant du temps, correspondant aux modes propres des molécules. Les calculs sont alors formellement identiques à ceux de la diffusion Rayleigh sauf que la fréquence ω de la vibration dédouble le spectre en deux contributions centrées à $\omega_o \pm \omega$.

En fait le caractère quantique du phénomène modifie cette image. La différence principale est l'incohérence de cette diffusion : le photon diffusé perd l'information de phase. Il n'y a donc plus d'interférence possible entre les divers photons diffusés. Cette diffusion ne donne donc d'information que sur des processus monomoléculaires. Une autre conséquence est la dissymétrie du spectre, l'absorption d'un quantum par la molécule étant plus probable que son émission.

Le calcul de la diffusion Raman par une molécule isolée doit donc se faire de façon quantique. Par contre le mouvement d'une molécule dans un liquide (en particulier la rotation) est très dépendant de l'environnement et rejoint la limite classique. Les modes de vibration étant généralement anisotropes donneront lieu chacun à une raie polarisée étroite et une raie dépolarisée large et dont la largeur sera directement liée au temps de réorientation des molécules. La comparaison entre la raie Raman dipolarisée et la raie Rayleigh dépolarisée permettra donc une évaluation des corrélations d'orientation intervenant dans cette dernière.

REFERENCES

a) J. Yvon, La propagation et la diffusion de la lumière (Hermann, Paris, 1937)

b) D. Beysens, J. Chem. Phys. 64, 2579 (1976)

c) R.D. Mountain, J.M. Deutch, J. Chem. Phys. 50, 1103 (1969)
P. Calmettes, Thèse de 3ème cycle, Faculté des Sciences de Paris (1969)

d) D. Hoel, D. Kivelson, J. Chem. Phys. 62, 1323 (1975)

e) E.N. Ivanov, JETP 18, 1041 (1975)

f) D.A. Pinnow, S.J. Candau, T.A. Litovitz, J. Chem. Phys. 49, 347 (1968)

g) D.J. Coumou, J. Hijmans, E.L. Mackor, J. Trans. Faraday Soc, 60, 1539 (1964)

h) G.R. Alms, D.R. Bauer, J.I. Brauman, R. Pecora, J. Chem. Phys. 59, 5310 (1973)

i) S.J. Bertucci, A.K. Burnham, G.R. Alms and W.H. Flygare, J. Chem. Phys. 66, 605 (1977)

j) A. Bourgou Thèse, Université de Tunis (1982)

C H A P I T R E II

Introduction aux transitions de phase

II.1 - Symétries brisées

Dans la nature, certains systèmes macroscopiques présentent l'intéressante propriété d'exister dans des états de symétrie différents selon les valeurs de certains paramètres thermodynamiques. Ainsi si l'on change un de ces paramètres, ces systèmes peuvent "préférer" diminuer leur symétrie : l'état stable d'un système ne correspond pas forcément à la solution la plus symétrique des équations qui le régissent. Parmi les exemples les plus connus de symétrie brisée, nous citerons l'écoulement turbulent, les phénomènes de convection et les transitions de phase.

Dans certains cas on peut définir quantitativement la rupture de symétrie au moyen d'un paramètre dit paramètre d'ordre. Ce paramètre peut être un scalaire (transition liquide gaz), un vecteur (transition ferromagnétique) ou un être mathématique plus compliqué (hélium superfluide).

II.2 - Mélanges binaires

Dans le cas de mélanges binaires la brisure de symétrie correspond au passage d'une phase homogène à deux phases distinctes, de concentrations différentes. Le paramètre d'ordre a la dimension d'une concentration donc est scalaire.

Soient n_A et n_B les nombres de molécules de A et B dans 1 gramme du mélange. Si m_A et m_B sont les masses moléculaires de A et B, on a la relation

$$n_A m_A + n_B m_B = 1$$

On voit que les proportions du mélange sont entièrement déterminées par la connaissance de la concentration en masse c du constituant A (par exemple) :

$$c = n_A m_A$$

A volume et entropie constants, toute variation de n_A et n_B entraîne une variation de l'énergie interne du système égale à :

$$d\varepsilon = \mu_A \, dn_A + \mu_B \, dn_B$$

où μ_A et μ_B sont les potentiels chimiques des constituants A et B dans le mélange. La variation de l'énergie interne peut encore s'écrire :

$$d\varepsilon = \mu dc$$

définissant ainsi le potentiel chimique du mélange :

$$\mu = \frac{\mu_A}{m_A} - \frac{\mu_B}{m_B}$$

Certains mélanges, préparés à une concentration c_o, à une température T_1, se séparent en deux phases qui sont chacune des mélanges de concentrations c_1 et c'_1 (voir figure a).

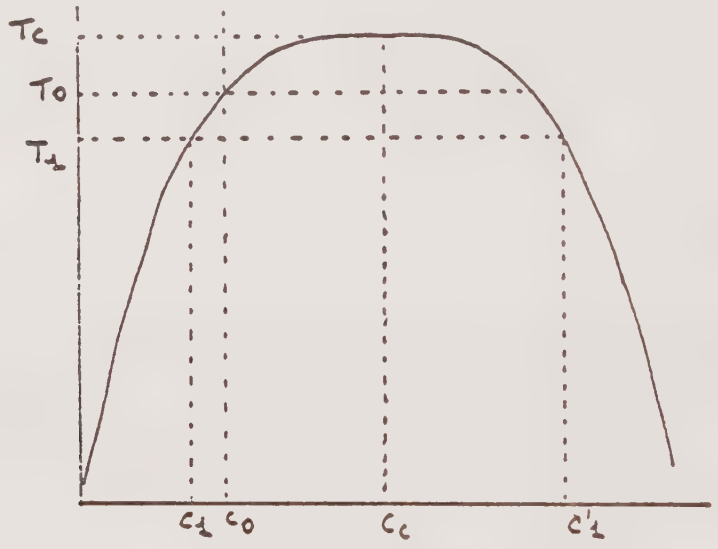

Figure a

Lorsqu'on élève la température, les concentrations c_1 et c'_1 se rapprochent l'une de l'autre jusqu'à ce que, pour $T = T_o$, le système ne comporte plus qu'une phase de concentration c_o. La température T_o de la transition est une fonction de la concentration c_o et passe par un maximum☆ qui correspond au point critique et définit ainsi la température et la concentration critique T_c et c_c. Le paramètre d'ordre de la transition est dans ce cas $c - c_c$.

☆ ou dans certains cas par un minimum

Au voisinage du point critique, le paramètre d'ordre varie comme une loi en puissance de l'écart à la température critique. L'exposant de cette loi est le même pour chacune des branches de la courbe de coexistence :

$$c - c_c = \pm B \left(\frac{T_c - T}{T_c} \right)^{\beta} \qquad \text{avec} \quad \beta \simeq 0{,}325$$

Pour un mélange ayant la concentration critique, on voit que, à une température $T = T_c - dT$, les deux phases qui coexistent ont des concentrations aussi voisines que l'on veut : $c_1 = c_c - dc$ et $c'_1 = c_c + d_c$ avec $dc \propto (dT)^{\beta}$. La condition d'équilibre s'écrit :

$$\mu\ (p,T,c) = \mu\ (p,T,c + dc)$$

ce qui entraîne :

$$\left(\frac{\partial \mu}{\partial c}\right)_{p,T} = 0 \qquad \text{au point critique}$$

De plus cette quantité varie comme une loi en puissance de $|T-T_c|$, ce qui permet de définir un deuxième exposant critique γ tel que

$$\left(\frac{\partial \mu}{\partial c}\right)_{p,T} = \left(\frac{\partial \mu}{\partial c}\right)_{pT} \left(\frac{T-Tc}{T_c}\right)^{\gamma} = \frac{1}{c^+}\, t^{\gamma} \qquad \text{au voisinage de } T_c$$

et qui vaut : $\gamma \simeq 1.24$

De même l'isotherme critique a la forme

$$(\mu - \mu c) = D\ (c - c_c)^{\delta} \qquad \text{avec} \qquad \delta \simeq 4{,}8$$

et sur l'isochore critique, la chaleur spécifique à pression constante a une singularité :

$$C_p^{sing} = A^+\, t^{-\alpha} \qquad \text{avec} \quad \alpha \simeq 0{,}110$$

II.3 - Universalité et lois d'échelle

Cet ensemble de phénomènes se retrouve dans des systèmes physiques très différents, par exemple les transitions ferromagnétiques. Cette

similitude est due au fait que les distances caractéristiques mises en jeu dans les transitions de phase deviennent beaucoup plus grandes que les distances microscopiques d'interaction. Les systèmes "oublient" le détail de leurs propriétés pour obéir à de nouvelles lois. Il est donc logique que ces lois soient les mêmes pour des systèmes différents : c'est l'hypothèse d'universalité. Dans cette hypothèse le comportement d'un système au voisinage d'une transition dépend essentiellement de deux paramètres : la dimensionnalité de l'espace d et celle du paramètre d'ordre n. Le cas des mélanges binaires correspond à d = 3, n = 1. Dans la discussion théorique suivante, nous allons utiliser des notations issues du vocabulaire magnétique :

paramètre d'ordre : M

champ conjugué : H

température réduite $t = \frac{T - T_c}{T_c}$

Cette insensibilité aux détails microscopiques a été exploitée pour la première fois par Kadanoff et al [a] qui ont exprimé la similitude entre le système initial et celui où l'objet élémentaire est la réunion de L^d objets élémentaires. L'équivalence des deux systèmes s'exprime par l'égalité des potentiels thermodynamiques :

$$W(t,H) = W(\tilde{t},\tilde{H})$$

où $\tilde{t}$ et $\tilde{H}$ sont des modifications des variables t et H. Kadanoff a proposé la transformation :

$$\tilde{t} = L^y t \quad ; \quad \tilde{H} = L^x H$$

Une variation du potentiel W s'écrira :

$$\delta\left(\frac{W}{k_B T}\right) = \int M \, \delta H \, d^d r = \int \tilde{M} \, \delta \tilde{H} \, \frac{d^d r}{L^d}$$

d'où $\tilde{M} = L^{d-x} M$

L'équation d'état s'écrit :

$$M = f_1 (t,H)$$

Si l'on suppose les deux systèmes identiques, on doit avoir aussi :

$$\tilde{M} = f_1 (\tilde{t},\tilde{H})$$

d'où

$$f_1(t,H) = L^{(x-d)} \quad f_1(L^y t, L^x H)$$

quelque soit L , ce qui n'est possible que si la fonction est homogène :

$$f_1(t,H) = |t|^{(d-x)/y} \quad f\left(\frac{t}{H^{y/x}}\right)$$

La forme de la fonction f n'est pas connue mais l'équation ci-dessus permet d'exprimer tous les exposants thermodynamiques en fonction de x et y. Il n'y aura donc que 2 exposants indépendants, les autres étant liés par les "lois d'échelle".

Sur la courbe de coexistence on obtient :

$$\beta = (d-x)/y$$

sur l'isotherme critique :

$$\delta = (d-x)/x$$

En dérivant,par rapport à H, sur l'isochore critique :

$$\gamma = (2x-d)/y$$

En intégrant par rapport à H et dérivant deux fois par rapport à t :

$$\alpha = 2 - \frac{d}{y}$$

d'où les relations

$$\alpha + 2\beta + \gamma = 2$$
$$\alpha = \beta (\delta - 1)$$

De même il existe des relations entre les amplitudes telles que :

$$B C^+ D^{\delta-1} = R_x$$

$$\frac{A^+ C^+}{B^2} = R_c$$

où R_c et R_x sont des constantes universelles, dépendant exclusivement de d et n. Bien que les arguments ci-dessus soient inexacts, ils ont permis de mettre en évidence l'origine des lois d'échelle. Ils sont au départ d'une théorie plus rigoureuse, dite du "groupe de renormalisation" due à Wilson [b] qui a permis de calculer les exposants et les combinaisons d'amplitude de façon satisfaisante. Une autre théorie, fondée sur des séries hautes températures, a également permis de calculer ces quantités. Après quelques péripéties ces deux théories donnent des résultats tout-à-fait concordants [c] et en bon accord avec l'expérience (voir chapitre VI).

II.4 - Fluctuations

Dans le chapitre précédent, nous avons calculé la valeur quadratique moyenne des fluctuations en développant l'accroissement d'entropie dû à ces fluctuations. Dans le cas d'un mélange binaire critique, le terme de plus bas ordre a un coefficient nul au point critique, ce qui correspondrait à des fluctuations infinies. Il est clair que dans ce cas il faut inclure des termes supplémentaires. En fait quand les fluctuations deviennent importantes, le milieu ne peut plus être considéré comme homogène et le terme qui s'ajoute dépend du gradient de la fluctuation. Nous avons donc, en respectant les conditions de symétrie :

$$\Delta S \sim \left(\frac{\partial H}{\partial M}\right)_T (\delta M)^2 + \frac{b}{2} (\vec{\nabla}\delta M)^2$$

dans l'espace conjugué nous avons donc :

$$\omega(\delta M) \sim \exp - \frac{V}{2k_B T} \sum_k \left[\left(\frac{\partial H}{\partial M}\right)_T + bk^2 \right] \left| dM \left(|k>\right) \right|^2$$

Cette expression montre que les fluctuations δM ($|k>$) sont statistiquement indépendantes et obéissent à une distribution de Gauss. La valeur quadratique moyenne vaut :

$$\left\{ \left|\delta M(k)\right|^2 \right\} = \frac{k_B T}{V\left[\left(\frac{\partial H}{\partial M}\right)_T + bk^2 \right]} = \frac{k_B T}{V} \left(\frac{1}{\frac{\partial H}{\partial M}} \right)_T \frac{1}{1+k^2\xi^2}$$

La longueur $\xi = \sqrt{b\left(\frac{\partial M}{\partial H}\right)_T}$ qui s'introduit naturellement est dite longueur de corrélation. Elle diverge avec un exposant appelé ν . D'après la théorie de perturbation que nous faisons, on a $\nu = \gamma/2$. Par transformation de Fourier on obtient la fonction de corrélation :

$$< \delta M(o) \quad \delta M(r) > \; = G(r) \sim \frac{1}{r} \; \exp - \frac{r}{\xi}$$

valable pour les grandes valeurs de r.

Du fait de la divergence des fluctuations, le développement en perturbation ne peut donner que des indications qualitatives et est foncièrement incorrect. La fonction de corrélation correcte s'écrit :

$$G(r) \sim \frac{1}{\gamma^{1+n}} \; f \; (\frac{r}{\xi})$$

L'intégrale de G(r) devant donner la susceptibilité, on en déduit la relation d'échelle :

$$\gamma = (2 - \eta)\nu$$

L'application à la fonction de corrélation des hypothèses de Kadanoff donne de façon évidente :

$$\nu = \frac{1}{y}$$

d'où la loi d'échelle :

$$d.\nu \; = 2 - \alpha$$

et la relation entre les amplitudes ξ_o de la longueur de corrélation et A de la chaleur spécifique :

$$A / \xi_o^{\,d} = \text{cte universelle.}$$

La forme la plus satisfaisante de G(r) a été établie par Bray [d] mais est particulièrement compliquée. Dans la pratique on en utilise des approximations.

Dynamique

D'une façon générale le temps de retour à l'équilibre d'une fluctuation est donné par le rapport d'un coefficient de transport à la susceptibilité correspondante (ou d'une somme de tels termes). Les premières théories supposaient les coefficients de transport réguliers près du point critique, ce qui entraînait, par exemple, que la relaxation des fluctuations du paramètre d'ordre varie avec un exposant γ , ce qui est en contradiction flagrante avec l'expérience qui montre un exposant voisin de ν .

La première approche fructueuse de ce problème est due à Kawasaki [e] qui a reconnu que l'anomalie critique du coefficient de transport du paramètre d'ordre provenait du couplage de ces fluctuations avec celles de la vitesse transverse. Il en a donc déduit des équations intégro-différentielles liant ce coefficient de transport et la viscosité de cisaillement. Ces équations sont insolubles dans le cas général, mais en première approximation Kawasaki a obtenu pour la largeur de la raie associée au paramètre d'ordre =

$$\Gamma(k,\xi) = \frac{k_B T}{6\pi\eta^* \xi} \; q^2 \; \Omega(k.\xi)$$

avec

$$\Omega(\eta,\xi) = \frac{3}{4} \frac{1}{k^2\xi^2} \left[\; 1 + k^2\xi^2 + (k^3\xi^3 - \frac{1}{k\xi}) \; \text{Ar tg } k\xi \; \right]$$

où η^* est la viscosité "haute fréquence", régulière au point critique. Cette formule a donné un bon accord avec l'expérience. Cependant diverses corrections y ont été apportées. Ainsi la viscosité "haute fréquence" η^* a été remplacée par la viscosité de cisaillement effectivement mesurée.

La théorie du groupe de renormalisation dynamique [f] a également apporté des modifications à cette formule, la multipliant par un coefficient R = 1.2. De plus ces mêmes théories ont abouti à l'expression suivante pour la viscosité de cisaillement

$$\eta = \eta_{reg} \; t^{-y} \qquad \text{avec } y \simeq 0{,}04$$

où η_{reg} est une partie régulière, généralement prise de forme Arhénius. Des théories plus récentes [g] ont abouti à une nouvelle valeur de R = 1.075.

La détermination expérimentale de R est encore hésitante. Elle exige une détermination préalable de ξ par des méthodes statiques. De fait il existe dans la littérature des données compatibles soit avec R = 1, soit avec R = 1.2.

Les autres coefficients de transport restent finis au point critique d'un mélange binaire, à l'exception possible de la viscosité de volume dont le comportement est difficile à déterminer. En effet les résultats ci-dessus sont valables à la limite des fréquences nulles. Les anomalies proviennent des couplages entre les modes et sont donc susceptibles de se modifier si

les fréquences considérées sont très différentes de celles des autres modes. On a pu montrer que la viscosité de cisaillement diminuait lorsqu'on montait en fréquence. Quant à l'absorption du son, il existe encore de sérieuses difficultés pour l'exprimer par une fonction universelle du rapport de la fréquence de mesure à la fréquence caractéristique des paramètres d'ordre [h].

REFERENCES

a) L.P. Kadanoff, W. Götze, D. Hamglen, R. Hecht, E.A.S. Lewis, V.V. Palciauskas, M. Rayl, J. Swift, D. Aspnes and J. Kane Rev. Mod. Phys. 39, 395 (1967)

b) K. Wilson, Phys. Rev. B4, 3174 (1971)

c) J. Zinn-Justin, J. Physique 42, 783 (1981)

d) A.J. Bray, Phys. Rev. B14, 1248 (1976)

e) K. Kawasaki, Annals of Physics 61, 1 (1970)

f) E.D. Siggia, B.I. Halperin and P.C. Hohenberg, Phys. Rev. B13, 2110 (1976)

g) G. Paladin and L. Peliti, J. Physique Lettres 43 L15 (1982)

h) D.B. Fenner, Phys. Rev. A23, 1931 (1981)

CHAPITRE III

Techniques expérimentales

III.1 - Introduction

Dans les études expérimentales constituant cette thèse, nous avons le plus souvent rencontré le problème de l'analyse d'une raie peu intense voisine d'une raie quasi élastique beaucoup plus intense. Le problème peut se poser dans le cas de raies déplacées en fréquence (raies Brillouin) comme dans le cas de raies centrées sur la fréquence de la lumière incidente (raie Rayleigh). Les domaines spectraux que nous avons eus à étudier imposaient l'emploi d'interféromètres de Fabry-Pérot l'un confocal (Intervalle spectral libre 213 MHz) l'autre plan (ISL = 6 - 1100 GHz) et d'un spectromètre à réseau. Nous allons d'abord étudier les limitations d'un montage traditionnel puis décrire ceux plus performants que nous avons utilisés.

III.2 - Montage classique

Les limitations d'un montage de Fabry-Pérot classique nous sont apparues lors des premières études de la diffusion dépolarisée dans le mélange de nitrobenzène et n-hexane. Dans ce système la raie dépolarisée (raie Rayleigh de largeur ≃ 15 GHz) apparaît surmontée d'une raie quasi élastique (diffusion multiple) qui devient très intense près de la température critique.

Lorsque la largeur de la raie devient de l'ordre de l'ISL, les raies des différents ordres de l'interféromètre se recouvrent. Il en résulte une diminution de l'amplitude apparente et surtout de la largeur apparente qui ne peut évidemment dépasser le quart de l'ISL. La correction de largeur reste théoriquement possible jusqu'à des valeurs de la largeur réelle élevées mais elle ajoute dans ce cas beaucoup d'incertitude. La limite pratique se situe pour une demi-largeur réelle égale environ au tiers de l'ISL.

Lorsque, au contraire, la largeur de la raie diminue, il va devenir délicat de la séparer de la fonction d'appareil due à la raie quasi élastique. Ces deux raies ont en effet la même forme. Si l'on considère, par exemple, le cas à priori favorable d'une raie trois fois plus large et spectralement trois fois plus intense que la fonction d'appareil, on obtient un profil qui ne diffère que de $\pm 5\,\%$ d'une seule raie lorentzienne d'intensité spectrale 4 et de largeur égale à 2,55 fois celle de la FA. On voit donc dans cet exemple qu'il est difficile d'estimer le montant de l'inten-

sité quasi élastique d'après le profil expérimental et que les erreurs sur la largeur peuvent être considérables.

Si la raie s'élargit davantage, on pourra la détecter avec une intensité spectrale plus faible. L' aile de la fonction d'appareil décroissant comme le carré de la fréquence, l'amplitude minimale de la raie large doit varier également comme le carré de sa largeur.

Ces considérations ont été résumées dans la figure a qui montre les régions où la mesure a un sens, pour un Fabry-Pérot de finesse ≃ 40. Dans le cas du mélange nitrobenzène - n-hexane, les mesures sont possibles lorsque $T - T_c$ dépasse quelques degrés.

On peut bien sûr gagner par rapport à la situation précédente en utilisant un interféromètre présentant une meilleure finesse. Toutefois ce gain est assez limité car la finesse est limitée pratiquement à environ 100, soit un gain d'un facteur 25, en contraste, ce qui reste insuffisant. Il est donc nécessaire d'utiliser un second interféromètre en série avec le premier pour obtenir un contraste adéquat. Comme il faut que les deux cavités restent parfaitement accordées devant le balayage, la seule façon pratique de réaliser cela est d'utiliser deux parties du champ d'un même interféromètre. On peut éventuellement réitérer ce processus et utiliser jusqu'à 5 passages.

La fonction d'appareil théorique d'un interféromètre double passage est le carré de la F.A simple passage. La finesse est donc assez peu modifiée mais les ailes de la fonction d'appareil, susceptibles de cacher un spectre sont virtuellement supprimées.

III.3 - Fabry-Pérot plan

Nous avons utilisé un interféromètre plan à épaisseur variable réalisé par les établissements Sopra. L'interféromètre est vertical, il a été entièrement construit en acier Invar et est placé dans une enceinte étanche thermostatée à $\pm$ 5.10^{-2}°C, de façon à obtenir une stabilité maximale. Le balayage de l'interféromètre est assuré par trois cales piezo électriques alimentées par un générateur de dent de scie non linéaire. Chaque dent de scie est formée de 16 segments dont la pente peut être modifiée jusqu'à 1 % par bonds de 0,1 %. On peut ainsi compenser la non-linéarité intrinsèque des cales.

Les lames sont à haute réflectivité (R = 0,985) et planes à $\lambda/400$ Un essai de ces lames en simple passage sur une ouverture de 4 cm a donné une finesse de 110. En double passage le diamètre utile a bien sûr été divisé par 2. La réflexion entre les deux passages est assurée par un coin de cube qui permet d'obtenir le parallélisme nécessaire sans ajustement. Comme le bord des lames est utilisé, la finesse est réduite à 70 et la transmission est d'environ 5 %. La stabilité de l'ensemble donne après 24 h une diminution de transmission d'environ 10 %. D'autre part le revêtement des lames a une réflectivité constante ($\pm$ 0.7 %) entre 4600 Å et 6500 Å, permettant l'utilisation de diverses longueurs d'onde sans perte de performances.

III.4 - Fabry-Pérot confocal

Lorsque l'épaisseur d'un interféromètre dépasse son diamètre utile, la géométrie confocale devient plus intéressante que la géométrie plane d'une part par sa meilleure étendue optique, d'autre part par sa stabilité. Nous avons utilisé un interféromètre confocal de 375 mm de longueur fabriqué par Jobin-Yvon (soit un ISL de 213 MHz). Sa finesse est de 100 mais les raies quasi-élastiques apparaissent élargies par la dérivé rapide ("Jitter") d'un laser à argon monomode (finesse apparente $\simeq$ 50). Le contraste par contre est peu affecté par cet effet. Cet interféromètre peut également être utilisé en double passage en envoyant la lumière l'ayant traversé légèrement de biais grâce à un miroir sphérique. Cette lumière est ensuite recueillie par un miroir troué. Ce miroir recueille également un peu de lumière réfléchie par la première lame de l'interféromètre. Pour éliminer cela, il suffit de tourner de 90° la polarisation de la lumière ayant traversé la FP grâce à une lame quart-d'onde placée entre l'interféromètre et le miroir optique. La lumière réfléchie par la 1ère lame est éliminée par un polariseur.

III.5 - Ensemble de montage

L'obtention d'un bon rapport signal/bruit nécessite en général un temps d'acquisition de données assez long. Pendant ce temps, le laser comme l'interféromètre peuvent dériver de façon significative. Il est donc nécessaire de resynchroniser le balayage périodiquement. Pour celà on envoie à travers l'interféromètre une fraction de la lumière laser, prélevée par réflexion sur une lentille (L1) et convenablement atténuée (fig.1).

Un dispositif électronique approprié, placé après le détecteur envoie un signal de synchronisation un temps fixé après le centre du pic de transmission. La lumière élastique est alors éteinte par le chopper T_2 et l'enregistrement déclenché. Les spectres successifs se superposent exactement dans la mémoire (analyseur multicanaux). La période choisie est de 2 secondes, rendant les dérivés négligeables. A intervalles réguliers (1 enregistrement sur dix) on enregistre, dans une autre partie de la mémoire, une diffusion élastique, dans une géométrie aussi voisine que possible, afin d'obtenir la vraie fonction d'appareil et éventuellement un étalon d'intensité. Ceci est réalisé grâce à l'action d'autres choppers. Chaque spectre est enregistré dans 2000 canaux de la mémoire et les vitesses de balayage sont ajustées de sorte qu'un ISL corresponde à 1024 canaux.

III.6 - Analyse de spectre

Nous avons vu à propos du Fabry-Pérot simple passage la difficulté d'extraire d'un spectre expérimental les caractéristiques d'une raie, principalement une raie Rayleigh. Pour pouvoir profiter pleinement des possibilités d'un Fabry-Pérot double passage, il est nécessaire d'utiliser des moyens informatiques évolués. Nous utilisons un programme de raffinement statistique non-linéaire dû à M. Tournarie [6] . Ce programme calcule le produit de convolution du spectre théorique par la fonction d'appareil expérimentale et on varie les paramètres jusqu'à l'obtention du meilleur accord avec le spectre expérimental. Il donne alors deux paramètres permettant de juger la qualité de l'accord. Il calcule d'abord l'erreur quadratique totale moyenne :

$$E_T = \frac{1}{N} \sum_i \left(\frac{Y_i exp - Y_i calc}{\Delta Y_i} \right)^2$$

et l'erreur systématique ou corrélée :

$$E_e = \frac{1}{N-1} \sum_i \left(\frac{Y_i exp - Y_i calc}{\Delta Y_i} \right) \left(\frac{Y_{i+1} exp - Y_{i+1} calc}{\Delta Y_{i+1}} \right)$$

D'où il est déduit :

l'erreur statistique moyenne : $E = E_T - E_c$

le coefficient de qualité : $Q = E / E_T$

Deux problèmes surviennent cependant lorsque le pic quasi élastique

devient trop important (le rapport maximal des intensités spectrales que nous avons étudiées est de l'ordre de 5000).

Le premier est lié au fait que la fonction d'appareil enregistrée n'est pas rigoureusement la même que le pic quasi élastique puisque les géométries ne peuvent être rigoureusement identiques. Une distortion systématique de 10^{-3} peut être de l'ordre de grandeur du spectre. Pour éviter que le programme ne trouve plus "économique" d'accorder le pic central que la raie large, il faut donc diminuer fortement le poids de cette région (augmenter les ΔY_i) en fixant à priori l'intensité du pic. Cette région "aveugle" couvre entre 5 % et 8 % de l'ISL (fig. 3). Le second est lié au bruit statistique de la fonction d'appareil expérimentale (enregistrée 9 fois moins longtemps que le spectre) qui, s'ajoutant au bruit intrinsèque du spectre, peut noyer l'information utile. Il faut donc remplacer la F.A. expérimentale par une fonction théorique sans bruit qui la décrit au mieux. Nous avons utilisé la fonction :

$$AF(\nu) = \frac{X_1}{1+X_2\nu^2+X_3\nu^3+X_4\nu^4} + C_1 +$$

$$C_2\nu + X_5(\nu+C_3)\ (\nu+C_4)\ (\nu+C_5)\ e^{-X_6\nu^2}$$

$$+ \begin{cases} C_6 \exp - \left(\frac{\nu}{C_7}\right) & \text{si} \quad \nu > 0 \\ \\ C_8 \exp - \left(\frac{\nu}{C_9}\right) & \text{si} \quad \nu < 0 \end{cases}$$

où les C_i ont été imposés et les X_i déterminés par un programme d'affinement (ces paramètres n'ont aucune signification intrinsèque). Les termes des deuxième et troisième lignes contribuent pour moins de 0,5 % de l'amplitude totale. Dans les cas où la comparaison a pu être faite l'utilisation de cette FA "lissée" n'a pas sensiblement modifié les résultats obtenus mais a réduit les incertitudes.

III.7 - Spectromètre à réseau

Le spectromètre utilisé était un spectromètre Coderg de type T800 (T pour triple monochromateur, 800 pour 800 mm de distance focale).

Cet appareil conçu et réalisé au début des années 70 était et reste inégalé par ses concurrents. Il allie une haute luminosité à une

bonne résolution, la rejection des lumières parasites est très élevée et la distorsion très réduite. La figure b montre un schéma simplifié du trajet optique.

Un objectif de 125 mm de focale et d'ouverture 1:2,2 collecte la lumière diffusée à 90° de la lumière excitatrice par l'échantillon. Le faisceau diffusé est focalisé sur la fente d'entrée de l'appareil. Une lunette permet à l'opérateur de régler l'optique d'entrée pour former l'image de diffusion sur la première fente. La lumière est renvoyée par un système de six miroirs concaves de 800 mm de focale sur trois réseaux de 1800 traits par mm. Les trois réseaux sont fixés et ajustés en position sur une même barre à faible torsion, ce qui réduit les risques de déréglage. A chaque réseau est associée une fente droite de 20 mm de long dont la commande électronique permet une ouverture continue de 0 à 2 mm. L'ouverture se fait symétriquement par rapport à l'axe optique de l'appareil. Cette disposition présente entre autres l'avantage de garder à la fonction d'appareil une forme de triangle isocèle.

La détection était effectuée par comptage de photons grâce à un photomultiplicateur refroidi.

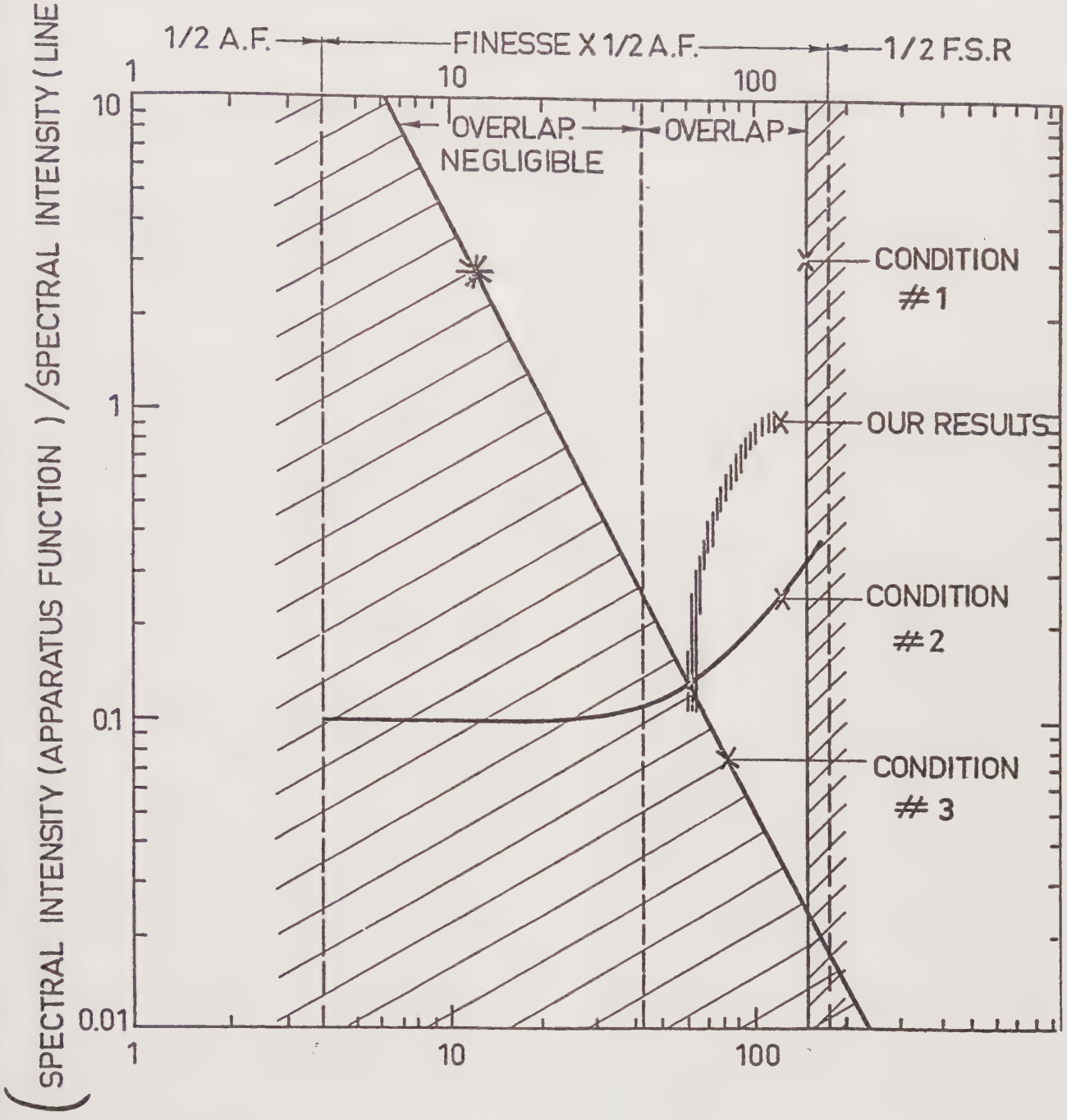
1/2 A.F.
FINESSE X 1/2 A.F.
1/2 F.S.R
1
10
100
OVERLAP
NEGLIGIBLE
OVERLAP
CONDITION #1
OUR RESULTS
CONDITION #2
CONDITION #3
10
1
0.1
0.01
1
10
100
(SPECTRAL INTENSITY (APPARATUS FUNCTION) / SPECTRAL INTENSITY (LINE))

Figure a

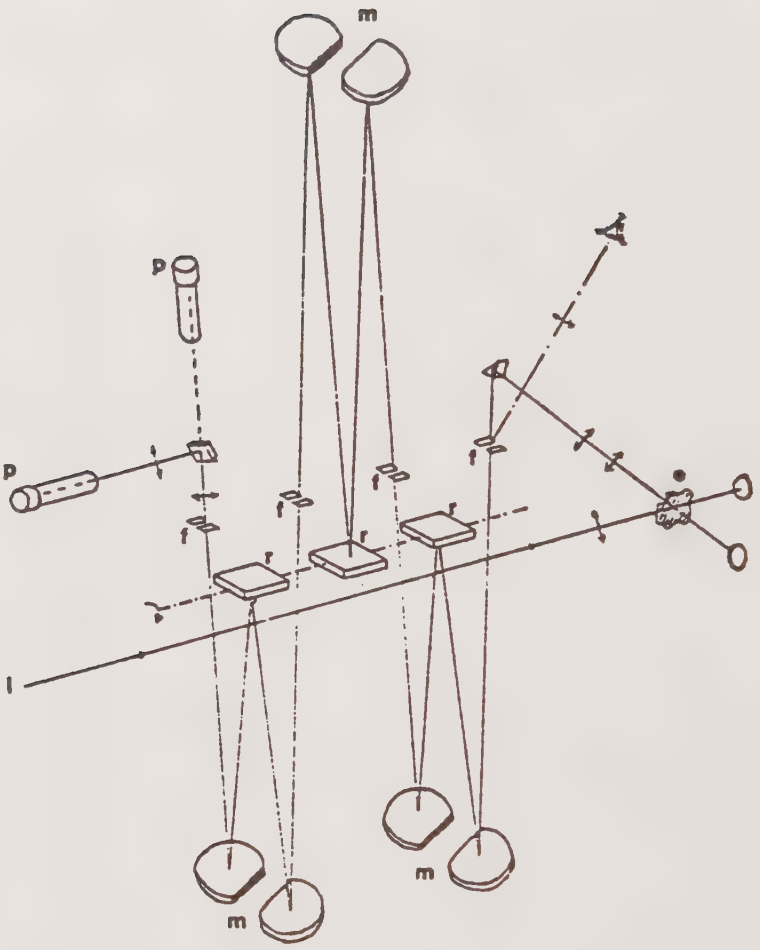

Fig. 6 - Schéma optique du T800

e : échantillon
f : fentes
l : faisceau laser
m : mircirs
p : photomultiplicateurs
r : réseaux

Volume 23, number 1 OPTICS COMMUNICATIONS October 1977

STUDY OF RAYLEIGH LINES IN PRESENCE OF STRONG ELASTIC SCATTERING: A HIGH PERFORMANCE FABRY-PÉROT EXPERIMENT

D. BEYSENS and G. ZALCZER

Commissariat à l'Energie Atomique, Division de la Physique, Service de Physique du Solide et de Résonance Magnétique, CEN Saclay, Boite Postale no. 2, 91190 Gif-s/Yvette, France

Received 2 August 1977

A new high performance Fabry-Perot experiment is presented that enables resolution of Rayleigh lines to be obtained even in presence of elastic scattering which is 5000 times more spectrally intense. A double-passed interferometer is used. Automatic compensation of frequency drifts and stability of the interferometer allow spectra to be accumulated for more than 24 hours. The apparatus function is simultaneously recorded using exactly the same geometry. A sophisticated computing program gives both the true linewidth and the intensity.

1. Introduction

In this paper we describe a high performance set-up capable of resolving non displaced lines (Rayleigh lines) which in a conventional experiment would be buried by the wings of very intense elastic or quasi-elastic scattering lines [1]. Obviously, such a set-up can also resolve displaced lines (Brillouin lines), although in this case alternative methods, such as iodine filters, can be used.

The main features of this experiment are: a plane multipass Fabry-Perot (F-P), with high contrast and long time stability, simultaneous recording of both the apparatus function (A-F) and the spectrum in an identical scattering geometry, automatic compensation of frequency drifts of the laser line, and use of a sophisticated deconvolution computing program.

This set-up was used to study the depolarized spectrum of a critical mixture of nitrobenzene and n-hexane where the very intense quasi-elastic depolarized (multiple) scattering has, up to now, prevented meaningful measurements being made close to the critical point, i.e. in the region of greatest interest.

2. Set-up and operation

The experiment is shown in fig. 1. Its use has already been described in ref. [2] for the case of a confocal double-passed F-P. The spectrum and the A-F are alternatively recorded (period 20 s) by using convenient choppers. Nevertheless, with a plane F-P the geometrical conditions need to be closely identical: We thus used as an A-F the spectrum of the very intense polarized spectrum, which is a low frequency spectrum [3] (linewidth ≈1 kHz) not resolved by the F-P and having an identical scattering geometry as the depolarized spectrum ‡. Since the selection of the depolarized (VH) component of the scattered field is achieved by a Glan prism set before the photomultiplier (P-M), we only need rotate the field by 90° to select the A-F. This is performed by the chopper C_3 which inserts a half-wave plate just before the Glan prism while the chopper C_1 places an attenuator to adjust the signal levels. We accumulate usually 9 spectra for one A-F at each period, but other ratios are possible.

The compensation of the frequency drifts is obtained by starting recordings at a maximum of transmission of the F-P when illuminated by the laser beam. For this purpose, a part of the laser beam obtained by reflexion on lens L_1, is sent through the chopper C_2 into the F-P using the reflexion on lens L_2. When the

‡ It is possible to generalize this method if one can separate the elastic scattering from the spectrum, either by polarization, or by frequency drifts as for Brillouin lines.

Volume 23, number 1 OPTICS COMMUNICATIONS October 1977

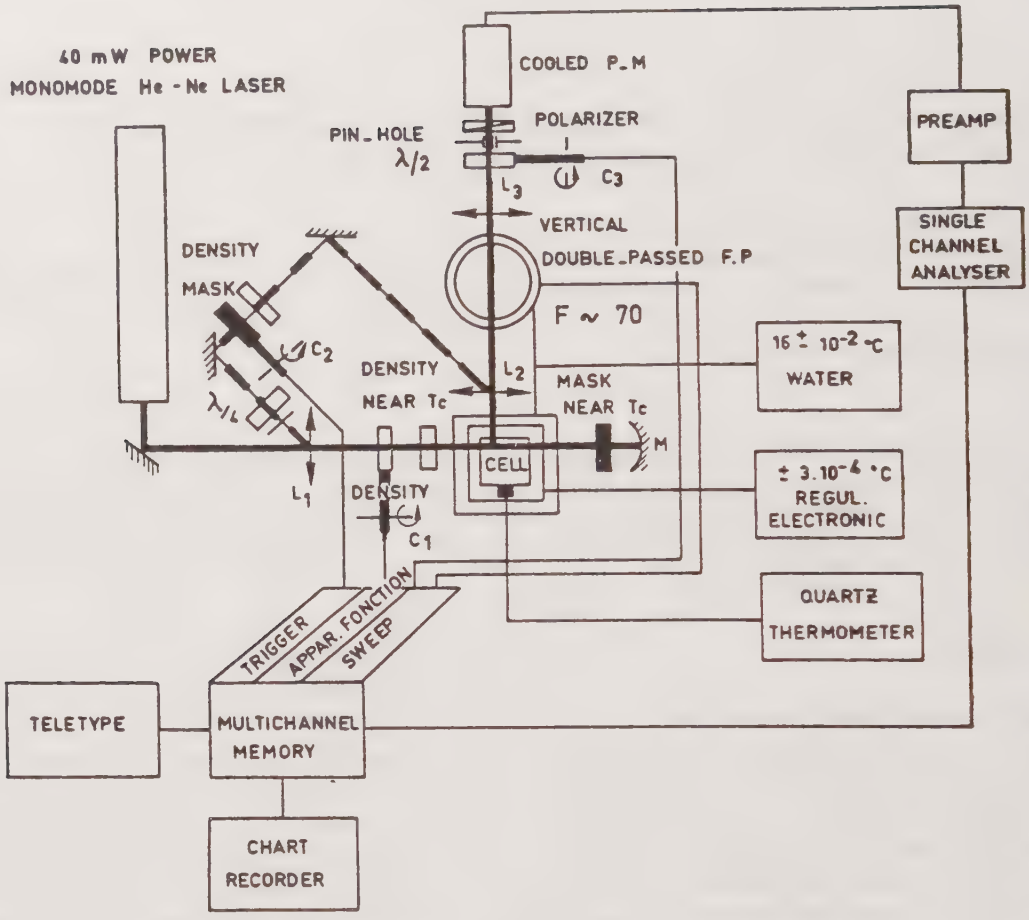

Fig. 1. General description of the set-up, C_1, C_2, C_3 are the three choppers.

maximum is detected, C_2 stops this beam. Its intensity is adjusted by an attenuator, and in order to allow the system to work whatever the position of C_3, this light is circularly polarized by a quarter-wave plate.

The exciting beam is provided by a He-Ne laser (λ = 6328 Å) of 60 mW power (40 mW in a single mode with a F-P in the cavity). The lens L_1 focuses this beam into the sample. The beam is reflected by a spherical mirror (M) in order to increase the intensity in the cell. 5 or more passages are possible (when the transmission of the cell is sufficient) without disturbing the laser provided that the reflected beam is slightly misaligned. This method is obviously possible only at a scattering angle of 90° or when the spectrum of the scattered light shows no angular dependance.

In some cases however it is necessary to reduce the incident intensity in order to avoid additional heating of the sample or the saturation of the counting chain. Attenuations up to 30 had to be used. The scattering volume was as close as possible to the entry and exit windows of the cell to minimize the effects of both turbidity ‡ and multiple scattering [e.g. 4].

The sample was placed in a two-stage thermostat inside a room with temperature stability ±0.3°C. The resulting temperature stability was $\pm 5 \times 10^{-4}$°C, or better during 24 hours.

The light analysed by the F-P is detected by a P-M. The photocathode is cooled by circulating gazeous nitrogen. The nitrogen pressure is high enough to

‡ The turbidity (τ) is the rate of decrease of the incoming beam intensity (I_0) per unit length. If I is the transmitted light through a sample of length (l), one can write: $I = I_0 e^{-\tau l}$, τ can be deduced by interpreting the first scattering.

avoid frost, so no windows are necessary.

An amplifier and a single channel analyser allow the photoelectrons to be counted in a multichannel memory (2 × 2000 channels), with chart recording and teletype as outputs. The generating rate (2 MHz) of the single channel analyser that we used imposed an upper limit to the counting, so when elastic scattering was too intense, the intensity of the beam and then the intensity of the spectrum, must be reduced. To obtaine the same signal-to-noise ratio an increase in the recording time, up to more than 24 hours was necessary. Of course this limitation can be removed in other experiments where the shape of the elastic scattering is not required.

3. The F-P interferometer

The F-P (built by Ets. Sopra), is constructed in invar, with a vertical optical axis giving the best mechanical stability. It is placed in a thermally stabilized air tight cylinder ($\pm 10^{-2}$°C) so that either pressure scanning or piezo-electric scanning at constant pressure can be performed. The three piezo-electric transducers are driven by a digital non linear saw tooth generator made up of 16 adjustable slope segments (adjustments ±1% by plots of 1‰) through 3 independent amplifiers. Bigger non-linearities can be reduced by using parallel resistors or capacitors. The total reproducibility is better than 5×10^{-4}, which corresponds to the tenth of a A-F full width, with finesse 100 and 2 free spectral range (F.S.R.) recorded. The period of the sawtooth can be adjusted from 0.5 s to 5×10^3 s. We used a period of 2 s.

The spacing between the plates is variable up to 50 cm. It can be measured either by the method of rings, when the spacing is small, or with a cathetometer. Typical uncertainty is 1%. In the considered example, the F.S.R. of 78 GHz has been chosen for giving reasonable overlappings from neighbouring orders [1]. The plates have 7 cm total and 5 cm useful diameters. We used a pair of high reflectivity plates (0.985), of λ/100 quality, suitable for single or double pass. But the F-P can work either in 3, 4 or 5 pass with plates of lower reflectivity but better quality (λ/200). Theoretical finesse and contrast are about identical when the first set is used in the double pass arrangement and when the second is used in the triple pass arrangement. The reflectivity is constant (±0.7%) between 4600 Å and 6500 Å. We obtained a finesse of 110 in single-pass with an aperture of 4 cm, and 70 in double-pass with an aperture of 2 cm. This result is due to the fact that we did not use the center of the plates with double pass. The theoretical contrast (double pass) is about 10^7, experimentally certainly better than 10^6. Transmission is about 5% in double pass.

The whole experiment is set on a granite table isolated from the ground by 6 tyre inner tubes [2] in order to eliminate mechanical vibrations. Overall stability corresponds to a deformation of the A-F of less than 10% (±5%) over 24 hours.

4. Analysis of the spectra

We therefore obtain the experimental spectrum, $S(\nu)$ and the experimental A-F, $H_{\mathrm{exp}}(\nu)$. $S(\nu)$ is the convolution of the true spectrum $\sigma(\nu)$ with the true A-F, $H_{\mathrm{true}}(\nu)$, and can be analysed as the sum:

$$S(\nu) = [\sigma(\nu) * H_{\mathrm{true}}(\nu)] + (\text{background}) + (\text{noise}).$$

The background comes from larger lines and can have a small slope due to some systematic distortions. $H_{\mathrm{exp}}(\nu)$ can be assumed to be $H_{\mathrm{exp}}(\nu) = [\delta(\nu) + P(\nu)] * [H_{\mathrm{true}}(\nu) + \text{systematic distortion}] + (\text{noise})$. $P(\nu)$ is composed of "parasitic" lines, i.e. in our case of the Brillouin lines plus $\sigma(\nu)$, whose relative spectral intensity $P(0)$ is in most cases, completely negligible (see below). $\sigma(\nu)$ can be assumed here to be a single lorentzian function [1,5], plus a Dirac function which represents in this range of frequency [3] the contribution of single scattering due to polarizer defects, and multiple scattering.

$$\sigma(\nu) = I \frac{\Gamma/\pi}{\Gamma^2+\nu^2} + D\,\delta(\nu)\,.$$

The experimental spectrum looks therefore like a quasi-lorentzian line $[\sigma(\nu) * H_{\mathrm{true}}(\nu)]$ on which is superimposed a peak $[D\,\delta(\nu) * H_{\mathrm{true}}(\nu)]$ (fig. 2) whose relative heights are in the ratio of spectral intensities $r = (I/D)(\delta\nu)/\pi\Gamma$ (where $\delta\nu$ in the half width of the A-F). This ratio can, in this experiment, be as large as 5×10^3.

The computing program we used is due to Tournarie [6]. In order to determine the unknown quantities

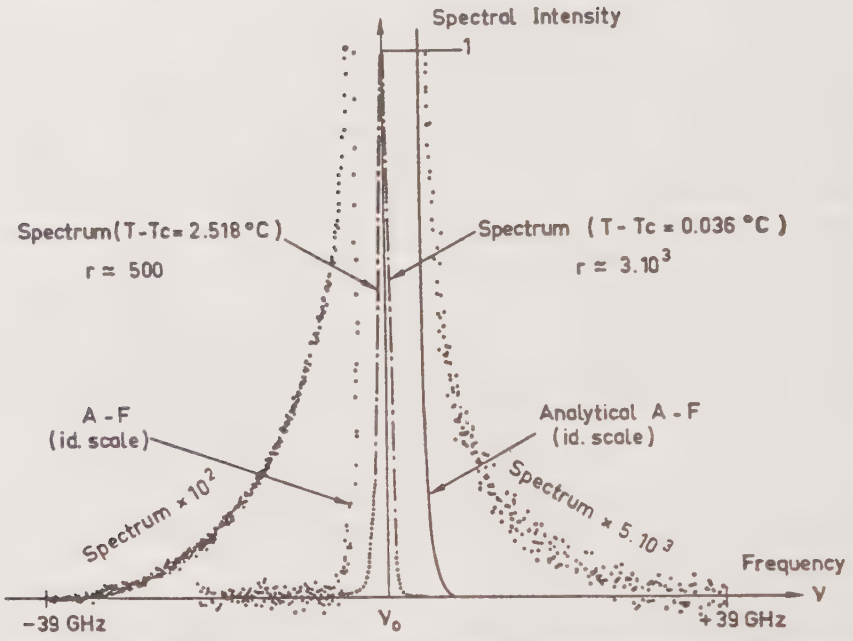

Fig. 2. Typical spectra with the same reduced scale. The A-F are shown with the same spectral intensity at frquency ν_0. Both experimental and analytical A-F are shown. r is the ratio of spectral intensities (peak/line) at frequency ν_0.

such as Γ, I, D... the experimental A-F, $H_{exp}(\nu)$, is convoluted with the true spectrum $\sigma(\nu)$ and compared with the experimental spectrum $S(\nu)$. Convolution is performed by fast Fourier transform, which atomatically accounts for periodicity (overlappings). In the normal form of the program, the uncertainty on each point is assumed to obey Gaussian statistics, i.e. it is taken equal to the square root of the number of photoelectrons in each channel.

Since a systematic distortion between the calculated and experimental peaks as small as 10^{-3} can be of the order of magnitude of the spectrum, we had to modify the weighing in the peak. So, the uncertainties have been strongly increase in the peak region, while the peak intensity was fixed "a priori". The parasitic lines $P(\nu)$ in the A-F have been dealt with in the same way. Typically this "blind" area concerns from 5% to 8% of the data, according to the value of r, and at most 12% when brillouin lines are present.

Another problem concerning the difference between an ideal and an experimental A-F is the noise: the intensity of $H_{exp}(\nu)$ is usually 0.1 times the intensity of the peak in $S(\nu)$ (the ratio of recording times). So $[H_{exp}(\nu) * \sigma(\nu)]$ introduces important noise when fitting with $S(\nu)$. This has been solved by replacing the experimental A-F by the analytical fit of $H(\nu)$. We used the following empirical formula

$$H_{exp}(\nu) = \frac{X_1}{1 + X_2\nu^2 + X_3\nu^3 + X_4\nu^4} + C_1 + [C_2\nu + X_5(\nu + C_3)(\nu + C_4)(\nu + C_5)] \times \exp(-X_6\nu^2) + \begin{cases} \nu > 0: C_8 \exp(-\nu/C_7) \\ \nu < 0: C_8 \exp(+\nu/C_9) \end{cases}$$

X_i are adjustable parameters, C_i are constants. The terms in the bracket represent less than 0.5% of the total function. Most values obtained with the experimental A-F did not change significantly when the analytical A-F was used, but the uncertainties decreased.

The difference between experimental values $S(\nu)$ and calculated values $[\sigma(\nu) * H_{exp}(\nu)]$ divided by the standard deviation δ are vizualized (fig. 3), whereas a coefficient (Q) measures the ratio of the statistical error to the total error: when Q is equal to one, the deviation is purely random. All the spectra we analyzed gave a Q value between 1 and 0.5, which is also a good justification concerning the assumptions on the shape of $\sigma(\nu)$ ‡.

‡ The same spectrum was analysed with a much wider free spectral range (1087 GHz), where the same hypotheses were no longer valid: Q got very low, showing a strong systematic distortion. Another Rayleigh line had to be added [7].

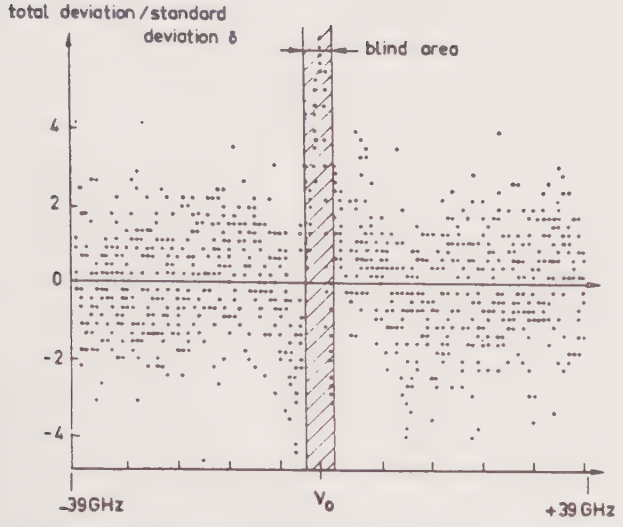

Fig. 3. Reduced deviation versus frequency for a spectrum recorded at $T - T_c = 0.0290°C$ with a ratio of spectral intensities $r \approx 5000$. The quality coefficient is $Q = 0.54$, due to the distortions in the "blind" region where the peak is situated.

The interesting parameters can therefore be obtained: intensity i of $H(\nu)$, intensity I and linewidth Γ of $\sigma(\nu)$, intensity D of the peak. Γ-units are referred to the F-S-R of the interferometer, whereas the polarized quasi-elastic scattering intensity (i) has been chosen as a standard for both I and D. In fact it accounts very exactly for the incident power, the loss of scattered intensity by turbidity, the transmission of the F-P, etc. Let us point out that the ratio I/D can also be a standard, but D has not the same spatial variation in the sample, and its variation with temperature, which is here our physical variable, is not known with the same accuracy as the polarized scattering. The results give an experimental scatter in the values of about ±3% for the intensities, and ±5% for the linewidths. Moreover, in order to test this program, identical spectra with very different D values have been analysed, verifying that the linewidth Γ did not change within the limits of the uncertainties.

As a conclusion, this F-P experiment allows a quantitative study to be made of weak lines (Rayleigh or Brillouin) adjacent to very strong elastic or quasi-elastic scattering. Both linewidths and intensities can be accurately measured.

We used this set-up to study the depolarized spectrum of the critical mixture of nitrobenzene and n-hexane near its critical mixing point [7] (T_c). With a conventional F-P experiment, reliable results could be obtained only in the range $\Delta T_c > 3°C$ [1,5]. With this new arrangement, we achieved measurements as close as $0.026°C$ to T_c, and we emphasize that the main limitation arose from the saturations of the recordings.

References

[1] D. Beysens and G. Zalczer, Opt. Comm. 22 (1977) 236.
[2] D. Beysens, Rev. Appl. 8 (1973) 175.
[3] D. Beysens and G. Zalczer, Phys. Rev. A15 (1977) 765.
[4] D. Beysens, A. Bourgou and H. Charlin, Phys. Lett. 53A (1975) 236;
L.A. Reith and H.L. Swinney, Phys. Rev. A12 (1975) 1094;
D. Beysens, A. Bourgou and C. Zalczer, J. Phys. (Paris) C1 (1976) 225.
[5] D. Beysens, A. Bourgou and G. Zalczer, Opt. Comm. 15 (1975) 436.
[6] M. Tournarie, J. Physique 30 (1969) 47.
[7] D. Beysens and G. Zalczer, to be published.

C H A P I T R E IV

Etude expérimentale de la diffusion dépolarisée dans les fluides critiques

IV.1 - Nitrobenzène - n-hexane

Introduction

La première étude de la diffusion dépolarisée dans un mélange critique est due à Fabelinski et al. [7-10] et portait sur le mélange de nitrobenzène et n-Hexane. Elle concluait à la présence de plusieurs raies, fortement anormales près du point critique tant par leur intensité que par leur largeur. Ces résultats étaient très suprenants du fait que l'anomalie observée pour la largeur était beaucoup plus forte que celle de la viscosité d'une part, et d'autre part que les fréquences caractéristiques de ces phénomènes sont beaucoup plus hautes que les fréquences de relaxation admises pour les parties critiques des grandeurs thermodynamiques.

Nous avons alors repris ces mesures en arrivant aux conclusions suivantes :

- le spectre dépolarisé d'un mélange binaire critique est dominé près du point critique par la diffusion multiple ou rediffusion de la diffusion primaire. Cette diffusion est quasi élastique et apparaît donc comme une fonction d'appareil, et son intensité croît environ comme le carré de la diffusion primaire (avec un exposant $2\gamma = 2,48$). Il semble que la méconnaissance de ce phénomène soit la cause de l'erreur d'interprétation de Fabelinski et Al. L'étude des autres composantes du spectre ne peut se faire avec des moyens classiques, qu'au-delà de quelques degrés du point critique.

- Dans cette région et avec un intervalle spectral libre (ISL) de 60 GHz, on n'observe qu'une seule raie lorentzienne dont la largeur varie sensiblement comme la viscosité et l'intensité décroît légèrement avec la température. Cependant il ne nous avait pas été possible de préciser si la largeur de la raie dépolarisée suivait la très faible anomalie de la viscosité, ni de rendre quantitative la variation de l'intensité.

Montage expérimental

Le montage expérimental a été décrit dans un chapitre précédent.

Résultats

- Raie large

Avec l'ISL de 1087 GHz, nous avons mis en évidence l'existence d'une raie large. Cette raie est très peu intense et son étude est difficile. Nous nous sommes contentés de la mesurer à 0,1°, 1°, 5° de T_c.

A 0,1° de T_c, la raie n'était pas visible. Aux autres températures, sa largeur était voisine de 145 GHz, et son intensité environ 15 % de celle de la raie étroite.

Son intensité spectrale est donc 100 fois plus faible et elle ne peut apparaître que comme un fond continu quand un ISL de 75 GHz est utilisé.

Par la suite nous avons réexaminé cette raie au moyen d'un triple monochromateur : nous avons alors constaté que cette raie n'est en fait pas lorentzienne mais se décrit plutôt sur un large intervalle de fréquence par une formule de la forme :

$$i(\omega) \simeq \sqrt{\omega}\, e^{-\frac{\omega}{\omega_o}} \quad \text{avec } \omega_o = 715 \text{ GHz}$$

qui correspond à un mécanisme collisionnel [a] (fig. a)

La même forme de courbe a été trouvée également pour le nitrobenzène pur avec $\omega_o \simeq 850$ GHz.

- Raie étroite : largeur

Nous avons regroupé trois séries de résultats :

a) $T - T_c = (0{,}016°K - 40K)$ effectuée avec l'interféromètre double passage et le laser monomode

b) $T - T_c = (0{,}1°K - 15°K)$ effectuée avec un laser multimode

c) $T - T_c = (3\ K - 50\ K)$ effectuée avec un interféromètre simple passage.

Nous avons essayé de décrire ces résultats par une formule analogue à celle de la viscosité de cisaillement

$$\eta = \eta_o \exp\left(\frac{E}{T}\right) t^{-Y\eta}$$

avec $\eta_o = (143 \pm 5)\ 10^{-T}$, $E = 10$

$(136 \pm 5)\ 10^{-4} P_o$, $E = 3.58 \times T_c = 1050$ K

soit en laissant y_η libre, soit en l'imposant à zéro.

Nous avons effectué la même analyse avec $\frac{\eta}{T}$ à la place de η.

Les résultats sont résumés dans la table III. Il en résulte :

- que les deux formes donnent les mêmes exposants
- que l'exposant laissé libre évolue vers une valeur significativement différente de zéro
- que l'on retrouve l'énergie d'activation de la viscosité si l'on utilise la première formule avec l'exposant non nul
- que l'exposant trouvé est légèrement inférieur à l'exposant de la viscosité.

Nous avons également comparé nos résultats à ceux obtenus dans des mélanges non critiques de nitrobenzène à la température de 24°C :

$$\tau = a\eta + \tau_o$$

Si l'on utilise les valeurs a et τ_o obtenues par ailleurs, on obtient la valeur $\tau = 12{,}6.10^{-12}$ s à 24°, assez proche de la valeur expérimentale de $16{,}2.10^{-12}$s.

Si par contre on suppose les coefficients a et b indépendants de la température et qu'on veut appliquer cette formule à l'ensemble des résultats, on obtient le meilleur accord pour des valeurs a_1 et b_1 telles que :

$$\frac{a_1}{a_o} \simeq 3 \qquad \frac{b_1}{b_o} \simeq \frac{1}{4}$$

ce qui ne peut être considéré comme satisfaisant.

Signalons ici que l'étude de la réorientation moléculaire du nitrobenzène dans le même mélange critique a, depuis lors été menée par une technique complètement différente : l'effet Kerr picoseconde [b] . Les temps observés varient de la même façon que dans nos mesures, avec un exposant voisin mais légèrement inférieur à celui de la viscosité. Par contre, ils sont systématiquement environ deux fois plus petits.

- Raie étroite : intensité

L'intensité de la raie étroite est obtenue par comparaison avec,

soit la diffusion polarisée, soit la diffusion multiple enregistrées simultanément. Le tracé de ces résultats suggère la forme empirique :

$$I = I_o \, t^{-\Omega}$$

avec $\Omega \simeq 0{,}2$

Les mesures de la série c) avaient déjà été comparées avec les résultats de mélange non critique de nitrobenzène à 24°C à la même concentration. Nous trouvons :

$$\frac{I \text{ critique}}{I \text{ non critique}} = 0.82$$

l'amplitude de l'anomalie est donc relativement faible.

Il est à noter que les théories monomoléculaires ne peuvent rendre compte que d'une variation proportionnelle à la densité. Dans l'intervalle que nous avons étudié, la densité ne varie que de quelques %, l'intensité dépolarisée d'un facteur 4. Il s'agit donc d'un phénomène collectif.

IV.2 - Nitroéthane-isooctane

Introduction

Les résultats précédents sont donc particulièrement surprenants. Il était donc intéressant de voir si on les retrouvait dans d'autres systèmes.

Nous avons choisi un système où les difficultés expérimentales sont limitées : si la diffusion élastique est très faible, la raie anisotrope sera beaucoup plus facile à mesurer. Nous avons donc utilisé le mélange de nitroéthane et d'isooctane. Une autre différence imposée par ce choix réside dans la différence des fréquences mises en jeu, de l'ordre de 100 GHz au lieu de 10 GHz dans le nitrobenzène-n-hexane.

Montage expérimental

Le montage utilisé est le montage interférométrique décrit précédemment, l'intervalle spectral libre étant fixé à 1087 GHz.

Résultats

- Constituants purs et mélange non critique

Nous avons d'abord étudié la diffusion dépolarisée par les composants du mélange. L'isooctane a une diffusion dépolarisée quatre fois plus faible que le nitrobenzène, aussi nous n'avons pas regardé sa variation avec la température. La largeur de raie dans le nitroéthane varie avec une loi d'Arrhénius, avec une énergie d'activation de 750 $\pm$ 170 K, comparable à celle de la viscosité 824 K alors que l'intensité reste à peu près constante. Nous avons aussi tenté d'étudier la variation de cette intensité en fonction de la concentration dans un mélange non critique avec du CCl_4. Les mesures sont peu précises du fait de la difficulté de comparer des intensités de diffusion dans des cellules différentes, mais indiquent une courbure beaucoup plus faible que dans le mélange de nitrobenzène et n-hexane.

Il semble donc que les corrélations d'orientation soient beaucoup plus faibles dans ces systèmes.

- Mélange critique

Les résultats couvrent le domaine $T - T_c$ = (2mK - 60 K).

Il en ressort tout d'abord que la largeur de la raie n'a pas d'anomalie critique, contrairement au cas du nitrobenzène - n-hexane. Cette largeur est bien décrite par une loi d'Arrhénius :

$$\Gamma = \Gamma_o \exp \frac{E}{T}$$

La viscosité du nitroéthane à laquelle on doit comparer ces résultats a été analysée selon la formule habituelle :

$$\eta = \eta_o \, t^{-y_\eta} \exp \frac{E}{T}$$

- soit en laissant y_η libre :

$\eta_o = 2{,}18\ 10^{-2}$ cPo $\quad y_\eta = 0{,}0045 \pm 0{,}0013$

$E = 920 \pm 180$ K

- soit en la fixant à sa valeur admise : $y_\eta = 0,04$

$$\eta_o = 1,83.10^{-2} \text{ cPo}$$

$$E = 980 \pm 20$$

Les énergies d'activation trouvées sont donc égales. Ceci peut être interprété comme le fait que la diffusion dépolarisée dans ce mélange n'est sensible qu'à la partie régulière de la viscosité. L'intensité de la diffusion dépolarisée ne diverge pas non plus près du point critique. Cependant dans la région $T - T_c < 30°$ elle croît fortement et sensiblement linéairement quand T décroît, alors qu'elle est constante au-delà. Le caractère linéaire de cette variation ne permet pas de déterminer si l'augmentation est due au voisinage du point critique. De plus, un comportement semblable a été observé dans le nitrobenzène pur.

Une autre formule a été récemment proposée qui décrit assez bien ces phénomènes par analogie avec certains corps présentant une transition vitreuse.

$$I\alpha \frac{I_o}{T - T_g}$$

où Tg est la température de transition. Dans les deux cas que nous avons cités, cette température ne peut être définie que de façon arbitraire, ce qui limite beaucoup la portée de cette suggestion.

IV.3 - Dioxyde de carbone

Introduction

Les fluides purs critiques appartiennent à la même classe d'universalité que les mélanges binaires critiques. Les caractères physiques dominants, liés au point critique sont donc très voisins dans ces deux classes de système. Il nous a donc paru opportun d'étudier également la raie dépolarisée d'un fluide pur de molécules anisotropes près de son point critique.

Le dioxyde de carbone a été choisi pour des raisons pratiques évidentes.

Montage expérimental

La cellule critique a été élaborée par MM. Le Neindre, Tufeu et Garrabos. Elle est composée d'un corps en dural noirci par oxydation anodique. Les fenêtres en verre de borosilicate sont collées sur des supports en acier inoxydable pour éviter la biréfringence due à des déformations mécaniques.

Cette cellule a d'abord été dégazée puis rincée au CO_2 et enfin remplie à la concentration critique, déterminée d'après la littérature (31-32). Elle était thermostatée - 40°C $\pm$ 0,07 et la pression du gaz contrôlée grâce à une balance de pression.

La source de lumière était un laser à argon ionisé et la lumière diffusée était analysée par un triple monochromateur Coderg.

Résultats

L'analyse des spectres obtenus est compliquée par la superposition de plusieurs phénomènes. En plus de la diffusion dépolarisée due à l'anisotropie permanente des molécules, vont intervenir les phénomènes transitoires dus à l'action conjuguée de plusieurs molécules : interaction dipole-dipole induit, déformation des nuages électroniques par collision, etc.

Ces phénomènes existaient aussi dans les liquides, mais l'ordre de grandeur des temps caractéristiques y est très différent. Dans un gaz tel que le CO_2 ces temps se rapprochent. Les spectres obtenus ont la forme d'une lorentzienne pour les basses fréquences ($\nu \lesssim 50$ cm^{-1}), exponentielle au-delà. Il est cependant encore possible de définir une largeur pour la partie lorentzienne.

En raison de la forte augmentation de la pression au-dessus de T_c, les mesures n'ont pu être effectuées au-delà de $T - T_c = 10$ K. Du fait de la divergence de la compressibilité et de l'instabilité d'un fluide critique, il est impossible d'effectuer des mesures pour $T - T_c \leqslant 10^{-2}$K.

Les variations de la largeur de la partie centrale du spectre et de son intensité sont reportées dans la figure 8.

On peut constater qu'aucun comportement critique n'est visible. La gamme de température accessible ne permet pas de caractériser le comportement régulier de ces grandeurs.

Nous avons également étudié les raies Raman dépolarisées de ce gaz et trouvé leur largeur légèrement supérieure à celle des raies Rayleigh dépolarisées et également sans variation notable. Il faut toutefois prendre garde que des mécanismes Rayleigh-Raman font apparaitre une raie parasite exactement comme la diffusion multiple dans le cas de la raie Rayleigh.

IV. 4 - Conclusion

Nous avons étudié expérimentalement la diffusion dépolarisée dans trois systèmes fluides critiques et observé trois comportements différents : dans le nitrobenzène - n-hexane, la largeur de la raie et son intensité présentent des anomalies. Celle de la largeur de raie s'explique assez bien par l'intervention de la viscosité de cisaillement, bien que la fréquence considérée soit bien plus élevée que la fréquence de coupure prévue. Celle de l'intensité par contre, fait intervenir un nouvel exposant, voisin de 0,2 et son mécanisme reste pour l'instant inexpliqué. Dans le mélange de nitroéthane et isooctane la largeur de raie a un comportement régulier au point critique et suit la partie régulière de la viscosité de cisaillement. L'intensité par contre croît mais de façon linéaire avec la température, ce qui rend impossible l'attribution de ce comportement à une partie régulière ou à une partie critique. Enfin pour le dioxyde de carbone, pur, les deux grandeurs restent constantes au voisinage du point critique. Dans ce dernier cas cependant la gamme de température accessible était trop limitée pour permettre une caractérisation de la variation régulière.

La diffusion dépolarisée n'obéit donc pas à une universalité évidente, comme celle liée au paramètre d'ordre. Cependant on peut penser que la fréquence intervient, en "relaxant" les anomalies. On constate en effet que (voir tableau) ces anomalies sont d'autant moins ressenties que la fréquence caractéristique du phénomène est élevée, ce qui est attendu dans les phénomènes dynamiques du fait des couplages entre modes. Cependant elles restent présentes bien au-delà de ce que prévoit la théorie habituelle des modes couplés.

L'autre facteur pouvant expliquer cette diversité de comportements est d'origine microscopique. On peut penser en effet que la rotation

moléculaire est plus sensible que les modes hydrodynamiques aux détails du potentiel d'interaction des molécules, et en particulier à leur moment dipolaire. Il a été montré dans des systèmes non critiques que le moment dipolaire intervenait de façon significative dans les corrélations d'orientation. Or on constate bien que les anomalies sont d'autant plus importantes que le moment dipolaire est grand, dans les systèmes que nous avons étudiés.

Le choix entre ces deux explications n'est pas possible à l'heure actuelle. Il ne le deviendra qu'à la suite de l'obtention de nombreuses données expérimentales ou de travaux théoriques convaincants. Compte tenu de la difficulté des uns et des autres et du développement actuel des recherches en ce domaine, il semble que la question ne puisse être tranchée dans un proche avenir.

Système	Fréquence	Largeur de raie	Intensité
nitrobenzène +n-hexane	10 GHz	$\sim$ viscosité exp $\simeq 0.03 \pm 0.01$	divergence exp $\simeq 0.22 \pm 0.01$
nitrohetane + isooctane	100 GHz	$\sim$ partie régulière de la viscosité	anomalie linéaire
CO_2	750 GHz	pas de divergence	pas de divergence

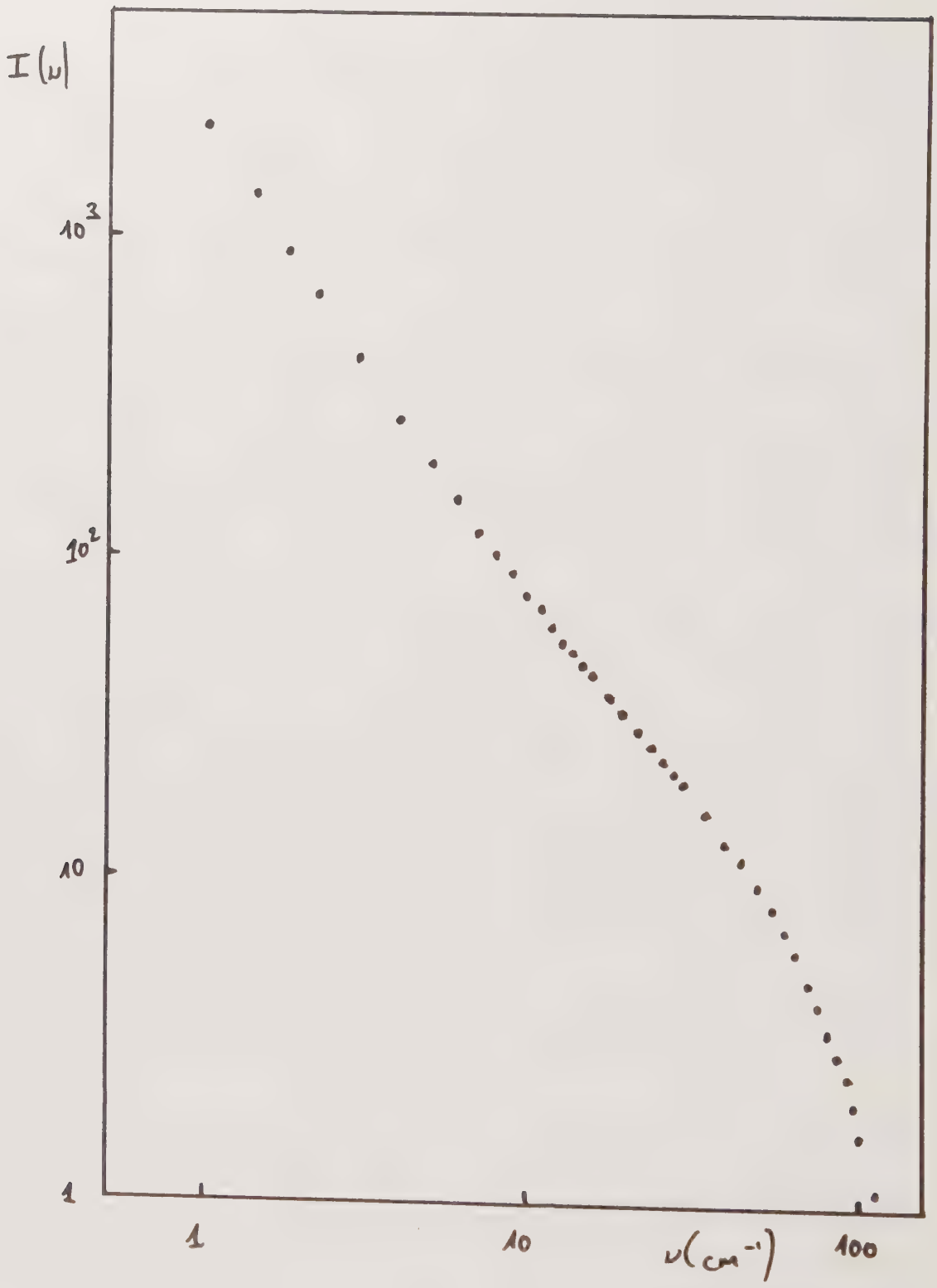

Figure a : Aile de la raie Rayleigh (l'intensité spectrale au centre est de 8.10^4).

Références

[a] H.B. LEVINE and G. BIRNBAUM
Phys. Rev. Lett. 20, 439 (1968)

[b] D. LITSTER and C.E. COOPER
in "Proceedings of the topical meeting in picosecond phenomena"
E. Ippen and C.V. Shank editors (North Falmouth, Mass. 1980).

PHYSICAL REVIEW A VOLUME 18, NUMBER 5 NOVEMBER 1978

Anomalies of linewidth and intensity in the reorientation spectra of a critical mixture

D. Beysens and G. Zalczer

Commissariat a l'Energie Atomique, Service de Physique du Solide et de Resonance Magnetique, Centre d'Etudes Nucleaires de Saclay, Boîte Postale No. 2, 91190 Gif-sur-Yvette, France

(Received 30 November 1977)

The critical behavior of the depolarized Rayleigh spectrum in the system nitrobenzene-*n*-hexane has not been previously accurately assessed because in usual Fabry-Pérot experiments the multiple-scattering contribution completely overwhelms the spectrum within a few degrees of the critical temperature T_c. By using a high-performance double-pass Fabry-Pérot interferometer, we have been able to obtain accurate measurements of both linewidth and intensity, from 50°C to temperatures as close as 0.026°C to T_c. Two lines due to nitrobenzene molecules in solution are visible. The first line (1) is intense and narrow, while the second line (2) is weak and broad. The spectral intensity of (2) is about 10^{-2} times that of (1). The linewidth of (1) is seen to behave as the inverse shear viscosity, with a critical divergence with exponent $Y \approx 0.04$. The intensity of (1) exhibits a power-law divergence with exponent $\Omega \approx 0.2$. These results are compared with data obtained in pure nitrobenzene and *n*-hexane, and in noncritical mixtures of nitrobenzene.

I. INTRODUCTION

Depolarized light scattering has previously been widely used to study short-range effects in liquids[1-4] and in liquid mixtures.[5,6] However, it is only recently that this technique has been applied to binary mixtures near their critical point by Fabelinskiĭ *et al.*,[7-10] followed by Aref'ev[11] and ourselves.[12]

The results obtained in this field strongly disagree with each other: Fabelinskiĭ *et al.* found a strong anomaly in the width of the reorientation lines, whereas other measurements are compatible with at most a weak anomaly related to the behavior of the shear viscosity near the transition point.[13] This discrepancy can be explained on purely experimental grounds,[14] as Fabelinskiĭ *et al.* did not take sufficient account of multiple scattering, which in most critical mixtures becomes very important near the transition temperature (T_c).

In any case, the behavior of the reorientation lines close to T_c cannot be inferred from the existing results. Moreover, the variation of the corresponding intensities is not well understood.[12] The present work consequently tries to answer the following questions: (i) Are there several depolarized lines? (ii) Is there a strong, weak, or in fact no anomaly at all in the behavior of both the linewidth and intensity of this (these) line(s)? (iii) More precisely, is the close relation generally observed between the shear viscosity and the reorientation linewidth still valid near T_c?

We chose for this study the binary mixture of nitrobenzene and *n* hexane. Indeed, the molecules of nitrobenzene are very anisotropic, giving rise to an intense depolarized scattering, and they have a high permanent dipole moment which is a possible source of strong orientation correlations (orientational local order). Furthermore, nitrobenzene has been widely studied by light scattering, both neat and in solution. *n* hexane is nonpolar, weakly anisotropic, and plays the role of an isotropic solvent. Moreover, this critical mixture has been studied in great detail near T_c by many authors.[15-20]

On the other hand, since the refractive indices of the components are very different, multiple scattering occurs near T_c, so that a high-performance setup is required. With a double-pass Fabry-Perot (FP) interferometer with variable thickness, which allows the multiple-scattering line to be separated from other depolarized contributions, we could obtain intensity and linewidth measurements in the frequency range 2–400 GHz and in the temperature range $T - T_c = 0.026–50$ °C. We show that there are two lines present, which is also the case in pure nitrobenzene.[21] The first line is a sharp and intense Lorentzian with a linewidth behaving roughly like the inverse viscosity, while the corresponding intensity approximately diverges with a power law (exponent $\Omega \approx 0.22$). The second line is nearly 15 times broader with an intensity seven times lower, thus the spectral intensity is so weak that it is no longer detectable when $T - T_c$ is smaller than a few degrees.

II. EXPERIMENTAL

The liquids used were of spectroscopic grade and filtered through 0.2-μm Teflon filters in order to remove dust particles. The binary mixture has

 © 1978 The American Physical Society

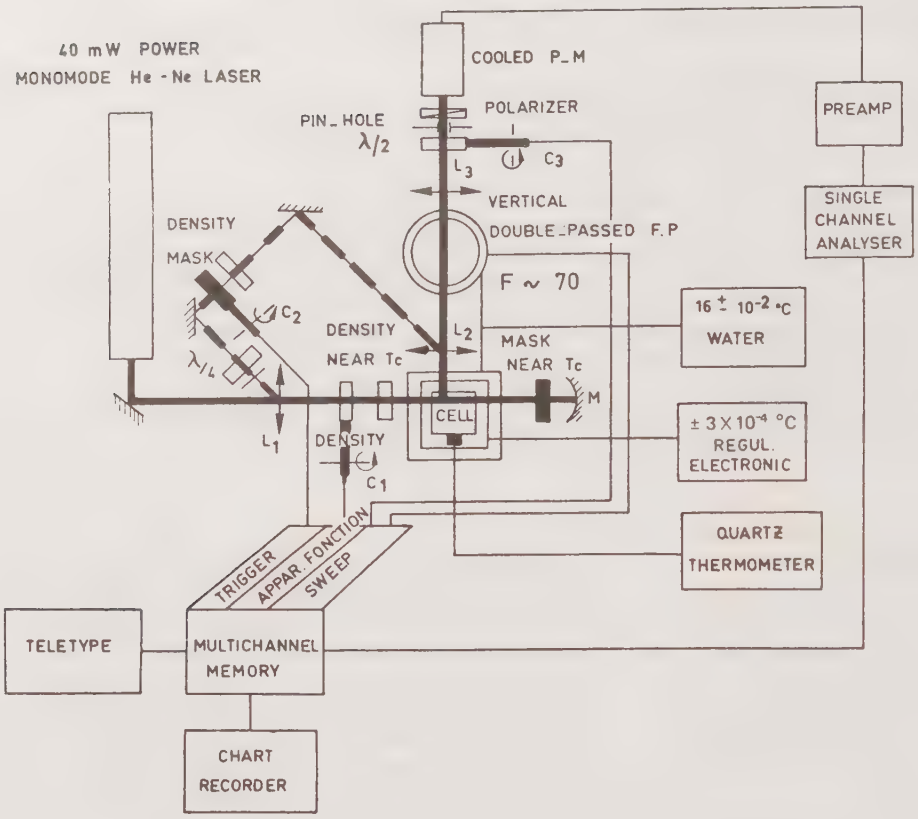

FIG. 1. General description of the setup. L_1, L_2, and L_3 are lenses; C_1, C_2, and C_3 are choppers.

a critical concentration of 0.51 wt% of nitrobenzene (0.42 mol%).[15] The experimental concentration was 0.509 ± .002, and the meniscus appeared in the middle of the cell, which is a good test for verifying the critical concentration. The temperature is measured by means of a quartz thermometer allowing relative measurements to be performed with a resolution of 10^{-4} °C. Precise absolute-temperature measurements were not required ($T_c \approx 20$ °C). The sample was located in a copper oven, itself inside a thermally regulated box. The temperature fluctuation was less than 5.10^{-4} over more than 24 h.

The detailed description of the spectrometer and its operation can be found in Ref. 22. The main features are (see Fig. 1): (i) A plane double-pass FP interferometer, working in a vertical position, which gives a passive stability allowing experiments to be continued over more than 24 h. The FP interferometer is placed in an air-tight box at a constant temperature and is piezoelectrically scanned. The spacing between the plates is variable and we used two different free spectral ranges (FSR), 78 GHz and 1087 GHz. The plates that we used give a contrast better than 10^6, a finesse of 70, and a transmission of 5% with a 2-cm useful aperture. (ii) A He-Ne laser ($\lambda = 6328$ Å) as incident light, monomode (40 mW power) when a 78 GHz FSR was used. (iii) Quasisimultaneous recording of both the apparatus function (AF) and the spectrum, by sequences of 9 spectra (9 × 2 sec) and one AF (2 sec) over a time period up to 48 h. The AF was provided by the very intense low-frequency (~1 KHz) polarized spectrum. (iv) Automatic compensation of frequency drifts of the laser line. (v) Photon counting (maximum rate 5×10^5 sec^{-1}).

A Glan prism selects the VH polarization when the spectrum is recorded. A half-wave plate rotates the polarization of the detected light by $\frac{1}{2}\pi$ when the AF is recorded.

In order to minimize the effects of both turbidity[23] and multiple scattering,[18,19] the scattering volume was set close to the entrance and exit windows. Near T_c, we had to attenuate the incident beam strongly (up to 1.3 mW) in order, first, to avoid extra heating of the sample, and second, to maintain the scattered light (dominated by the multiple scattering) below the saturation level of the counting chain. Therefore, close to T_c recording times longer than 24 h are necessary in order to obtain a reasonable signal-to-noise ratio.

A program of statistical refining, due to Tournarie,[24] determines the best fit of the experimental spectrum. The "quality" of the fit is measured by a coefficient Q, which gives the contribution of the statistical error to the total deviation: A purely random deviation would give $Q = 1$, whereas a systematic distortion drastically lowers Q.

Figure 2 shows a spectrum with a FSR of 1087 GHz. A weak, broad line can be detected, as in pure nitrobenzene,[21] in addition to a central peak which contains at least a narrow line plus an AF. The fitting program failed when the convolution product of the AF by only one Lorentzian line plus a Dirac function, due to the quasielastic scattering (both polarized scattering and multiple scattering), was considered. So we fitted the experimental spectra to an AF plus two Lorentzian lines, representing the convolution of the AF by a true spectrum composed of a Dirac function and two Lorentzian lines. Of course, correction of half-widths and overlapping from neighboring interferometer orders were taken into account. We tried also an exponential shape for the broad line, which gave a fit as good as that previously obtained, with a characteristic frequency of the same order of magnitude. It is worth noticing that a simple fit of only the wings of the spectrum to one single line gives quite different results, showing that the wings of the narrow line cannot be neglected.

Figure 3 shows two spectra at two temperatures with a FSR of 78 GHz, i.e., much smaller than the former FSR. These spectra have been successfully analyzed (Fig. 4) by considering them as the convolution product of the AF by a true spectrum composed of a flat background (nonresolved lines), a Lorentzian line (anisotropy line), and a Dirac function accounting for the quasielastic scattering, as in pure nitrobenzene.

The linewidths obtained in the computing proprograms are expressed in units of FSR, which itself can be measured with an accuracy of about 1%. The final uncertainty is near 5%.

The numbers I_1^*, I_2^*, D^*, and P^* given by the computer for the intensities of, respectively, the narrow and wide Lorentzian lines, the quasielastic depolarized scattering, and the polarized scattering, are meaningless unless corrected by many factors, such as laser intensity, turbidity, FP interferometer transmission, aperture angles, etc. However, the ratios of these numbers, for a given recording, are automatically corrected for all these factors; thus the variations of the true intensities I_1, I_2, D, and P can be deduced from the variations of one of them. Obviously, the polarized scattering intensity P is the best known,[19,20]

$$P(T - T_c) \propto \frac{T}{T_c} \frac{(T - T_c)^{-1.22}}{1 + 0.0286(T - T_c)^{-1.22}}.$$

So we get $I_{1,2} = (I_{1,2}^*/P^*)P$. This method has been used for the set of experiments α in Table I. Typical uncertainties are 8%.

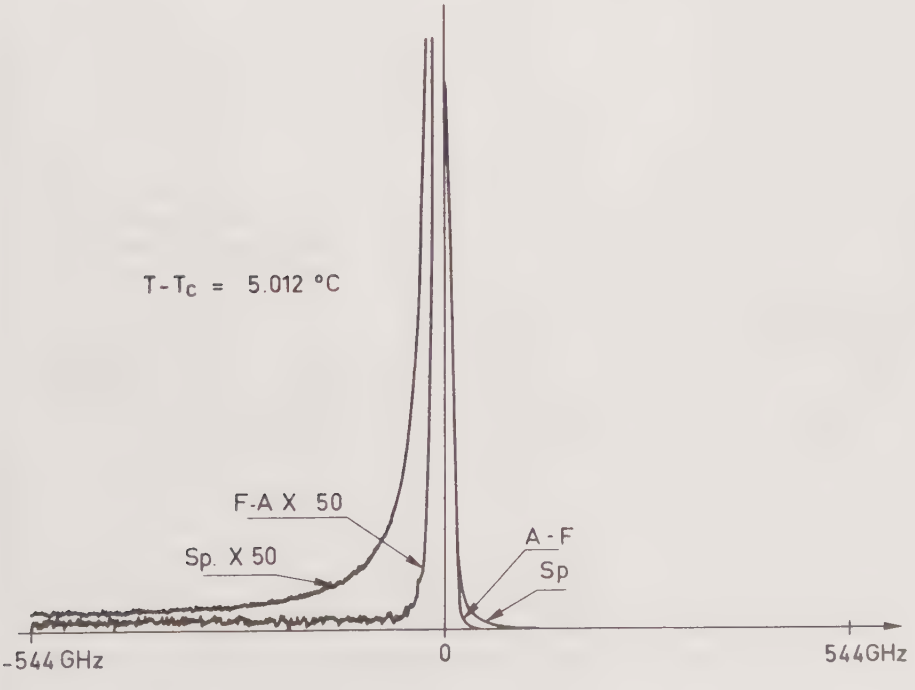

FIG. 2. Total spectrum with a FSR of 1087 GHz at two different scales showing (right) the narrow spectrum plus a strong AF (quasielastic scattering), and (left) the broad spectrum.

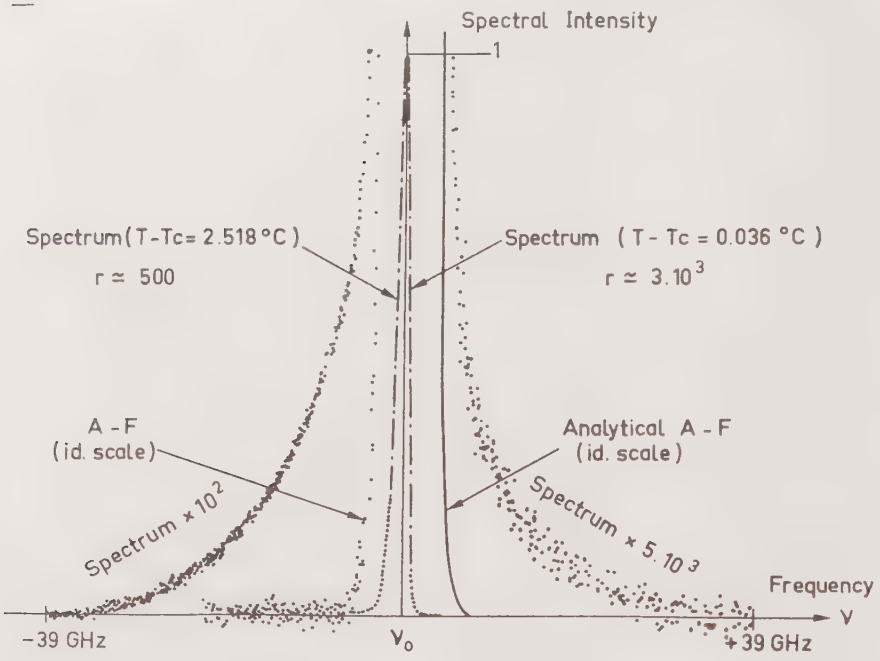

FIG. 3. Typical narrow spectra with the same reduced scale. The AF are shown with the same spectral intensity at frequency ν_0. Both experimental and analytical AF are shown. r is the ratio of spectral intensities (peak/line) at frequency ν_0.

In set β of Table I, P^* could not be accurately measured, so we calibrated the intensity by the depolarized quasielastic scattering D^*. A difficulty with this method is that the spatial variation around the exciting beam is not the same as the polarized or depolarized single scattering.[18] Nevertheless, since the set β was performed in the same experimental conditions as the set α, we

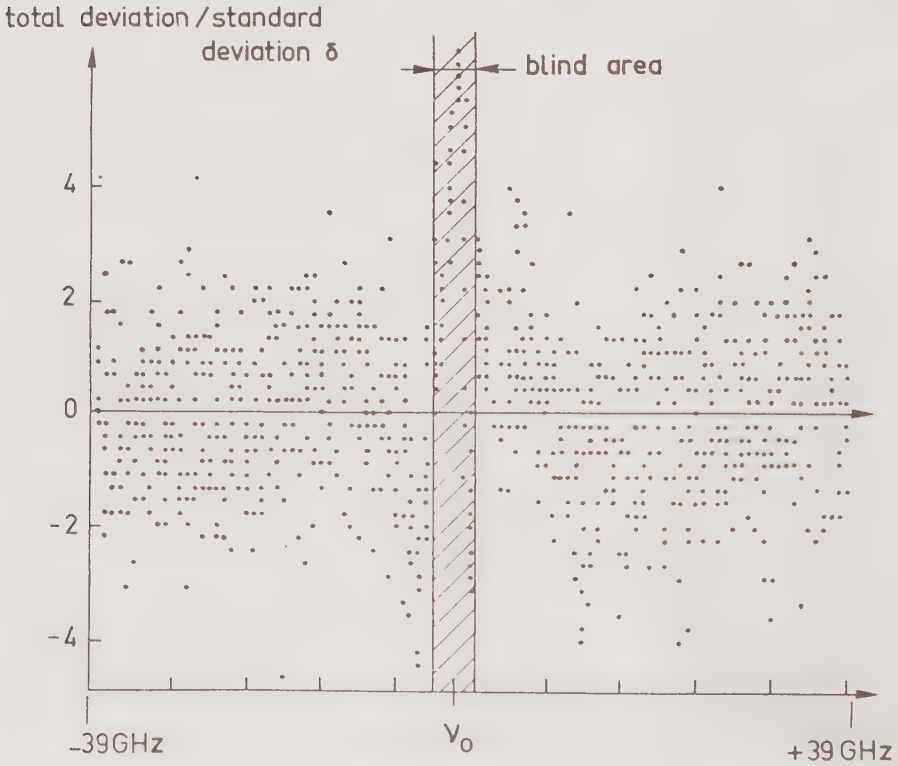

FIG. 4. Reduced deviation vs frequency for a narrow spectrum recorded at $T-T_c = 0.0290$ °C with a ratio of spectral intensities $r \simeq 5000$. The quality coefficient is $Q = 0.54$, due to the distortions in the "blind" region where the peak is situated.

can infer from set α the experimental ratio

$$D^*/P^* = a + bP(T - T_c),$$

$$a = 19.1 \pm 0.5, \quad b = (9.4 \pm 1.4) \times 10^{-2}.$$

The first term (a) is due to polarizer defects, the second (b) arises from double scattering and depends on the actual experimental geometry.

From the computed intensity I^* it is then straightforward to obtain

$$I(T - T_c) = \frac{I^*}{D^*}\frac{D^*}{P^*}P(T - T_c)$$

$$= \frac{I^*}{D^*}[aP(T - T_c) + bP^2(T - T_c)].$$

The results for set β can be found in Table I. Typical uncertainties are 12%.

We also give in Table I early (graphical) published experiments[12] (set γ) where the intensity was referred to the incident power. Both FP

TABLE I. Measurements for sets α, β, and γ.

Set α			Set β		
$(T/T_c) - 1$	$\tau_1 (\times 10^{-12} s)$	$I_1 \pm 10\%$	$(T/T_c) - 1$	$\tau_1 (\times 10^{-12} s)$	$I_1 \pm 12\%$
1.31×10^{-1}	9.87 ± 0.26	4.67	7.66×10^{-2}	11.9 ± 1	6.6
1.211×10^{-1}	10.45 ± 0.32	4.90	7.66×10^{-2}	12.7 ± 1	
1.03×10^{-1}	9.97 ± 1.4	5.49	5.1×10^{-2}	14.8 ± 1.3	7.91
8.57×10^{-2}	10.82 ± 0.32	6.38	3.5×10^{-2}	15.3 ± 1.1	9.60
6.04×10^{-2}	11.9 ± 2.1	7.19	2.7×10^{-2}	14.6 ± 1.1	7.01
5.05×10^{-2}	15.2 ± 0.45	7.25	2.32×10^{-2}	15.3 ± 1.1	12.6
3.72×10^{-2}	12.4 ± 0.32	6.40	1.63×10^{-2}	17.4 ± 1.3	9.95
3.36×10^{-2}	12.6 ± 0.53	8.23	1.50×10^{-2}	15.7 ± 1.1	9.24
1.99×10^{-2}	14.2 ± 2.75	9.01	1.50×10^{-2}	16.3 ± 1.3	
1.54×10^{-2}	15.6 ± 0.48	7.04	1.09×10^{-2}	13.5 ± 4.5	11.7
9.54×10^{-3}	15.2 ± 0.45	9.54	8.97×10^{-3}	16.5 ± 1.3	13.9
8.594×10^{-3}	15.6 ± 0.32	10.8	6.18×10^{-3}	16.1 ± 1.3	10.9
5.78×10^{-3}	16.9 ± 0.32	11.8	3.77×10^{-3}	16.1 ± 2.4	13.2
5.017×10^{-3}	16.07 ± 0.32	14.5	3.47×10^{-3}	15.7 ± 1.1	11.3
3.778×10^{-3}	16.07 ± 0.32	13.7	3.2×10^{-3}	15.0 ± 2.4	14.0
2.43×10^{-3}	17.0 ± 3.2	13.3	2.9×10^{-3}	16.4 ± 1.1	14.1
1.66×10^{-3}	17.4 ± 0.48	7.79	2.58×10^{-3}	16.3 ± 1.1	15.5
1.177×10^{-3}	16.07 ± 0.53	13.6	2.3×10^{-3}	16.5 ± 1.1	17.5
8.055×10^{-4}	14.1 ± 0.48	13.7	1.7×10^{-3}	16.8 ± 1.1	18.5
4.73×10^{-4}	16.87 ± 0.37	30.8	1.7×10^{-3}	16.9 ± 1.1	16.1
4.266×10^{-4}	18.46 ± 0.58	18.5	1.37×10^{-3}	16.6 ± 1.1	20.5
3.53×10^{-4}	19.0 ± 0.69	15.4	1.0×10^{-3}	18.0 ± 1.1	25
2.96×10^{-4}	17.7 ± 0.42	22.5	9.3×10^{-4}	19.1 ± 1.5	20.9
2.64×10^{-4}	18.7 ± 1	25.1	8.43×10^{-4}	18.7 ± 6.3	24.8
2.59×10^{-4}	20.1 ± 0.70	...	5.7×10^{-4}	18.0 ± 1.5	26.6
2.33×10^{-4}	17.88 ± 0.37	24.7	5.0×10^{-4}	20.0 ± 1.6	26.0
1.79×10^{-4}	20.9 ± 0.50	19.1	2.7×10^{-4}	18.0 ± 1.3	29.7
1.706×10^{-4}	15.7 ± 0.53	26.6			
1.481×10^{-4}	13.05 ± 2.6	27.8			
1.365×10^{-4}	20.9 ± 1.3	26.1			
1.27×10^{-4}	27.00 ± 1.6	21.3			
1.229×10^{-4}	18.3 ± 0.58	27.0			
9.9×10^{-5}	17.2 ± 0.58	22.9			
8.87×10^{-5}	20.90 ± 4.1	27.4			

TABLE I. (Continued)

Set γ					
$(T/T_c)-1$	$\tau_1(10^{-12}$ sec) ± 10%	I_1 ± 12%	$(T/T_c)-1$	$\tau_1(10^{-12}$ sec) ± 10%	I_1 ± 12%
1.73×10^{-1}	9.92	2.90	2.9×10^{-2}	16.4	4.25
1.65×10^{-1}	8.86	2.85	2.76×10^{-2}	13.6	
1.61×10^{-1}	8.86	1.54	2.72×10^{-2}	15.4	
1.54×10^{-1}	9.92	2.35	2.70×10^{-2}	14.0	
1.46×10^{-1}	10.0	2.45	2.55×10^{-2}	15.6	4.35
1.38×10^{-1}	9.8	2.70	2.50×10^{-2}	15.3	5.20
1.35×10^{-1}	8.9	3.70	2.13×10^{-2}	16.4	
1.31×10^{-1}	10.3	2.55	2.04×10^{-2}	14.8	
1.28×10^{-1}	10.0	3.30	2.00×10^{-2}	13.5	
1.23×10^{-1}	10.8	4.05	2.00×10^{-2}	14.7	4.75
1.20×10^{-1}	9.9	2.85	1.98×10^{-2}	15.2	5.00
1.18×10^{-1}	11.0		1.90×10^{-2}	15.2	4.75
1.18×10^{-1}	10.0	3.85	1.90×10^{-2}	16.8	4.80
1.05×10^{-1}	11.3	3.05	1.60×10^{-2}	16.8	
1.01×10^{-1}	10.6	4.05	1.40×10^{-2}	16.2	4.80
9.41×10^{-2}	11.5	3.25	1.40×10^{-2}	19.5	4.80
8.82×10^{-2}	11.7	3.85	1.38×10^{-2}	18.5	
7.86×10^{-2}	12.7	3.60	1.14×10^{-2}	16.9	
6.73×10^{-2}	13.3	3.95	1.13×10^{-2}	19.3	5.40
6.25×10^{-2}	13.7	3.50	1.10×10^{-2}	19.7	5.55
5.70×10^{-2}	12.4	5.10	1.04×10^{-2}	17.7	5.15
5.06×10^{-2}	15.2	4.20	9.89×10^{-3}	a	5.20
4.4×10^{-2}	12.9	4.40	8.19×10^{-3}	···	4.95
4.23×10^{-2}	13.5	4.95	7.51×10^{-3}	···	5.20
4.13×10^{-2}	12.9	3.9	6.48×10^{-3}	···	5.10
4.02×10^{-2}	15.3		6.48×10^{-3}	···	5.40
3.98×10^{-2}	12.8		5.80×10^{-3}	···	5.00
3.85×10^{-2}	13.5		4.78×10^{-3}	···	5.60
3.84×10^{-2}	14.2		3.75×10^{-3}	···	6.00
3.83×10^{-2}	14.2		3.75×10^{-3}	···	5.10
3.49×10^{-2}	15.6	4.60	2.73×10^{-3}	···	4.60
3.41×10^{-2}	13.8	4.05			
3.37×10^{-2}	14.0				
3.36×10^{-2}	16.6				
3.36×10^{-2}	16.6				
3.24×10^{-2}	14.0				
3.17×10^{-2}	13.1				
3.05×10^{-2}	14.9				

[a] τ_1 accuracy is much worse than the I_1 accuracy in the range $T-T_c=1-3\,^\circ$C.

interferometer transmission and turbidity were nearly constant in this experiment (single-pass FP interferometer, $T-T_c>1\,^\circ$C).

III. EXPERIMENTAL RESULTS

A. Pure components

n hexane is a quasi-isotropic solvent. A depolarized spectrum recorded with a FSR of 1087 GHz shows a line of about 20 GHz, which is probably the Rayleigh-Brillouin components broadened by the aperture angle: the ratio of the depolarized intensity to the polarized intensity is of the order of magnitude of 10^{-3}, i.e., the polarization ratio.

Nitrobenzene exhibits two lines of half-width (at $T=20\,^\circ$C) $\Gamma_1=5$, 50 GHz[2] and $\Gamma_2\simeq300$ GHz.[21] The first line (1) is a sharp and intense Lorent-

zian which shows when resolved a structure due to a coupling with shear waves.[25] This phenomenon, the unusual weak value of the linewidth, and the high corresponding intensity, suggest a strong local-orientation order. The temperature variation of the intensity[2] is roughly linear but much more important than the density variation. The second line (2) is weak and broad: the ratio of intensities $I(2)/I(1) \approx \frac{1}{20}$,[21] so that the ratio of spectral intensities is weaker by about $\sim 10^{-3}$. This fact explains the polemic about its existence, since a contrast of much more than 10^3 is needed, which is rather difficult to obtain with a single-pass FP interferometer. The first line has a temperature dependence like the inverse viscosity following an Arrhenius law with activation energy of 2.4×10^{-13} erg.[2,4] The temperature dependence of the second line has not been investigated.

We neglect, of course, the influence of broader lines related to anisotropy-induced effects (linewidth $\sim 10^3$ GHz),[26] inertial phenomena, etc. These lines cannot be seen in the FSR of 78 and 1087 GHz. The following discussion will therefore refer to the two lines of nitrobenzene in solution with *n* hexane. Nevertheless, before considering the critical mixture, let us recall some results concerning noncritical mixtures of nitrobenzene in isotropic or quasi-isotropic solvents.

B. Noncritical mixtures of nitrobenzene

We will be chiefly concerned with spectrum (1). A study of nitrobenzene in carefully chosen solvents enables the variation of Γ_1 or $\tau_1 = (1/2\pi\Gamma_1)$ with the shear viscosity (η_s) and/or the volume percent (x) of nitrobenzene to be examined. The following empirical formula was found by Alms *et al.*,[6] where u and τ_0 are empirical functions of x

$$\tau_1(x, \eta) = u(x)\eta + \tau_0(x) . \qquad (1)$$

The temperature dependence was not investigated ($T \simeq 24\,^\circ\mathrm{C}$). The solvent seems to have no action on the reorientation time, the meaningful parameters being the concentration and the viscosity. Nevertheless, the signification of $\tau_0(x)$ is not clear; it could be related to inertial effects due to dilution, i.e., an influence of the molecules of the solvents.

The intensity is strongly correlated to the dilution following the variation with N, the number of molecules per unit volume,

$$I_1(N) \propto N(1 + fN) ,$$

where f is a parameter related to the strength of local static orientation correlations. Its value is close to 1; this means roughly that in neat nitrobenzene, several molecules cooperatively scatter. And for the concentration $x = x_c$, one finds: $I_1(x_c)/I_1(1) \approx 0.22$ following Refs. 5 and 6.

The variations of the time τ_1 and of the corresponding intensity I_1 seem to indicate the presence of a strong local-orientational order, which decreases with increasing dilution, to reach a "monomolecular" scattering at infinite dilution. To our knowledge, the behavior of both the reorientation time τ_2 and the intensity I_2 have not been previously investigated. We will now consider the behavior of these two lines in a critical mixture.

C. Critical mixture nitrobenzene *n* hexane

1. Broad line

As we have already pointed out, the analysis of this line, with weak spectral intensity, in the presence of strong quasielastic scattering and a narrow depolarized spectrum, with the presence of non-negligible overlapping from neighboring interferometer orders, is not easy. So we cannot expect very accurate results, and did not investigate this line extensively. Four spectra, at $T - T_c = 0.1$, 1, 5, and 12 °C, were recorded. Due to the drastic increase of the quasielastic scattering near T_c, at $T - T_c = 0.1\,^\circ\mathrm{C}$ the broad line is no longer visible. In the range 12–1 °C, the linewidth is nearly constant: $\Gamma_2 \approx 145$ GHz. We will further see that this linewidth corresponds at $T - T_c = 1\,^\circ\mathrm{C}$ to the ratio between the broad and narrow linewidths

$$\Gamma_2/\Gamma_1 \approx 15 .$$

The ratio of the intensities is nearly

$$I_2/I_1 \approx 0.15 .$$

So, the spectral intensity of the broad line is therefore about 1% of the narrow line. These results ensure that the broad line appears as a weak and flat background when a FSR of 78 GHz is used.

2. Narrow line: Study of the linewidth

The results for three sets of experiments can be found in Table I: (i) set α: $T - T_c = 0.026$–40 °C; (ii) set β: $T - T_c = 0.1$–25 °C. These data concern preliminary measurements performed with a nonmonomode laser. (iii) set γ: $T - T_c = 3$–50 °C. These measurements (in the range 1–50 °C) have been already published in Figs. 3 and 4 of Ref. 12. They were performed with a single-pass FP interferometer and a nonmonomode laser. Following a previous analysis,[14] we suppress the range 1–3 °C where the uncertainties

were much bigger.

We tried first to compare our data to Eq. (1), i.e., at $T = 24\,^{\circ}C$, and for the viscosity and concentration of the critical mixture:

$$x = x_c = 0.42 \text{ mol \%}$$

$$u(x_c) \simeq 8.75\ 10^{-12} \text{ sec } cP_0^{-1} \quad \text{(Ref. 6)},$$

$$\tau_0(x_c) \simeq 7.5\ 10^{-12} \text{ sec} \quad \text{(Ref. 6)},$$

$$\eta_s^c(24\,^{\circ}C) \simeq 0.585\ cP_0 \quad \text{(Ref. 13)}.$$

Equation (1) gives a reorientation time of

$$\tau_1(x = x_c,\ \eta_s = \eta_s^c,\ T = 24\,^{\circ}C) \simeq 12.6 \times 10^{-12} \text{ sec},$$

whereas our measurements give a mean value of about

$$\tau_1(\text{experimental}) \simeq 16.2 \times 10^{-12} \text{ sec}.$$

The agreement is therefore reasonable, and one could expect a weak influence from the critical properties on the reorientation time.

Second, we tried to fit Eq. (1) to our linewidth data, η_s being considered as a variable (function of $T - T_c$), and u and τ_0 being the adjustable parameters, called u^* and τ_0^*. The values of η_s are inferred from shear viscosity measurements of Ref. 13 performed close to T_c and which exhibit the usual critical anomaly, i.e., an increase of about 20% near T_c

$$\eta_s^c = \eta_0 \exp\left(\frac{E}{kT}\right)\left(\frac{T - T_c}{T_c}\right)^{-Y}, \qquad (2)$$

where $\eta_0 = (143 \pm 5) \times 10^{-6} P_0$, and $E = (1.450 \pm 0.016) \times 10^{-13}$ erg; $Y = 0.0430 \pm 3.10^{-4}$ is a critical exponent. k is the Boltzmann constant.

The results of the fit are shown in Table II, where we can see that the statistical quality is quite good, justifying Eq. (1). Nevertheless, τ_0^* is found to be negligible small, whereas u^* is significantly bigger than $u(x_c)$ [indeed, at $24\,^{\circ}C$, $u(x_c)\eta_s^c + \tau_0(x_c) \approx u^* \eta_s^c$]. Therefore, either both $u(x_c)$ and $\tau_0(x_c)$ have a strong temperature dependence, at least of the same order of magnitude as the viscosity and there is no meaningful information to be drawn from this comparison, or τ_0 is a function of the solvent, and its influence

TABLE II. Fit to $\tau_1 = u^* \eta_s^o + \tau_O^*$

Set	u^* (10^{-12} sec.c Po^{-1})	$\pm\Delta u^*$	τ_O^* (10^{-12} sec)	$\pm\Delta\tau_0^*$	Q
α	22.6	1.7	1.7	1	0.99
β	20.0	4	4.6	2.4	0.77
γ	27.8	0.4	0.01	0.05	0.98
$\alpha+\beta+\gamma$	21.9	0.7	2.5	0.5	0.83

TABLE III.

Set	Fit	τ_1^o (10^{-12} sec)	$\tau_1^o \exp(E_1^o/1+\epsilon)\epsilon^{-Y_O}$ (Ref. a) $\pm\Delta\tau$ (10^{-12} sec)	E_1^o	$\pm\Delta E_1^o$	Y_O	$\pm\Delta Y_0$	Q	δ (Ref. b)	τ_1^1 (10^{-12} sec)	$\tau_1^1(1+\epsilon)^{-1} \exp(E_1^1/1+\epsilon)\epsilon^{-Y_1}$ $\pm\Delta\tau_1^1$ (10^{-12} sec)	E_1^1	$\pm\Delta E_1^1$	Y_1	$\pm\Delta Y_1$	Q	δ (Ref. b)
α	Y free	0.50	0.3	3.3	0.7	0.036	0.01	0.99	0.9	1.5	1	2.2	0.7	0.036	0.01	0.99	0.9
	$Y = 0$	0.10	0.05	5.2	0.5	0	0	0.81	1	0.27	0.14	4.1	0.5	0	0	0.81	1
β	Y free	0.77	0.8	3.0	1	0.025	0.015	0.64	1	2.1	2	1.9	1	0.025	0.012	0.64	1
	$Y = 0$	0.17	0.09	4.6	0.6	0	0	0.52	1	0.46	0.2	3.6	0.5	0	0	0.52	1
γ	Y free	1.2	1	2	1	0.1	0.06	0.80	0.8	3.7	0.4	0.5	1	0.15	0.05	0.80	0.8
	$Y = 0$	0.15	0.05	4.7	0.3	0	0	0.96	1	0.44	0.1	3.7	0.3	0	0	0.95	1
$\alpha+\beta+\gamma$	Y free	0.41	0.12	3.56	0.3	0.030	0.005	0.94	0.9	0.96	0.1	2.7	0.1	0.026	0.004	0.94	0.9
	$Y = 0$	0.12	0.03	4.99	0.25	0	0	0.83	1	0.34	0.08	3.9	0.25	0	0	0.82	1

[a] $\epsilon = (T - T_c)/T_c$.

[b] δ: reduced standard deviation (for each set).

would be negligible in this particular mixture.

The reorientation time seems to behave as the inverse viscosity with its critical behavior. A more sensitive test is to fit the data to the same critical variation (2) found for the viscosity

$$\tau_1 = \tau_1^\circ \exp\left(\frac{E_1^0}{kT}\right)\left(\frac{T-T_c}{T_c}\right)^{-Y_1^0}. \qquad (3)$$

τ_1^0, E_1^0, and Y_1^0 are adjustable parameters. In order to assess the point that the very weak exponent Y_1^0 is well determined, we fit also the data with $Y_1^0 = 0$.

Table III shows the results. One can notice that (i) the quality Q of the fit increases when $Y_1^0 \neq 0$, (ii) the reduced standard deviation δ decreases when $Y_1^0 \neq 0$, (iii) the activation energy E_1^0 is quite different from the shear viscosity activation energy when $Y_1^0 = 0$ is assumed.

It is obvious that the best measurement of Y is performed in set α where the data are closest to T_c. The corresponding parameters of both the shear viscosity and the reorientation time are nearly identical. We have for set α:

$$E_1^0/E = 0.9 \pm 0.2\,, \quad Y_1^0/Y_1 = 0.84 \pm 0.3\,,$$

and for sets $\alpha+\beta+\gamma$:

$$E_1^0/E = 1.00 \pm 0.08\,, \quad Y_1^0/Y = 0.7 \pm 0.2\,.$$

In Fig. 5 are shown sets α, β, and γ with these last values.

It is also convenient to compare the reorientation time with the viscosity divided by T, following an hydrodynamic model of rotation (Brownian model of rotation). The following formula has been tested

$$\tau_1 = \tau_1^1 \frac{1}{T} \exp\left(\frac{E_1^1}{kT}\right)\left(\frac{T-T_c}{T_c}\right)^{-Y_1^1}. \qquad (4)$$

The results, shown in Table III, are qualitatively the same as for the variation (3), with the same standard deviation and quality of fits. In particular, the values of the exponent Y are the same: $Y_1^1 = Y_1^0$. The variation in T^{-1} does not influence obviously the behavior near T_c, but modifies the activation energy. We have for set α:

$$\frac{E_1^1}{E} = 0.6 \pm 0.3\,, \quad \frac{Y_1^1}{Y} = \frac{Y_1^0}{Y} = 0.84 \pm 0.3\,,$$

and for set $\alpha+\beta+\gamma$:

$$\frac{E_1^1}{E} = 0.75 \pm 0.05\,, \quad \frac{Y_1^1}{Y} = \frac{Y_1^0}{Y} = 0.7 \pm 0.2\,.$$

The conclusion to be drawn following the study of this reorientation time is therefore that there is a weak anomaly of the $T - T_c$ behavior, this anomaly being close to the anomaly of viscosity. The variation seems to be described best by Eq. (3).

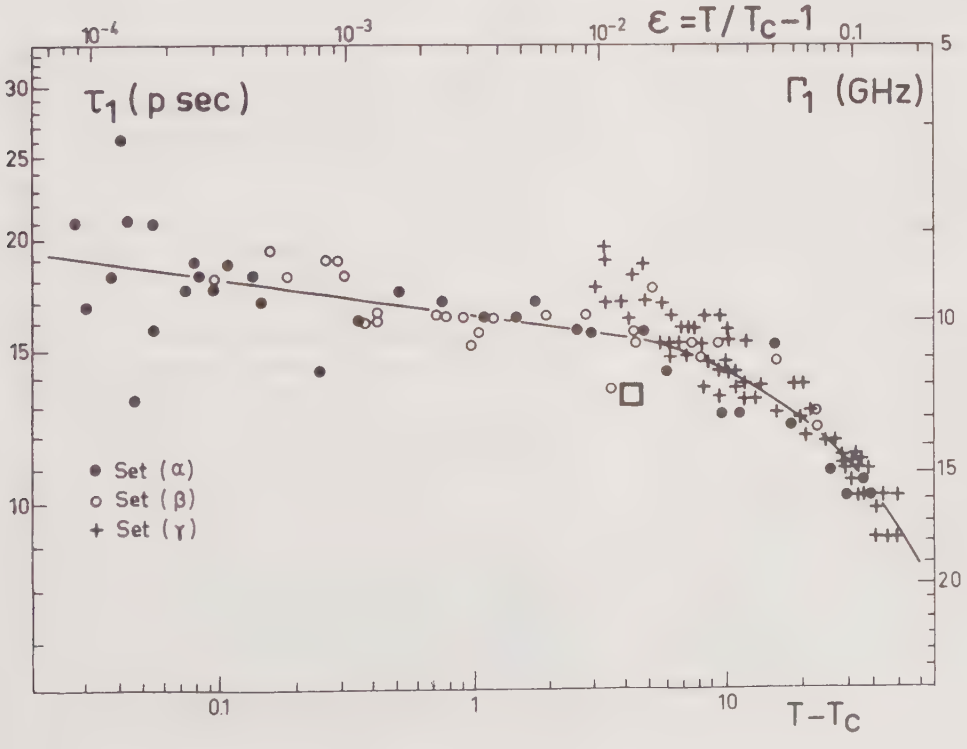

FIG. 5. Variation of linewidth τ_1 vs $T - T_c$. The line is the fit to the expression: $\tau_1 = \tau_1^0 \exp(E_1^0/kT)\cdot[(T-T_c)/T_c]^{-Y_1^0}$. The square is the value inferred from measurements in a non critical mixture (see text).

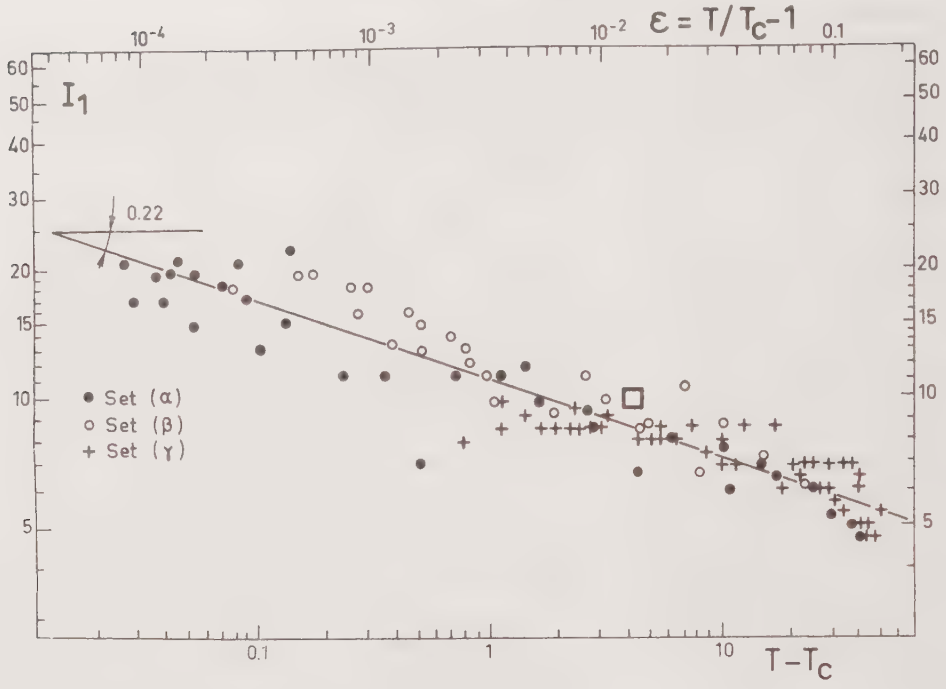

FIG. 6. Variation of intensity I_1 vs $T - T_c$. The line corresponds to the variation: $I_1 \propto (T - T_c)^{-\Omega}$. The square is the value obtained in noncritical mixtures (see text).

3. Narrow line: Study of the intensity

As we have previously pointed out, the variation of the integral I_1 of the narrow line (1) has been obtained by three different methods, according to the set of experimental results. They are compatible to within a multiplying constant with a power-law variation with an exponent $\Omega \simeq 0.22$ as shown in Fig. 6. More precisely, we performed a fit following the formula

$$I_1 = A_{\alpha,\beta,\gamma}(T - T_c)^{-\Omega} .$$

The results are shown in Table IV, the value of Ω ranging from 0.18 to 0.26 according to the set of experiments. The value

$$\Omega = 0.222 \pm 0.008$$

is obtained when fitting all sets.

Measurements of set γ have been referred to the intensity of line (1) in pure nitrobenzene, at the temperature of 24 °C[12]

TABLE IV. Fit to $I_1 = X_1 \epsilon^{-\Omega}$. $\epsilon = (T - T_c)/T_c$.

Set		X_1	$\pm\Delta X_1$	Ω	$\pm\Delta\Omega$	Q
α		0.34	0.03	0.222	0.013	0.53
β		0.34	0.035	0.26	0.02	0.75
γ		2.2	0.15	0.18	0.02	0.70
$\alpha+\beta+\gamma$	α, β	0.36	0.02	0.222	0.008	0.85
	γ	2.0	0.7			

$$I_1(x = x_c, \text{critical})/I_1(x = 1) \approx 0.18 , \quad T - T_c = 4\,^{\circ}\text{C} .$$

When comparing with noncritical mixtures of nitrobenzene, but at the same concentration[5,6] we find

$$I_1(x = x_c, \text{noncritical})/I_1(x = 1) \approx 0.22 \quad T = 24\,^{\circ}\text{C} .$$

Hence the ratio $I_1(x = x_c, \text{critical})/I_1(x = x_c, \text{noncritical})$ can be evaluated. Its value $\simeq 0.82$ is nearly equal to one. Therefore the anomaly of the intensity is seen to be, as the anomaly of the linewidth, a weak anomaly in absolute size.

IV. DISCUSSION

A. Origin of the two lines

Several models are usually considered to explain a depolarized spectrum built up to two Lorentzian lines, one sharp and narrow, the other broad and weak:

(i) The "monomolecular model," which attributes these two lines to two rotational motions around different axes of the single molecule.[27,28] In noncritical mixtures, this model is shown not to be valid by the fact that the intensity of the narrow line does not vary linearly with the concentration of the anisotropic liquid, suggesting some orientation correlations.

(ii) The correlations have been taken into account by Keyes and Kivelson,[29] who obtained for

the narrow line

$$I_1 \sim N(1+fN), \quad \tau_1 = [(1+fN)/(1+gN)]\tau_s,$$

where f and g are the static and dynamic correlation coefficients, N is the number of anisotropic molecules per unit volume, and τ_s is the reorientation time of a single molecule. In this model, however, only the case of a cylindrical symmetric molecule is considered, and the question concerning the origin of the second line is left open. Alms *et al.*[6] used this model and calculated τ_s with the monomolecular model. They also suggested the presence of a second line due to reorientation around another axis of the same anisotropic molecule.

(iii) An alternative model has been elaborated by Quentrec[30,31] that accounts for the wide line by introducing a second local-order tensor, related to the short-range position correlations, while the treatment of the narrow line is very similar to that of Keyes and Kivelson.

A full discussion of this point would need a careful comparison of linewidths and intensities in different experimental cases and will be the subject of a future paper.[21] In this paper, we would rather focus our attention on the behavior of the narrow line at the critical concentration. We only note that all these models lead to a Lorentzian shape for the narrow line, i.e., refer to a diffusive process for the reorientation.

B. Anomaly of the intensity of the narrow line

In the monomolecular model at constant concentration, the intensity can vary only through the density or the local electric field. Now the density does not vary more than 5% throughout the considered temperature range. Even in pure nitrobenzene, the intensity varies much faster than the density at these temperatures but it varies roughly linearly with the temperature,[2,25] while we have here a power-law behavior. Refractive-index measurements near the critical point of a binary mixture[32,33] show that the combined effect of both factors remains very small. Therefore, this model is not consistent with the observed anomaly.

The correlation model leads to the following variation

$$I = I_0 N(1+fN),$$

where I_0 and f can vary with the temperature. Since the factor fN is expected to be of order of unity from noncritical mixtures data,[6] a power-law behavior of f should not lead to a power-law behavior of I. However, experimental uncertainties are large enough to prevent us from a clear-cut conclusion.

C. Anomaly of the width of the narrow line

The linewidth has been seen to exhibit the same behavior as the inverse macroscopic viscosity. This is compatible with the monomolecular theory in which each molecule rotates in a continuous medium, and the diffusion coefficient(s) is (are) related to the shear viscosity through the boundary conditions at the surface of the molecule (slip, stick, or other[34,35]). Although this model cannot explain the intensity variation, we can consider it as valuable for calculating the single-molecule rotation time τ_s, as in Ref. (6). This hypothesis requires the ratio

$$(1+fN)/(1+gN)$$

to be temperature independent. Since f and g are very different in noncritical nitrobenzene mixtures ($fN = 1.3$ and $gN = 0.1 \pm 0.1$ in pure nitrobenzene), it is somewhat unlikely that they would vary with $T - T_c$ in such a way that this ratio keeps constant. This is then another indication that f and g are constant—although the opposite proposition cannot be strictly discounted.

In other respects, Quentrec's theory relates this linewidth to a new formal coefficient α_{33}, α_{11} being the viscosity, and therefore does not provide any new insight.

Nevertheless, in all cases, these results raise the question of the nature of the coupling between the low-frequency long-wavelength critical modes and a fast and short-ranged phenomenon like depolarized scattering. For instance, Carini *et al.*[36] have shown that the shear viscosity measured by usual methods exhibits a relaxation, a fact which clearly does not appear in our experiment, where a naive reasoning would lead to assert that the measuring frequency is about $\Gamma \simeq 10$ GHz and the typical length is the extent of local order, which cannot exceed 100 Å.

V. CONCLUSION

In order to try to answer the questions concerning the existence of two lines in the high-frequency depolarized spectrum of the critical mixture of nitrobenzene and n hexane, and the variations of their linewidths and intensities near the critical point, we set up a very high contrast and high-resolution Fabry-Perot interferometer in double passed arrangement and with two free spectral ranges.

Two lines are visible. One is broad and has a very weak spectral intensity so that it could not

be studied accurately. The other is narrow and intense and could be studied in the range $T - T_c = 0.026-50\,^{\circ}C$. The wide line is 15 times wider and 7 times less intense than the narrow line at $T - T_c = 1\,^{\circ}C$.

The width of the narrow line is seen to behave like the inverse of the macroscopic shear viscosity, in particular it exhibits a weak anomaly in $(T - T_c)^{Y}$, where $Y \approx 0.04$. The intensity of this line also shows a divergence which can be expressed in the form $(T - T_c)^{-\Omega}$ with exponent $\Omega \approx 0.2$.

The existing theories do not provide an adequate frame for the discussion of these results which raise many questions, mainly concerning the nature of the coupling between the order parameter and the orientation fluctuations. New experiments are currently underway in order to try to understand the origin of the anomalies in both the linewidth and intensity.

---

[1]D. A. Pinnow, S. J. Candau, and T. A. Litovitz, J. Chem. Phys. 49, 347 (1968).
[2]E. Zamir, N. Gershon, and A. Ben-Reuven, J. Chem. Phys. 55, 3397 (1971).
[3]S. J. Bertucci, A. K. Burnham, G. R. Alms, and W. H. Flygare, J. Chem. Phys. 66, 605 (1977).
[4]J. Rouch, J. P. Chabrat, L. Letamendia, A. Marcou, and C. Vaucamps, Acta Phys. Pol. A 50, 503 (1976).
[5]D. J. Coumou, J. Hijmans, and E. L. Mackor, Trans. Faraday Soc. 60, 2244 (1964).
[6]G. R. Alms, D. R. Bauer, J. I. Brauman, and R. Pecora, J. Chem. Phys. 59, 5310 (1973).
[7]A. K. Atakhodzhaev, L. M. Kashaeva, L. M. Sabirov, V. S. Starunov, T. M. Utarova, and I. L. Fabelinskiĭ, JETP Lett. 17, 65 (1973).
[8]I. L. Fabelinskiĭ, V. S. Starunov, A. K. Atakhodzhaev, L. M. Sabirov, and T. M. Utarova, Opt. Commun. 15, 432 (1975).
[9]I. L. Fabelinskiĭ, G. I. Kolesnikov, V. J. Sheiner, and V. S. Starunov, Phys. Lett. A 59, 408 (1976); I. L. Fabelinskiĭ, G. I. Kolesnikov, and V. S. Starunov, Opt. Commun. 20, 130 (1977).
[10]I. L. Fabelinskiĭ, V. S. Starunov, A. K. Atakhodzhaev, L. M. Sabirov, and J. M. Utarova, Opt. Commun. 20, 135 (1977).
[11]I. M. Aref'ev, Opt. Commun. 10, 277 (1974).
[12]D. Beysens, A. Bourgou, and G. Zalczer, Opt. Commun. 15, 436 (1975).
[13]D. Beysens, S.H. Chen, J. P. Chabrat, L. Letamendia, J. Rouch, and P. Vaucamps, J. Phys. (Paris) Lett. 38, L203 (1977).
[14]D. Beysens and G. Zalczer, Opt. Commun. 22, 236 (1977).
[15]S. H. Chen and N. Polonski, Opt. Commun. 1, 64 (1969).
[16]C. C. Lai and S. H. Chen, Phys. Rev. Lett. 29, 401 (1972).
[17]C. C. Lai, S. H. Chen, Phys. Lett. A 41, 259 (1972).
[18]D. Beysens, A. Bourgou, and H. Charlin, Phys. Lett. A 53, 236 (1975).
[19]D. Beysens, A. Bourgou, and G. Zalczer, J. Phys. (Paris) Colloq. C 1, 225 (1976).
[20]D. Beysens, G. Zalczer, Phys. Rev. A15, 765 (1977).
[21]D. Beysens and G. Zalczer (unpublished).
[22]D. Beysens and G. Zalczer, Opt. Commun. 23, 142 (1977).
[23]V. Puglielli and N. Ford, Phys. Rev. Lett. 25, 143 (1970).
[24]M. Tournarie, J. Phys. (Paris) 30, 47 (1969).
[25]G. I. A. Stegeman and B. P. Stoicheff, Phys. Rev. A 7, 1160 (1973).
[26]B. Simic-Glavaski and D. A. Jackson, J. Phys. (Paris) Colloq. 33, C1-183 (1972).
[27]E. N. Ivanov, JETP 18, 1041 (1975).
[28]R. Pecora, J. Chem. Phys. 49, 1036 (1968).
[29]T. Keyes and D. Kivelson, J. Chem. Phys. 56, 1057 (1972).
[30]B. Quentrec, J. Phys. (Paris) 37, 1255 (1976).
[31]B. Quentrec, Phys. Rev. A15, 1304 (1977).
[32]C. L. Hartley, D. T. Jacobs, R. C. Mockler, and W. J. O'Sullivan, Phys. Rev. Lett. 33, 1129 (1974).
[33]D. T. Jacobs, D. J. Anthony, R. C. Mockler, and W. J. Sullivan, Chem. Phys. 20, 219 (1977).
[34]C. M. Hu and R. Zwanzig, J. Chem. Phys. 60, 4354 (1974).
[35]D. Hoel and D. Kivelson, J. Chem. Phys. 62, 1323 (1975).
[36]G. Carini Jr., G. Maisano, P. Migliardo, and F. Wanderlingh, Phys. Rev. A 11, 1755 (1975).

Depolarized Rayleigh scattering near the critical point of the nitroethane–isooctane mixture

G. Zalczer and D. Beysens

Commissariat a l'Energie Atomique, Division de la Physique, Service de Physique du Solide et de Resonance Magnetique, DPh-G/PSRM, Cen.Saclay, Boite Postale N°2, 91190 GIF-s/Yvette, France
(Received 2 March 1979; accepted 10 September 1979)

Intensity and linewidth measurements of the depolarized Rayleigh line in the critical mixture of nitroethane and isooctane in the temperature range $T - T_c = 2$ m°K – 60°K are reported. The linewidth presents no anomaly and behaves like the regular part of the viscosity. The intensity however exhibits a linear anomaly which levels off for $T - T_c > 35$°K.

INTRODUCTION

Depolarized light scattering from critical binary mixtures has been investigated only recently. The first mixture studied was that of nitrobenzene and n-hexane where the spectrum was analyzed as three superposed Lorentzian components, with dramatic variations.[1–3] Soon after Aref'ev[4] noticed only slight effects in the nitroethane–isooctane system which exhibits very weak critical opalescence and suggested that multiple scattering was responsible for the large effects that had been previously observed. Subsequently, we showed that the narrowest of these lines is due to multiple scattering[5,6] which is merely repeated single scattering by concentration fluctuations. This phenomenon, which has been widely studied,[5,7–11] is well understood, but it may considerably affect the measurements of the wide lines if special care is not taken.[12] Two ways are possible for overcoming this difficulty; either by using a very high contrast interferometer as in Ref. 13 or by choosing a mixture where the refractive indices are matched, which ensures that concentration scattering and therefore, multiple scattering are weak.[4,14] However since noncritical mixtures with different anisotropic species can exhibit different orientation correlation,[15] depolarized scattering measurements from different critical mixtures could also lead to different results.

Until now most of the results on these subjects[4,16] are only of a qualitative nature and only show that there is no strong anomaly as reported in Refs. 1–3. In Ref. 14 two different trial functions, one regular and one singular were fitted to the linewidth data. Unfortunately no indication was given concerning the relative quality of these fits. Indeed, to correctly decide between different slowly varying functions, it is necessary to measure over a sufficiently wide temperature range (in fact, much wider than the 0.1°–8 °C range used in Ref. 14). However these authors did conclude that the linewidth variation was smaller than that of the viscosity. Their statement about the regular part of the viscosity is not appropriate for it has been proved[17] that such a partition of the viscosity is meaningless. Obtaining meaningful values of parameters such as an exponent or an activation energy would require both measurements over a wide temperature range and the knowledge of an appropriate function for the viscosity. Only in Ref. 13, where the nitrobenzene–n-hexane system was investigated, were these conditions fulfilled. The linewidth was there seen to behave like the shear viscosity, that is, it diverged near the critical point with a very small exponent. Moreover, the intensity variation could be well described by the power law $(T - T_c)^{-\Omega}$ with $\Omega \simeq 0.22$.

DEPOLARIZED RAYLEIGH SCATTERING

Depolarized Rayleigh scattering arises from the anisotropy of the molecules. A treatment[18] of the electromagnetic problem for individual molecules leads in the more general case to five lines. Collective treatments[19–21] however usually lead to a smaller number of lines. Experimentally only two lines at most have ever been observed and only the narrower line could be accurately studied. Depolarized scattering that arises by other mechanisms such as collisions or DID can usually be identified, for this scattering involves higher frequencies and has a different (exponential) spectrum shape.[22]

In noncritical mixtures with an isotropic solvent, the intensity of this narrow line can behave in two different ways when the concentration c of the anisotropic solute is changed.[15] Either this intensity varies linearly with c, as, for example, in benzene solutions suggesting an independent behavior of the molecules, or as for nitrobenzene solutions in which it shows a parabolalike variation suggesting the relevance of orientation correlations. The width Γ of this line is related to the viscosity η of the mixture. Most theoretical models predict that Γ varies as the inverse of the shear viscosity with different coefficients according to the boundary conditions at the "surface" of the molecule (slip, stick, or other).[23,24] The experimental study of Alms *et al.*[25] has shown that the relation is not so simple, namely

$$1/\Gamma = a\eta + b$$

where a and b are functions of the concentration. The temperature dependence was not investigated. Another important experimental result is that anisotropic molecules of nearly identical shapes can have very different orientation correlations depending upon their dipolar moments.[26] Near the critical point, the position correlations and the viscosity diverge and we wish to examine whether and how these divergences affect the depolarized Rayleigh scattering in a mixture other than nitrobenzene-n-hexane.

EXPERIMENTAL

We choose the mixture of nitroethane and isooctane because of its very weak concentration scattering. Its

 0021-9606/80/010348-05$01.00 © 1980 American Institute of Physics

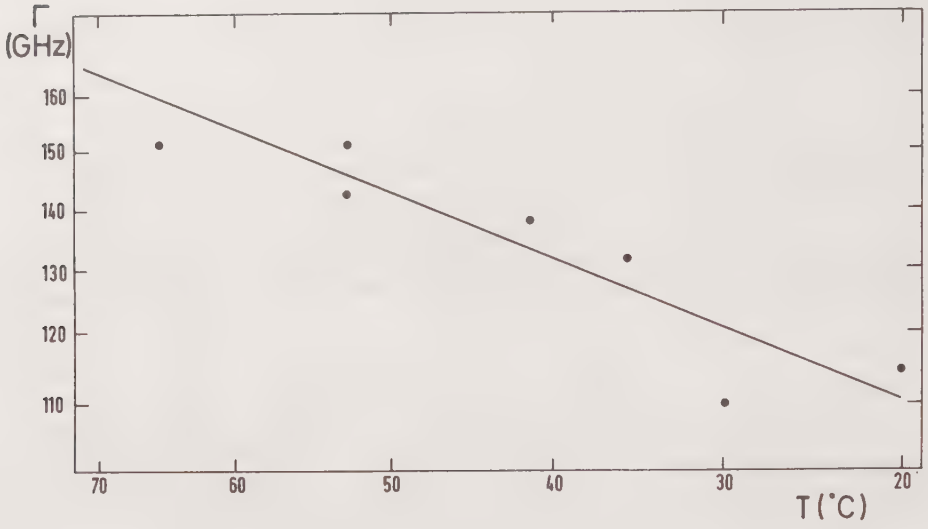

FIG. 1. Linewidth of the depolarized scattered spectrum from pure nitroethane. The solid line is the Arrhenius fit (units: vertical scale: logΓ; horizontal scale: $1/T$).

coexistence curve has been carefully studied,[27] and a few measurements of depolarized Rayleigh scattering have already been performed.[4] In other respects, the nitroethane molecule has a strong dipolar moment (between 2.75 and 3.6 D according to different measurements).[28]

We used the critical concentration determined in[27] (0.535 mass fraction of isooctane) and used the same device for determining the critical point: The laser beam is reflected by the input and output windows of the cell. These reflected beams interfere and the interference order is directly related to the refractive index of the mixture. The temperature is lowered by small steps. After having crossed the critical point, the refractive index varies much more rapidly and the equilibrium value is attained after a much longer time. This allows the determination of T_c to within ± 1 m °K.

The light scattering setup and the two stage thermostat are the same as those used in Ref. 13 and are fully described in Ref. 29, except that we selected the $HH+HV$ polarizations, using a half-wave plate in the incident beam and increased the focal length of the collecting lens. We used a 20 mW He–Ne laser and a double-pass Fabry–Perot interferometer (free spectral range 1087 GHz, finesse 70, contrast 10^6) stable enough to allow recordings for up to 24 h. The spectrum and the apparatus functions are alternatively recorded. The experimental apparatus function or an analytical fit to it is used for fitting each spectrum, using a statistical refining program due to Tournarie.[29,30]

Contrary to the case of the nitrobenzene–n-hexane system, the quasielastic polarized scattering which we use for calibrating the intensities is not due only to the concentration fluctuations, but also to pressure (Brillouin lines) and entropy fluctuations. In order to determine its variation, we recorded polarized spectra at different temperatures in a short time interval so that parameters such as F.P. transmission or laser intensity were constant. These data could be fairly well described by the sum of the usual polarized intensity and a constant,

$$I = \frac{I_0}{(T - T_c)^{\gamma} + a} + I_1$$

This formula has been used for calibrating the intensities.

RESULTS

A. Pure constitutents and noncritical mixtures

The depolarized spectra of pure components were investigated first. Isooctane has a much weaker (four times) depolarized scattering than nitroethane so its scattering was not investigated at different temperatures. The nitroethane spectrum width varies, within experimental uncertainties, following an Arrhenius law with an activation energy of 750 ± 170 K (Fig. 1), to be compared with that of the viscosity: 824 K,[31] while its intensity remains nearly constant (Fig. 2). We then tried to check the variation of the intensity versus the concentration of nitroethane in a noncritical mixture (solvent CCl_4). The measurements were somewhat imprecise because of the difficulty of comparing intensities from different cells but consistent with, at most, a small curvature, much weaker than for nitrobenzene solutions.

B. Critical mixture

The depolarized spectrum of the critical mixture was investigated in the temperature range 2 m °K $\leq T - T_c \leq$ 60 °K. The results are reported in Table I. A log–log plot of the linewidth (Fig. 3) shows unambiguously there is no critical divergence. In the range 0.002 °K $< T - T_c <$ 2 °K, the expected divergence with exponent $y_\eta \simeq 0.04$ would lead to a variation of about 30%. The data follow fairly well an Arrhenius law with an activation energy of 955 ± 65 K, as shown in Fig. 3.

For the intensity, no theoretical prediction presently exists which can be compared with the data. We have plotted the results in Fig. 4 using linear scales. Obviously the intensity varies much more than in pure nitroethane and much more than does the density, indicating that some kind of orientation correlations are present. This plot shows that the intensity decreases

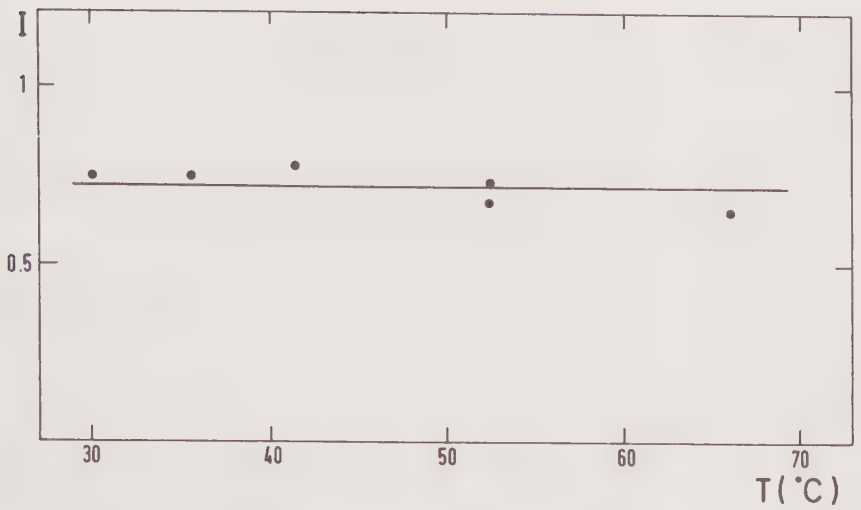

FIG. 2. Depolarized scattered intensity from pure nitroethane (arbitrary units).

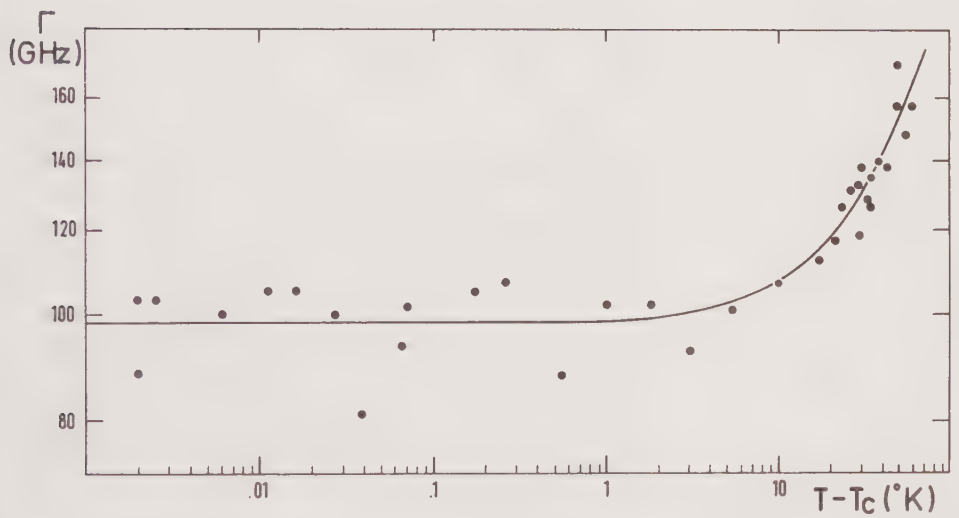

FIG. 3. Linewidth of the depolarized scattered spectrum from the critical mixture of nitroethane and isooctane. The solid line is the best Arrhenius fit.

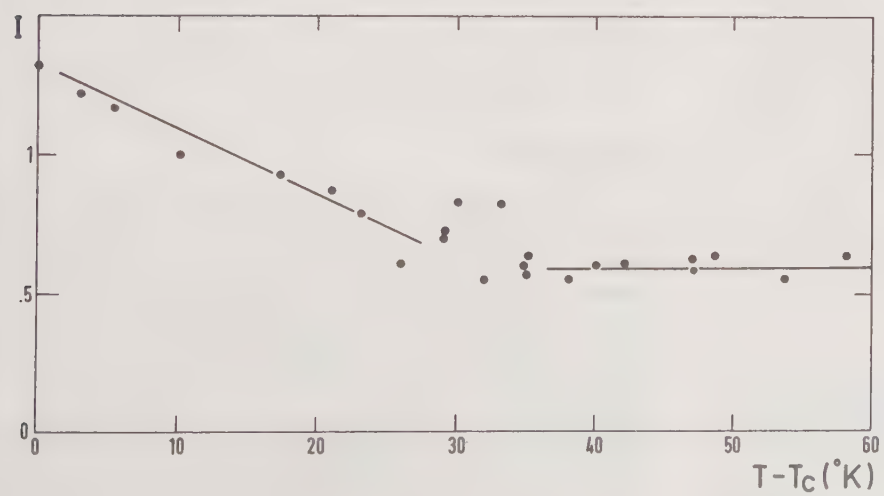

FIG. 4. Depolarized scattered intensity from the critical mixture.

TABLE I. Linewidth and intensity measurements from the critical mixture.

$T - T_c$ (°C)	Γ (GH_z)	I (arbitrary units)
58	157	0.65
53.5	148	0.57
48	172	0.65
46.7	158	0.59
40	138	0.63
38	141	0.55
34.6	136	0.63
33	127	0.82
32	129	0.56
30	138	0.83
29	133	0.71
29	119	0.72
26	132	0.61
23	127	0.79
21	118	0.87
17	113	0.93
10	107	1.0
5.3	102	1.17
3	92	1.22
1.0	103	1.59
0.54	88	...
0.27	108	1.43
0.17	105	1.27
$9.5\ 10^{-2}$	101	1.31
$7\ 10^{-2}$	103	1.13
$6.5\ 10^{-2}$	93	1.52
$3.8\ 10^{-2}$	81	1.07
$2.7\ 10^{-2}$	101	1.48
$2.5\ 10^{-2}$	104	1.35
$1.6\ 10^{-2}$	105	1.63
$1.1\ 10^{-2}$	109	1.60
$6.\ 10^{-3}$	101	1.30
$2.\ 10^{-3}$	88	1.30
$2.\ 10^{-3}$	104	1.36

linearly from T_c to $T - T_c = 35$ °K and remains constant beyond this temperature. The same kind of variation has already been observed in pure nitrobenzene.[32]

DISCUSSION

The linewidth of the reorientation line was always found to be related to the viscosity. In nitrobenzene–*n*-hexane, the only critical mixture until now which has been investigated over a sufficient temperature range for quantitative conclusion to be possible,[13] the linewidth follows the same variation as the shear viscosity, that is it exhibits a divergence with a very small ($\simeq 0.04$) exponent. Here there is clearly no divergence while the viscosity[33] fits well to the same law as in many other critical systems[17]

$$\eta = \eta_0 \left(\frac{T - T_c}{T_c} \right)^{-y_\eta} \exp\left\{ \frac{\theta}{T} \right\}$$

with $\eta_0 = 2.82 \times 10^{-2}$ *cPO*, $y_\eta = 0.045 \pm 0.013$, $\theta = 920 \pm 180$ K. The linewidth data however are fairly well fitted by an Arrhenius law with an activation energy $\theta' = 955 \pm 65$ K. The fact that these two activation energies are so close to each other is probably significant. This could mean that the regular part of the multiplicative law can be directly observed. To our knowledge this is the first time that a direct observation of this regular viscosity has been made.

Our results can be compared with those of Petrula *et al.*[14] who studied the mixture of nitroethane and 3-methyl pentane. Indeed this mixture has the same anisotropic constitutent and in noncritical mixtures the isotropic solvent affects the reorientation linewidth only through the viscosity of the mixture.[25] These authors fitted their data to both a power law in $T - T_c$ and an Arrhenius law but were not able to choose between the two laws, because as already stated the temperature interval studied was too small to allow the difference to be evidenced and *a fortiori* it was meaningless to try using a more complicated formula. In the light of our present results, the Arrhenius behavior seems to be more likely.

Contrary to the linewidth, the intensity exhibits a variation that cannot be explained by standard theories. Since this kind of behavior has already been observed in pure nitrobenzene, it might not be due to the critical point. Anyway the precise nature of such a mechanism which affects the intensity but not the linewidth is not clear.

The results are quite different from those obtained with the same setup in the mixture of nitrobenzene and *n*-hexane.[13] This could be due to two causes. One is the difference (by a factor of about ten) of the frequencies involved, which could relax the critical contribution to the viscosity. The possible cutoff frequencies, following Kadanoff and Swift[34] correspond to the coupling with mass diffusive modes and acoustic modes. Carini *et al.*[35] have experimentally shown that a relaxation occurs at the frequency of the mass diffusive mode. In our case the cutoff frequency would be between 15 and 100 GHz, i.e., about of the order of magnitude of the sound mode cutoff.

The second possible cause lies in the nature of the molecule which could more or less favorize orientation correlations. An indication of the presence of this process is given by the different behavior of the depolarized intensity vs concentration of CCl_4 solutions of both species. Moreover, the nitroethane molecule has a weaker dipolar moment than the nitrobenzene molecule (respectively, about 3D and 4D) and its shape seems less favorable to steric effects.

CONCLUSION

We have studied the depolarized Rayleigh spectrum of the critical mixture of nitroethane and isooctane in a wide temperature range. We did not notice any critical anomaly in the linewidth. The observed variation of the linewidth reflects that of the regular part of the viscosity, provided that the multiplicative law is admitted. The intensity however shows a linear anomaly which levels off 35 K above T_c. The difference with the results previously obtained in the nitrobenzene–*n*-hexane system could be related either to the frequencies involved or to the nature of the molecule, as indicated by

the different variations of the depolarized intensity from both species in an isotropic solvent.

ACKNOWLEDGMENTS

We gratefully thank P. Calmettes and J. Hodges for their comments on the manuscript.

[1]A. K. Atakhodzhaev, L. M. Kashaeva, L. M. Sabirov, V. S. Starunov, T. M. Utarova, and I. L. Fabelinskii, Zh. Eksp. Teor. Fiz. Pisma Red. 17, 95 (1973).
[2]I. L. Fabelinskii, V. S. Starunov, A. K. Atakhodzhaev, L. M. Sabirov, T. M. Utarova, Opt. Commun. 15, 432 (1975).
[3]G. I. Kolesnikov, V. S. Starunov, and I. L. Fabelinskii, Zh. Eksp. Teor. Fiz. Pisma Red. 24, 73 (1976).
[4]I. M. Aref'ev, Opt. Commun. 10, 277 (1974).
[5]D. Beysens, A. Bourgou, and G. Zalczer, Opt. Commun. 15, 436 (1975).
[6]D. Beysens, A. Bourgou, and G. Zalczer, J. Phys. (Paris) Colloq. C 1, 225 (1976).
[7]D. Beysens, A. Bourgou, and H. Charlin, Phys. Lett. A 53, 236 (1975).
[8]L. A. Reith and H. L. Swinney, Phys. Rev. A 12, 1034 (1975).
[9]Y. Garrabos, R. Tufeu, and B. Le Neindre, J. Chem. Phys. 68, 495 (1978).
[10]D. Beysens and G. Zalczer, Phys. Rev. A 15, 765 (1977).
[11]D. Beysens and G. Zalczer, Opt. Commun. 26, 172 (1978).
[12]D. Beysens and G. Zalczer, Opt. Commun. 22, 236 (1977).
[13]D. Beysens and G. Zalczer, Phys. Rev. A 18, 2280 (1978).
[14]J. R. Petrula, H. L. Strauss, K. Q. H. Lao, and R. Pecora, J. Chem. Phys. 68, 623 (1978).
[15]D. J. Coumou, J. Hijmans, and E. L. Mackor, Trans. Faraday Soc. 60, 2244 (1964).
[16]G. D. J. Phillies, P. J. Chappell, and D. Kivelson, J. Chem. Phys. 68, 4031 (1978).
[17]P. Calmettes, Phys. Rev. Lett. 39, 1151 (1977).
[18]R. Pecora, J. Chem. Phys. 49, 1036 (1968).
[19]T. Keyes and D. Kivelson, J. Chem. Phys. 56, 1057 (1972).
[20]B. Quentrec, J. Phys. (Paris) 37, 1255 (1976).
[21]B. Quentrec, Phys. Rev. A 15, 1304 (1977).
[22]B. Simic-Glavaski and D. A. Jackson, J. Phys. (Paris) Colloq. 33 C1 183 (1972).
[23]C. M. Hu and R. Zwanzig, J. Chem. Phys. 60, 4354 (1974).
[24]D. Hoel and D. Kivelson, J. Chem. Phys. 62, 1323 (1975).
[25]G. R. Alms, D. R. Bauer, J. I. Brauman, and R. Pecora, J. Chem. Phys. 59, 5310 (1973).
[26]S. J. Bertucci, A. K. Burnham, G. R. Alms, and W. H. Flygare, J. Chem. Phys. 66, 605 (1977).
[27]D. Beysens, J. Chem. Phys. 71, 2557 (1979).
[28]A. L. McClellan, *Tables of Experimental Dipole Moments* (Freeman, San Francisco, 1963).
[29]D. Beysens and G. Zalczer, Opt. Commun. 23, 142 (1977).
[30]M. Tournarie, J. Phys. (Paris) 30, 47 (1969).
[31]B. C. Tsai and D. McIntyre, J. Chem. Phys. 60, 937 (1974).
[32]G. I. A. Stegeman and B. P. Stoicheff, Phys. Rev. A 7, 1160 (1973).
[33]K. Lyons, Ph.D. thesis, University of Colorado (1973).
[34]L. P. Kadanoff and J. Swift, Phys. Rev. 166, 89 (1968).
[35]G. Carini, Jr., G. Maisano, P. Migliardo, and F. Wanderlingh, Phys. Rev. A 11, 1755 (1975).

Rayleigh and Raman scattering near the critical point of carbon dioxide

Yves Garrabos, Roland Tufeu, and Bernard Le Neindre

Laboratoire des Interactions Moléculaires et des Hautes Pressions, Centre Universitaire Paris-Nord, Avenue Jean-Baptiste Clément, 93430 Villetaneuse, France

Gilbert Zalczer and Daniel Beysens

Service de Physique du Solide et de Résonance Magnétique, DPH-G/PSRM, CEN. Saclay, Boite Postale n° 2, 91190 Gif-Sur-Yvette, France

(Received 7 August 1979; accepted 11 December 1979)

An experimental study of the behavior of depolarized Rayleigh and Raman spectra of carbon dioxide when approaching the critical temperature along the critical isochore is presented. The study of the depolarized Raman scattering was carried out on the Fermi diad ν_1, $2\nu_2$ and was supplemented by a study of the polarized Raman scattering. Contributions to the different physical mechanisms which can give rise to the depolarized spectra are carefully analyzed. We have shown that the orientational dynamics of CO_2 molecules are unchanged by critical slowing down of the diffuse hydrodynamical mode associated to fluctuations of the order parameter in the range $0.01\,°C < T - T_c < 10\,°C$. Moreover we found that the frequency variation of the polarized Fermi diad can be well described using only density terms. The variation of the spectral intensities of the different polarized and depolarized bands is well explained in terms of only turbidity and multiple scattering phenomena owing to the intensive quasielastic polarized Rayleigh scattering.

I. INTRODUCTION

A. Theory

The close vicinity of the critical point of a pure fluid is characterized by large fluctuations of the order parameter $\rho - \rho_c$ (the difference between the density ρ and the critical density ρ_c). In fluids cooperative phenomena extend to large distances (several hundred Å) with respect to classical molecular parameters (several Angstroms), leading to singular behavior of several thermodynamical properties of the fluid when approaching its critical point. Thus, as a consequence of the divergence of the isothermal compressibility κ_T [$\kappa_T = \rho^{-1}(\partial\rho/\partial p)_T$, where p is the pressure and T the temperature] the critical opalescence is certainly the longest known manifestation of these important fluctuations of the order parameter near this unusual point of the phase diagram.

Simultaneous developments of experimental techniques[1,2] and theories[3,4] in recent years have enabled the characterization of the decay rate of fluctuations of the order parameter approaching the critical point to be obtained. The phenomenon known as critical slowing down pertaining to regression of fluctuations of the order parameter which becomes slower as these fluctuations become larger can also now be explained. As the fluid gets closer to its critical point, the time necessary to reach equilibrium becomes longer. The main point here concerns the important cooperative aspect of the phenomena, which is particular to the vicinity of the critical point and which is based on the translational correlations over large distances between the molecules of the fluid. The extent of spatial correlations is such that the exact nature of local order on the scale of one molecule or even a few molecules is not relevant to the qualitative description of the behavior of these cooperative phenomena, and even yields the universality concept for the same class of transition points.[4,5] However, it is evident that we must not ignore the important role that is played by the exact nature of local order on the quantitative description of these phenomena.

The development of the static and dynamic aspects of local order in the pure fluid approaching the critical point remains an open question and to date only a few experimental studies have been made.

From neutron scattering experiments along the critical isochore of neon, Mozer[6] found that the static structure factor $S(k)$ was not modified approaching T_c for momentum transfers larger than $1.5\ Å^{-1}$. The fact that the position and the intensity of the first peak of $S(k)$ are not modified approaching to the critical point shows, as can be expected, that a spatial structure defined by the closest neighbors of a molecule continues to exist even under critical conditions. In other words, the appearance of cooperative phenomena related to the approach of the critical point of a pure fluid such as neon can be attributed only to a new phenomenon: In this region of the phase diagram, the range of spatial correlations between the molecules can extend to larger distances than the mean distance of separation between their near neighbors.

Concerning the dynamical aspect of this local order in a pure fluid near its critical point, we are not aware of any experimental investigation of this problem. However, it was studied recently[7-11] near the demixing point of critical binary mixtures, which is analogous to the gas–liquid critical point of simple fluids.[12] Two of us (D. B. and G. Z.) have investigated the phenomena[13,14] which must be taken into account[15] in the studies of depolarized Rayleigh scattering of light by different critical binary mixtures.

B. The depolarized Rayleigh spectrum

The depolarized Rayleigh scattering of light by a fluid or a binary liquid mixture, whether close or far from a

 0021-9606/80/084637-15$01.00 © 1980 American Institute of Physics

transition point, is due to the polarizability anisotropy of the component molecules. The main difficulty is the complexity of the physical mechanisms which perturb the molecular anisotropy when molecules are not considered to be isolated from one another. This is obviously the case in liquid mixtures or dense fluids which are of interest here. The theoretical approaches to the subject are presently being developed. Experimentally, many studies using this technique have helped to clarify the relative importance of these mechanisms.

For atomic noble gases in the dense gas or liquid phase, we observe in the high frequency range a quasi-exponential decrease of the spectral intensity of the depolarized Rayleigh band (decay rate > 300 GHz). The interpretation of this result can be given in terms of the anisotropy induced in atoms by molecular interactions. Thus, in the restrictive hypothesis of a binary interaction, the collisional Rayleigh wing of compressed noble gases is described by taking into account both the dynamics of an unbound transient dimer formed by the interacting pair of atoms and the degree of distortion of their respective electron configurations in terms of the intermolecular distance of separation.[16]

When we study pure liquid or liquid solutions made of complex molecules which have a permanent polarizability (benzene, nitrobenzene, polyalcohol), the observed depolarized Rayleigh spectrum is generally composed of two bands.

Only the narrower band can be characterized with accuracy. Its profile is well represented by a Lorentzian with full width at half-maximum (FWHM) located in the frequency range below 150 GHz. The interpretation of this result can be made only in terms of the reorientation motion of molecules. The contributions to the depolarized spectrum of other mechanisms are negligible because these contributions must occur at significantly higher frequencies. For instance, collisional phenomena induce a small modification of the permanent anisotropy. On theoretical grounds it is not easy to separate contributions coming from individual reorientation of molecules from those due to correlations between reorientation of several neighboring molecules.[17] Simpler theoretical models of molecular reorientation are preferred and these models will be compared not only with results obtained from depolarized Rayleigh scattering but also with those obtained by nuclear magnetic resonance, neutron scattering, Raman scattering, and infrared absorption. These various methods provide identical or complementary information about the monomolecular character of the reorientation or about the presence of strong correlations in the reorientation of several neighboring molecules. Up to now, one of the most significant results of all experimental studies carried out on liquids consisting of complex anisotropic molecules (pure liquid or mixtures with an isotropic solvent) has been expressed as a linear relation between the width of the Rayleigh band and the reciprocal shear viscosity of the liquid or the mixture.[18] It is usely admitted that this relation reflects the presence of strong reorientation correlations in these liquids. Another important experimental result is that anisotropic molecules with similar shapes and sizes can have very different depolarized Rayleigh profiles; this would show t essential role of the dipolar nature of the molecules to favor more or less the reorientation correlations.[19]

Near the gas–liquid critical point of a pure fluid or near the demixing point of a binary critical mixture, the divergence of the shear viscosity is weak[20] owing to the coupling between the diffusive mode associated with the fluctuations of the order parameter and the transverse local velocity.[21,22] It is important to know if this divergence can modify the depolarized Rayleigh spectrum. We have investigated this question for binary critical mixtures of nitrobenzene–*n*-hexane[13] or nitroethane–iso-octane.[14] In the nitrobenzene–*n*-hexane critical mixture the depolarized Rayleigh linewidth follows the same variation as the shear viscosity, namely, a divergence with a very small exponent. In nitroethane-iso-octane the linewidth of the reorientation line is clearly not divergent, although the viscosity well fits the same law as for many other critical systems.[20]

The present work is concerned with this subject in the critical region of a pure fluid. Among the fluids th we have previously studied near their respective critical points,[23] we have chosen carbon dioxide because the strong anisotropy of the polarizability of the molecule suggests that important orientational effects should exist. Moreover, for this fluid, the phenomenon was studied only at low density in the gaseous phase[24] or at very high density in the liquid phase[25,26] without obtaining enough accurate conclusions on the evolution of the dynamical behavior of reorientation over large temperature and pressure ranges. Thus, through the specific problem associated with the critical region, this experimental contribution provides some information on the nature of the reorientation motion of the carbon dioxide molecule at moderate density ($\rho_c = 0.468$ g cm^{-3}) and in the single phase range ($T_c = 31 < T < 40$ °C).

Measurements of depolarized Rayleigh scattering we supplemented by measurements of polarized and depolarized Raman scattering for the ν_1 symmetrical frequency vibration in Fermi resonance with the $2\nu_2$ harmonic of same symmetry.[27] In fact, for carbon dioxide in the relatively dense phase (the liquid density at the triple point is only twice the critical density), the interpretation of the depolarized Rayleigh spectrum will be delicate because we are between the two extreme cases previously mentioned. Without explaining the method o Raman scattering, its use in this study is justified by its complementarity with Rayleigh scattering. As was shown by Litovitz[28] who made the hypothesis of a separation between internal and external motions of molecules the depolarized Raman scattering provides the reorientation time of one molecule and the depolarized Rayleig scattering gives information on the collective reorientation time of several molecules when they are correlate The ratio of reorientational times $\tau_{\text{Rayleigh}}/\tau_{\text{Raman}}$ deduc from these measurements is proportional to the factor of static correlation orientation.[29] Thus, the comparis of respective results of depolarized Rayleigh and Rama scattering enables us to investigate the influence of nea neighbors on the reorientation motion of the individual molecules.

After a description in Sec. II of the experimental devices used in our study, we give in Sec. III the main results deduced from our measurements of the width of the polarized Rayleigh band by the photon correlation method when T_c is approached along the critical isochore. This enables us to verify the critical slowing down of the dynamical behavior of entropy fluctuations along the critical isochore of carbon dioxide as already observed by Swinney *et al.*[30] using different analysis techniques. In Sec. IV we discuss the data extracted from the intensity variations and from the position in frequency of the two vibrational polarized Raman bands ν_1 and $2\nu_2$ in Fermi resonance. These fluctuations well illustrate the scattering mechanisms which take place in critical opalescence phenomena in the optical cell. In Secs. V and VI we carefully analyze the recordings of depolarized Raman and Rayleigh bands taken with a triple monochromator; we consider the physical phenomena which can be at the origin of depolarized spectra in order to correctly characterize the evolution of orientational dynamics of CO_2 along the critical isochore. In Sec. VII we discuss results obtained from Rayleigh and Raman depolarized spectra which are interpreted simply in terms of mechanisms which take place in the cell during its critical opalescence.

II. EXPERIMENTAL

A. The scattering cell

The scattering cell is similar to that used previously in the study of multiple scattering, near the critical point of some pure fluids.[23] The high pressure vessel is made of aluminum alloy. Its surfaces are blackened by anodal oxydation. The optical windows are made of borosilicate and are stuck on supports made of stainless steel to avoid the accidental birefringence effect due to mechanical deformation.

B. Temperature control

The temperature control device consists of two independent regions. The first is the scattering cell setup inside a spherical furnace made of copper with an external diameter of 160 mm. The temperature control of the furnace is obtained by a commercial controller (A. T. N. E.) using a platinum resistance sensor. The heating power is provided by a heating element embedded in the external surface of the sphere. The furnace and the scattering cell are then introduced into a second environment which is adaptable to several experimental conditions.

This second region is in fact an enclosure where temperature is monitored at a slightly lower temperature than the critical temperature of the fluid under study. Two kinds of external enclosures have been used: one made of aluminum alloy with a double water flow is used for filling of the optical cell and for the polarized Rayleigh scattering study, and the other made of wood with convective air circulation is used for polarized Raman scattering and for depolarized Rayleigh and Raman scattering studies. The use of the two temperature controls yields a stability temperature of the scattering cell which is better than $\pm 2\times10^{-4}$ K over several hours. The temperature measurement is obtained with two complementary devices. The precise absolute value is obtained to $\pm 10^{-2}$ K with a previously calibrated platinum resistance. The temperature differences are measured with a Hewlett-Packard quartz crystal thermometer with an accuracy of $\pm 5\times10^{-4}$ K and a resolution of $\pm 1\times10^{-4}$ K.

C. The filling of the cell at the critical density for CO_2

Prior to filling with carbon dioxide, the scattering cell was degassed at high temperature (250°C) for 2 days. It was pumped for 48 h, then cleaned by successive filling and emptying with 99.998% pure carbon dioxide under pressure at room temperature.

The final filling of the scattering cell with carbon dioxide was performed in the supercritical range at 40°C at a pressure corresponding to the critical density. Unfortunately, the accuracy of the absolute determination of the critical density of carbon dioxide given in the literature is far lower than the relative accuracy given by our filling method. At $T = 40$°C, which is far enough from the critical temperature ($T - T_c \simeq 9$°C), we used the precise p, V, T data of Michels *et al.*[31] for 40.087 and 40.105°C isotherms and p, T data of Levelt-Sengers and Chen[32] along the critical isochore to determine the filling pressure data. The pressure is measured with a dead weight gauge (Desgranges and Huot) with an accuracy better than 0.1%. Using the previously described temperature controller, the temperature stability is better than 10^{-3} K and the filling temperature of 40°C is known with an accuracy better than $\pm 10^{-2}$ K. The sealing of the cell is made with a microvalve which introduces a slight decrease in volume which is negligible in comparison to the volumes of the cell and dead weight gauge. Thus, the filling density of the scattering cell is known with an accuracy better than 0.1% for nominal values of the order of 0.47 g cm^{-3}.

We chose to fill up the cell at the density of 0.468 g cm^{-3}, that is to say at 40°C under a pressure of 88.125 atm. This choice agrees with the measured value $\rho_c = 0.4678 \pm 0.0022$ g cm^{-3} of Moldover[33] and is compatible with a rectilinear diameter law even close to the critical temperature.[34,35] A possible bending of the diameter implies that the densities obtained by extrapolation of the rectilinear diameter are in fact underestimated. However, as was shown recently by Sengers *et al.*,[36] the error introduced in ρ_c is generally less that 0.5% even though the theoretical predictions of the bending are important. Thus, we estimate that our cell was filled at the critical density with an accuracy of 0.5%.

Probably the best measure of the purity and correct critical density of the sample is the critical temperature. The critical temperature measurement was obtained by a visual observation method of gas–liquid separation. We found $T_c = (30.99 \pm 0.01)$°C. The most accurate determination of T_c gives (30.977 ± 0.004)°C.[33] This excellent agreement between the critical temperature values confirms the good filling of our carbon dioxide scattering cell.

D. Experimental arrangements in depolarized scattering

In Sec. III we briefly report our experimental arrangement in the polarized Rayleigh line study.

In this paragraph we describe the analysis technique in the polarized Raman band and depolarized Rayleigh and Raman band studies. The experimental setup is standard but several particular points must be underlined.

We used, as excitation light, the green line $\lambda = 5145$ Å given by a Spectra Physics laser model 165. We have used several different monitored incident powers, depending on the gap between the experimental temperature and the critical temperature so as to avoid any perturbation of thermal equilibrium. This is a necessary condition to obtain a correct recording of scattering spectra. For $T - T_c > 0.5$ °C, we used powers up to a few hundred milliwatts; the typical value used for the calibration of the spectra was 100 mW. When $T - T_c$ was of the order of 0.01 K the incident power was attenuated with neutral filters to a few milliwatts.

The light scattered at 90° is analyzed by a triple monochromator (Coderg T 800). The four slits are always used with identical widths and have symmetrical openings. For all recorded spectra the width of slits was chosen narrow enough to avoid corrections in the analysis of the profile. A slit width equal to $\frac{1}{5}$ of the FWHM of a Lorentzian profile causes a distortion lower than 5%.

The image of the illuminated volume by the incident laser beam focused on the scattering cell is formed through a lens in focus condition on the entrance slit of the first monochromator. A telescope set up behind this slit enables us to insure the symmetry with respect to the illuminated beam.

The component $HH + HV$ of the light scattered at 90° was recorded, so that the useful signal was maximum. The gain of the signal is especially appreciable for recordings near T_c because the incident intensity is attenuated by turbidity phenomena.[23] The spectrometer collects an entirely depolarized intensity ($HH + HV$) when the incident laser beam is horizontally polarized and a partial polarized intensity ($VV + VH$) when the laser beam is vertically polarized. Although the depolarization influences the response of the gratings of the monochromators which is only correct when the light falling on them is circularly polarized, we did not take it into account for the following reasons: One reason is that we are not looking for an absolute measurement of the depolarization ratio of the bands studied. The other reason comes from the experimental observation at temperatures far from T_c where the depolarization ratio measured is close to the theoretical value (at 40 °C, we verified that the ratio I_{VH}/I_{VV} was equal to 0.75 for an adequate light scattering analysis).

The spectral intensity of the scattered light was detected by a photomultiplier tube (EMI 9358 A) cooled by Peltier effect in a chamber (Products of Research). The photomultiplier tube works in the pulse counting regime with a commercial amplifier–discriminator electronic system. Its output is connected to a digital voltmeter and to a graphical recorder. The various conditions of recording the spectra are described in the text.

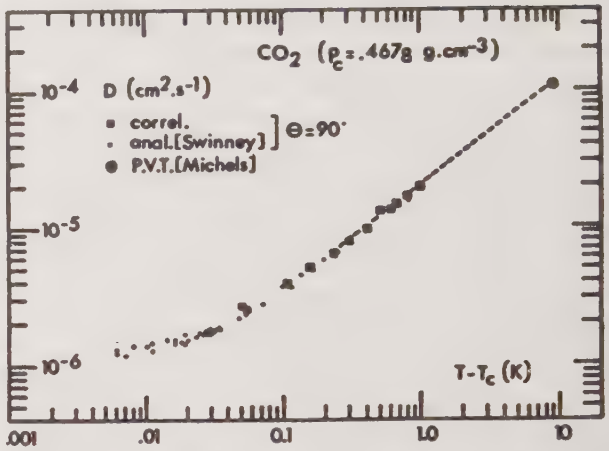

FIG. 1. D as a function of $T - T_c$ for CO_2 on the critical isochore. □: Correl., our data obtained with a digital correlator ($\theta = 90°$); ●: Anal., data of Swinney and Cummins (Ref. 37) obtained with a spectrum analyzer ($\theta = 90°$); ●: Thermodynamic values (see text and Refs. 31, 38, and 39).

III. POLARIZED RAYLEIGH LINE

To give a complete set of our results we report Rayleigh polarized scattering linewidth measurements approaching the critical temperature along the critical isochore of CO_2.

We used a Spectra Physics He–Ne laser model 125. The optical cell and thermostated enclosures were described in the previous section. The scattered light at 90° is focused on a pinhole in front of a photomultiplier tube RCA 31000 A working in the photon-counting regime. The analysis of photon-counting fluctuations was made with an ATNE 250-channel digital autocorrelator. The correlation functions are well represented by single exponential curves with a decay rate τ. The reproducibility of the measured value of τ is better than 1% in all the explored critical range, i.e., $0.01 < T - T_c < 1$ °C.

For $T - T_c = 1$ °C, we obtained $\tau = 1.04$ μs and for $T - T_c = 0.053$ °C τ reached 7.8 μs. These two values clearly show the well known critical slowing down of the entropy fluctuations.

We compared our results with those obtained by Swinney *et al.*[37] in similar experimental conditions (homodyne detection) although they used a conventional spectrum analyzer. We calculated the thermal diffusivity coefficient $D = \lambda/\rho C_p$ related to τ by $\tau^{-1} = Dq^2$, where λ is the thermal conductivity coefficient and C_p is the specific heat at constant pressure. The modulus of the momentum transfer q is the same in both experiments and equal to 1.556×10^{-3} Å (corresponding to the same scattering angle $\theta = 90°$ and the same exciting line $\lambda_0 = 6328$ Å). Figure 1 shows the agreement between the results. For comparison we plotted also the calculated value of D at $T - T_c = 9$ °C using thermodynamic measurements of λ,[38] ρ,[31] and C_p.[39] Although there is good

agreement between different measurements of D, the theoretical interpretation of its variation as a function of $T - T_c$ is still unsatisfactory: first, as the analysis of the data is doubtful because of the uncertainty of 30% for the value of the amplitude of the correlation length; second, because the separation between regular and critical parts of thermodynamic and transport properties of pure fluids is still poorly supported theoretically.[40] A study is being carried out to try to improve these two aspects in particular by an analysis of experimental results in terms of theoretical predictions of the renormalization group recently developed. In this paper, in light of the agreement shown in Fig. 1, we have used the critical data given by Swinney and Henry in their review paper (Table III in Ref. 30). Only the data on the isothermal compressibility were modified and not taken from Ref. 30 as we used our own determination for this quantity.[23] All the quantities calculated in below will use this set of data.

IV. POLARIZED RAMAN STUDY OF THE FERMI DIAD

We recorded the evolution of the polarized Fermi diad and the different combination bands and associated hot bands in a temperature range $0.005 < T - T_c < 10$ K. At each temperature, several records (at least three) were made allowing the monitoring of the stability of experimental conditions, mainly the incident laser intensity, the geometrical position of the cell relatively to the beam, and the focus of the beam lighting the input slit of the spectrometer. The experimental conditions, similar for all the recorded spectra, were as follows: The width of the slits was the same for all four slits and equal to 300 μm corresponding to a resolution of 2.4 cm^{-1} for the green band of excitation $\lambda = 5145$ Å. The displacement speed of the grating was 25 cm^{-1} per min with a time constant of 1 s. We used a scale calibration on recording paper of 5 cm^{-1}/cm. The reproducibility of the results allows us to estimate the relative intensity of the polarized Raman bands within 10% and their frequency positions within ± 0.5 cm^{-1}.

Figure 2 shows a typical recording of polarized Fermi diad at $T = 40$ °C. The unresolved bands look like triangular apparatus functions and are easy to read. The measured intensity corresponds to the height of the triangle, and the position in frequency is the position of the peak of the triangle. On the other hand, we always verified the symmetry of the triangular function in the above experimental conditions (the influence of the combination bands and hot bands on the profile of the two main bands is not observed because the frequency shift is large enough). The depolarized band was resolved, and consequently larger than the triangular function while the background intensity was small enough to be similar to a flat background. However, close to the critical temperature these conditions are less satisfactory owing to the presence of large turbidity and multiple scattering phenomena (see our analysis of results).

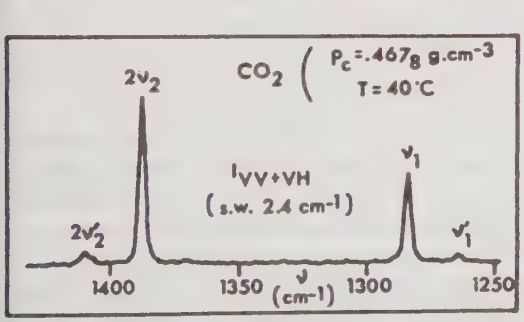

FIG. 2. Observed Raman polarized spectra ($VV + VH$) in the region of the Fermi diad ν_1, $2\nu_2$ of CO_2 at $T = 40$ °C ($\rho_c = 0.468$ g cm^{-3}) (vertical scale: relative intensity in arbitrary units). The spectral slit width is 2.4 cm^{-1}.

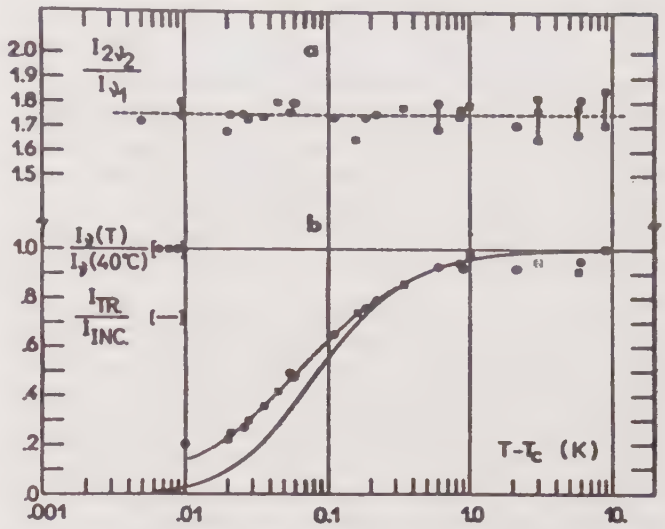

FIG. 3. (a) Plot of the Raman intensity ratio of the polarized Fermi diad ν_1, $2\nu_2$ in CO_2 versus a $\log(T - T_c)$ scale. (b) Plot of the Raman intensity ratio of the polarized $2\nu_2$ line at T °C to that at 40 °C, versus a $\log(T - T_c)$ scale. The solid line is the ratio of the transmitted laser intensity to the incident laser intensity.

A. Experimental results

We followed the behavior of the intensity and the position of the diad band while approaching the critical temperature along the critical isochore.

In the temperature range $0.005 < T - T_c < 9$ °C, no shift was observed in the frequency positions of the diad to within experimental accuracy. Moreover, as Fig. 3(a) shows, the ratio of the intensities of the two bands is constant in this temperature range though, for $T - T_c < 3$ °C, the respective intensity of each band is attenuated by the turbidity of the incident light.

Figure 3(b) shows the attenuation of the ratio of the measured intensity of the $2\nu_2$ band at temperature T to the corresponding value at $T = 40$ °C for the same band versus $\log(T - T_c)$. This ratio can be compared to the ratio of the transmitted laser intensity to the incident laser intensity for the following reasons: On one hand, the optical paths for the transmitted radiation and the scattered radiation are the same in the construction of our optical cell and in taking into account the observation geometry imposed by the spectrometer. On the other hand, for $T > T_c + 3$ °C, the transmitted intensity is equal at least to 96% of the incident intensity for an

optical path of 20 mm in the cell.

Near T_c ($T - T_c < 0.3\,^\circ\mathrm{C}$) Fig. 3(b) shows that the measured values $I^{\text{Raman}}_{VV+VH}(T)/I^{\text{Raman}}_{VV+VH}(40\,^\circ\mathrm{C})$ depart significantly from those which are expected from the turbidity. The explanation for this can be found in multiple scattering which occurs from very intense primary scattering and which is the origin of the progressive extension of the scattering volume up to that of the whole volume of the cell (critical opalescence phenomenon).

The quantitative interpretation of the supplementary contribution to the scattered light has been extensively studied in the past[41] in the framework of a mechanism of large uncorrelated Rayleigh–Rayleigh double scattering. In the same way we can introduce a mechanism of uncorrelated Rayleigh–Raman double scattering. The Raman–Raman terms, being of second order, do not contribute significantly because of the ratio of 10^{-3} which exists for the cross section of Raman to Rayleigh scattering. We did not attempt to make experimental study of this kind of multiple scattering because the experimental conditions associated with the Coderg spectrometer do not enable us to define the geometrical parameters which are necessary. Moreover, we shall see that the depolarized Raman scattering allows a better understanding of this phenomenon.

B. Discussion

Although the polarized Raman bands ν_1 and $2\nu_2$ are not resolved, the results are enough accurate to show that these bands are not perturbed by the cooperative modes characterizing the critical point. This behavior is in contrast to the anomalous behavior observed in the shift of the Raman Q branch of oxygen near the critical point as reported by Clouter *et al.*[42] Before giving a more detailed interpretation of our results we shall note that the process used by these authors to approach the critical point by working along the critical isotherm can explain their observation of anomalous behavior. In fact, by using this method of approach in the case of xenon[43] we have noted that when $T - T_c < 1\,^\circ\mathrm{C}$, it is almost impossible to know the exact value of the density in the scattering cell by measuring the pressure outside the cell. This comes from convective instabilities due to the existence of a large temperature variation of the pressure gauge which is independent of the knowledge of pVT data in that range.

We know that the perturbations of the energy level of molecules in fluids under pressure are interpreted in terms of intermolecular forces. The range of interaction of these forces is of the order of a few nm.[44] Thus, the shift in frequency of the ν_1 and $2\nu_2$ bands of gaseous carbon dioxide was studied as a function of the density (from 0.03 to 1.05 g cm^{-3}) at 40 °C.[45] This shift reflects only the molecular interactions as confirmed by recent measurements[46] along the coexistence curve. This last experiment shows that the temperature variation between −30 to 40 °C does not affect the vibrational energy levels of vibration. We can compare the results of these measurements with those obtained with our cell filled at the critical density. In this regard, we have completed our recordings in the single phase region by some recordings

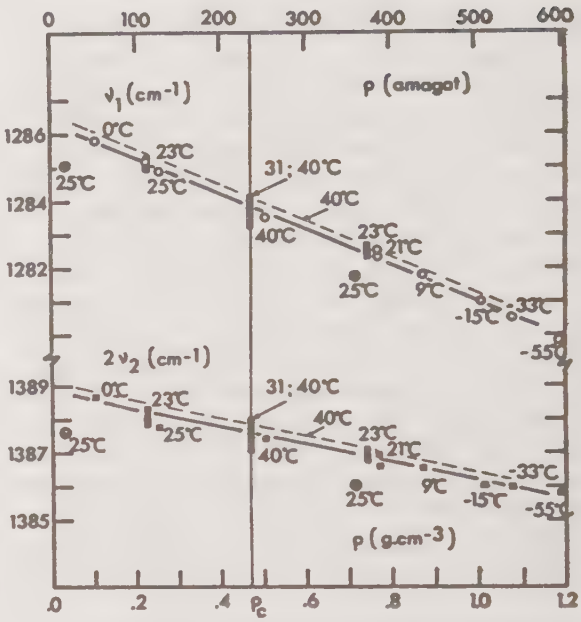

FIG. 4. Density dependence of the Raman frequencies for ν_1 and $2\nu_2$ vibrations in CO_2. ⊟: our results obtained with the critical isochoric optical cell (see text); o, ■: results obtained along the coexistence curve and at $T = 40\,^\circ\mathrm{C}$, $\rho = 0.5$ g cm^{-3} (Ref. 46); ⊖: results of Welsh, Pashler, and Stoicheff (Ref. 47); ---: results of Wright and Wang along the $T = 40\,^\circ\mathrm{C}$ isotherm (Ref. 45).

of the polarized Raman diad in the two phase region, in each phase at $T = 23$ and 28 °C and in the liquid phase at $T_c - T = 0.076$ and 0.006 °C. Figure 4 shows the good agreement between all the results of the frequency position fitted by the following linear relations:

$$\omega(\nu_1) = 1286.3 - 5.337\rho\,,$$

$$\omega(2\nu_2) = 1388.8 - 2.69\rho\,,$$

where ρ and ω are given, respectively, in g cm^{-3} and in cm^{-1}. Consequently, the approach to the critical point does not influence the energy transfer between the two levels in the Fermi resonance. Likewise we compared the ratio $I_{2\nu_2}/I_{\nu_1}$ of the intensity of the two bands. In Fig. 5 are clearly shown that the values of $I_{2\nu_2}/I_{\nu_1}$ obtained at the critical density are consistent with those obtained along the coexistence curve.[46] This monotonous behavior which is linear in first approximation near the critical density is associated with the variation of the frequency difference $2\nu_2 - \nu_1$ of the two levels in Fermi resonance when the density varies (Fig. 4). It is clear now that the density is the main variable in the description of the behavior of the Fermi resonance.

As a conclusion of this study of the polarized Raman diad ν_1, $2\nu_2$ of CO_2, it appears that the vicinity of the critical point does not modify the short range molecular interaction, which in turn only influences the energy levels of vibration. A continuous and linear change in the position of the corresponding Raman bands as a function of the density was observed over the whole critical region. Furthermore, we can reasonably assume that the width of these bands has a similar continuous change not perturbed in the critical region.

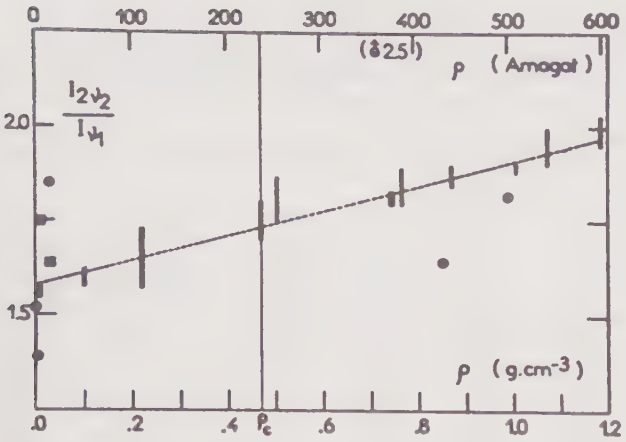

FIG. 5. Density dependence of the Raman intensity ratio of the polarized fermi diad ν_1, $2\nu_2$ in CO_2. ⊟: this work (critical isochoric cell: see text); ▮: Ref. 46 (along the coexistence curve); ○: Ref. 47; □: Ref. 48; ■: Ref. 49; ●: Ref. 50. The dashed line is the best linear density dependence fit of points of Ref. 46.

Knowing that the theory of critical phenomena suggests a universal character for pure fluids which is insensitive to the characteristics of the constituent molecules, we can generalize the above conclusion: Owing to interactions at large distances which are characteristic of the critical regime, the main cooperative effects do not influence the vibrational energy levels of constituent molecules, which are perturbed only by short range molecular interactions.

V. STUDY OF THE DEPOLARIZED RAYLEIGH BAND OF CARBON DIOXIDE

A. Results

We studied the evolution of the depolarized Rayleigh band of carbon dioxide at the approach to the critical temperature along the critical isochore by especially looking at $HV+HH$ (Table I). The experimental conditions generally used to record this component were chosen to take account of the fact that the FWHM of the spectra was about 25 cm^{-1}. The widths of the four slits of the spectrometer were identical and fixed at 200 μm, corresponding to a resolution of 1.6 cm^{-1} for the exciting band $\lambda = 5145$ Å. We used a grating displacement speed of 5 cm^{-1} per min and the recording paper displacement speed was 1 cm per min. The time constant was 2.5 s.

To test the reproducibility of our results we made several recordings of this component for one or two temperatures which are characteristic of each studied decade in $T - T_c$. Then the central part ($\Delta\omega < 50$ cm^{-1}) of the band was obtained with the maximum resolution allowed by the spectrometer (0.35 cm^{-1}), that is to say a slit width of 40 μm. The grating displacement speed was 1 cm^{-1} per min for a paper displacement speed of 1 cm per min with a time constant of 5 s. Moreover, we made an accurate measurement of the profile of the far side of the band ($\Delta\omega > 30$ cm^{-1}). To do so we maximized the spectral intensity by using a larger slit width (up to 600 μm), or a stronger laser power (up to 500 mW), or both. Our choice was determined by high stability of the temperature inside the scattering cell and shape of the recorded profile unperturbed by the width of slits.

To improve the quality of these recordings of the $HV+HH$ component, we recorded also the $VH+VV$ component under the same conditions. Then, when the temperature of the experiment was not too close to T_c ($T - T_c > 0.5$ °C), we verified that the spectral densities of these two components were in the ratio 6/7 (the values obtained varied from 0.85 to 0.90). Near T_c the presence of multiple scattering significantly modified this ratio because they act with factors which depend on the observation geometry and are different for VV, VH, and HH components.[51] Moreover, comparison of the recordings of the center of each component at high resolution allows us to see the influence of the wing of the polarized Rayleigh band, the intensity of which increases strongly approaching T_c.[23] We verified that the profile of the depolarized band was not modified as soon as the shift in frequency was larger than 2 cm^{-1}.

B. Profile analysis

We recall that this study was carried out to investigate a possible modification of local dynamical behavior of a pure fluid consisting of anisotropic molecules under the influence of important cooperative phenomena in the neighborhood of its critical point. The analysis of our results concerns chiefly the determination of a possible distortion of the depolarized band profile which is characteristic of the local dynamics approaching T_c. Therefore, independently of the exact physical meaning attached to the process of spectral analysis used, it is important to note that this process must yield one or several parameters typical of local dynamics, the development of which will be followed in terms of $T - T_c$. It is apparent from recent studies of the behavior of fluids using depolarized light scattering experiments that the main problem lies in the type of dynamics in question and the proposed solutions are controversial. That is to say that at present it is difficult to assess which phenomena gives rise to this scattering and to what extent.

In the case of fluids composed of atoms or spherical molecules, the anisotropic part of the polarizability tensor responsible for the depolarized scattering can be induced only by collisions (Rayleigh) and unsymmetrical vibrations (Raman). Experimentally, a quasiexponential decrease of the spectral intensities in the wings of the Rayleigh band is observed for compressed noble gases and atomic or molecular liquids. The theoretical interpretation involves anisotropic induction by binary interactions. The problem is to know how the anisotropic character of the polarizability is induced in terms of the distance between the two interacting atoms or molecules. When this distance is large enough, the model of one dipole inducing another dipole is well suited.[16(a),(c)] For smaller distances, we must take into account electronic overlaps and distortion of the molecular framework.[16(b)]

For fluids composed of nonspherical molecules (case of CO_2) the permanent anisotropy of the polarizability owing to orientational fluctuations of molecules also

TABLE I. Measurements of spectral intensities of the Stokes side of the depolarized $HH+HV$ Rayleigh line in CO_2 near its critical point. The measurements are referred to the one intensity value at the 20 cm^{-1} frequency shift. For each measurement the spectral intensities are corrected by factors including both the frequency dependence of the total spectral response of the photomultiplier tube and the detailed balance principle of quantum effects. Three sets of experiments are reported with their respective symbols ⊖, ⊟, ⊗ inferred in the different figures.

$T-T_c$ (°G) \ $\Delta\omega$ (cm^{-1})	5	10	15	20	25	30	35	40	45	50	55
⊟ 9.00	1.618	1.400	1.194	1.000	0.844	0.700	0.589	0.496	0.409	0.338	0.268
⊖ 6.07	1.622	1.420	1.201	1.000	0.851	0.722	0.603	0.505	0.422	0.340	0.277
⊟ 5.77	1.652	1.405	1.190	1.000	0.828	0.692	0.583	0.485	0.403	0.326	0.265
⊖ 4.00		1.508	1.190	1.000	0.823	0.699	0.585	0.485	0.403	0.339	0.273
⊟ 3.00	1.666	1.419	1.208	1.000	0.835	0.693	0.576	0.482	0.397	0.320	0.258
⊖ 2.15	1.655	1.410	1.201	1.000	0.822	0.680	0.568	0.469	0.386	0.314	0.251
⊟ 1.01	1.691	1.438	1.205	1.000	0.827	0.692	0.579	0.484	0.398	0.334	0.255
⊗ 0.870	1.704	1.424	1.196	1.000	0.831	0.695	0.582	0.477	0.382	0.310	0.246
⊖ 0.855	1.689	1.461	1.224	1.000	0.835	0.709	0.591	0.483	0.394	0.320	0.257
⊗ 0.596	1.685	1.431	1.206	1.000	0.825	0.684	0.569	0.472	0.388	0.319	0.251
⊟ 0.354	1.700	1.429	1.183	1.000	0.822	0.675	0.560	0.467	0.386	0.312	0.251
⊖ 0.218	1.657	1.442	1.213	1.000	0.831	0.696	0.572	0.478	0.392	0.317	0.252
⊖ 0.185	1.625	1.426	1.204	1.000	0.822	0.671	0.560	0.468	0.386	0.310	0.241
⊟ 0.157	1.694	1.412	1.174	1.000	0.824	0.688	0.571	0.474	0.389	0.306	0.245
⊗ 0.110											
⊟ 0.100	1.658	1.430	1.210	1.000	0.825	0.681	0.574	0.469	0.383	0.303	0.257
⊗ 0.059	1.699	1.418	1.204	1.000	0.829	0.681	0.575	0.474	0.392	0.312	0.249
⊖ 0.054	1.652	1.461	1.216	1.000	0.805	0.675	0.550	0.465	0.378	0.310	0.251
⊟ 0.046	1.691	1.414	1.204	1.000	0.835	0.691	0.569	0.474	0.386	0.306	0.251
⊟ 0.036	1.664	1.465	1.228	1.000	0.828	0.679	0.568	0.469	0.385	0.323	0.258
⊟ 0.028	1.639	1.407	1.204	1.000	0.820	0.667	0.542	0.450	0.373	0.312	0.254
⊗ 0.026	1.653	1.429	1.209	1.000	0.833	0.691	0.577	0.481	0.398	0.321	0.257
⊟ 0.021	1.637	1.433	1.211	1.000	0.842	0.702	0.582	0.488	0.395	0.329	0.260
⊗ 0.020											
⊗ 0.009_5	1.694	1.444	1.203	1.000	0.837	0.697	0.575	0.479	0.392	0.328	0.262
⊗ 0.005		1.418	1.184	1.000	0.838	0.690	0.570	0.471	0.386	0.322	0.254

	60	65	70	80	90	100	110	120	130	140	150
⊟ 9.00	0.212	0.169	0.132	0.0758	0.0450	0.0273	0.0171	0.0114	0.0074	0.0048	0.0040
⊖ 6.07	0.223	0.175	0.141	0.0840	0.0514	0.0317	0.0128	0.0139			
⊟ 5.77	0.208	0.165	0.128	0.0769	0.0451	0.0266	0.0164	0.0099	0.0070	0.0049	0.0032
⊖ 4.00	0.226	0.177	0.145	0.0870	0.0542	0.0316	0.0198				
⊟ 3.00	0.208	0.165	0.129	0.0770	0.0457	0.0275	0.0170	0.0107	0.0067	0.0044	0.0033
⊖ 2.15	0.203	0.162	0.128	0.0804	0.0511	0.0326	0.0202				
⊟ 1.01	0.204	0.160	0.127	0.0743	0.0438	0.0254	0.0154	0.0106	0.0070	0.0040	
⊗ 0.870	0.196	0.156	0.122	0.0714	0.0422	0.0251	0.0154	0.0099	0.0071	0.0043	0.0031
⊖ 0.855	0.205	0.160	0.124	0.0782	0.0492	0.0292					
⊗ 0.596	0.204	0.158	0.124	0.0737	0.0441	0.0270	0.0177	0.0118	0.0074	0.0049	0.0034
⊟ 0.354	0.200	0.156	0.121	0.0707	0.0442	0.0262	0.0161	0.0100	0.0070	0.0046	
⊖ 0.218	0.204	0.160	0.126	0.0783	0.0474	0.0255	0.0183				
⊖ 0.185	0.193	0.154	0.123	0.0722	0.0442	0.0282	0.0175				
⊟ 0.157	0.197	0.157	0.124	0.0709	0.0438	0.0258	0.0156	0.0103			
⊗ 0.110											
⊟ 0.100	0.200	0.158	0.125	0.0731	0.0448	0.0271	0.0180				
⊗ 0.059	0.195	0.153	0.120	0.0718	0.0431	0.0266	0.0181	0.0115	0.0069		
⊖ 0.054	0.199	0.155	0.121	0.0746	0.0462	0.0264					
⊟ 0.046	0.201	0.159	0.123	0.0749	0.0443	0.0256	0.0155				
⊟ 0.036	0.204	0.160	0.128	0.0767	0.0436	0.0295					
⊟ 0.028	0.204	0.164	0.129	0.0765	0.0460	0.0296					
⊗ 0.026	0.204	0.163	0.130	0.0767	0.0433						
⊟ 0.021	0.203	0.164	0.129	0.0762	0.0455	0.0288					
⊗ 0.020											
⊗ 0.009_5	0.208	0.168	0.134	0.0800							
⊗ 0.005	0.198	0.158	0.123								

gives rise to depolarized scattering. In this case, there will be simultaneous orientational and collisional dynamics. The functional form of the spectrum arising from these two types of dynamics and their possible mutual interaction is not theoretically understood. On the experimental level, the arbitrary character of the separation of these two effects can be found in the literature in which relative intensities are reported, which varied over one order of magnitude for a fluid under similar conditions. However, from these different ap-

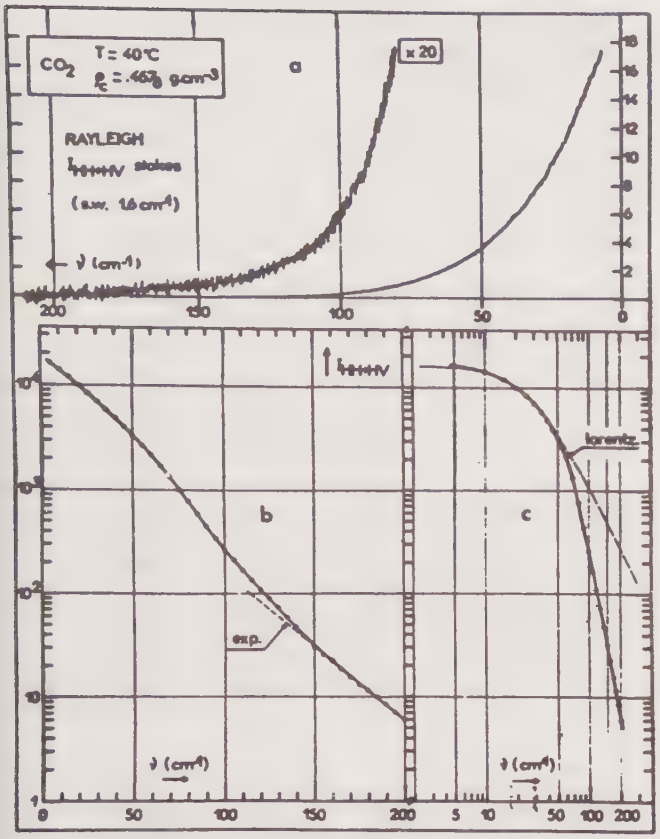

FIG. 6. (a) Linear chart recording of the Stokes side of experimental CO_2 depolarized Rayleigh spectra at $T = 40\,°C$, $\rho_c = 0.468\ g\,cm^{-3}$, with $1.6\ cm^{-1}$ of the spectral slit width. The critical scale change represents a factor of 20 in arbitrary units. (b) Logarithmic representation of the spectral intensity versus a linear scale of the frequency shift. (c) Log–log representation of the depolarized Rayleigh spectrum. The dashed line is the best Lorentzian profile adjusted in the limited range 5 to 50 cm^{-1} of the frequency shift.

proaches the following general considerations can be drawn: For liquids composed of simple polyatomic anisotropic molecules (N_2, O_2, CO_2), the profile of the depolarized Rayleigh spectra is not Lorentzian,[52,53] while showing the presence of orientational dynamics since the induced anisotropy contribution can be neglected even for relatively high densities. On the other hand, organic liquids formed of strongly anisotropic molecules show, at room temperature, a depolarized Rayleigh profile well fitted by a Lorentzian.[54] This is explained by using large cooperative effects in the reorientational motions and as for diatomic molecules, only the orientational dynamics contributes in a sensitive way to the scattering.

Following these considerations, we were first interested in the depolarized Rayleigh spectra of CO_2 recorded far from the critical point, i.e., when $T - T_c > 3\,°C$. These conditions allow us to be sure that the influence of multiple scattering phenomena is negligible (Fig. 10, Ref. 23). Spectra are suitably analyzed up to frequency shifts of 250 cm^{-1} with respect to the exciting frequency. The spectral intensity decreases over four decades. Figure 6(a) shows the Stokes part of the *HH* + *HV* spectrum obtained for $T - T_c = 9\,°C$, i.e., at $T = 40\,°C$. The functional complexity of the profile is illustrated in parts (b) and (c) of this figure. We have used semilogarithmic and logarithmic coordinates to put in evidence the exponential and Lorentzian profiles.

For frequency shifts larger than 100 cm^{-1}, the profile is exponential. This exponential tail which extends beyond 200 cm^{-1} is found in all liquids and compressed gases studied to date and its presence appears to be independent of molecular shape. This profile should be connected to an interaction mechanism at short distance where the anisotropy can result from the overlap of the electronic clouds and the distortion of molecular geometry. The time range concerned is equivalent to the collision time for which the precise form of the correlation function is not very important. Spectral intensities are small [<1/100 of I (20 cm^{-1})] and we can reasonably think that this type of contribution is negligible. Unfortunately, near T_c, where the useful signal is attenuated by the turbidity, we cannot determine correctly this part of the profile.

We have still to characterize the central part of the spectrum ($\Delta\omega < 100\ cm^{-1}$). Initially, we assume that the contribution to the spectral intensity owing to induced anisotropy phenomena of D.I.D. type is of the order of a few percent. This hypothesis seems to be justified by the previous measurements[23] of the depolarization ratio $\eta = I_{HH+HV}/I_{VV}$ for a distance from T_c of 10 °C. Figure 11 of Ref. 23 shows that the contribution of this mechanism, which is the only one possible for all spherical molecules of Xe and SF_6, is one order of magnitude weaker than the total measured value in the case of CO_2. This was confirmed experimentally[52,53] for diatomic molecules N_2, O_2, and CO which are simpler than the CO_2 molecule and also for more complex anisotropic molecules.[54] We thus assign the central part of the depolarized Rayleigh profile of CO_2 uniquely to the reorientation motions of the molecule in its neighborhood.

As shown in Fig. 6(c) the experimental profile cannot be reproduced correctly by one Lorentzian. This result is analogous to the one obtained with diatomic molecules.[52] However, we make use of the fact that the fit is right over about one decade to define the two first parameters which will allow us to follow the behavior of the spectral shape. Of course, these parameters will be the half-width at half-height and the height at the center of the Lorentzian. For each temperature shift, from the critical temperature we have always worked out the best fit in the frequency range defined by the recorded spectrum at 40 °C, that is to say $7 < \Delta\omega < 70\ cm^{-1}$.

Finally, we calibrated all our Stokes spectra at unit spectral intensity for a shift of 20 cm^{-1} with regard to the exciting frequency. Every spectrum is registered at intervals of 1 cm^{-1} when the instrumental resolution is 0.35 cm^{-1} and every 5 cm^{-1} when the resolution is 1.6 cm^{-1}. Frequency ranges cover from 3 to 30 cm^{-1} in the first case and 5 to 100 cm^{-1} in the second case. Then we can see a possible modification of the depolarized Rayleigh profile approaching the critical temperature through the variations of the numbers connected to each of the frequency shifts.

TABLE II. Measurements of the normalized spectral intensities of the Stokes side of the depolarized *HH+HV* Raman band centered at the $2\nu_2$ frequency of the polarized Raman–Fermi diad of CO_2. See Sec. VI and Table I.

$T-T_c$ (°C) \ $\Delta\omega$ (cm^{-1})	5	10	15	20	25	30	35	40	45	50
9.00	1.528	1.337	1.163	1.000	0.868	0.736	0.615	0.521	0.417	0.337
6.07	1.500	1.333	1.147	1.000	0.853	0.726	0.612	0.510	0.422	0.337
5.77	1.478	1.304	1.145	1.000	0.870	0.754	0.638	0.530	0.444	0.368
4.00										
3.00	1.517	1.328	1.148	1.000	0.852	0.724	0.593	0.500	0.414	0.328
2.15	1.511	1.323	1.149	1.000	0.851	0.723	0.602	0.511	0.425	0.355
1.01	1.561	1.393	1.179	1.000	0.869	0.714	0.590	0.499	0.404	0.339
0.870	1.503	1.310	1.144	1.000	0.847	0.722	0.608	0.508	0.419	0.337
0.855	1.479	1.324	1.153	1.000	0.850	0.716	0.592	0.490	0.408	0.329
0.596		1.300	1.141	1.000	0.865	0.737	0.619	0.512	0.423	0.346
0.354	1.473	1.299	1.135	1.000	0.856	0.731	0.615	0.500	0.423	0.346
0.218										
0.185	1.552	1.358	1.170	1.000	0.845	0.716	0.582	0.479	0.400	0.320
0.157	1.516	1.344	1.163	1.000	0.864	0.733	0.634	0.534	0.430	0.317
0.110	1.552	1.347	1.163	1.000	0.868	0.732	0.605	0.487	0.395	0.316
0.100										
0.059	1.491	1.302	1.140	1.000	0.868	0.743	0.615	0.491	0.409	0.325
0.054										
0.046	1.423	1.319	1.154	1.000	0.868	0.744	0.619	0.497	0.414	0.327
0.036	1.492	1.311	1.133	1.000	0.850	0.717	0.606	0.487	0.400	0.324
0.028										
0.026										
0.021	1.526	1.328	1.160	1.000	0.861	0.746	0.604	0.478	0.428	0.333
0.020	1.495	1.322	1.141	1.000	0.862	0.740	0.610	0.477	0.420	0.340
0.009_5	1.500	1.334	1.152	1.000	0.857	0.715	0.592	0.488	0.404	0.318
0.005	1.493	1.307	1.132	1.000	0.868	0.730	0.605	0.497	0.400	0.315

	55	60	65	70	75	80	85	90	95	100
9.00	0.260	0.201	0.149	0.115	0.0868	0.0694	0.0590	0.0382		
6.07	0.271	0.212	0.163	0.128	0.0951	0.0745	0.0549	0.0431	0.0392	
5.77	0.293	0.232	0.180	0.148	0.1190	0.1014	0.0826	0.0580	0.0377	
4.00										
3.00	0.269	0.207	0.138	0.097	0.0759	0.0586	0.0414	0.0345		
2.15	0.294	0.234	0.181							
1.01	0.286	0.225	0.171	0.132	0.1000	0.0714	0.0464	0.0357		
0.870	0.267	0.214	0.171	0.137	0.1030	0.0797	0.0683			
0.855	0.268	0.218	0.176	0.137						
0.596	0.282	0.231	0.186	0.146	0.1130	0.0833	0.0615	0.0436	0.0321	0.0256
0.354	0.289	0.240	0.198	0.164	0.1290	0.0962	0.0769			
0.218										
0.185	0.283	0.209	0.144	0.090						
0.157	0.272	0.200	0.140							
0.110	0.263	0.211	0.158	0.127	0.0921					
0.100										
0.059	0.257	0.200	0.162	0.143	0.0981	0.0757				
0.054										
0.046	0.272	0.214	0.154	0.115						
0.036	0.274	0.198	0.133							
0.028										
0.026										
0.021	0.270	0.210	0.152							
0.020	0.276	0.220	0.170							
0.009_5	0.282	0.191								
0.005	0.260									

VI. STUDY OF THE DEPOLARIZED RAMAN SCATTERING OF FERMI DIAD

A. Results

The *HH+HV* spectra of the ν_1, $2\nu_2$ diad were recorded (Table II) with a slit width of 600 μm which corresponds to a resolution of 4.8 cm^{-1} for the exciting line $\lambda = 5145$ Å. A check of the good definition of the profile was mad for each temperature farthest from T_c where spectra ar well recorded with a resolution two times larger (slits of 300 μm). We used a grating displacement speed of 2.5 cm^{-1} per min with a paper recording speed of 0.5 cm per min and a time constant of 5 s. The frequency scale on the paper is the same as that for the recording

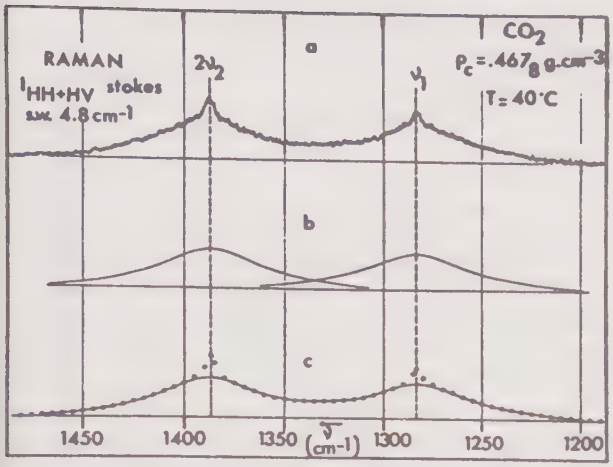

FIG. 7. (a) Linear chart recording of the Stokes side of experimental depolarized Raman Spectra in the region of the ν_1, $2\nu_2$ Fermi diad of CO_2 at $T=40\,°C$, $\rho_c=0.485\ g\,cm^{-3}$, with 4.8 cm^{-1} of the spectral slit width. (b) Estimated intensity profile of each rotovibrational Raman band of the ν_1, $2\nu_2$ Fermi diad of CO_2 (see text). (c) Comparison of the additional result of estimated profiles of part (b) with experimental depolarized Raman spectra [part (a)]. ●: experimental profile. ---: estimated profile.

of the polarized Raman doublet and this allows a direct comparison of the frequency position of bands. A good definition of the base line is guaranteed by recording up to 200 cm^{-1} on either side of the center of each band of the diad. The frequency was swept from 950 to 1600 cm^{-1}.

B. Profile analysis

The theoretical analysis of the Raman profile of a dense fluid is not well known (and subject to several hypotheses to be described by one analytical formulation). Moreover, in the case of CO_2, bands have to be added for possible energy transfers owing to the Fermi resonance. We followed the same steps based on general considerations that were worked out in the profile analysis of the depolarized Rayleigh band. The analysis method used takes into account the quality of the recorded spectra for temperatures far from T_c and gives a result substantiated by the following analysis.

Figure 7(a) shows a spectrum of a depolarized Raman diad recorded at $T=40\,°C$. It underlines the fact that the separation between the two vibrational bands ν_1 and $2\nu_2$ in Fermi resonance indicates an important overlapping of corresponding depolarized Rayleigh wings in the frequency range between ν_1 and $2\nu_2$, which can modify slightly the profile of the central part of these bands. Furthermore, this last part is modified by an intensive polarized component owing to interference depolarization (by optical windows and nonzero openings of the slits).

Only the high frequency and low frequency parts of this depolarized diad located further than 20 cm^{-1} from the respective center of each band can be considered as not perturbed by mutual overlapping.

However, we can simultaneously treat each depolarized band associated with the corresponding vibrational band as being isolated. This means that we consider the depolarized bands as profiles with a purely rotational origin. This is reasonable. Clearly, high and low frequency parts of the diads which show broad enough profiles ($\simeq 28\ cm^{-1}$) are insensitive to the vibrational relaxation arising from intermolecular forces. Furthermore, Fig. 4 shows that the shift of two polarized bands ν_1 and $2\nu_2$ stays small at the critical density, showing a small influence from molecular interactions and consequently a width of depolarized vibrational bands which can be neglected. Moreover, the respective spectral intensity of two depolarized wings unperturbed by overlapping are very close [the low frequency part is slightly (10%) smaller than the high frequency part] which is consistant with the hypothesis of separation of rotational and vibrational motions because it involves the fact that the only possible energy transfer owing to the Fermi resonance is that of vibrational energy.

First, we fitted the low and high frequency parts of the diad beginning at 20 cm^{-1} from the respective center of each band. Then these fitted profiles were drawn symmetrically with respect to those centers in the ν_1 and $2\nu_2$ interval. Then we added the spectral intensities in the overlapping range to obtain with satisfactory accuracy the experimental profile in this range. At least the central part of every band was fitted taking into account the far wing contribution of the other band and by removing the polarized spectrum contribution. We obtain a symmetrical profile for every depolarized band of the diad which correctly reproduces the experimental profile by simple addition [Fig. 7(c)].

This method was repeated for all recorded spectra at different distances from the critical temperature. The characterization of the various profiles was carried out in an analogous manner to the depolarized Rayleigh profiles. As for these Rayleigh profiles, the depolarized Raman profiles cannot be fitted by one Lorentzian over the whole spectral range but only over a range large enough (from 10 to 70 cm^{-1}) to have a significant fit. Here too, for all spectra, the fit was obtained in the same spectral interval defined in the recorded spectrum at 40 °C. We followed the behavior of the half-width at half-height and the intensity of the Lorentzian in terms of $T-T_c$.

VII. DISCUSSION OF RESULTS OBTAINED IN DEPOLARIZED RAYLEIGH AND RAMAN SCATTERING

The two main parts of this discussion concern the variation of the $\Gamma_{Lorentz}$ and $I_{Lorentz}$ parameters, along the critical isochore approaching the critical point. These parameters characterize the Lorentzian profiles adjusted to the experimental Rayleigh and Raman profiles, following methods developed in Secs. V and VI. We will obtain some fundamental results without having to interpret the nature of local dynamics responsible for the exact shape of experimental profiles. From these results, in the last part of the Discussion, we will provide some phenomenological background for reorientational motions in carbon dioxide near its critical point.

A. Intensities

The behavior of the intensity of the fitted Lorentzian bands is reported in the lower part of Figs. 8 and 9. As for the Raman polarized band (Fig. 3, Sec. IV) we are interested in the evolution of the ratio of the intensity of the Lorentzian profile fitted on the spectrum at T °C and the corresponding ratio at 40 °C as a function of the $\log(T - T_c)$. Here also we observe a decrease of this ratio with decreasing $T - T_c$. For $0.5 < T - T_c < 9$ °C this behavior is mainly due to turbidity phenomena which progressively attenuate the intensity of the incident and scattered light crossing the cell.

For $T - T_c < 0.3$ °C the ratio $I_{\text{Lorentz}}(T\,°\text{C})/I_{\text{Lorentz}}(40\,°\text{C})$ significantly deviates from I_{TR}/I_{INC}. We get here a similar result to that obtained with the intensity of the polarized Raman diad. In a similar way we explain this fact in terms of multiple scattering phenomena owing to very intensive entropy fluctuations.

We will give a clear picture of this complementary contribution by following the evolution of the total spectrum of the depolarized Raman diad approaching T_c. On Fig. 10 are reproduced five recordings corresponding to characteristic $T - T_c$ differences between 10 and 0.01 °C.

As soon as $T - T_c < 0.3$ °C, we see on Fig. 10 a significant increase of two unresolved narrow bands which are positioned on the ν_1 and $2\nu_2$ frequencies of polarized bands. This increase which is associated with the decrease of the corresponding large band intensity leads to the depolarized doublet spectrum having a similar shape to that of the polarized diad (Fig. 2).

We then can define the intensity of these unresolved

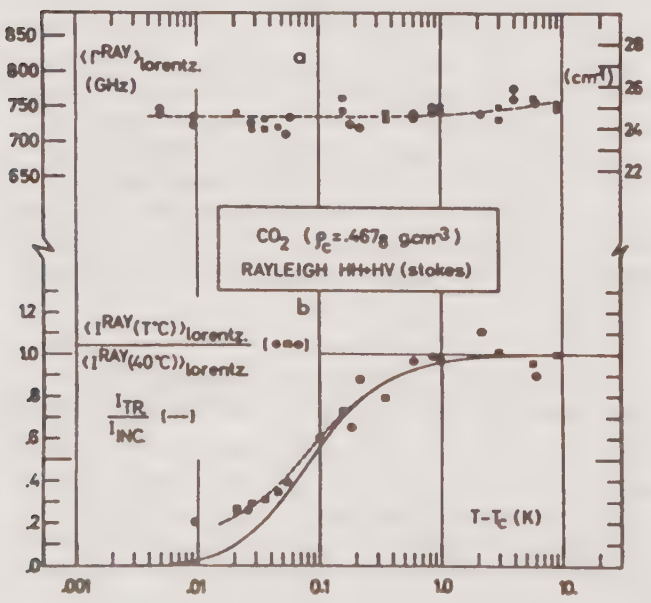

FIG. 8. (a) Plot of the HWHM of the Lorentzian profile adjusted on the limited frequency shift range at the experimental Rayleigh spectrum (see text) versus a $\log(T - T_c)$ scale. (b) Plot of the intensity ratio of this Lorentzian profile at T °C to that at 40 °C versus a $\log(T - T_c)$ scale. The solid line is the ratio of the transmitted laser intensity to the incident laser intensity.

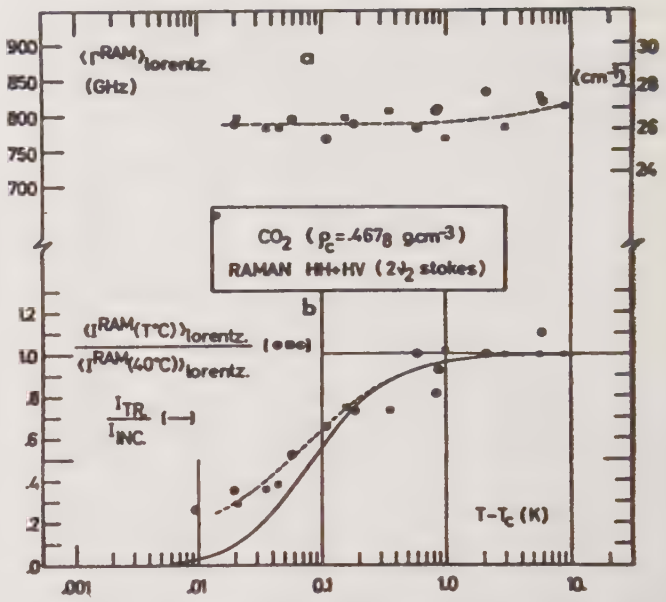

FIG. 9. (a) Plot of the HWHM of the Lorentzian profile adjusted on the limited frequency shift range at the estimated $2\nu_2$ Raman profile (see text) versus a $\log(T - T_c)$ scale. (b) Plot of the intensity ratio of the Lorentzian profile at T °C to that at 40 °C versus a $\log(T - T_c)$ scale. The solid line is the ratio of the transmitted laser intensity to the incident laser intensity.

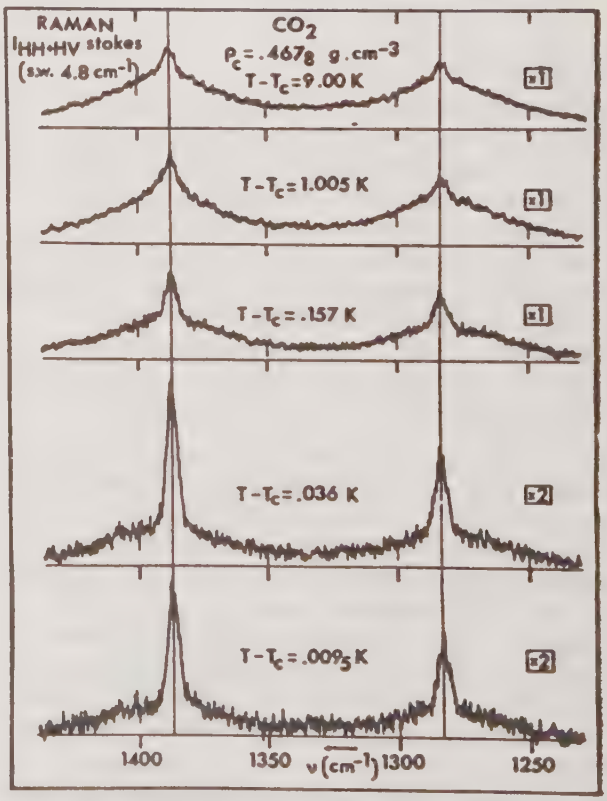

FIG. 10. Stokes side of experimental depolarized Raman spectra in the region of the ν_1, $2\nu_2$ Fermi diad of CO_2 obtained at various $T - T_c$ along the critical isochore (the spectral slit width was 4.8 cm^{-1}). The vertical scale of this different spectral intensities is in the same arbitrary units.

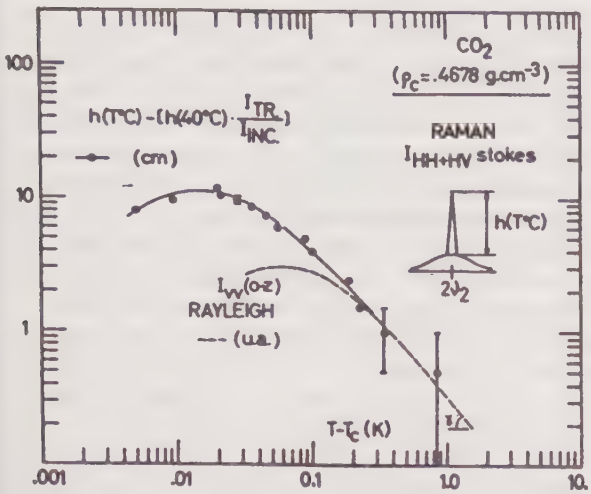

FIG. 11. Plot of corrected height (see text) of the superimposed depolarized Raman peak at the $2\nu_2$ frequency versus $T-T_c$ (log–log scales). The dashed line is the intensity of the polarized Rayleigh line calculated in the Ornstein–Zernike approximation (see text) (vertical scale: arbitrary units).

narrow bands in arbitrary units by their height h above the wide bands (in our case we directly use the measured height). To interpret the behavior of h in terms of $T-T_c$ by rescattering mechanisms, it is necessary to recall some considerations developed in our analysis of the depolarized Raman profile recorded at 40 °C (Sec. V).

Far away from the critical point, peaks centered at ν_1 and $2\nu_2$ above the wide profiles are only due to a part of the corresponding polarized contribution, due to parasite depolarized phenomena. Thus, the peak intensity is proportional to the polarized Raman intensity. In the absence of rescattering phenomena and with the reasonable hypothesis that the parasite depolarization ratio is constant for temperature variations in the range from 31 to 40 °C, the evolution of intensities of the observed 40 °C peaks, approaching T_c, must be ruled by the turbidity alone which affects the scattered Raman polarized intensity, i.e., that with our notation, the heights measured at T °C and $T=40$ °C must be related by

$$h(T)=h(40\,^{\circ}\mathrm{C})\times\frac{I_{TR}}{I_{INC}}\,.$$

The result is that the difference between the measured height at T °C and the value expected from the turbidity attenuation is a measure of multiple rescattering contributions. Figure 11 shows the evolution in logarithmic coordinates of this rescattering in terms of the distance from the critical temperature. This behavior is comparable to that observed in the previous studies of Rayleigh rescattering mechanisms owing to entropy fluctuations in the critical region.[23] In the present case, we must obviously introduce into the series of Rayleigh rescattering a Raman scattering process. However, all the other features developed in the previous studies remain valid. In particular, the fact that we observed a depolarized spectrum analogous to the polarized spectrum is still only explained by geometrical considerations. Only the first scattering takes place necessarily in the volume illuminated by the laser beam. The successive rescatterings can occur in any point of the cell. The last scattering takes place necessarily in the volume observed by the detector. If, as is the case in our experiment, the observation geometry is fixed and if we make the hypothesis that the main contributions are those due to a second rescattering uncorrelated to the first one, we can predict the relative behavior of the intensity of the narrow Raman depolarized band which grows above the corresponding wide band. Indeed, as there are only two scattering mechanisms, one is necessarily Rayleigh and the other Raman.

Approaching T_c, the Rayleigh scattering intensity due to entropy fluctuations diverges. In the $q\xi<1$ range, the divergence is described correctly by the Ornstein–Zernike theory corrected for turbidity effects (in our case $q\xi<1$ corresponds to $T-T_c>0.03$ K). We have seen that the intensity of polarized Raman scattering has a regular behavior which can be explained only in terms of turbidity and multiple scattering phenomena. Then, in the framework of uncorrelated double scatterings, the abnormal behavior of the intensity of the narrow Raman band is due only to the critical behavior of the polarized Rayleigh scattering. This can be verified in Fig. 11 where the points furthest from T_c, though having a large experimental uncertainty, are compatible with this theoretical prediction. The dashed line curve represents the relative behavior of the Rayleigh intensity I_{VV}^{Ray} calculated in the Ornstein–Zernike approximation and corrected for the turbidity effect. We find again here a result previously observed for pure fluids.[23] In the range $0.1<T-T_c<1$ °C, i.e., when the corrections owing to the turbidity effect are not too important and can be determined correctly from the values of I_{TR}/I_{INC}, we observe the behavior of multiple scattering in describing it qualitatively in terms of the only contributions owing to an uncorrelated double scattering. For $T-T_c<0.1$ °C the divergences observed in Fig. 11 are certainly related to higher order scattering. Moreover, the important corrections of turbidity which take into account the geometrical observation conditions are not satisfactorily represented by the ratio I_{TR}/I_{INC}.

Obviously, our analysis of the behavior on the approach to T_c of the intensity of the narrow depolarized Raman bands in terms of multiple scattering can be generalized for other bands. For this it is sufficient to include in the series of rescatterings the scattering mechanism of interest. So we explain all the observed deviations between the relative measured intensities and those expected from the turbidity phenomena as well as in the case of depolarized Rayleigh band (Fig. 8), as in the cases of the narrow polarized Raman bands (Fig. 3) and of the wide depolarized Raman bands (Fig. 9).

This phenomenon should explain the surprising strong narrowing of the depolarized Raman lines of nitrobenzene in a critical solution with *n*-hexane as reported in Ref. 7(c). A high resolution is indeed needed to distinguish the multiple scattering peak. When the resolution is not high enough the spectrum + peak looks like a single line which seems to become stronger and narrower near T_c.

The most direct experimental result which confirms this analysis was the recording of the profiles of the depolarized Rayleigh polarized and depolarized ν_1, $2\nu_2$ Raman diad by observing a volume of fluid which does not contain the excitator laser beam. This observation was made at $T - T_c = 0.020$°C.

B. Bandwidths

As is clearly shown in Fig. 8(a), the half-width at half-height of the Lorentzian adjusted to the depolarized Rayleigh experimental profile does not vary significantly approaching T_c. The same behavior occurs in the case of the depolarized Raman band centered on the $2\nu_2$ frequency of the Fermi diad [Fig. 9(a)]. Tables I and II generalize this behavior to the whole profiles. In fact, spectrum intensities, normalized to unity for $\Delta\omega = 20$ cm^{-1}, are constant for the same distance from the central frequency over the three decades in $\log(T - T_c)$ $(0.01 < T - T_c < 10$°C). Consequently, if molecular reorientational motions show a collective behavior (Rayleigh scattering), they remain extremely fast and their spatial range short. Also, this behavior is not influenced by the low frequency-large distance critical modes associated to fluctuations of the order parameter $\rho - \rho_c$. These results are different to those obtained in depolarized Rayleigh scattering in critical binary mixtures. In the case of CO_2 near its critical point, the frequencies for reorientational motions (~750 GHz in the Rayleigh case) remain one order of magnitude higher that cutoff frequencies of sound modes or relaxation phenomena of the critical contribution to the viscosity.[55]

C. Reorientational motions

The results just analyzed show some features of the orientational local order of carbon dioxide near its critical point. In addition, it is necessary to remember that even if the critical density value is large, the liquid density value at the triple point is three times greater. Consequently, in the critical region, we can limit the study of the local order to the contributions of the near neighbors of one CO_2 molecule. This is confirmed experimentally by the similarity of depolarized Raman and Rayleigh profiles (Tables I and II) and by the close values of the half-width at half-height of Lorentzian profiles adjusted in almost identical conditions to the experimental spectra: Γ(Rayleigh) ~ 750 GHz; Γ(Raman) ~ 800 GHz. It follows that statistical orientation correlations are small. Consequently, a symmetry (in the meaning of Quentrec[44]) of local orientation order exists where the lifetime is certainly greater than the characteristic reorientation time of a single molecule. This can be justified in terms of the correlation function $\phi(t)$ obtained by Fourier transform of the depolarized spectrum owing to reorientational motion of linear molecules[56]

$$\phi(t) = \sum_j \langle P_2(\cos\theta_{i,j}(t))\rangle \Big/ \sum_j \langle P_2(\cos\theta_{i,j}(0))\rangle \ ,$$

where $\theta_{i,j}(t)$ is the angle between the axis of the ith molecule at time 0 and the axis of the jth molecule at time t and where $P_2(x)$ is the second order Legendre Polynomial of the variable x. The Rayleigh scattering is sensitive both to crossed correlation and self-correlation terms.

The previous discussion shows that the contribution of crossed terms is small and takes place significantly at large times of $\phi(t)$. In this case the single molecular character for fast reorientational motions dominates at short times.[57] Consequently, we can compare the experimental correlation function $\phi(t)$ for short times to correlation functions obtained from theoretical models or reorientational motions of one particle.[56] We can expect large motions of the free rotator type. Unfortunately, difficulties mentioned in the introduction limit the range of this comparison because we are unable to treat the other contributions to the depolarized Rayleigh (for instance, the induced anisotropy). Close to T_c no anomaly of depolarized Rayleigh and Raman spectra was seen, showing that these spectra can be attributed to the single molecular nature of the phenomenon. The range of the static orientation correlation which can modify the characteristic time of this reorientation lies in a range of the interaction potential (a few Å). This range is smaller than the range of translational position correlations which are at the origin of anomalies of equilibrium and transport properties near the critical point of a pure fluid.

For this purpose, the existence of background terms in viscosity and thermal conductivity coefficients hinder a coherent interpretation of critical dynamic phenomena[20] where its importance depends on the nature of the fluid.[30] Such experimental results which specify microscopic phenomena at the scale of the interaction potential are of great interest for estimating the potential contribution to transport coefficients in the critical region.[58]

VIII. GENERAL CONCLUSION

When carbon dioxide approaches its critical temperature along the critical isochore, the behaviors of the intensity of polarized and depolarized Raman bands ν_1 and $2\nu_2$, respectively, and the depolarized Rayleigh band can be explained uniquely by turbidity and multiple scattering phenomena. These phenomena are due to the quasi-elastic intensive polarized Rayleigh scattering which is associated to the critical divergence (with the γ exponent) of the isothermal compressibility. In particular, the specific variation of unresolved depolarized Raman diad originates from multiple scattering (Fig. 10). In an adequate $T - T_c$ range, an uncorrelated double scattering Rayleigh–Raman mechanism accounts for the quantitative behavior of the height of diad bands.

In the temperature range $0.01 < T - T_c < 10$°C no anomalous variation of the profiles of depolarized Rayleigh and Raman bands was observed. Their analysis shows that molecular reorientational motions remain extremely fast and their range small enough to exhibit a single molecular behavior. Consequently, they are not influenced by critical modes at low frequency associated to fluctuations of the order parameter.

The experimental study of the behavior of the polarized Raman Fermi diad ν_1, $2\nu_2$ of carbon dioxide confirms the existence of molecular interactions at short distance which are not modified in the critical region and which are the only interactions responsible for their frequency shift.

ACKNOWLEDGMENTS

We would like to thank Mr. Drifford who put the triple monochromator at our disposal and Mr. Dalbiez, Mr. Nectoux, and Mr. Vinit for their valuable collaboration in its use. We are very grateful to Mr. Chandrasekharan for his interest in this study and his enlightening discussions. We thank Mr. Mozer, Mr. Oxtoby, and Mr. Hodges for their judicious comments and their critical reading of the manuscript.

[1]B. Chu, *Laser Light Scattering* (Academic, London, 1974).
[2]*Photon Correlation and Light Beating Spectroscopy*, edited by H. Z. Cummins and E. R. Pike (Plenum, New York, 1974).
[3]H. E. Stanley, *Introduction to Phase Transitions and Critical Phenomena* (Clarendon, Oxford, 1971).
[4]S. K. Ma, *Modern Theory of Critical Phenomena* (Benjamin, Reading, Mass., 1976).
[5]P. G. de Gennes, in *Fluctuations, Instabilities, and Phase Transitions*, edited by Tormod Riste (Plenum, New York, 1975), p. 1.
[6]B. Mozer (private communication).
[7](a) A. K. Atakhodzhaev, L. M. Kashaeva, L. M. Sabirov, V. S. Starunov, T. M. Utarova, and I. L. Fabelinskii, Zh. Eksp. Teor. Fiz. 17, 95 (1973); (b) G. I. Kolesnikov, V. S. Starunov, and I. L. Fabelinskii, Zh. Eksp. Teor. Fiz. 24, 73 (1976); (c) I. L. Fabelinskii, G. I. Kolesnikov, and V. S. Starunov, Opt. Commun. 20, 130 (1977).
[8]I. M. Arefev, Opt. Commun. 10, 277 (1974).
[9]D. Beysens, A. Bourgou, and G. Zalczer, Opt. Commun. 15, 436 (1975).
[10]J. R. Petrula, H. L. Strauss, K. Q. H. Lao, and R. Pecora, J. Chem. Phys. 68, 623 (1978).
[11]G. D. J. Phillies, P. J. Chappell, and D. Kivelson, J. Chem. Phys. 68, 4031 (1978).
[12]M. R. Moldover and J. S. Gallagher (private communication).
[13]D. Beysens and G. Zalczer, Phys. Rev. A 18, 2280 (1978).
[14]G. Zalczer and D. Beysens, J. Chem. Phys. 72, 348 (1980).
[15]D. Beysens and G. Zalczer, Opt. Commun. 22, 236 (1977).
[16](a) M. Thibeau and B. Oksengorn, Mol. Phys. 15, 579 (1968); J. Phys. (Paris) 30, 47 (1969); (b) H. B. Levine and G. Birnbaum, Phys. Rev. Lett. 20, 439 (1968); (c) P. Lallemand, Phys. Rev. Lett. 25, 1079 (1970); J. Phys. (Paris) 32, 119 (1971); (d) J. I. Gersten, R. E. Slusher, and C. M. Surko, Phys. Rev. Lett. 25, 1739 (1970); (e) W. M. Gelbart, Adv. Chem. Phys. 26, 1 (1974).
[17]R. Pecora, J. Chem. Phys. 49, 1036 (1968).
[18](a) G. R. Alms, D. R. Bauer, J. I. Brauman, and R. Pecora, J. Chem. Phys. 59, 5310 (1973); (b) B. J. Berne and R. Pecora, *Dynamic Light Scattering with Applications to Chemistry, Biology, and Physics* (Wiley, New York, 1976).
[19]S. J. Bertucci, A. K. Burnham, G. R. Alms, and W. H. Flygare, J. Chem. Phys. 66, 605 (1977).
[20]P. Calmettes, Phys. Rev. Lett. 39, 1151 (1977).
[21]R. Perl and R. Ferrell, Phys. Rev. A 6, 2358 (1972).
[22]D. W. Oxtoby, Phys. Lett. A 50, 459 (1975); J. Chem. Phys. 62, 1463 (1975).
[23]Y. Garrabos, R. Tufeu, and B. Le Neindre, J. Chem. Phys. 68, 495 (1978).
[24]R. A. J. Keijser, M. Jansen, V. G. Cooper, and H. F. P. Knaap, Physica (Utrecht) 51, 593 (1971).
[25]P. Van Konynenberg and W. A. Steele, in *Advances in Raman Spectroscopy*, edited by J. P. Mathieu (Heyden, London, 1973), Vol. 1, p. 450.
[26]M. Perrot, J. Devaure, and J. Lascombe, Mol. Phys. 30, 97 (1975).
[27]G. Amat and M. Pimbert, J. Mol. Spectrosc. 16, 278 (1965).
[28]F. J. Bartoli and T. A. Litovitz, J. Chem. Phys. 56, 413 (1972).
[29]T. Keyes and D. Kivelson, J. Chem. Phys. 56, 1057 (1972).
[30]H. L. Swinney and D. L. Henry, Phys. Rev. A 8, 2586 (1973).
[31]A. Michels, C. Michels, and H. M. Wouters, Proc. R. Soc. (London) Ser. A 153, 214 (1935); A. Michels, B. Blaisse, and C. Michels, Proc. R. Soc. (London) Ser. A 160, 358 (1937).
[32]J. M. H. Levelt-Sengers and W. T. Chen, J. Chem. Phys. 56, 595 (1972).
[33]M. R. Moldover, J. Chem. Phys. 61, 1766 (1974).
[34]J. Zollweg and G. Mulholland, J. Chem. Phys. 57, 1021 (1972).
[35]J. Weiner, K. Langley, and N. C. Ford, Jr., Phys. Rev. Lett. 32, 879 (1974).
[36]J. V. Sengers and J. M. H. Levelt-Sengers, "Critical Phenomena in Classical Fluids," in *Progress in Liquid Physics*, edited by C. A. Croxton (Wiley, Chichester, 1978), p. 103.
[37]H. L. Swinney and H. Z. Cummins, Phys. Rev. 171, 152 (1968).
[38]B. Le Neindre, R. Tufeu, P. Bury, and J. V. Sengers, Ber. Busenges. Phys. Chem. 77, 262 (1973).
[39]A. Michels and S. R. de Groot, Appl. Sci. Res. Sect. A 1, 94, 102 (1948).
[40]J. V. Sengers and P. H. Keyes, Phys. Rev. Lett. 26, 70 (1971).
[41]See for example Ref. 23 and D. Beysens and G. Zalczer, Phys. Rev. A 15, 765 (1977); A. Reith and H. L. Swinney, Phys. Rev. A 12, 1094 (1975).
[42]M. J. Clouter, H. Kiefte, and N. Ali, Phys. Rev. Lett. 40, 1170 (1978).
[43]Y. Garrabos, R. Tufeu, and B. Le Neindre, C. R. Acad. Sci. Ser. B 282, 313 (1976).
[44]B. Quentrec, J. Phys. (Paris) 37, 1255 (1976); Phys. Rev. A 15, 1304 (1977).
[45]R. B. Wright and C. H. Wang, J. Chem. Phys. 58, 2893 (1973).
[46]Y. Garrabos (unpublished results).
[47]H. L. Welsh, P. E. Pashler, and B. P. Stoicheff, Can. J. Phys. 30, 99 (1952).
[48]I. Hanson, Phys. Rev. 46, 122 (1934).
[49]A. Langseth and J. R. Nielsen, Phys. Rev. 46, 1057 (1934).
[50]H. E. Howard-Lock and B. P. Stoicheff, J. Mol. Spectrosc. 37, 321 (1971).
[51]A. J. Bray and R. F. Chang, Phys. Rev. A 12, 2594 (1975).
[52]J. Bruining and J. M. R. Clarke, Chem. Phys. Lett. 31, 355 (1975).
[53]A. de Santis, M. Sampoli, P. Morales, and G. Signorelli, Mol. Phys. 35, 1125 (1978).
[54]D. A. Pinnow, S. J. Candau, and T. A. Litovitz, J. Chem. Phys. 49, 347 (1968).
[55]D. W. Oxtoby, Phys. Lett. A 50, 459 (1975); J. Chem. Phys. 62, 1463 (1975).
[56]R. G. Gordon, J. Chem. Phys. 43, 1307 (1965); 44, 1830 (1966).
[57]A. Ben Reuven and N. D. Gershon, J. Chem. Phys. 51, 893 (1969).
[58]D. W. Oxtoby, "Transport in Dense Fluids," in *High Pressure Science and Technology*, edited by K. D. Timmerhaus and M. S. Barker (Plenum, New York, 1979), Vol. 1, p. 379.

C H A P I T R E V

Diffusion Rayleigh-Brillouin dans le mélange de nitroéthane et isooctane

V.1 - Introduction

Comme nous l'avons vu, le spectre de diffusion polarisée d'un mélange binaire se compose de deux raies Rayleigh dues aux fluctuations de la concentration et de l'entropie et d'un doublet Brillouin dû aux ondes sonores (fluctuations de pression adiabatiques). A celà s'ajoutent pratiquement la contribution de la diffusion dépolarisée et Raman et la lumière élastique parasite due aux poussières ou à des réflexions. Dans la pratique, lorsque l'ensemble de ce spectre veut être analysé au moyen d'un Fabry Pérot, les raies centrales se fondent en une seule fonction d'appareil et la raie dépolarisée et les raies Raman apparaissent comme une ligne de base sans structure.

Les paramètres que nous pouvons obtenir d'un tel spectre sont le décalage et la largeur des raies Brillouin et les intensités du pic central, des raies Brillouin et de la ligne de base. Lorsque nous faisons une étude en fonction de la température, les trois composantes du pic central peuvent être évaluées car elles ont des comportements très différents.

V.2 - Montage expérimental

Nous avons utilisé le mélange de nitroéthane et isooctane en raison de la faible intensité de la raie de concentration.

Le spectre Rayleigh Brillouin de ce mélange avait déjà été étudié [16] mais avec un interféromètre simple passage, ce qui limitait la précision des résultats. Dans la suite nous comparerons les résultats des deux expériences.

La cellule avait déjà été utilisée pour des mesures d'indice de réfraction de part et d'autre du point critique [20] , qui avaient prouvé qu'elle était bien à la concentration critique (c = 0,5344 $\pm$ 0,0008 en masse d'isooctane). La stabilité thermique était de l'ordre de $\pm$ 2.10^{-4} K sur 24 h et la température critique était repérée grâce au système de franges décrit plus loin (Chpt. VI. fig. a) donnant :

$$T_c = 30,1605°C \begin{cases} \pm\ 0,0015°C \text{ en valeur relative} \\ \pm\ 0,1°C \quad \text{en valeur absolue} \end{cases}$$

L'ISL de Fabry Pérot plan était fixé à 5,92 $\pm$ 0,02 GHz. Le laser utilisé était un laser à argon ionisé (Spectra-Physics 165) fonctionnant à 4880 Å . Il était rendu monomode par l'utilisation d'un étalon intra-cavité et donnait une puissance maximale de 250 mW. Près du point critique le faisceau était atténué jusqu'à 1 mW pour éviter l'échauffement de la cellule (0,5 mK/mW).

L'angle de diffusion moyen était de 90° $\pm$ 5' et l'ouverture angulaire de 1°.

La figure 3 de l'article montre deux spectres typiques, l'un loin de T_c ($T - T_c = 6,27$ K) l'autre très près ($T - T_c = 2,2$ mK). Dans ce dernier cas, la hauteur du pic central est environ 40 fois celle des raies Brillouin ce qui justifie l'emploi d'un interféromètre double passage.

V.3 - Analyse de spectre

Dans ce cas où les raies Brillouin sont nettement séparées du pic central, il est possible d'effectuer l'analyse en grande partie"à la main". Il est toutefois nécessaire de calibrer les résultats ainsi obtenus en les comparant aux résultats de calcul sur machine, au moins pour un échantillon de situations typiques. La ligne de base était prise égale aux points les plus bas du spectre puis on mesurait les hauteurs h_B et h_R et les largeurs apparentes $2\Gamma_B^*$ et $2\Gamma_R$ des raies Brillouin et Rayleigh. Par comparaison avec les résultats exacts nous obtenons les formules suivantes pour les valeurs de la largeur Brillouin :

$$2\Gamma_B = 1,35\ (2\Gamma_B^* - 2\Gamma_R)$$

l'intensité Rayleigh :

$$I_R = 1.12\ h_R \cdot 2\Gamma_R$$

et l'intensité Brillouin :

$$I_B = 0.96 \cdot \pi \cdot h_B \cdot 2\Gamma_B$$

la moyenne sur les deux raies étant prise dans ce cas. Les incertitudes sont de 0,5 % pour le décalage Brillouin et d'environ 3 % pour la largeur Brillouin près du point critique et croissant jusqu'à 8 % loin de T_c du fait du recouvrement partiel des raies Brillouin d'ordres consécutifs.

V.4 - Résultats

a) Vitesse hypersonique

Le décalage Brillouin a été obtenu avec une précision de 0,5 %. Les résultats obtenus (voir fig. 4) montrent sans ambiguité qu'à cette précision il n'y a pas d'anomalie visible de décalage dans l'intervalle $T - T_c = \{1mK, 60\ K\}$ et que la variation est linéaire, ce qui est compatible avec les mesures hypersoniques et ultrasonores déjà effectuées sur ce même mélange.

Si l'on compare maintenant avec les résultats obtenus dans d'autres mélanges, la situation est moins nette. Dans le mélange de nitroéthane et 3-méthylpentane aucune anomalie n'a été vue par diffusion Brillouin. Dans le mélange de nitrobenzène et n-hexane certaines expériences Brillouin donnent une anomalie (- 10 %) et d'autres pas, alors que les mesures d'ultrasons en donnent une très faible (0,5 %). Il faut toutefois noter que ces expériences ont été réalisées avec des techniques différentes : celle montrant une anomalie avec un interféromètre simple passage et celle n'en montrant pas avec un double passage. Il paraît donc probable que cette anomalie soit un artifice expérimental. Enfin une anomalie de + 10 % a été observée dans le mélange d'eau et triéthylamine. Cependant ce mélange étant assez fortement diffusant et un interféromètre simple passage ayant été utilisé, ce résultat est à considérer avec réserves.

La vitesse du son s'obtient d'après la formule :

$$v = 2\pi \frac{\Delta\nu}{q} = \frac{\lambda_o}{\sqrt{2}} \frac{\Delta\nu}{n}$$

$\Delta\nu$ étant linéaire avec la température, n peut être développé en série en se limitant au premier terme, on obtient alors :

$$= v\,(T_c) + \frac{(T - T_c)}{n(T_c)} \left[\frac{\lambda_o}{\sqrt{2}} \cdot \frac{\partial(\Delta\nu)}{\partial T} - v(T_c) \left(\frac{\partial n}{\partial T}\right)_P \right]$$

$$= (1115 \pm 10)\ m\ s^{-1} - (T - T_c)\ (4{,}04 \pm 0{,}05)\ ms^{-1}\ K^{-1}$$

b) Atténuation du son

La largeur mesurée des raies Brillouin est représentée sur la

figure 5. On voit qu'elle ne présente non plus aucune anomalie. Ces mesures sont en accord avec celles de Arefev et coll. sur le même système, quoique ces dernières données soient beaucoup moins précises. Les seules autres données que nous ayons concernent le mélange de nitrobenzène et n-hexane : Chen et coll.,ont mesuré un effet critique mais nous avons vu que l'usage d'un interféromètre simple passage rendait ces résultats peu fiables. D'autre part Wang, avec un double passage a observé un léger effet qu'il n'a pas étudié quantitativement.

La comparaison avec les mesures sonores n'a pas de signification à cause de la différence des fréquences. En effet, l'atténuation du son provient de couplages avec les autres modes. Pour qu'il y ait couplage efficace, il faut que les temps caractéristiques de ces modes ne soient pas trop longs par rapport à la fréquence de l'onde sonore, ce qui n'est pas le cas ici (4GHz comparés à 10 kHz).

Nous avons vu que l'absorption du son est liée aux viscosités de cisaillement η_s et de volume η_b par la formule :

$$\Gamma q^2 = \frac{q^2}{2\rho} \left(\frac{4}{3}\ \eta_s + \eta_b\right)$$

Le comportement de la viscosité de cisaillement à basse fréquence est

$$\eta_s = \eta_s^{reg}\ \ t^{-y_\eta}$$

avec $y_\eta \simeq 0.04$. Dans le mélange de nitroéthane et isooctane, nous avons :

$$\eta_s = \eta_o \exp \frac{E}{T}\ \ t^{-y_\eta} \quad \text{avec } \eta_o = 218.10^{-2} \text{ cPo}$$

$$E = 920 \pm 180 \text{ K}$$

$$y_\eta \simeq 0{,}045 \pm 0{,}013$$

Si nous reportons ces valeurs de la viscosité dans la formule ci-dessus, nous obtenons une contribution inférieure à la largeur de la raie ($\sim$ 150 MHz à 60° de T_c, 240 MHz à 1°, à comparer avec les mesures respectivement 240 et 350 MHz). Comme la viscosité haute fréquence est inférieure à la viscosité basse fréquence, on voit que la viscosité de volume a une influence importante.

Nous avons essayé de décrire quantitativement les résultats

expérimentaux avec les formules suivantes :

a) $\Gamma q^2 = X_2 \exp\{\frac{X}{T}\}$ ce qui revient à supposer le même comportement pour les deux viscosités. L'accord avec l'expérience est bon mais la valeur trouvée pour l'énergie d'activation $X_1 = 751 \pm 13$ K est très basse, ce qui indique que la variation de la viscosité de volume est plus faible que celle de la viscosité de cisaillement.

b) $\Gamma q^2 = X_2 \exp\{\frac{X}{T}\} + X_3$, ce qui suppose que la viscosité de volume est constante. De plus, nous avons imposé à X_1 sa valeur dans la viscosité de cisaillement : 920 ± 180 K.

Nous obtenons $X_2 = 5{,}9 \pm 3{,}6$ MHz

$X_3 = 33{,}4 \pm 17$ MHz

soit à T_c $\frac{\eta_s}{\eta_B} \simeq 4{,}3$

c) $\Gamma q^2 = X_2 \exp(\frac{X_1}{T}) \times X_3 \exp(\frac{X_4}{T})$

Nous trouvons alors $X_4 = 24 \pm 200 \simeq 0$. Nous sommes donc ramenés au cas précédent.

c) Intensité Brillouin

La variation de l'intensité Brillouin avec la température a été portée sur la figure 6 . L'intensité Brillouin varie doucement et linéairement avec la température. L'ordre de grandeur de la variation peut être estimé d'après la formule

$$I_B \propto T \left[\rho \left(\frac{\partial (n^2)}{\partial \rho}\right)_{T_c} \right]^2 \cdot \frac{1}{\rho v^2}$$

L'évaluation numérique donne :

$$\frac{1}{I_B} \frac{dI_B}{dT} \approx 0.01\ K^{-1}$$

en bon accord avec les données.

d) Intensité Rayleigh et rapport Rayleigh-Brillouin

L'intensité de la raie Rayleigh comprend les contributions de la

raie d'entropie, de la raie de concentration et éventuellement de la lumière élastique parasite (due à des réflexions ou des poussières). Nous avons d'abord vérifié que la lumière élastique était négligeable en considérant la région loin de T_c, où la raie de concentration est négligeable. Comme la partie divergente de C_p est très faible, le rapport $\frac{Cp}{C_v} = \gamma_o$ doit être constant, et l'intensité des deux raies varier de la même façon. S'il y a de la lumière élastique, indépendante à priori de la température, l'intensité Rayleigh doit moins varier que l'intensité Brillouin. La figure (6) montre de façon nette que l'on est dans le premier cas donc qu'il n'y a pas de lumière élastique parasite.

Nous aurons donc à comparer nos résultats avec la formule :

$$\frac{I_{Rayleigh}}{I_{Brillouin}} = \frac{I_{entropie} + I_{concentration}}{I_{Brillouin}}$$

Nous avons déjà remarqué que ce rapport était indépendant de la théorie de diffusion de la lumière considérée. Par simplicité nous choisirons maintenant celle d'Einstein où la relation entre la fluctuation de l'indice et la fluctuation des paramètres thermodynamiques est supposée la même qu'entre la variation de l'indice pour une variation homogène des paramètres thermodynamiques. Nous obtenons alors :

$$\frac{I_R}{2I_B} = \left\{ \frac{\left[\frac{\partial(n^2)}{\partial c}\right]^2_{P,T}}{\left[\rho \frac{\partial(n^2)}{\partial \rho}\right]^2_{T,C}} \cdot \frac{\rho v^2}{\left(\frac{\partial \mu}{\partial c}\right)^o_{P,T}} \cdot t^{-\gamma} \cdot G(q\xi) \right\} + \gamma_o - 1$$

ce qui, une fois introduites les valeurs numériques se réduit à :

$$\frac{I_R}{2I_B} = Ac \left[1 + s(T - T_c) \right] \left(\frac{T - T_c}{T_c}\right)^{-\gamma} G(q\xi) + \gamma_o - 1$$

où G (qξ) a été défini au chapitre 2

où $Ac = \frac{\left[\left(\frac{\partial(n2)}{\partial c}\right)_{P,T}\right]^2}{\left[\rho \left(\frac{\partial(n2)}{\partial \rho}\right)_{T,C}\right]^2} \cdot \frac{\rho v^2}{\left(\frac{\partial \mu}{\partial c}\right)^o_{P,T}}$ évalué à la température critique

et $s = 1.6.10^{-3}\ K^{-1}$. Nous avons accordé cette formule aux valeurs expérimentales en variant les paramètres Ac, ξ_o, ν , γ et γ_o.

Nous avons d'abord constaté que la valeur de s ne change pas significativement (moins de 0,5 %) les valeurs obtenues pour les autres paramètres fixant s à ($-1{,}6.10^{-3}$ K^{-1}), ($1{,}6.10^{-3}$ K^{-1}) et ($1{,}6.10^{-2}$ K^{-1}).

Ensuite, si nous laissons évoluer librement tous les paramètres, la détermination de ξ_o est très fortement corrélée avec celle de ν et celle de A_c avec celle de γ. Sur la figure 8 nous avons tracé les valeurs de ξ_o en fonction de ν et de A_c en fonction de γ pour à peu près la même qualité d'accord. Il est donc impossible de déterminer indépendemment toutes les variables. Cependant les exposants γ et ν sont universels et ont été évalués à $\gamma = 1{,}240$; $\nu = 0{,}630$, dans les mélanges binaires. Nous obtenons alors :

$$A_c = (2{,}94 \pm 0{,}04).10^{-4}$$
$$\xi_o = 2{,}42 \pm 0{,}04 \text{ Å}$$
$$\gamma_o = 1{,}270 \pm 0{,}001$$

où l'incertitude sur ξ_o tient aussi compte de l'incertitude sur q.

V.5 - Relation d'amplitudes

De la valeur de A_c que nous avons obtenue, nous pouvons déduire l'amplitude

$$\left(\frac{\partial \mu}{\partial c}\right)^o_{P,T} = \left\{ \frac{\left(\frac{\partial (n^2)}{\partial c}\right)_{P,T}}{\rho \left(\frac{\partial (n^2)}{\partial \rho}\right)_{T,C}} \right\}^2 \frac{\rho v^2}{A_c} = 134 \pm 20 \text{ J cm}^{-3}$$

Et en appliquant la même analyse aux résultats d'Aref'ev et coll. [16] nous obtenons :

$$\left(\frac{\partial \mu}{\partial c}\right)^o = 103 \pm 20 \text{ J cm}^{-3}$$

En utilisant la valeur de ξ_o que nous venons de déterminer, nous pouvons calculer la constante universelle

$$R_\xi^+ R_c^{-1/3} = \xi_o \left[B^2 \frac{\left(\frac{\partial \mu}{\partial c}\right)^o_{PT}}{k_B T_c} \right]^{1/3} = \begin{array}{l} 0{,}72 \pm 0{,}07 \text{ (nos résultats)} \\ 0{,}66 \pm 0{,}07 \text{ (Aref'ev)} \end{array}$$

En bon accord avec les valeurs théoriques de 0,650 par la méthode des séries haute température et de 0,667 par la méthode du groupe de renormalisation [40-41] .

V.6 Conclusion :

La résolution du spectre de Rayleigh Brillouin nous a permis de mettre en évidence le caractère régulier des variations de la vitesse du son et de son absorption dans le domaine hypersonore près du point critique du mélange de nitroéthane et d'isooctane.

Ces spectres nous ont permis d'étudier la variation de l'intensité de la raie de concentration et donc de déduire la valeur de la longueur de correlation ξ_o, alors que cette raie aurait été noyée par les autres sources de diffusion si l'on ne l'avait séparée spectralement. Enfin nous avons pu par ce moyen déterminer sans aucune hypothèse l'amplitude de la susceptibilité osmotique, même si le nombre de paramètres impliqués limite la précision statistique, ce qui, à notre connaissance, n'est possible par aucune autre méthode.

PHYSICAL REVIEW A VOLUME 25, NUMBER 2 FEBRUARY 1982

High-resolution Rayleigh-Brillouin spectroscopy in the critical mixture nitroethane-isooctane

Y. Garrabos,* G. Zalczer, and D. Beysens

Commissariat à l'Energie Atomique, Division de la Physique, Service de Physique du Solide et de Résonance Magnétique, Boite Postale No. 2, 91190 Gif sur Yvette, France

(Received 12 March 1981)

We report new measurements of the Rayleigh-Brillouin spectrum of a critical binary mixture and review the existing data in this field. We used a double-pass Fabry-Pérot interferometer and a weakly scattering system (nitroethane-isooctane) so that the Brillouin lines were not affected by the wings of the Rayleigh line, even in the immediate vicinity of the critical point. No anomaly was detected in the shift or width or intensity of the Brillouin lines. From the ratio of the intensities of the Rayleigh and Brillouin lines we deduced the ratio of specific heats γ_0, the correlation length ξ_0, and the susceptibility amplitude $(\partial c/\partial\mu)^0_T$, without any hypothesis about light-scattering amplitudes. These values lead to an amplitude ratio $R_\xi^+ R_c^{-1/3}$ in full agreement with the theoretical values.

I. INTRODUCTION

The study of the dispersion and attenuation of sound in critical systems has stimulated theoretical[1-5] and experimental[6-16] interest. The order parameter is not directly observable in this case, but it affects the behavior of other physical quantities through couplings. In most experiments the dispersion and attenuation of sound have been studied with induced ultrasound. The anomalous absorption observed in many systems has been well explained by mode-coupling theories and dynamical scaling[1,5] in the frequency range achievable ($\lesssim$50 MHz). These ultrasonic techniques are accurate but subject to some spurious phenomena: Large volumes are needed whose temperature control is difficult and the ultrasonic pulses can perturb the medium. Light scattering is not affected by these difficulties but other problems arise, mainly the strong increase of the Rayleigh scattering near the critical point (critical opalescence), which can overwhelm the Brillouin lines. Thus, special care must be taken such as using a multipass Fabry-Pérot (FP) interferometer in order to achieve a very high contrast, or using a weakly opalescent system. Finally, the frequency range which the FP experiment investigates is much higher than for ultrasonic experiments, typically about 5 GHz.

The purpose of this paper is to report new experimental results obtained using both a weakly opalescent system (nitroethane-isooctane) and a double pass FP spectrometer, and to review the status of the experimental situation.

Until now three systems have been investigated by both ultrasonic and Brillouin techniques. Ultrasonic measurements have always shown weak negative anomalies in the sound velocity and strong positive anomalies in the sound damping, whereas Brillouin spectroscopy has detected either a corresponding—but much bigger—anomaly in the sound velocity (nitrobenzene+n-hexane,[9-11] nitroethane+isooctane[15,16]), or no anomaly at all (nitrobenzene+n-hexane,[13] nitroethane+3-methylpentane[12]), or an anomaly in the other direction (triethylamine+water).[7] An anomaly in the sound attenuation has also been reported (nitrobenzene+n-hexane,[11,13] nitroethane+isooctane[16]). However, all the light-scattering experiments which claimed the observation of some anomalies in the sound velocity or the sound damping suffer from the same criticism, namely, using a low-contrast spectrometer which makes it impossible to obtain reliable results near the critical temperature T_c. This limitation still applies to such a weakly opalescent system as nitroethane+isooctane: We will see that the remaining Rayleigh scattering near T_c is spectrally 20 times more intense than the Brillouin lines, which can lead to erroneous conclusions.

II. THEORETICAL BACKGROUND

The spectrum of the light scattered at a transfer wave vector $\vec{q}$ by a liquid mixture consists of three contributions from the three independently decaying thermodynamic parameters: concentration c, entropy s, and pressure p.[17] Each has the structure

$$S_i(q,\omega)=A\left(\frac{\partial(n^2)}{\partial i}\right)^2 k_B T\chi_i G_i(q)\, s_i^0(q,\omega)\,,$$

where A includes the geometrical and electromagnetic factors and is the same for all variables c,s,p; $(\partial(n^2)/\partial i)^2$ expresses the coupling between the light and the fluctuation of the parameter i (the other two are kept constant). The exact structure of this factor is still open to controversy. Indeed, though we can calculate the change in local polarizability, none of the proposed formulas has been universally admitted.[18] However, since the controversial part does not refer to any thermodynamic variable, it is the same for all the con-

 © 1982 The American Physical Society

tributions. Therefore, the ratios of these contributions are independent of the choice of the formula and we can use any one for their interpretation. χ_i is the susceptibility associated with the parameter i (the other two kept constant) and k_B is the Boltzmann constant so that $k_B T \chi_i$ is the amplitude of the thermal fluctuation of the parameter i. These first three terms express the integrated scattered light at zero wave vector. $G_i(q)$ describes the angular dependence of the integrated intensity, and $s_i^0(q, \omega)$ is a normalized function describing how this light is distributed in the frequency space.

Since the concentration is the order parameter, the associated susceptibility diverges near the critical point as

$$\left(\frac{\partial c}{\partial \mu}\right)_{p,T} = \left(\frac{\partial c}{\partial \mu}\right)^0_{p,T} t^{-\gamma},$$

where t is the reduced temperature difference $(T - T_c)/T_c$ and γ the universal critical exponent $\simeq 1.24$. Moreover, the correlation length ξ of the concentration fluctuations also diverges as

$$\xi = \xi_0 t^{-\nu},$$

where $\nu \simeq 0.63$. Near the critical point this length is no longer negligible compared to λ so the function $G_c(q)$ significantly departs from unity for typically $T - T_c \lesssim 0.3$ K at a scattering angle of 90°.

The time behavior of the concentration fluctuations is also anomalous but since the characteristic frequency (0.5 to 50 kHz) is much smaller than the resolution of our present experiment (100 MHz), we can consider here the line $S_1 = S_c(q, \omega)$ as a δ function of the frequency.

The line $S_2 = S_s(q, \omega)$ associated with entropy fluctuations is isotropic and low frequency (5 MHz). Its intensity is given by

$$I_2 = A \frac{k_B T^2}{C_p} \left(\frac{d(n^2)}{dT}\right)^2_{c,p}$$

$$= A \frac{C_p - C_v}{C_v} \frac{k_B T}{\beta_s} \left(\frac{\partial (n^2)}{\partial p}\right)^2_{c,s},$$

where β_s is the adiabatic compressibility.

The third contribution $S_3 = S_p(q, \omega)$ is due to pressure fluctuations (Brillouin lines). Its spectrum consists of two symmetrical lines with respect to the incident frequency. The displacement $\pm vq$ is related to the sound velocity v in the mixture. The order of magnitude at a scattering angle of 90° is 4 GHz (2.5×10^{10} rad sec^{-1}):

$$2S_3(q, \omega) = A \frac{k_B T}{\beta_s} \left(\frac{\partial (n^2)}{\partial p}\right)^2_{c,s} \frac{1}{2\pi} \left(\frac{\Gamma q^2}{(\omega + vq)^2 + (\Gamma q^2)^2} + \frac{\Gamma q^2}{(\omega - vq)^2 + (\Gamma q^2)^2} \right).$$

Γ, the attenuation coefficient of the sound wave, is expressed as

$$\Gamma = \frac{1}{2\rho} \left\{ (\tfrac{4}{3}\eta_S + \eta_B) + (\gamma - 1)\rho D_T + \frac{v^2}{\rho} D \left(\frac{\partial \mu}{\partial c}\right)^{-1}_{p,T} \left[\left(\frac{\partial \rho}{\partial c}\right)_{p,T} + \frac{K_T}{C_p} \left(\frac{\partial \rho}{\partial T}\right)_{p,c} \left(\frac{\partial \mu}{\partial c}\right)_{p,T} \right]^2 \right\}.$$

ρ is the mass density, D_T is the thermal diffusivity, D is the mass diffusivity, and K_T is the thermal diffusion ratio. The first term represents the damping of sound by the shear viscosity η_S and the bulk viscosity η_B. Typically, at a scattering angle of 90°, the corresponding linewidth is in the range 500 MHz (3×10^9 rad sec^{-1}). This very high value makes the contributions of the other terms negligible, which corresponds to the coupling with the entropy mode (linewidth $\simeq 5$ MHz) or to the mass diffusion mode (linewidth $\lesssim 5$ kHz). So we can write

$$\Gamma \simeq \frac{1}{2\rho} (\tfrac{4}{3}\eta_S + \eta_B).$$

Other contributions, such as depolarized lines which cannot be resolved because they are too broad, look like a flat background B (see below). Other contributions such as quasielastic scattering from dust in the sample, etc., add a nearly Dirac function $D\delta(\omega)$ to $S(q, \omega)$.

Finally $S(q, \omega)$ can be put under the following form (Fig. 1):

$$S(q, \omega) = S_1(q, \omega) + S_2(q, \omega) + 2S_3(q, \omega) + D\delta(\omega) + B.$$

III. EXPERIMENTAL

Close to T_c the intensity from the line $S_1(q, \omega)$ strongly increases, giving rise to spurious effects. So we used both a system where $(\partial(n^2)/\partial c)_{p,T}$ is very low and a high-contrast FP spectrometer.

This mixture consists of nitroethane and isooctane, the refractive indices of which are matched within $\sim 10^{-3}$.[19] We already used the very same sample for refractive index[19-21] and depolarized scattering[22] measurements. The purity of nitroethane was better than 99.5%, as verified by chromatography and NMR measurements. The isooctane used had the quality "reference substance for gas chromatography." The isooctane mass fraction was $c = 0.5344 \pm 0.0008$, close to the critical value 0.5350 ± 0.0006.[19] The mixture was frozen

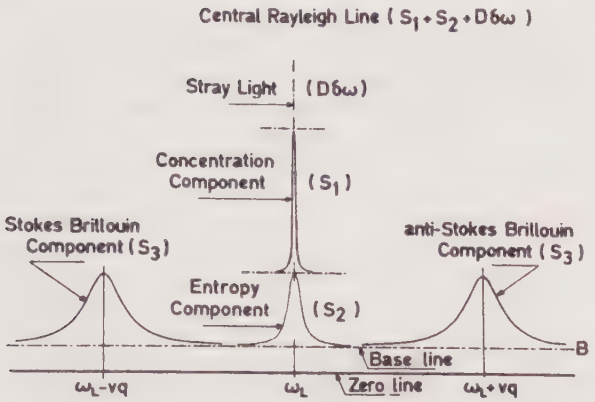

FIG. 1. Schematic Rayleigh-Brillouin spectrum of a binary mixture. In an actual experiment, the three central lines appear as a single apparatus function, and the whole spectrum is periodically repeated with possible overlaps of the Brillouin lines.

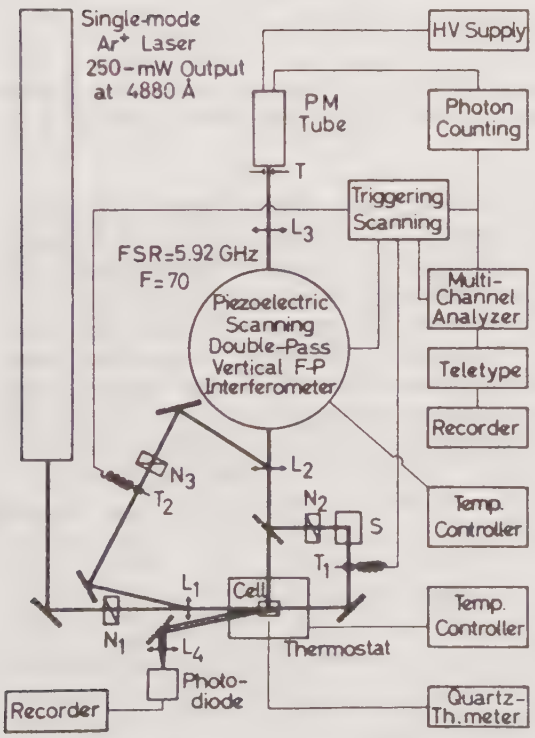

FIG. 2. Experimental setup. N_1, N_2, N_3 are attenuators, L_1–L_4 are lenses. T is a pinhole. When the chopper T_1 is open, the system records an apparatus function from the elastic scatterer S. When T_2 is open, laser light is sent through the interferometer for synchronization. Fringes are formed on the plane of the photodiode by the beams reflected from both walls of the cell.

in liquid nitrogen and sealed under vacuum.

The cell was placed into a thermally stabilized copper oven, itself enclosed in an air-regulated box allowing a thermal stability of $\pm 2 \times 10^{-4}$ K to occur for more than one day, as verified by a quartz thermometer.

Owing to the nearly perfect matching of the refractive indices, no visible opalescence occurs at T_c, and even the meniscus is hardly visible. Therefore, special care was necessary to determine the critical temperature. We set up an experiment as in Ref. 23, where the beam reflected from the input window of the sample interferes with the beam reflected from the output window. This is a very simple, sensitive, and accurate way to determine the refractive index variation. At T_c, due to the phase-separation process, the variation of the refractive index with temperature increases sharply.[19] Moreover, the equilibrium value is reached only after a very long time. This allows us to determine accurately the critical temperature. The value was $T_c = 30.1605 \pm 0.0015$ °C. The absolute value is accurate only within 0.1 °C.

The light-scattering setup (Fig. 2) is almost the same as in Ref. 24 except for the laser which worked on a single mode with a power of about 250 mW at a wavelength $\lambda = 4880$ Å. Near the critical point, heating by the laser beam was detected in the sample (about 0.5 mK/mW), so the power had to be reduced down to 1 mW.

The mean scattering angle was $90° \pm 5'$. The refractive index extrapolated at 4880 Å and 30 °C from Ref. 25 is $n = 1.392 \pm (1 \times 10^{-3})$ (for a complete discussion see below). The mean transfer wave vector is $q = (2.534 \pm 0.002) \times 10^5$ cm^{-1}. The aperture angle was about 1°, broadening the Brillouin lines certainly no more than 35 MHz (2.2×10^6 rad sec^{-1}). This is completely negligible with respect to other broadenings, such as the apparatus function (AF) of the spectrometer (see below), as shown by the similarity of the spectra recorded with the full aperture and with the aperture reduced by a factor of 3.

In order to calibrate the intensity, we recorded every 20 sec the elastic light scattered from a solid opalescent medium, used as a standard, which was illuminated by the transmitted beam. The corresponding spectrum looked like an apparatus function. This allows us to know the exact shape of the apparatus function, which can vary in time because of misadjustments, and to automatically correct for the variations of the laser intensity, the transmission of the FP, etc., though we found *a posteriori* that this last factor kept remarkably constant.

The free spectral range (FSR) of the FP was 5.92 ± 0.01 GHz. It was determined by measuring

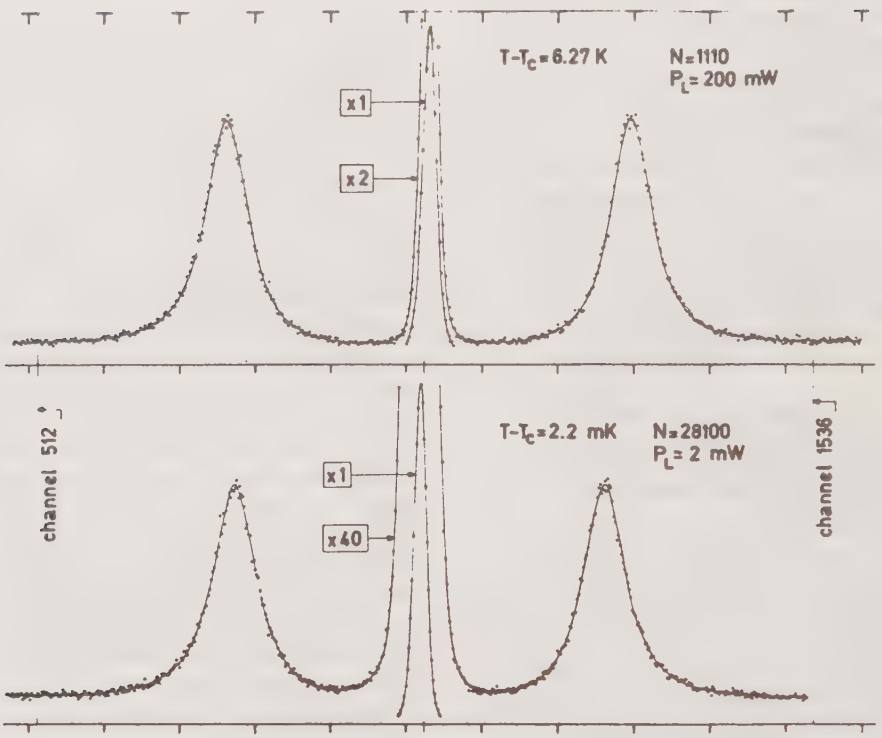

FIG. 3. Two typical spectra. Close to T_c the laser power was reduced to 2 mW, requiring the accumulation of 38 000 scans of 2 sec each. Far from T_c, with 200 mW, 1100 scans are enough to obtain a good signal-to-noise ratio.

the spacing between the plates by means of a cathetometer. The finesse was typically 70, corresponding to a half-width at half-height of the apparatus function of 50 MHz, and the contrast was found to be better than 10^6. The adjustments were stable enough to allow recording during 24 h or more, but the typical duration time of a recording was 1 or 2 h, except near T_c where the laser power was considerably reduced, as explained above.

Figure 3 shows two typical spectra obtained far from T_c (6.27 K) or very close to T_c (2.2 mK). The ratio of the central peak height to the Brillouin height varies typically from 2–40 (that of the integrated intensities from 0.3–6.5). The resolution of 50 MHz merges the entropy and concentration lines into an apparatus function, but the Brillouin linewidth is clearly evidenced. The baseline is different from zero, due in part to the unresolved broad depolarized lines.

The parameters, which can be determined at each temperature, are the shift, linewidth, and intensity of the Brillouin lines, the intensity of the central peak, and the intensity of the baseline (Table I). The experimental spectra are the convolution of $S(q, \omega)$ by the apparatus function. We analyzed the recordings as follows: Only a few spectra, each considered as typical of a given $T - T_c$ range, were analyzed using the apparatus function recorded simultaneously. We used a program of statistical refining due to M. Tournarie,[28] which allows the determination of the above quantities. But this kind of analysis is long and expensive, and we found it possible to simplify this analysis by some practical considerations. The background was deduced from the lowest points of the spectrum and then the heights h_B, h_R and apparent widths at half-height $2\Gamma^*$, $2\Gamma_R^*$ of the Brillouin and Rayleigh lines were measured. The true Brillouin linewidth is then given by

$$2\Gamma = 1.35(2\Gamma^* - 2\Gamma_R^*)$$

and the intensities of the Brillouin and Rayleigh lines by

$$I_R = 1.12\, h_R 2\Gamma_R ,$$

$$I_B = 0.96\pi h_B 2\Gamma \quad \text{(average of both lines)} .$$

The uncertainties are 0.5% for the Brillouin shift, 3% for the intensities, and range from 3–8% for the Brillouin linewidth, the larger value applying far from T_c, where the Brillouin lines of consecutive orders overlap.

TABLE I. Measured values of the Brillouin shift ($\Delta\nu$) and linewidth (Γ) and the intensities of the Rayleigh line (I_R), the Brillouin lines ($2I_B$), and the background (B). These intensities are referred to as the elastic scatterer (I_{AF}) so that their scale is arbitrary.

N	$T-T_c$ (°C)	$\Delta\nu$ (GHz)	Γ (MHz)	$\frac{I_R}{2I_B}$	$\frac{2I_B}{I_{AF}}$	$\frac{I_R}{I_{AF}}$	B
01	60.64	3.4185	241.9	0.270	1.92	0.72	0.68
02	52.44	3.561	241.9	0.265	1.85	0.685	0.72
03	47.64	3.647	249.8	0.270	1.72	0.65	0.69
04	43.34	3.708	253.7	0.270	1.50	0.57	0.61
05	39.14	3.7885	273.2	0.270	1.63	0.615	0.75
06	36.64	3.838	265.4	0.275	1.73	0.67	0.83
07	34.74	3.8665	277.1	0.280	1.50	0.59	0.72
08	29.34	3.9625	284.9	0.280	1.47	0.58	0.76
09	23.64	4.071	300.5	0.275	1.23	0.475	0.63
10	18.14	4.1555	304.4	0.285	1.57	0.63	0.93
11	13.74	4.254	312.2	0.290	1.25	0.52	0.85
12	9.95	4.3065	327.8	0.30	1.18	0.50	0.82
13	6.2675	4.381	331.7	0.305	1.17	0.50	0.86
14	4.25	4.410	339.5	0.33	1.20	0.555	0.88
15	3.968	4.419	343.4	0.35	1.21	0.60	1.03
16	3.7345	4.430	339.5	0.36	1.17	0.59	0.96
17	2.83	4.435	351.2	0.37	1.13	0.585	0.97
18	2.54	4.4555					
19	2.03	4.446	343.4	0.445	1.11	0.69	0.92
20	1.7345	4.465	351.2	0.46	1.08	0.70	
21	1.695	4.467	351.2	0.47	1.11	0.735	0.93
22	1.18	4.465	347.3	0.57	1.20	0.96	0.89
23	1.135	4.4755					
24	0.84	4.479	351.2	0.69	1.06	1.02	0.87
25	0.755	4.4755	343.4	0.755	1.09	1.16	0.85
26	0.7455	4.482	351.2	0.745	1.17	1.22	1.08
27	0.6895	4.477	347.3	0.81	1.23	1.39	1.00
28	0.6203	4.486	359.0	0.90	1.12	1.42	1.16
29	0.5747	4.482	359.0	0.93	1.04	1.35	0.82
30	0.565	4.482					
31	0.560	4.482	351.2	0.945	1.12	1.49	0.93
32	0.469	4.483	347.3	1.07	1.19	1.78	0.95
33	0.4325	4.488	355.1	1.14	1.28	2.04	1.20
34	0.356	4.485	343.4	1.30	1.05	1.92	0.96
35	0.28	4.482					
36	0.2762	4.493	347.3	1.60	1.15	2.54	1.17
37	0.270	4.495	355.1	1.625	1.12	2.56	0.93
38	0.2655	4.492	359.0	1.76	1.16	2.86	0.89
39	0.2433	4.493	359.0	1.86	1.07	2.79	0.86
40	0.2415	4.486	347.3	1.73			0.97
41	0.2375	4.493	355.1	1.94	1.15	3.13	0.87
42	0.2185	4.4915	347.3	2.00	1.16	3.26	0.86
43	0.2180	4.478	355.1	1.95			1.04
44	0.1985	4.4955	359.0	2.20	1.11	3.42	0.85
45	0.1970	4.492	362.9	2.16	1.12	3.40	0.90
46	0.1918	4.494	347.3	2.25	1.09	3.45	0.81
47	0.1765	4.486	355.1	2.40	0.96	3.22	0.97
48	0.1698	4.492	359.0	2.43	1.07	3.66	0.85
49	0.1673	4.495	355.1	2.57	1.10	3.97	0.86
50	0.1568	4.493	351.2	2.65	1.09	4.05	0.85
51	0.1490	4.486	351.2	2.60	0.99	3.60	0.90
52	0.1375	4.496	347.3	2.75	1.06	4.10	1.12
53	0.1315	4.490	351.2	2.84	1.11	4.40	0.89
54	0.1213	4.4845	359.0	2.85	1.19	4.75	1.10
55	0.1195	4.489	355.1	3.25	1.14	5.20	1.12
56	0.1114	4.4915	359.0	3.20	1.13	5.05	1.11
57	0.1018	4.497	362.9	3.50	1.09	5.25	1.26
58	0.092	4.486	355.1	3.60	1.13	5.7	1.21
59	0.079	4.499	351.2	4.00	1.11	6.25	1.26
60	0.070	4.490	347.3	4.20	1.09	6.4	1.10
61	0.063	4.4955	355.1	4.70	1.12	7.4	1.20
62	0.059	4.493	351.2	4.40	1.11	6.9	1.08
63	0.047	4.492	355.1	4.75	1.17	7.8	1.12
64	0.035	4.495	355.1	5.50	1.06	8.2	1.07
65	0.026	4.491	343.4	5.90	1.11	9.2	1.10
66	0.024	4.495	362.9	5.85	1.10	9.0	1.12
67	0.018	4.487	355.1	6.05	1.10	9.3	1.09
68	0.0125	4.494	359.0	6.50	1.04	9.5	1.02
69	0.0022	4.489	351.2	6.50	1.11	10.1	1.10
70	0.0010	4.496	359.0	7.50	1.15	12.0	1.15

IV. RESULTS AND DISCUSSION

A. Hypersound velocity

Primarily we have determined the hypersound velocity of the pure components. The setup which consisted of 2 FP in tandem allowed the velocity to be determined at two frequencies: High frequency with only the plane FP (back scattering $\theta \simeq 150°$, shift $\Delta\omega \simeq 5$ GHz, and "low" frequency with the plane FP used as a filter and a confocal FP used as an analyzer (forward scattering $\theta \simeq 25°$, $\Delta\omega \simeq 1$ GHz). The velocities $v = 2\pi\Delta\omega/q$ are listed in Table II, where they can be compared to ultrasonic measurements at 24 MHz. The uncertainty is typically 1%, and is due chiefly to the uncertainty on q (see below). A weak positive dispersion can be deduced, which is commonly found in liquids. This dispersion was already detected with ultrasonic measurements.[14]

The nitroethane-isooctane mixture is ideal within 1% with respect to the volume additivity.[20] We consider the relationship $v^2 = (\rho\beta_s)^{-1} = (\partial\rho/\partial p)^{-1}_{s,c}$ and the volume additivity, which lead to the density formulation $\rho^{-1} = c\rho_1^{-1} + (1-c)\rho_2^{-1}$ with c the mass fraction of isooctane. Subscripts 1 and 2 refer to, respectively, isooctane and nitroethane. In this case, it is straightforward to deduce the ideal velocity v_{id} from the velocity of each component v_1 and v_2:

TABLE II. Velocity measurements from hypersonic and ultrasonic techniques near the critical point of binary mixture.

Systems	FP technique	Hypersonic measurements: Frequency measurement (GHz)	Hypersonic measurements: Temperature measurement (°C)	Hypersonic measurements: Linear variation v_c (m sec^{-1})	Hypersonic measurements: Linear variation dv/dT (m sec^{-1} K^{-1})	Hypersonic measurements: Critical anomaly	Ultrasonic measurements: Critical anomaly	Ultrasonic measurements: Temperature measurement (°C)	Ultrasonic measurements: Linear variation v_c (m sec^{-1})	Ultrasonic measurements: Linear variation dv/dT (m sec^{-1} K^{-1})	Ultrasonic measurements: Frequency measurements (MHz)	Ultrasonic measurements: Dispersion
nitroethane	2 FP[a]	5.7	23 ± 0.5	1320 ± 50[a]	?			32	1262[b]	?	24	negligible[b] up to 4 GHz
	tandem	0.789	23 ± 0.5	1320 ± 10[a]								
isooctane	2FP[a]	4.8	23 ± 0.5	1110 ± 50[a]	?			11	1050[b]	?	24	weak after[b] 1 GHz
	tandem	1.15	23 ± 0.5	1120 ± 10[a]								
nitroethane + isooctane	1 pass[c]	3.42	30.16[d]	1088 ± 1[e]	−3.8 ± 0.5[e]	No (± 1%)	No (± 0.2%)	30.16[d]	1088 + 24[e]	−4.0 ± 0.2[g]	10.24	?
				1088 ± 10[f]	−3.8 ± 0.5[f]							
	2 pass[a]	4.49	30.16[a]	1115.42 ± 0.18[e]	−4.04 + 0.02[e]	No (± 0.5%)						
				1115 ± 10[f]	−4.04 ± 0.05[f]							
	ideal value[a]			1146 ± 10						1077		
nitrobenzene	1 pass[h]	7.59	20.20	1548 ± 10[f]	−5.8 + 1.3[i]							
n-hexane	1 pass[h]	4.82	20.20	1110 ± 10[f]	−4.9 ± 1.3[i]							
nitrobenzene	1 pass[j]	3.94	20.00	1226 ± 12[j]	−4.7 ± 1[i]	Yes: −10% at $T - T_c = 0.1$ °C						
+	1 pass[h]	5.59	20.20	1229 ± 12[f]	−4.1 ± 1[i]	Yes: −10% at $T - T_c = 0.1$ °C	Yes (−0.5%)	20.6	1215 ± 2[k]	−3.64 ± 0.05[k]	15	?
n-hexane	2 pass[i]	4.63	20.90	1170 ± 12[f]	−4.0 ± 0.5[i]	No (± 1%)						
	ideal value[a]			1135 ± 10								
nitroethane 3-methylpentane	2FP[o] tandem	~5	26.38			No						
water + triethy-amine	1 pass[m]	5	18	1385 ± ?	~ −11	Yes: +10% at $T - T_c = 0.1$ °C	Yes: (−1%)		1330[a]	−11.5[a]	0.6	

[a] This work.
[b] Reference 14.
[c] Reference 16.
[d] For sake of comparison, we have extrapolated the value at the same temperature $T_c = 30.16$ °C. The value found in c was $T_c = 30.91$ °C. The isooctane mass fraction in c is 0.503, here it is 0.5344. The influence is weak: $dv/dc \sim -6$ m sec^{-1}.
[e] The uncertainty concerns the relative values directly deduced from the Brillouin shift.
[f] Absolute value and corresponding error.
[g] Reference 15.
[h] Reference 11 (0.42 mole fraction of nitrobenzene).
[i] Reference 13. Same sample as in h.
[j] Reference 9 (0.40 mole fraction of nitrobenzene). With $dv/dc \simeq 8.4$ m sec^{-1}, the velocity becomes 1218 m sec^{-1} at 0.42 mole fraction.
[k] Reference 8.
[l] We have taken into account the thermal variation of the refractive index (see text).
[m] Reference 7.
[n] Reference 6.
[o] Reference 12.

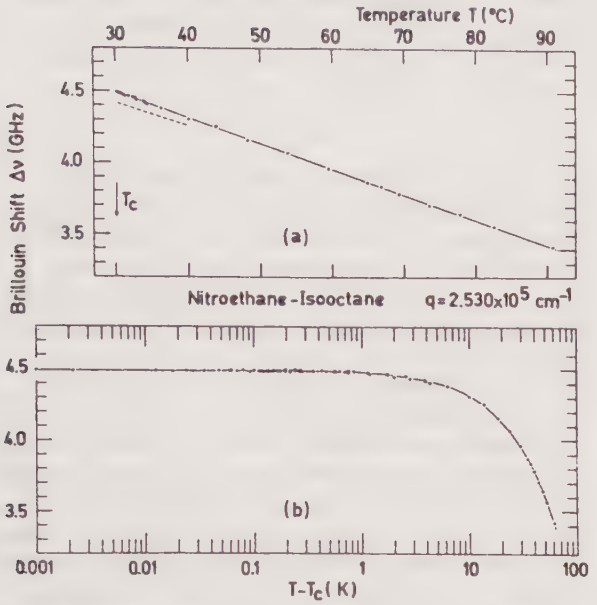

FIG. 4. Plot of the Brillouin shift versus the temperature in linear and semilog coordinates. No anomaly has been detected. The dotted line shows the results of Aref'ev *et al.* (Ref. 16).

$$(\rho v_{id})^{-2} = c(\rho_1 v_1)^{-2} + (1-c)(\rho_2 v_2)^{-2}.$$

The value found for the nitroethane-isooctane system is in Table II, together with that found for the nitrobenzene–*n*-hexane mixture, where hypersonic measurements are available in the literature. In both cases, comparison with experimental data shows relatively good agreement, within 4–5%.

The Brillouin shift of the mixture has been obtained with an accuracy better than 0.5%, this uncertainty taking into account the nonlinearity of the FP scanning. Figure 4 shows unambiguously that within a 0.5% precision, no anomaly of the shift can be detected in the range $T - T_c = 1$ mK–60 K, ($t = 3.3 \times 10^{-6}$–0.2). Only a linear dependence is seen, which is compatible with the hypersonic data of Aref'ev *et al.*[16] (no anomaly within 1%) and the ultrasonic measurements of Anisimov *et al.*,[15] which were both performed with the nitroethane-isooctane mixture. There is also agreement with the Brillouin measurements of Kruer *et al.*[12] on the nitroethane–3-methylpentane system, and with Wang's[13] data on the nitrobenzene–*n*-hexane mixture. Ultrasonic experiments on the last mixture by d'Arrigo *et al.*[8] have shown only a 0.5% negative anomaly near T_c.

On the other hand, our results contrast with Brillouin-shift measurements in the water + triethylamine and nitrobenzene + *n*-hexane mixtures reported by Aref'ev *et al.*[7,10] and Chen *et al.*[11] where, respectively, a +10% and −10% shift anomaly has been observed close to T_c. Let us notice, however, that the FP technique used (single pass) is not well adapted to these opalescent mixtures, as we have discussed above, so these data cannot be regarded as conclusive.

From the Brillouin shift $\Delta\nu$, it is straightforward to obtain the hypersound velocity $v = 2\pi\Delta\nu/q$. The shift, being a linear function of T, can be written as

$$\Delta\nu = \Delta\nu_c + \left(\frac{d(\Delta\nu)}{dT}\right)(T - T_c).$$

The critical anomaly of the refractive index has been found negligible in this mixture.[20,21] We can therefore write

$$q = q_c\left[1 + \frac{1}{n_c}\left(\frac{dn}{dT}\right)_p (T - T_c)\right]$$

so that

$$v(T) = v(T_c) + (T - T_c)\left[\frac{2\pi}{q_c}\frac{d(\Delta\nu)}{dT} - \frac{v_c}{n_c}\left(\frac{dn}{dT}\right)_p\right].$$

The values of n and $(dn/dT)_p$ have been accurately determined in Refs. 21 and 25 for the wavelength $\lambda = 6328$ Å. Since we used $\lambda = 4880$ Å, we had to evaluate the dispersion correction. An order of magnitude for the dispersion correction of the refractive index of the mixture can be evaluated by comparison with the data for pure components.[27] We have estimated the refractive index at 30 °C and 4880 Å to $n = 1.392 \pm 0.001$.

The wavelength dependence of $(dn/dT)_p$ is certainly very weak and we can adopt the value measured at 6328 Å: $(dn/dT)_p = -(4.936 \pm 0.002) \times 10^{-4}$ K^{-1}. Apart from the determination of the shift, uncertainties about the absolute value of the velocity arise from uncertainties in the free spectral range (0.15%) and the transfer wave vector q (0.2%). The total uncertainty is therefore about 1%.

The values of the velocity have been listed in Table II, together with other data concerning ultrasonic or hypersonic measurements in the same system and in two other binary mixtures. For these mixtures we have determined the velocity and its thermal derivative as above. When necessary (nitroethane-isooctane by Aref'ev *et al.*,[16] we have taken into account the small corrections due to the differences in critical concentrations or critical temperatures (see the caption of Table II). The agreement between ultrasonic and hypersonic measurements is good and our data show a very small positive dispersion (+2.5% ± 1%), contrary to other measurements by Aref'ev *et al.* (0 ± 1%).[16]

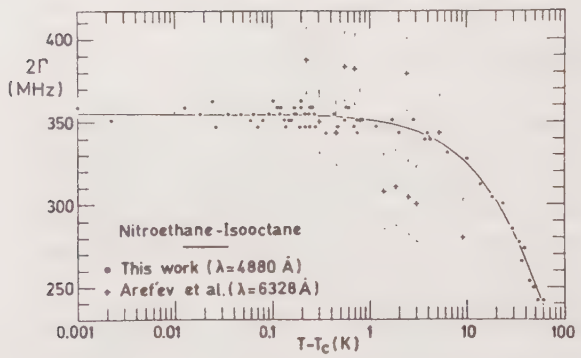

FIG. 5. Brillouin full linewidth 2Γ versus the logarithm of $T-T_c$. The behavior is regular and follows an Arrhenius law (solid curve). Also shown are the data of Ref. 16.

B. Hypersound attenuation

The true full linewidth 2Γ of the Brillouin lines, deduced from the experimental spectrum as explained above, is shown in Fig. 5 versus $T-T_c$ (semilog plot). The accuracy is typically 3%, which allows the thermal variation to be clearly evidenced in a wide range of $T-T_c$ (1 mK–60 K). Also are reported the data of Aref'ev *et al.*[16] from the same mixture, taking into account the difference in the q wave vectors. Although the precision of these data is rather low, they appear to be in agreement.

As for the Brillouin shift, no anomaly in the vicinity of the critical point is visible. This is in contradiction with the data on the nitrobenzene–*n*-hexane mixture in which a critical broadening of the linewidth has been seen. Chen *et al.*[11] used a single-pass FP and the results might have been influenced near T_c by the strong opalescence of the system. Wang,[13] using a double-pass FP, reported also some critical broadening of the linewidth, although he was not able to measure the effect.

It is interesting to note that a strong absorption of the sound is commonly observed at a low frequency near T_c. This is due to the coupling between the sound modes (frequency ω_S) and the critical concentration modes (frequency ω_c). Indeed, an adiabatic pressure fluctuation generates a temperature fluctuation which has a strong influence near T_c on the concentration fluctuation. This coupling is efficient only if the pressure fluctuations have enough time to "feel" the concentration fluctuations, i.e., if $\omega_S \lesssim \omega_c$. Since ω_c is low, ($\omega_c/2\pi < 0.01$ MHz), Brillouin experiments cannot be concerned with this kind of broadening. It is well established now that this ultrasound absorption is strongly frequency dependent, and that no effects are visible for frequencies higher than $\simeq$0.1 GHz. We therefore, expect no contributions from this coupling in a Brillouin experiment working at $\simeq$5 GHz.

Sound absorption arises mainly from the shear and bulk viscosities. The shear viscosity η_S exhibits a critical behavior governed by the exponent $y_\eta \simeq 0.04$[28]:

$$\eta_S = \eta_S^{\text{reg}} t^{-y_\eta} .$$

η_S^{reg} is the regular part of the viscosity, which usually behaves as an Arrhenius law with an activation energy E. Therefore, $\eta_S = \eta_0 t^{-y_\eta} \exp[E/T_c(1+t)]$. As for the sound absorption, the critical part of the viscosity is due to the coupling between the viscous modes and the critical-concentration modes, and the same relaxation effect with frequency is expected. This has been verified by shear flow measurements.[29–31]

Concerning the bulk viscosity η_B, a strong $T-T_c$ dependence is expected[2,4,5]; this approach is quite similar to the direct study of the coupling between the sound mode and the concentration mode.[1,3] The same arguments as above concerning the frequency dependence of the coupling lead to the conclusion that the bulk viscosity should not have any critical anomaly at the Brillouin frequencies.

It is therefore logical to relate the Brillouin linewidth to the regular part of the viscosities:

$$\Gamma q^2 = \frac{q^2}{2\rho}\left(\tfrac{4}{3}\eta_S^{\text{reg}} + \eta_B^{\text{reg}}\right) .$$

We tried the following fits (see Table III):

(i) $\Gamma q^2 = X_2 \exp(X_1/T)$,

assuming the same Arrhenius temperature dependence for both η_S and η_B. The fit of the data is good, but the activation energy $X_1 = 751 \pm 13$ K corresponds to the lower limit of the activation energy obtained from the shear viscosity measurements $E = 920 \pm 180$ K.[22] This means that the bulk viscosity η_B should exhibit a temperature dependence weaker than η_S. So we tried the fit as follows.

(ii) $\Gamma q^2 = X_2 \exp(X_1/T) + X_3$,

with the restriction $X_1 = E = 920 \pm 180$ K, but the results show that the best fit is obtained with a poor determination of X_2 and X_3, which suggests that the temperature dependence of η_B, although weak, cannot be neglected. The 3rd fitting function was the following:

(iii) $\Gamma q^2 = X_2 \exp(X_1/T) + X_3 + X_4 T$,

where we have added a term linearly dependent on T.

With all parameters free or with $X_1 = E$ imposed as above, X_4 is undetermined. But the lower limit of X_2 is almost compatible with the value deduced

TABLE III. Fit of the half-linewidth of Brillouin lines to $\Gamma q^2 = X_2 \exp(X_1/T) + X_3 + X_4 T$. We have assumed $\Gamma q^2 = (q^2/2\rho)[(4/3)\eta_S^{reg} + \eta_B^{reg}]$ (see text). From shear flow measurements (Ref. 22) $\eta_S = \eta_0 \exp(E/T)\{[(T - T_c)/T_c]^{\gamma\eta}\}$ with $\eta_0 = 2.18 \times 10^{-4} P$, $E = (920 \pm 180)$ K, and $\gamma_\eta = 0.045 \pm 0.013$. We have used $\rho = 0.821$ g cm^{-3} at $T = 303$ K (Ref. 20) and $q = 2.53 \times 10^5$ cm^{-1} (see text). Q is a statistical quality coefficient (=1 if the uncertainties are randomly distributed, =0 if not).

X_1 (K)	X_2 (MHz)	X_3 (MHz)	X_4 (MHz K^{-1})	Q	$\sigma(\Gamma)$ (%)	Remarks
751 ± 13	14.8 ± 0.7	(0) imposed	(0) imposed	0.875	1.4	X_3, X_4 imposed to (0)
967 ± 14	5.9 ± 3.6	33.4 ± 17	(0) imposed	0.873	1.4	X_1 imposed to (920 ± 180) K
1134 ± 211	2.8 ± 2.5	90 ± 62	−0.10 ± 0.13	0.872	1.4	all free parameters
1000 ± 120	4.7 ± 2.4	77 ± 57	−0.10 ± 0.11	0.872	1.4	X_1 imposed to (920 ± 180) K

from the regular shear viscosity $X_2 = (q^2/2\pi)(2\eta_0/3\rho) = 1.80$ MHz (values from Table III caption).

From another point of view, these linewidth data can be regarded as measurements of the viscosity, and it seems interesting to compare these results with other indirect viscosity determinations, such as the linewidth of the molecular reorientation spectrum (depolarized scattering), which has been done in the same critical mixture.[22] In Table IV the data in terms of frequency-dependence viscosity for several mixtures are reported, using Brillouin or depolarized scattering, Kerr effect, and the usual shear flow viscosimeter determination. As expected the low-frequency measurements exhibit a divergence, which nevertheless levels off when the frequency of the measurement becomes comparable to the concentration fluctuation frequency.[29-31] As far as the nitroethane-isooctane system is concerned, only the regular behavior is detected for frequencies 5 and 100 GHz. This is well explained by relaxation phenomena as noticed above. The nitrobenzene–n-hexane mixture shows a different behavior, a diverging part being detected for frequencies up to 15 GHz. However, this system is very opalescent, and one could consider the data from Ref. 11 as not very reliable since they were obtained using a single-pass FP. The same difference of behavior has been noticed in the study of the reorientation motion, two techniques, double-pass FP,[32] and optical Kerr effect[33] with a picosecond laser giving the same results, although with somewhat different reorientation times (respectively, 10 and 15 GHz).

This rather puzzling situation suffers from a lack of data concerning other binary mixtures, which prevents any further considerations being made.

C. Brillouin intensity

As explained above, the ratio of the integrated spectral intensity of the Brillouin line $I_B = \int_{-\infty}^{\infty} S_3(\omega)\, d\omega$ to the intensity of the FP apparatus function allows the relative variation of I_B to be measured versus temperature. This is shown in Fig. 6, where a smooth linear variation with T is visible. If the difference between the temperature variation of the scattering volumes of the AF and the mixture are neglected, the intensity I_B must vary as

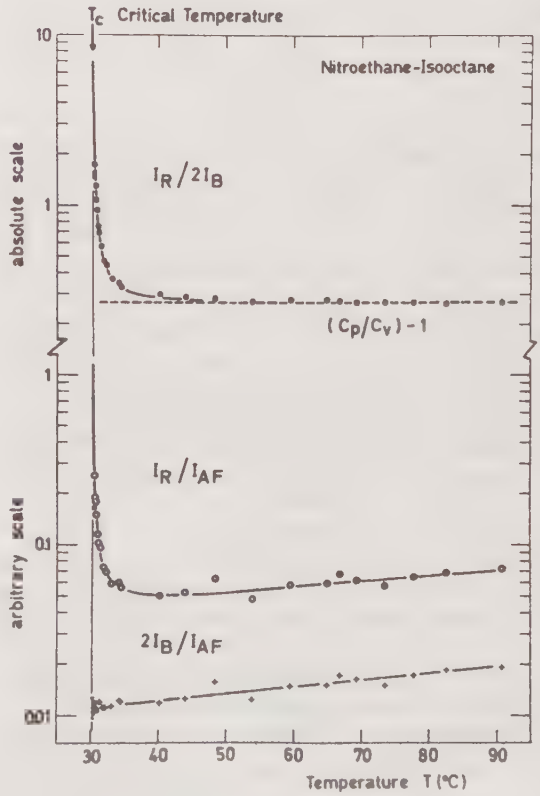

FIG. 6. Different ratios of the intensities of the Rayleigh line I_R, the Brillouin lines $2I_B$, and the intensity standard I_{AF}. The horizontal asymptote of $I_R/2I_B$ shows that strong light is negligible.

TABLE IV. Shear viscosity measurements by different methods and at various frequencies. As typical frequency in the shear flow viscosimeter experiments it has been taken the shear rate; [$t=(T-T_c)/T_c$ and $y_n \simeq 0.04$].

System	Optical Kerr effect Frequency (GHz)	Optical Kerr effect Behavior	Molecular reorientation Frequency (GHz)	Molecular reorientation Behavior	Brillouin spectrum Frequency (GHz)	Brillouin spectrum Behavior	Shear flow viscometer Frequency (GHz)	Shear flow viscometer Behavior
Nitroethane			100[a]	regular	4.5	regular	100[b]	regular
+								×
Isooctane				exp(E/T)		exp(E/T)		divergent
								$t^{-y_n}\exp(E/T)$
Nitrobenzene	15[c]	regular	10[d]	regular	5.5[e]	regular	100[f]	regular
+		×		×		×		×
		divergent		divergent		divergent		divergent
n-hexane		$t^{-y_n}\exp(E/T)$		$t^{-y_n}\exp(E/T)$		$t^{-y_n}\exp(E/T)$		$t^{-y_n}\exp(E/T)$

[a] Reference 22.
[b] This work.
[c] Reference 33.
[d] Reference 32.
[e] Reference 11.
[f] Reference 30.

$$k_B T \beta_s \left(\frac{\partial(n^2)}{\partial\rho}\right)^2_{T,c}.$$

Using the definition of β_s and the well-known relationship

$$\beta_s = (\rho v^2)^{-1}, \quad I_B \propto T\left(\rho \frac{\partial(n^2)}{\partial\rho}\right)^2_{T,c} \Big/ \rho v^2 .$$

An order of magnitude of the variation is given by

$$\frac{1}{I_B}\left(\frac{dI_B}{dT}\right) \simeq \frac{1}{T_c} - \frac{1}{\rho}\left(\frac{\partial\rho}{\partial T}\right)_p - \frac{2}{v_c}\frac{dv}{dT} + \frac{4n}{n^2-1}\left(\frac{dn}{dT}\right)_p ,$$

where the Rocard relation $[\rho\,\partial(n^2)/\partial\rho]^2_T = (n^2-1)^2$ was assumed[18] for simplicity (the Einstein or Yvon-Vuks formulations do not change the results appreciably). Each term is known, except $(1/\rho)(\partial\rho/\partial T)_p$, which can be estimated as $(-1.2 \times 10^{-3})\ \mathrm{K}^{-1}$ when looking at each component,[25] and one finally obtains $(1/I_B)(dI_B/dT) \simeq 10^{-2}\ \mathrm{K}^{-1}$, which agrees well with the data as shown in Fig. 6.

D. Background intensity

The recorded spectra show a non-negligible baseline due to broad lines, which cannot be resolved in the free spectral range of the FP. One component of this background is the scattering due to the anisotropy of the nitroethane molecules,[22] but other mechanisms (Raman, collision-induced, etc.) also contribute.

E. Rayleigh intensity: Rayleigh-Brillouin ratio

The Rayleigh intensity measures the nonresolved contributions from stray light, entropy fluctuations, and (critical-) concentration fluctuations. We first checked that the stray light, which is expected to have no temperature variation, was negligible. Stray light is exhibited far from T_c, where concentration fluctuations are negligible. Figure 6 shows that, far from T_c, the Rayleigh intensity normalized to the FP apparatus function varies as the Brillouin intensity, which proves that the stray light is effectively negligible versus the entropy contribution so that the ratio Rayleigh-Brillouin measures the ratio entropy-Brillouin, i.e., the Landau-Placzek ratio. It is well known that this ratio is equal to $(C_p/C_v)-1=\gamma_0-1$. In critical mixtures C_v is regular while C_p is the sum of a regular part and a diverging part, with the exponent $\alpha \simeq 0.1$. However, refractive-index measurements[20] have shown that the amplitude of the diverging part is very small in this mixture so that C_p can be considered as regular here, and the ratio γ_0 as independent of the temperature. The low value found $\gamma_0 = 1.27$ is a final check of the smallness of the stray light.

We then fitted the experimental Rayleigh-Brillouin ratio taking into account only the two contributions $S_1/2S_3$ and $S_2/2S_3$ (see Figs. 1 and 7):

$$\frac{I_R}{2I_B} = \left(\frac{\left(\frac{\partial(n^2)}{\partial c}\right)^2_{p,T}}{\left(\rho\frac{\partial(n^2)}{\partial\rho}\right)^2_{T,c}} \frac{\rho v^2}{\left(\frac{\partial\mu}{\partial c}\right)^0_{p,T}} t^{-\gamma} G(q,\xi) \right) + (\gamma_0 - 1).$$

As we have stressed above, this ratio is independent of the light-scattering theories. For simplic-

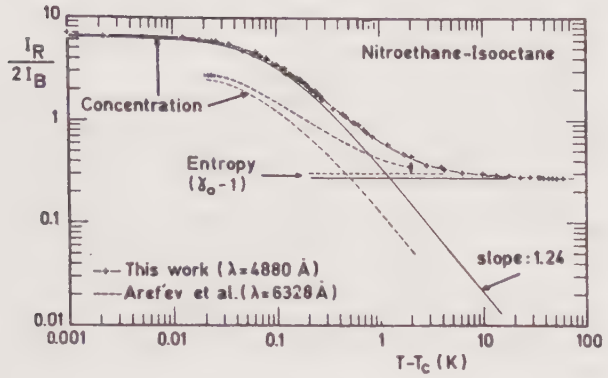

FIG. 7. Rayleigh-Brillouin ratio versus $T-T_c$ (log-log plot) showing the different contributions to the Rayleigh peak (this work and Ref. 16).

ity we shall use the Einstein formulation, where the factors $(\partial(n^2)/\partial c)_{\rho,T}$ and $(\partial(n^2)/\partial\rho)_{T,c}$ are mathematical derivatives and can be calculated using the Lorentz-Lorenz formula.

We know $(\partial n/\partial c)_{\rho,T}$ at $T \sim 30$ °C and $\lambda = 6328$ Å,[34]

$$\left(\frac{\partial n}{\partial c}\right)_{\rho,T} = (1.34 \pm 0.04) \times 10^{-3},$$

the dispersion correction can be estimated from the literature,[27]

$$\left(\frac{\partial n}{\partial c}\right)_{\rho,T}(4880\ \text{Å}) = \left(\frac{\partial n}{\partial c}\right)(6328\ \text{Å}) + (1.2 \pm 0.2) \times 10^{-3}$$
$$= (2.54 \pm 0.24) \times 10^{-3},$$

while the temperature dependence can be obtained by a straightforward application of the Lorentz-Lorenz theory and the data[20]

$$\frac{\partial n_1}{\partial T} = -4.961 \times 10^{-4}\ \text{K}^{-1},$$

$$\frac{\partial n_2}{\partial T} = -4.774 \times 10^{-4}\ \text{K}^{-1}.$$

We finally get

$$\frac{1}{\left(\frac{\partial(n^2)}{\partial c}\right)_{\rho,T}} \frac{\partial}{\partial T}\left(\frac{\partial(n^2)}{\partial c}\right)_{\rho,T} \simeq 7.7 \times 10^{-3}\ \text{K}^{-1}.$$

The evaluation of $\partial n/\partial\rho$ is not accurate if we differentiate the Lorentz-Lorenz formula, and it is better to calculate this ratio from its value in each component.[25] This leads to

$$\rho\left(\frac{\partial(n^2)}{\partial\rho}\right)_{T,c} = 2n\,\frac{\left(\frac{\partial n}{\partial T}\right)_{\rho,c}}{\frac{1}{\rho}\left(\frac{\partial\rho}{\partial T}\right)_{\rho,c}} = 1.14 \pm 0.05,$$

the thermal variation of which can be easily evaluated to $-2 \times 10^{-3}\ \text{K}^{-1}$. The factor ρv^2 exhibits also a T dependence, which can be easily estimated from the above results:

$$\frac{1}{\rho v^2}\frac{d}{dT}(\rho v^2) = -8.2 \times 10^{-3}\ \text{K}^{-1}.$$

$G(q,\xi)$ is the critical contribution of concentration fluctuations, and can be written under the following form, valid within 1% in the range $q\xi = (20 - 5 \times 10^{-4})$[35] [our experiment covers the range $q\xi = (20 - 2 \times 10^{-2})$].

$$G(q,\xi) = [1 + (\alpha_1 q\xi)^2]^{-(1-\eta/2)} + [1 + (\alpha_2 q\xi)^2]^{-\Omega} - [1 + (\alpha_3 q\xi)^2]^{-\Sigma},$$

with $\alpha_1 = 1.040\,056$, $\alpha_2 = 1.058\,947$, $\alpha_3 = 1.053\,932$, $\eta = 0.0315$, $\Omega = 1.554\,213$, $\Sigma = 1.627\,419$. We recall that $\xi = \xi_0[(T - T_c)/T_c]^{-\nu}$.

Finally, the experimental data had to be compared with the following temperature variations:

$$\frac{I_R}{2I_B} = \left[A_c[1 + m(T - T_c)]\left(\frac{T - T_c}{T_c}\right)^{-\gamma} G(q,\xi)\right] + (\gamma_0 - 1),$$

where

$$A_c = \frac{\left[\left(\frac{\partial(n_c^2)}{\partial c}\right)_{\rho,T}\right]^2}{\left(\rho\frac{\partial(n^2)}{\partial\rho}\right)^2}\,\frac{\rho_c v_c^2}{\left(\frac{\partial\mu}{\partial c}\right)_{\rho,T}^{\delta}}$$

and $m = 1.1 \times 10^{-2}\ \text{K}^{-1}$. The subscript c means that the value is taken at T_c. The coefficients A_c, ξ_0, ν, γ, and γ_0 are considered as free parameters.

First we have checked that the value of m does not influence the results very much; with (m) set to different values between $-1.6 \times 10^{-3}\ \text{K}^{-1}$ and $+1.6 \times 10^{-2}\ \text{K}^{-1}$, the values of the above parameters did not change within 0.5%, which was within the uncertainties.

Second, with all parameters free, the determination of the amplitude ξ_0 is strongly correlated with ν, as well as A_c with γ, which prevents accurate independent determinations (Fig. 8 reports the values found for ξ_0 as a function of ν, and A_c as a function of γ, for about the same quality of the fit). We thus fixed the exponents at their expected values in binary mixtures (Refs. 36 and 37) $\gamma = 1.2402 \pm 0.0009$, $\nu = 0.6300 \pm 0.0008$. The results of the fit are in Table V.

The values found lead to the following remarks.

i. The correlation length amplitude ξ_0. The uncertainty on ξ_0 is in fact slightly bigger than deduced from the fit, since the true variable is the product $q\xi_0$. Therefore,

$$\xi_0 = 2.42 \pm 0.04\ \text{Å}.$$

ii. The Landau-Placzek ratio $(\gamma_0 - 1)$. The value found for the ratio $C_p/C_v = \gamma_0 = 1.2702 \pm 0.0009$ is

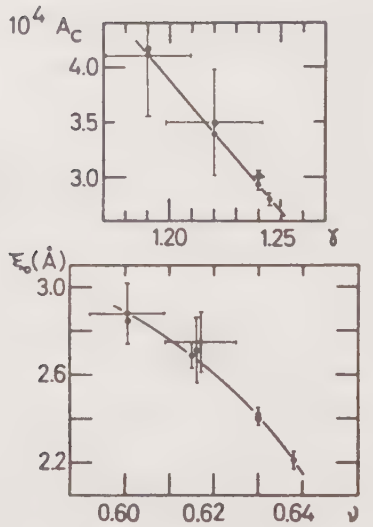

FIG. 8. "Best" values of the couples of correlated variables (A_c, γ) and (ξ_0, ν). It has been necessary to fix the values of the critical exponents to their universal values to determine accurately the amplitudes A_c and ξ_0.

usual in liquids. The comparison with the data of Ref. 16 (see also Fig. 7), where the value 1.30 was found, gives a satisfactory agreement.

iii. The amplitude $(\partial\mu/\partial c)^0_{\rho,T}$ and the universal amplitude ratio $R_t^+ R_c^{-1/3}$. From the value A_c we can infer

$$\left(\frac{\partial \mu}{\partial c}\right)^0_{\rho,T} = \left(\frac{(\partial(n_c^2)/\partial c)_{\rho,T}}{\rho(\partial(n_c^2)/\partial\rho)}\right)^2 \frac{\rho_c v_c^2}{A_c} = 134 \pm 20\ \mathrm{J\,cm^{-3}}.$$

We fitted the results of Ref. 16, performed at $\lambda = 6328$ Å, in the same way and got $A_c = (1.06 \pm 0.15) \times 10^{-4}$, which gives a value in agreement $(\partial\mu/\partial c)^0_{\rho,T} = (103 \pm 20)\ \mathrm{J\,cm^{-3}}$.

We can therefore deduce the amplitude of the diverging susceptibility without any assumptions concerning light-scattering theories (Einstein, Yvon-Vuks, or Rocard).[18] It is interesting to check the value found for the universal amplitude ratio

$$R_t^+ R_c^{-1/3} = \xi_0 \left[B^2 \left(\frac{\partial \mu}{\partial c}\right)^0_{\rho,T} \Big/ k_B T_c\right]^{1/3},$$

where B is the amplitude of the coexistence curve defined as $(c^+ - c^-)/2 = B|t|^\beta +$ corrective terms, whose value is $B = 0.915 \pm 0.008$ in this mixture.[19] Our data lead to $R_t^+ R_c^{-1/3} = 0.72 \pm 0.07$ and those of Ref. 16 to $R_t^+ R_c^{-1/3} = 0.66 \pm 0.07$, in good agreement with the theoretical predictions[38,39] of 0.650 by the high-temperature-series method and 0.667 by renormalization-group calculations.

V. CONCLUSION

The study of the linewidth and the intensity of the Rayleigh-Brillouin spectrum versus $T - T_c$ in the weakly opalescent mixture of nitroethane and isooctane using a high-contrast spectrometer has

TABLE V. Fit of the Rayleigh-Brillouin Ratio to

$$\frac{I_R}{2I_B} = \left[A_c[1 + m\ (T - T_c)]\left(\frac{T - T_c}{T_c}\right)^{-\gamma} G(q\xi)\right] + (\gamma_0 - 1),$$

where $G(q\xi) = \sum_i b_i[1 + (\alpha_i q\xi)^2]^{-\mu_i}$ and (see text)

$b_1 = +1$, $\alpha_1 = 1.040\,056$, $\mu_1 = 1 - \eta/2 = 0.984\,25$,

$b_2 = +1$, $\alpha_2 = 1.058\,947$, $\mu_2 = \Omega = 1.554\,213$,

$b_3 = -1$, $\alpha_3 = 1.053\,932$, $\mu_3 = \Sigma = 1.627\,419$,

$m = 1.6 \times 10^{-3}\ \mathrm{K^{-1}}$, $q = 2.530 \times 10^5\ \mathrm{cm^{-1}}$, $\xi = \xi_0(1 - T/T_c)^{-\nu}$.

The parameters A_c, ξ_0, and γ_0 are considered as free parameters. The critical exponents γ and ν are universal and imposed to their expected value from a renormalization-group (RG) calculation (Ref. 38): $\gamma = 1.2402 \pm 0.0009$ and $\nu = 0.6300 \pm 0.0008$ [the values estimated by a high-temperature-series analysis are about the same (Ref. 39)].

Parameters	Results of the fit	Remarks
γ	1.2403 ± 0.0009	imposed within RG uncertainties
ν	0.6294 ± 0.0005	imposed within RG uncertainties
A_c	$(2.94 \pm 0.04) \times 10^{-4}$	free
ξ_0	2.42 ± 0.03 (Å)	free
$\gamma_0 - 1$	0.270 ± 0.001	free

Statistical quality coefficient = 0.841
Mean relative uncertainty = 3.02×10^{-2}

shown that neither the hypersonic velocity, the hypersound attenuation, nor the intensity of the Brillouin lines exhibit an anomalous behavior when approaching the critical point. The values which have been determined for these quantities are in the usual range for liquids. Moreover, the Rayleigh-Brillouin intensity ratio has allowed the ratio γ_0 of the specific heats to be accurately determined, with the correlation length amplitude ξ_0 and the susceptibility amplitude $[(\partial\mu/\partial c)^0_{p,T}]^{-1}$. It is worthwhile to note that this last parameter can be obtained without the usual local-field hypotheses (Einstein, Yvon-Vuks, or Rocard) which yield an ambiguous determination. Therefore, the universal amplitude ratio $R_\xi^+ R_c^{-1/3}$ has been obtained in agreement with the expected theoretical value.

ACKNOWLEDGMENTS

We gratefully thank B. Mozer and B. Le Neindre for their comments about this manuscript.

---

*On leave from Laboratoire des Interactions Moléculaires et des Hautes Pressions, C. N. R. S. Université Paris Nord, Avenue J. B. Clement, 93430 Villetanneuse, France.

[1]M. Fixman, J. Chem. Phys. 36, 1961 (1962).
[2]K. Kawasaki and M. Tanaka, Proc. Phys. Soc. London 90, 791 (1967).
[3]W. Botch and M. Fixman, J. Chem. Phys. 42, 199 (1965).
[4]J. M. Deutch and R. Zwanzig, J. Chem. Phys. 46, 1612 (1967).
[5]K. Kawasaki, Phys. Rev. A 1, 1750 (1970); 3, 1097 (1971).
[6]A. G. Chynoweth and W. G. Schneider, J. Chem. Phys. 19, 1566 (1951).
[7]I. M. Aref'ev, Zh. Eksp. Teor. Fiz. Pis'ma Red. 7, 361 (1968) [JETP Lett. 7, 285 (1968)].
[8]G. D'arrigo and D. Sette, J. Chem. Phys. 48, 691 (1968).
[9]I. M. Aref'ev and N. V. Shilin, Zh. Eksp. Teor. Fiz. Pis'ma Red. 10, 138 (1969) [JETP Lett. 10, 87 (1969)].
[10]I. M. Aref'ev and V. J. Birynkov, Zh. Eksp. Teor. Fiz. Pis'ma Red. 12, 352 (1970) [JETP Lett. 12, 240 (1970)].
[11]S. H. Chen and N. Polonsky, Phys. Rev. Lett. 20, 909 (1968).
[12]M. R. Kruer and R. W. Gammon, Bull. Am. Phys. Soc. 16, 84 (1971).
[13]C. S. Wang, Opt. Commun. 5, 56 (1972).
[14]M. I. Shakparonov, Yu. G. Shoroshev, S. S. Aliev, M. G. Khalinlin, and P. K. Khabibullaev, Zh. Fiz. Khim. 43, 2543 (1969) [Russ. J. Phys. Chem. 43, 1425 (1969)].
[15]A. Anisimov, I. M. Aref'ev, A. V. Voronel, V. P. Voronov, Yu. F. Kiyachenko, and I. L. Fabelinskii, Zh. Eksp. Teor. Fiz. 61, 1524 (1971) [Sov. Phys.—JETP 34, 813 (1972)]; I. M. Aref'ev and I. L. Fabelinskii, J. Phys. (Paris) 33, C1–131 (1972).
[16]I. M. Aref'ev, I. L. Fabelinskii, M. A. Anisimov, Yu. F. Kiyachenko, and V. P. Voronov, Opt. Commun. 9, 69 (1973).
[17]R. D. Mountain and J. M. Deutch, J. Chem. Phys. 50, 1103 (1969); P. Calmettes, thesis, Paris, 1969 (unpublished).
[18]For review, see D. Beysens, J. Chem. Phys. 64, 2579 (1976).
[19]D. Beysens, J. Chem. Phys. 71, 2557 (1979).
[20]D. Beysens and J. Wesfreid, J. Chem. Phys. 71, 119 (1979).
[21]D. Beysens and A. Bourgou, Phys. Rev. A 19, 2407 (1979).
[22]G. Zalczer and D. Beysens, J. Chem. Phys. 72, 348 (1980). Note that the value of η_0 is erroneous and must be changed from 2.82×10^{-4} P to 2.18×10^{-4} P.
[23]D. Beysens, Rev. Sci. Instrum. 50, 509 (1979).
[24]D. Beysens and G. Zalczer, Opt. Commun. 23, 142 (1977).
[25]D. Beysens and P. Calmettes, J. Chem. Phys. 66, 766 (1977).
[26]M. Tournarie, J. Phys. (Paris) 30, 47 (1969).
[27]Vogel, J. Chem. Soc. 1852 (1948); Wibaut, Rec. Trav. Chim. Pays-Bas Belg. 58, 374 (1939): quoted in Landolt-Bornstein, *Eigenschaften der Materie in Ihren Aggregatzuständen 8 Teil Optische Konstanten* (Springer, Berlin, 1962).
[28]P. Calmettes, Phys. Rev. Lett. 39, 1151 (1977).
[29]G. Carini, G. Maisano, P. Migliaro, and F. Wanderlingh, Phys. Rev. A 5, 1755 (1975).
[30]D. Beysens, S. H. Chen, J. P. Chabrat, L. Letamendia, J. Rouch, and C. Vaucamps, J. Phys. Lett. (Paris) 38, L-203 (1977).
[31]D. Beysens, M. Gbadamassi, and L. Boyer, Phys. Rev. Lett. 43, 1253 (1979).
[32]D. Beysens and G. Zalczer, Phys. Rev. A 18, 2280 (1978).
[33]D. Lister and D. E. Cooper, in Proceedings of the topical meeting in picosecond phenomena, edited by E. Ippen and C. V. Shank, North Falmouth, Mass., 1980 (unpublished); and D. E. Cooper, thesis, M.I.T., 1980 (unpublished).
[34]Note that the formula used in Ref. 19 to obtain the refractive index difference of the components from $(\partial n/\partial c)_{p,T}$ was approximate. Indeed, the derivative of the Lorentz-Lorenz LL formula for binary mixtures with nearly matched refractive indices leads to $(\partial n/\partial c)^{LL}_{p,T} = [(n_1 - n_2)]\ [(\rho/\rho_1) + (\rho/\rho_2)]$. Therefore, $(n_1 - n_2)$ can be estimated at 30 °C and 6328 Å: $(n_1 - n_2) = (1.36 \pm 0.04)\times10^{-3}$, which is somewhat different from the value 0.95×10^{-3} which was proposed.
[35]D. Beysens, A. Bourgou, and P. Calmettes (unpublished).
[36]J. C. Le Guillou and J. Zinn-Justin, Phys. Rev. B 21, 3976 (1980) and references therein.
[37]Phase Transitions: Status of the experimental and theoretical situations, edited by M. Levy, J. C. Le Guillou, and J. Zinn-Justin, Cargèse Summer Institute, 1980 (in press).
[38]A. Aharony and P. C. Hohenberg, Phys. Rev. B 13, 3081 (1976).
[39]C. Bervillier, Phys. Rev. B 14, 4964 (1976).

C H A P I T R E V I

Détermination de combinaisons d'amplitudes dans le mélange critique de nitrobenzène et n-hexane

VI.1 - Introduction

La détermination des exposants critiques a longtemps été le problème principal des théories des points critiques. L'accord observé aujourd'hui entre les deux principales théories (Groupe de Renormalisation RG et Séries Haute Température HTS) et les résultats expérimentaux fait considérer ce problème comme résolu. Il est dès lors important de vérifier expérimentalement d'autres conséquences de ces théories, en particulier les valeurs prédites pour certaines combinaisons universelles d'amplitudes.

Bien que l'universalité de ces combinaisons, sinon leur valeur ait été prédite depuis longtemps [a], leur investigation expérimentale n'a débuté que récemment. La raison essentielle en est que la détermination de ces amplitudes nécessite impérativement la connaissance préalable des valeurs des exposants associés. L'objet de l'article présenté dans ce chapitre est de déterminer un certain nombre de ces combinaisons dans le mélange critique de nitrobenzène et n-hexane. L'introduction théorique en a été faite au chapitre II. Les combinaisons déterminées sont tabulées dans la table 1.

VI.2 - Contraintes expérimentales

La principale difficulté expérimentale est la nécessité de faire des mesures absolues. La détermination d'un exposant s'effectue par comparaison des mesures de la même quantité pour diverses valeurs de la variable (t ou M) : on peut donc négliger tous les paramètres expérimentaux constants. La détermination de combinaisons d'amplitudes de grandeurs différentes au contraire requiert que tous les paramètres soient parfaitement connus. Cela est souvent difficile expérimentalement et parfois impossible pour des raisons théoriques. Nous avons eu plusieurs fois l'occasion de voir (Ch. I et V) que la mesure d'une intensité diffusée ne permettait pas de remonter à l'amplitude absolue de la fluctuation diffusante. Les méthodes adaptées à la mesure des exposants ne conviennent pas forcément à celle des amplitudes.

Une autre difficulté provient du fait que les amplitudes sont beaucoup plus sensibles aux impuretés que les exposants. S'il est impos-

sible de préparer un échantillon rigoureusement pur, on peut cependant limiter l'influence des impuretés en utilisant - dans la limite du possible - un seul échantillon. Il est probable qu'une légère dérive des amplitudes se compense dans les combinaisons. De fait, sauf deux exceptions, nous avons effectué nos mesures sur un seul échantillon, scellé sous vide, celui décrit et utilisé au chapitre IV.

VI.3 - Résultats

Les différents montages utilisés sont décrits et les résultats présentés dans les divers appendices de l'article. Nous nous limiterons ici à un résumé succinct.

a) Courbe de coexistence

La composition de chaque phase est déterminée d'après son indice de réfraction. Pour mesurer celui-ci, on utilise le fait que la cellule est cylindrique, donc se comporte comme une lentille cylindrique dont la distance focale varie avec l'indice du liquide contenu. La position du foyer est déterminée par une conjugaison optique simple. L'incertitude sur les différences d'indices mesurées est de l'ordre de 10^{-4}. Notons que pour obtenir un bon accord de la fonction théorique avec les données expérimentales, il a fallu y introduire un terme correctif mais que celui-ci a très peu d'influence sur la valeur de l'amplitude B. La relation entre l'indice et la concentration a été déterminée par des mesures de réfractométrie mais il faut souligner que cette valeur se simplifie dans les combinaisons du fait du caractère optique des autres mesures. Néanmoins elle permet de constater un excellent accord entre nos mesures et celles de la littérature, effectuées selon des méthodes classiques.

b) Spectre Rayleigh Brillouin

L'intérêt d'une telle mesure du point de vue des relations d'amplitude a été montré au chapitre précédent. Nous disposions de quelques spectres à faible résolution (fig. AI.1), séquelles du chapitre IV qui nous ont montré qu'il n'y avait pas de correction significative à la loi asymptotique dans la région étudiée (fig. AI.2). Il suffisait donc d'enregistrer un seul spectre avec une résolution convenable (fig. AII.3).

c) Chaleur spécifique

La calorimétrie est inutilisable près d'un point critique. En effet, elle exige des variations de température relativement importantes, incompatibles avec une bonne proximité du point critique. La détermination de la partie critique de la chaleur spécifique exige donc une approche indirecte. Pour celà nous avons utilisé la relation :

$$C_{P,M} - C_{VM} = \alpha p \; V \; T_c \left(\frac{\partial T_c}{\partial P} \right)^{-1} \quad \text{où} \quad \alpha p = \frac{1}{V} \left(\frac{\partial V}{\partial T} \right)_{P,M}$$

que l'on peut séparer en partie régulière et partie critique :

$$C_{P,M}^{crit} = VTc \left(\frac{\partial Tc}{\partial p} \right)^{-1} \alpha_p^{crit}$$

Il suffit donc de mesurer la dilatation isobare du fluide. Ceci peut s'effectuer de deux manières : soit directement, par exemple par la méthode du réservoir et du capillaire, qui implique la préparation d'un autre échantillon, soit indirectement en attribuant au seul effet de la densité la variation de l'indice de réfraction.

Nous avons utilisé les deux méthodes dans un souci de justification réciproque.

La détermination de la variation de l'indice de réfraction se fait par une méthode interferométrique : on enregistre les franges d'interférence des deux réflexions d'un faisceau laser sur deux faces de la cellule (voir figure a).

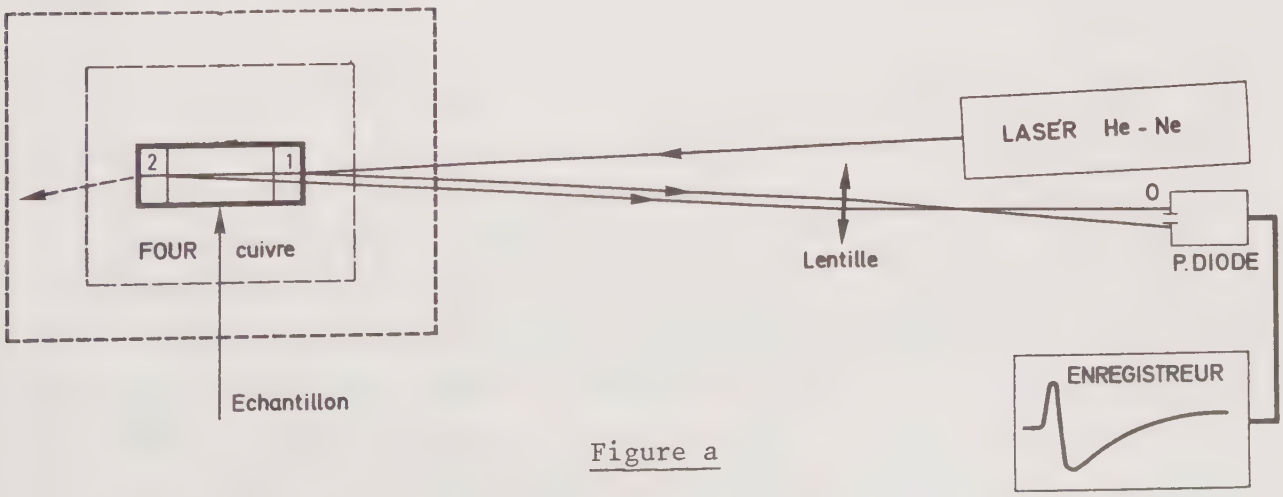

Figure a

L'ordre d'interférence sera $2\ ne/\lambda_o$. Le défilement des franges permet de mesurer les variations d'indice avec une précision de l'ordre de 10^{-6}.

Ces mesures étant tout-à-fait compatibles avec celles de volume et beaucoup plus précises, nous les avons utilisées pour déterminer l'amplitude A^+ et avons également conclu que les autres contributions éventuelles à l'anomalie de l'indice de réfraction étaient négligeables.

d) Turbidité

La diffusion de la lumière s'accompagne forcément d'une perte d'intensité du faisceau transmis de la forme

$$I = I_o\ e^{-\tau \ell}$$

où l est la longueur parcourue. τ est appelé la turbidité. Ce paramètre est évidemment l'intégrale sur les angles de la fonction $S(k)$, transformée de Fourier et la fonction de corrélation $G(r)$ et qui donne l'intensité diffusée au vecteur d'onde de transfert k. La détermination de la longueur caractéristique ξ à partir de la connaissance de $\tau(t)$ se déroule de la même façon qu'à partir de $S(k,t)$ comme il a été fait au chapitre précédent. Il faut souligner cependant que les mesures de turbidité sont sensiblement plus aisées et que les résultats obtenus sont absolus et permettraient également la détermination de l'amplitude de la susceptibilité, ne serait la méconnaissance que nous avons de la valeur du coefficient de couplage. Notons que la comparaison des mesures de turbidité et de rapport Rayleigh Brillouin permet de déterminer ce coefficient de couplage.

Nous avons effectué des mesures de turbidité sur les trois trajectoires principales : l'isochore critique, la courbe de coexistence et l'isotherme critique. Cette dernière ne pouvait être étudiée qu'avec une cellule à concentration variable. Pour les deux autres, nous avons utilisé les deux cellules. La cellule à concentration variable présentant une longueur optique de 5 mm permettait d'approcher plus près du point critique. De plus elle a permis de corriger le léger défaut de criticité de la cellule de référence. Enfin la comparaison des résultats des deux cellules, sur la courbe de coexistence, permet également de vérifier la calibration des mesures sur l'isotherme critique.

Ces mesures de turbidité nous ont permis de mesurer la longueur caractéristique ξ le long des trois trajectoires fondamentales et les rapports des amplitudes respectives de la susceptibilité.

e) Mesures dynamiques

Enfin nous avons effectué une série de mesures de temps de corrélation afin de déterminer la valeur de la constante dynamique R définie au ch. II. Des mesures analogues avaient déjà été effectuées [b] mais manquaient de précision. Nous avons utilisé cette fois-ci un corrélateur digital afin d'améliorer cette précision (fig. AV.1). Les résultats ont été comparés aux deux fonctions proposées avec des résultats très voisins, compatibles avec la valeur de 1 prédite par la théorie des modes couplés.

VI.4 - Conclusion

Nous avons mesuré de façon absolue les amplitudes de la longueur de corrélation et de la susceptibilité le long des trois trajectoires du diagramme de phase d'un mélange binaire critique pour lesquelles elles ont été calculées : isochore critique, isotherme critique et courbe de coexistence. A notre connaissance, les amplitudes relatives à l'isotherme critique n'avaient jamais été mesurées dans un mélange binaire. Nous avons également mesuré l'amplitude de la chaleur spécifique sur l'isochore critique et celle de la courbe de coexistence. Nous avons pu en déduire les relations présentées dans la table I.

Les valeurs prévues par les deux théories sont en général très proches de sorte qu'il est impossible de déclarer l'une d'elles plus proche de l'expérience, sauf dans le cas du rapport C^+/C^- où la valeur expérimentale est en bon accord avec la valeur R.G. mais pas avec celle des H.T.S.

Toutes les autres combinaisons mesurées sont en bon accord avec les théories puisque la différence dépasse à peine l'incertitude expérimentale dans les pires des cas. Nous pouvons donc en conclure que nos expériences constituent une preuve convaincante de la validité de ces théories.

Enfin la valeur obtenue pour la constante dynamique R est en accord avec la prédiction originale de la théorie des modes couplée et en désaccord avec celles du groupe de renormalisation.

Références

[a] P.G. WATSON
J. Phys. C2, 1883 (1969) et J. Phys. C2 , 2158 (1969)

[b] Thèse de IIIe cycle - Université Paris VI (1977)

COMMISSARIAT A L'ENERGIE ATOMIQUE

DIVISION DE LA PHYSIQUE

SERVICE DE PHYSIQUE DU SOLIDE
ET
DE RESONANCE MAGNETIQUE

AMPLITUDE COMBINATIONS IN THE CRITICAL BINARY FLUID NITROBENZENE AND N- HEXANE

by

G. Zalczer, A. Bourgou* and D. Beysens

*Permanent address :
Ecole Normale Supérieure, 43 rue de la Liberté, Le Bardo, Tunisie

CEN-SACLAY – 91191 GIF-sur-YVETTE CEDEX – FRANCE

ABSTRACT

We have determined experimentally the amplitudes of the correlation length and susceptibility along the three principal trajectories : critical isochore, coexistence curve and for the first time in a critical mixture, critical isotherm. We have also determined the amplitude of the coexistence curve and that of the specific heat along the critical isochore. These amplitudes allowed us to compute several universal amplitude combinations, which are all in agreement with the renormalization group theoretical predictions and except one exception (C^+/C^-) with the high temperature series ones. Moreover linewidth measurements allowed to determine the dynamic constant R, found to be close to unity in agreement with the original mode - coupling theory and in disagreement with the dynamical renormalization group predictions.

Submitted for publication to :
"Phys. Rev. A"

DPh-T/PSRM/82/2000
May 1982

I. INTRODUCTION

The hypothesis of universality has played a central role in the study of phase transitions. It arises from the fact that characteristic lengths near a critical point are much larger than the microscopic interaction scale. Therefore these details are forgotten and most of the observed quantities depend only on the dimensionalities of the space (d) and of the order parameter (n). For instance the 3d Ising model and the fluid and binary mixtures transitions belong to the same class of universality d=3, n=1. At the present state of the theory, the exponents are universal and related by the so-called scaling laws, while the microscopic nature of the system is reflected through 2 independent amplitudes, at least asymptotically close to the critical point. The other amplitudes can then be deduced using universal amplitude combinations.

While the exponents and the relations between them have been subjects of experiments for a long time, the amplitudes received attention only recently. The reason for that is that their study requires the gathering of results of different kinds of experiments and therefore the knowledge of many parameters, including the critical exponents themselves. These exponents are now well known and the theoretical methods which have therefore proved their reliability can be used to calculate these new constants.

A complete check of the theory however requires experimental determinations of these combinations. The purpose of the present paper is to determine some of these constants for the mixture of nitrobenzene and n-hexane. The different techniques involved are static and dynamic light scattering (self beating spectroscopy and Fabry Perot interferometry), interferometry, refractometry and volumetry. However, the measurements have been performed using the very same cell whenever possible.

Though the theory predicts the behaviour of a system along the three basic trajectories : critical isochore, critical isotherm and coexistence curve, most of the experiments so far have been limited to the critical isochore. However, in this paper, all these three trajectories will be studied.

II. THEORETICAL BACKGROUND

1. General

According to the standard terminology, we shall call M the order parameter, H the conjugate field, T_c the critical temperature and $t=(T-T_c)/T_c$ the reduced temperature. Along the critical isochore ($t>0$, $M=H=0$) the following quantities will behave :

susceptibility $$\chi = \left(\frac{\partial M}{\partial H}\right)_T = C^+ t^{-\gamma}/k_B T_c \qquad (1)$$

specific heat $$C_p = \frac{A^+}{\alpha} k_B t^{-\alpha} + \text{regular part} \qquad (2)$$

correlation length $$\xi = \xi_o^+ t^{-\nu} . \qquad (3)$$

Along the critical isotherm ($t=0$), whose equation is :

$$H = DM^{\delta} \qquad (4)$$

we have

$$k_B T\chi = C_c H^{-\gamma/\beta\delta} \equiv \frac{1}{\delta D^{1/\delta}} H^{-\gamma/\beta\delta} \qquad (5)$$

$$\xi = \xi_o^c H^{-\nu/\beta\delta} . \qquad (6)$$

Along the coexistence curve ($H=0$, $t<0$) whose equation is :

$$M = B(-t)^{\beta} \qquad (7)$$

we have

$$k_B T\chi = C^-(-t)^{-\gamma} \qquad (8)$$

$$C_p = k_B \frac{A^-}{\alpha} (-t)^{-\alpha} + \text{regular part} \qquad (9)$$

$$\xi = \xi_o^- (-t)^{-\nu} . \qquad (10)$$

All these formula hold asymptotically close to the critical point. Further away multiplicative corrective factors of the form

$$(1 + at^{\Delta} + \ldots) \qquad (11)$$

must be introduced[1].

The values admitted now for the exponents are[2] $\gamma = 1.240$, $\nu = 0.630$, $\alpha = 0.110$, $\beta = 0{,}325$, $\delta = 4.815$ and $\Delta = 0.50$, and we expect the combinations reported in table I to be universal.

We shall now consider the experimental determinations of the quantities involved.

2. Order parameter and coexistence curve

We have deliberately choosen magnetic notations to stress an important problem. The exact order parameter is not known in the case of binary fluids (it might be mass fraction or volume fraction or ...) as well as in pure fluids. This is of little importance as far as only exponents are of interest but it makes impossible to assign an amplitude to the order parameter or to the susceptibility without introducing an arbitrary factor. This factor cancels out in the final relations but one has to take care of using coherent conventions throughout. In fact any quantity linear in the concentration can be used as a "practical" order parameter. We must therefore keep in mind which parameter we use. This arbitrary choice will not however affect the value of the amplitude combinations defined above. If we chose the volume fraction φ, we shall define :

$$B_{\varphi} = \frac{1}{2} \lim_{t \to 0} (\varphi_1 - \varphi_2) |t|^{-\beta} = B \left(\frac{\partial \varphi}{\partial M}\right)_T \quad . \qquad (18)$$

3. Susceptibility

The conjugate field is the proper chemical potential difference (μ) of the components and $\chi = \left(\frac{\partial c}{\partial \mu}\right)_{p,T}$. However a chemical potential is not directly measurable and one has to deduce the susceptibility from the mean square of the order parameter fluctuations. This can be readily done by optical means, at the expense of several additional parameters, among them the coupling factor between the refractive index and the concentration fluctuations. This factor is known not to be the bulk derivative, as assumed in the Einstein theory. Indeed, we can calculate the increase of polarisability due to a fluctuation which is directly related to the bulk derivative, but there is no universaly accepted formula for the scattered electric field. For a discussion of this point see e.g. [11] . But this correction is obviously independent

of the nature of the fluctuation. Hence the following scheme, already used in [12] :

i) Find a fluctuation that couples with light and whose absolute amplitude or related susceptibility is known. (Practically the Brillouin doublet).

ii) Record both lines at the same time, in identical geometrical conditions but in a way they can be separated (Rayleigh-Brillouin spectrum).

iii) Determine the bulk derivatives.

This eliminates systematical errors but involves many parameters, so that the final statistical uncertainty cannot be expected small. When Rayleigh Brillouin spectra are not available, one can determine one amplitude for each form of the Rayleigh factor. This allows comparisons between different mixtures but not directly with theory.

The light scattered at a transfer wavevector $\vec{q}$ by a liquid mixture consists of three contributions (neglecting Raman, etc ...) from the three independently decaying thermodynamic parameters : concentration φ entropy S and pressure p, with the intensities (omitting geometrical factors),

$$I_i(q) = I_o \frac{\pi^2}{\lambda_o^4} S_n^2 \left(\frac{\partial n^2}{\partial i} \right)^2 G_i(q) \chi_i k_B T \quad , \qquad (19)$$

where λ_o is the light wavelength in vacuum, $\left(\frac{\partial n^2}{\partial i} \right)$ the bulk derivative of the squared refractive index relative to the variable i, and χ_i the susceptibility associated with the variable i. Therefore $k_B T \chi_i$ is the amplitude of the thermal fluctuations of the parameter i. The coupling of this fluctuation with light is expressed by the factors $S_n^2 \left(\frac{\partial n^2}{\partial i} \right)^2$ where S_n is unknown but function of n only. $G_i(q)$ is the interference term and is the Fourier transform of the normalized correlation function of the variable i. Except for the concentration fluctuations close to the critical point, $G_i(q)$ is equal to unity (see below). Therefore far

enough from the critical point, the ratio of two lines can be written :

$$\frac{I_i}{I_j} = \frac{\left(\frac{\partial n^2}{\partial i}\right)^2}{\left(\frac{\partial n^2}{\partial j}\right)^2} \quad \frac{\chi_i}{\chi_j} \quad . \tag{20}$$

The intensity of the entropy line is quite negligible in this mixture compared to that of the concentration one, which can be confounded with the whole Rayleigh peak.

We therefore have :

$$\frac{I_R}{2I_B} = \frac{\left(\frac{\partial n^2}{\partial \varphi}\right)^2 \left(\frac{\partial \varphi}{\partial M}\right)^2 \left(\frac{\partial M}{\partial H}\right)_T}{\left(\frac{\partial n^2}{\partial \rho}\right)^2 \rho \left(\frac{\partial p}{\partial \rho}\right)_{s,\varphi}} \quad . \tag{21}$$

Using the formulas :

$$\left(\frac{\partial n^2}{\partial p}\right)_s = \left(\frac{\partial n^2}{\partial \rho}\right) \left(\frac{\partial \rho}{\partial p}\right)_s = 2n \left(\frac{\partial n}{\partial T}\right)_p \left(\frac{\partial T}{\partial \rho}\right)_p \left(\frac{\partial \rho}{\partial p}\right)_s \tag{22}$$

and

$$\frac{1}{\rho} \left(\frac{\partial \rho}{\partial p}\right)_s = \frac{1}{\rho v^2} \tag{23}$$

where v is the sound velocity, we get

$$\frac{I_R}{2I_B} = \frac{\left(\frac{\partial n}{\partial \varphi}\right)^2}{\left(\frac{\partial n}{\partial T}\right)^2} \cdot \left[\frac{1}{\rho}\left(\frac{\partial \rho}{\partial T}\right)\right]^2 \rho . v^2 . \frac{C^+ t^{-\gamma}}{k_B T_c} \left(\frac{\partial \varphi}{\partial M}\right)^2 \quad . \tag{24}$$

If we define

$$C^+_\varphi = C^+ \left(\frac{\partial \varphi}{\partial M}\right)^2 . \tag{25}$$

We can notice that

$$\frac{C^+}{B^2} = \frac{C^+_\varphi}{B_\varphi^2} \tag{26}$$

and therefore the choice of the order parameter does not change the value of R_c^+ .

4. Specific heat

Direct specific heat measurements cannot be performed very near a critical point because of the contradictory requirements on the temperature jump which must be much smaller than the temperature difference to T_c but large enough to allow significant measurements. On the other hand, the weakness of the exponent and the importance of the background makes compulsory the measurements very close to T_c. We can make an indirect determination however by separating the thermodynamic formula

$$C_{P,M} - C_{V,M} = \alpha_p \; V T_c \left(\frac{\partial T_c}{\partial p} \right)^{-1} \text{ with } \alpha_p = \frac{1}{V} \left(\frac{\partial V}{\partial T} \right)_{P,M} \qquad (27)$$

into regular and critical part hence :

$$C_{P,M}^{crit} = V T_c \left(\frac{\partial T_c}{\partial p} \right)^{-1} \alpha_p^{crit} \; . \qquad (28)$$

The thermal dilatation coefficient is directly derived from density measurements. These can be performed either by volumetric methods or through refractive index determination, the latter method affording much better performances[13]. It is a little less direct because the refractive index anomaly arises, in principle, not only from the density anomaly but also from the fluctuations. Two contributions are expected[14]. One is in $t^{-\nu}$ and was demonstrated to be negligible through flow birefringence measurements[12]. The other is unfortunately also in $t^{-\alpha}$ and only the cross-check of both methods - as in appendix A.III - allows to estimate it negligible.

5. Correlation length

The correlation length appears in two different processes, one static and one dynamic. The static scattered intensity is directly related to the Fourier transform $G(k,\xi)$ of the correlation function. The determination of ξ can be performed by varying either the scattering wave vector or the temperature. The same information can also be obtained in an experimentally simpler way through turbidity measurements[16] (the integral over angles of the scattered intensity). A quantitative measurement of ξ requires a precise knowledge of the correlation function which has been available only recently[17].

The linewidth of the order parameter fluctuation is also a function of ξ. The previously admitted function was obtained by Kawasaki[18-19], using mode coupling techniques.

$$\Gamma(k,\xi) = R \frac{k_B T}{6\pi\eta\xi} k^2 . \Omega_K (k,\xi) \qquad (29)$$

where η is the shear viscosity and, using $x = k\xi$,

$$\Omega_K(x) = \frac{3}{4} \frac{1}{x^2} [1+x^2+(x^3 - \frac{1}{x}) \, tg^{-1} x] \quad . \qquad (30)$$

Originally the parameter R was believed to be unity. The value R=1.2 was then proposed (renormalization group theory)[20] and some experimental data agree better with the former[21] or the latter[22] value.

Very recently, using a fixed dimension R.G. calculation, Paladin and Peliti[23] proposed the modified version :

$$\Omega_{pp}(x) = (x^2+1)^{x_\eta - \eta/2} \, [\Omega_K(x)]^{1-x_\eta-\eta} \qquad (31)$$

where $x_\eta = y_\eta/\nu = 0.0635$ and with R = 1.075.

III. EXPERIMENTAL REMARKS

For sake of clarity, the experimental details have been defered in appendices. Even then they will be only sketched since most of them have been already described in other publications. The point we want to stress here is that all the measurements have been performed using the very same sample, except for those at varying concentration and for volume measurements, which could however be calibrated by comparison with the reference cell.

Indeed the amplitudes have been often seen to be strongly dependent on impurities, and it is sometimes difficult to match the amplitudes measured in different laboratories.

This sample was in a quartz cell, sealed under vacuum, of cylindrical shape with an inner length of 20.0 mm and an internal diameter of 18 mm. The liquids used were of spectroscopic grade and

filtered through 0.2 μm Teflon filters. The experimental concentration was 0.509 ± 0.002 weight fraction of nitrobenzene. It turned out in the study of the coexistence curve that the critical concentration was rather 0.525 ± 0.005. This difference clearly does not affect the measurements in the diphasic region and those above the critical point only in a very small temperature range, which can be estimated as $T_c\left(\frac{M}{B}\right)^{1/\beta} \simeq 2 \times 10^{-3}$K. Therefore all data closer than ~ 10 mK had to be removed ; they moreover showed systematic discrepancies with respect to current behaviors (see appendix A.IV).

IV. AMPLITUDE COMBINATIONS

We have determined in the appendices

$$B_\varphi = 0.77 \pm 0.02$$
$$C_\varphi^+ = (2.8 \pm 0.4)\ 10^{-29}\ m^3$$
$$A^+ = (1.05 \pm 0.15)\ 10^{27}\ m^{-3}$$
$$S_n^2 C_\varphi^+ = (2.45 \pm 0.04)\ 10^{-29}\ m^3$$
$$S_n^2 C_\varphi^- = (0.57 \pm 0.02)\ 10^{-29}\ m^3$$
$$\xi_o^+ = (2.65 \pm 0.07)\ 10^{-10}\ m$$
$$\xi_o^- = (1.4 \pm 0.1)\ 10^{-10}\ m$$
$$S_n^2 (\delta DB^{\delta-1})^{-1} = (0.29 \pm 0.05)\ 10^{-29}\ m^3$$
$$\xi_o^c (BD^{1/\delta})^{-\nu/\beta} = (0.93 \pm 0.10)\ 10^{-10}\ m^3$$

Hence we can determine the values reported in table I. It should be noticed first that the difference between both theoretical values is usually smaller than the uncertainty on the experimental value. Therefore we are not able to claim that one theoretical approach is in better agreement than the other. The only exception is the ratio C^+/C^- where the R.G. value agrees significantly better with our data.

The large uncertainty on the amplitude A^+ led us to construct the combination $R_\xi^+ R_c^{-1/3}$ which is free of this variable to have a closer check of the fit between theory and experiment. Except for the exception quoted above, the difference between the theoretical and experimental value is hardly bigger than one experimental standard

deviation in the worst cases. We consider this as a fairly convincing evidence of the accuracy of these theories.

We have also determined the value of the dynamical constant

$$R_K = 0.99 \pm 0.05$$

or

$$R_{PP} = 0.98 \pm 0.05$$

according to wether we use the Kawasaki or Peliti Paladin formulations. This value is in good agreement with the original mode-coupling prediction and clearly disagrees with the renormalization group one.

The comparison of the Rayleigh Brillouin and turbidity measurements allows also the determination of the light scattering prefactor S_n : the most widely used forms for this factor are :

$$\text{Einstein} : S_n = 1$$

$$\text{Yvon-Vuks} : S_n = \frac{9_n^2}{(n^2+2)(2n^2+1)} = 0.89$$

$$\text{Rocard} : S_n = \frac{3}{n^2+2} = 0.73$$

while we get Sn = 0.94 ± 0.08, about midway between Einstein's and Yvon's values. This value also enables us to determine the amplitude of the critical isotherm $D = (1.70 \pm 0.7)10^{29} m^{-3}$.

V. CONCLUSION

We have determined experimentally the amplitude of the susceptibility and correlation length along the three principal trajectories of the phase diagram : critical isochore, coexistence curve and critical isotherm. As far as we know, no data on the critical isotherm has ever been obtained previously. We have also determined the amplitude of the coexistence curve and that of the specific heat along the critical isochore. These amplitudes allowed to compute universal amplitude combinations. The experimental values are all in agreement with the renormalization group theoretical predictions. Except for the combination C^+/C^- they are also in agreement

with the high temperature series ones. Moreover we have performed linewidth measurements along the critical isochore which allowed to determine the dynamic constant R, found to be close to unity, in agreement with the original mode coupling theory and in disagreement with the dynamical renormalization group theory. Let us remind finally that all the measurements have been performed in a single cell or recalibrated according to that cell so that drifts associated with impurities should be minimized.

APPENDIX I - The coexistence curve

a) Method

Determining the coexistence curve of a mixture using a single sealed cell involves measuring at different temperatures a parameter directly related to the concentration in each phase. As already noted, the refractive index is an obvious choice for such a parameter. We choosed a refractometric method, rather than an interferometric one because very high accuracy was not needed and because it is much easier to use mainly when some degree of aboluteness is desired. The cylindrical shape of the cell and the necessity to investigate both phases dictated the set-up (fig. AI1). Two thin parallel light beams are sent through the cylindrical lens made by the cell. The image of the focus is made on a remote screen by a lens placed on a translation stage. The position of this lens allows then to know that of the focus and therefore the refractive index of the fluid in the cell, at the level of the beams. The cell is immersed in a thermostatic water bath (stability 1 mK) and mounted on a vertical translation stage which allows to investigate both phases. The absolute accuracy on a single measurement is only of about $\Delta n \sim 0{,}01$ because the distances are difficult to measure accurately. However a single point calibration (mixture just above the critical point, see below) allows to gain one order of magnitude. Moreover the differences between two measurements is limited only by the uncertainty on the position setting, which corresponds to $\Delta n \simeq 4.10^{-4}$.

The refractive index was measured in each phase at different heights and no significant gradients have been observed.

b) Results

The refractive index data are given in table AI1. A first evidence is that the cell is not exactly at the critical concentration. Indeed the meniscus appeared near the bottom of the cell. From the extrapolation of the diameter, we can deduce a more accurate value of the critical volume fraction 0.377 instead of 0.363[24]. The critical temperature is therefore $\sim$ 2 mK higher than the phase separation temperature.

The difference data have been fitted allowing the critical temperature to vary within 0.01K. A first fit, to a single power law with a fixed exponent :

$$n_1 - n_2 = 2B_n |t|^{0.325}$$

showed a systematic distortion. A corrective factor $(1+a|t|^{0.5})$ greatly improved the agreement with only a small change in B_n (fig. AI2). Further improvements of the function such as linear or 2β-power terms are therefore meaningless, though not excluded in principle. The residuals of the fit are reported in fig. AI2. The retained value is

$$B_n = 0.140 \pm 0.02$$

We have also measured the refractive index for different volume fractions at 22°C and 5890 Å, using an Abbe refractometer (Table AI2). The data can be fitted by

$$n = 1.3741 + 0.1989\varphi - 0.0214\ \varphi^2$$

which leads to $\left(\frac{\partial n}{\partial \varphi}\right)_{T,p} = 0.183 \pm 0.002$.

Hence we get :

$$B_\varphi = 0.77 \pm 0.02$$

c) Literature

The data of ref (25) have also been analysed[26] and, when fitted to the same formula give $\phi_c = 0.377$, $T_c = 19.06°C$, $B\phi = 0.767$, $a = 0.61$, and are therefore in excellent agreement with our result.

Appendix II - Rayleigh Brillouin spectra

Rayleigh Brillouin spectra in this sample had already been obtained as a by-product of the study of the depolarized Rayleigh scattering[27]. However, since the free spectral range of the interferometer was optimized for this study (fsr = 78 GHz), these spectra were of rather poor quality. At temperatures greater than 30° ($T - T_c > 10°$) the Brillouin doublet could be clearly evidenced (see fig. AII.1) but its intensity could not be measured accurately because of the difficult evaluation of the background and of the Rayleigh wing. By using the same approximations for all spectra, the variation could be studied, and is reported in fig. AII2. The conclusion is that no background term in the Rayleigh line is visible and that equation (21) applies.

Therefore we recorded a single Rayleigh Brillouin spectrum using a FSR of 5.92 GHz, at a temperature of 41.1°C ($T - T_c \simeq 21°$). For sake of brevity, we do not repeat the description of the set-up which can be found in ref. 28. The spectrum is shown in fig. AII3. Integration of the lines leads to a value

$$\frac{I_R}{2I_B} = 30$$

While the Brillouin shift gives the speed if sound at this temperature

$$v = 1140 \text{ ms}^{-1}$$

The other parameters involved in eq. 20 will be discussed in the following appendices.

We finally get

$$C_\varphi^+ = (2.8 \pm 0.4)10^{-29} \text{m}^3$$

Or, using a more usual terminology :

$$\left(\frac{\partial \mu}{\partial \varphi}\right)_T = \frac{k_B T_c}{C_\varphi^+} = 144 \text{ J cm}^{-3}$$

Appendix III - Refractive index and volume measurements

As explained above, the specific heat was not directly measured. Instead we determined a change of density (or volume), taking advantage of the formula

$$C_{p,M}^{crit} = -T_c\left(\frac{dT_c}{dp}\right)^{-1}\left(\frac{1}{\rho}\frac{\partial\rho}{\partial T}\right)_{\rho,M}^{crit} = \frac{A^+}{\alpha} k_B t^{-\alpha} \qquad \text{(AIII-1)}$$

The density itself was deduced from refractive index and volume measurements.

1. Refractive index

The refractive index has been measured using the simple interferometer described and used in ref[29]. The accuracy is of the order of magnitude of some 10^{-6} with the 2 cm sample length we used. The refractive indices of the pure components have been fitted to a linear variation :

$$n(T) - n(T_o) = \left(\frac{\partial n}{\partial T}\right)_P (T - T_o)$$

with $T_o \simeq T_c \simeq 20°C$. The results of the fit are reported in table AIII-1.

The data of the mixture are reported in table AIII-2 and have been fitted, according to (AIII-1),

$$n(t)-n(t_o) = \left(\rho\frac{\partial n}{\partial\rho}\right)\left(\frac{dT_c}{dp}\right) k_B \frac{A^+}{\alpha}\int_{t_o}^{t} [t^{-\alpha}+\alpha a_c t^{\Delta-\alpha}+ \ldots + \text{regulat terms}]dt$$

In fact no correction to-scaling was found necessary and the data were well described by

$$n(t) - n(0) = T_c\left(\frac{\partial n}{\partial T}\right)_{\rho,M}^{reg} t + R_n\, t^{1-\alpha}$$

The results are listed in table A-III-1, and the residuals of the fit are shown in fig.AIII-1. One can notice that the regular part $\left(\frac{\partial n}{\partial T}\right)_{\rho,M}^{reg} = 1.08\left(\frac{\partial n}{\partial T}\right)_{p,T}^{id}$ where the ideal part is deduced from the pure components measurements, $\left(\frac{\partial n}{\partial T}\right)^{id} = -(5.177 \pm 0.007)10^{-4}K^{-1}$.

2. Volume measurements

In order to check that only the density is responsible for the critical behaviour of the refractive index, we also performed volume measurements.

The dilatation of the mixture has been studied using the usual reservoir and capillary method. Owing to the small volume of the capillary a limited temperature range can be studied at a time (~ 2K). An auxillary reservoir allowed to adjust the amount of liquid without unsealing the cell. The pure components exhibited a linear expansion (see table AIII1). The non linearity of the expansion of the mixture cannot be evidenced in a single interval but the average slope changes with the mean temperature (see fig. AIII2). These measurements are less precise than refractive index ones.

Therefore it is impossible to deduce simultaneously the amplitude of the regular and singular parts. However, while the singular part of the refractive index might arise from a different process that the one of the density, this should not be the case for the regular part. So we imposed the regular part to be 1.08 times the ideal value as found in the refractive index data fit. The ratio of the singular to regular amplitudes for value measurements is 1.13 ± 0.15 times that found in refractive index measurements. This proves that the measured refractive index anomaly arises from the thermal expansion only. However, by comparing the changes in n and ρ, we can deduce :

$$\rho\left(\frac{\partial n}{\partial \rho}\right) = (4.72 \pm 0{,}08)\,10^{-4}$$

From the literature[32], the shift of T_c with pressure is obtained :

$$\left(\frac{\partial T_c}{\partial p}\right) = -(1.64 \pm 0.08)\,10^{-7}\,K.Pa^{-1}$$

Hence we get

$$A_n^+ = -\frac{\alpha(1-\alpha)}{k_B}\,\frac{R_n}{\rho\left(\frac{\partial n}{\partial \rho}\right)\left(\frac{\partial T_c}{\partial p}\right)} = (1.05 \pm 0.15)\,10^{27}\,m^{-3}$$

Appendix IV - Turbidity measurements

The turbidity alone does not allow to determine C^+, C^- or C_c but their product by the light scattering amplitude $\left(\frac{\partial n^2}{\partial M}\right)_{P,T}$, which is not a mere derivative and is not known. However turbidity measurements can be useful is two different ways. The first is that close to the critical point the turbidity is also sensitive to the correlation length ξ. It is therefore an easy way to measure the correlation length amplitude, since we know an appropriate form of the correlation function[17]. The second is that the ratios of turbidity amplitudes do not depend on $(\partial n^2/\partial M)_{p,T}$ and that the ratios C^+/C^- or C^+/C_c can be directly measured. Turbidity measurements are straightforward : a light beam of constant intensity is sent through the mixture and the emergent intensity is measured. The original formulation of the correlation function being very cumbersome, an approximation valid within 1% has been worked out[26] :

$$G(k\xi) = \sum_{i=1}^{3} C_i (1+a_i^2 k^2 \xi^2)^{-b_i}$$

which can readily be integrated over angles to give :

$$G'(X_o) = \sum_{i=1}^{3} c_i \left\{ \left[(1+2a_i^2 X_o^2)^{\mu_i} - 1 \right] \left[1 + a_i X_o^2 (2-\mu_i) + a_i^4 X_o^4 (2+\mu_i+\mu_i^2) \right] \right.$$

$$\left. - 2\mu_i X_o^2 (1+X_o^2) \right\} \left[a_i^6 X_o^6 \mu_i (1+\mu_i)(2+\mu_i) \right]^{-1} .$$

with $X_o = \sqrt{2}\, k_o \xi$. The a_i's are given in table (AIV1).

The turbidity has to be fitted to the function

$$\tau = \frac{2\pi^3}{\lambda_o^4} S_n^2 \left(\frac{\partial n^2}{\partial \varphi}\right)^2 (1+t) C_\varphi^i t^{-\gamma} G'(k\xi_o^i)$$

where the superscript i denotes the trajectory (i = +,-,C).

Since the reference cell was not exactly critical, it could not provide accurate data close to the critical point, which are important for the determination of the correlation length. Therefore we also used data from a variable concentration cell, the optical path of which was 0.5 cm. The range in concentration spanned was $\phi = \{\pm 4.2\ 10^{-2}\}$ and data were taken from above the critical isotherm down to the coexistence curve. These data are a by product

of a non equilibrium experiment[33].

We fitted together both series for the critical isochore and the coexistence curve (see tables AIV2 and AIV3 and fig. AIV1 and got :

$$S_n^2 \, C_\varphi^+ = (2.45 \pm 0.04) 10^{-29} m^3$$
$$S_n^2 \, C_\varphi^- = (0.58 \pm 0.02) 10^{-29} m^3$$
$$\xi_o^+ = (2.65 \pm 0.07) 10^{-10} m$$
$$\xi_o^- = (1.4 \pm 0.1) 10^{-10} m$$

The data can also be interpolated at the critical temperature, providing a way if determining both D and ξ_o^c. The analysis is the same, provided we replace t by $\left(\frac{M}{B}\right)^{1/\beta}$. We therefore get

(instead $S_n^2 \, C^\pm$) $\quad S_n^2 (\delta D B^{\delta-1})^{-1} = (0.29 \pm 0.05) 10^{-19} m^3$

(instead $\xi_o^\pm$) $\quad \xi_o^c (B D^{1/\delta})^{-\nu/\beta} = (0.93 \pm 0.10) 10^{-10} m$.

Appendix V - Correlation time measurements

Spectral measurements of the Rayleigh line in this sample had already been obtained. However we felt the need of more precise data. We used for that a clipped photon correlator (ATNE). The scattering angle was 90° and the incident radiation was issued from small power He-Ne laser (λ = 632.8 nm). No departure from an exponential decay was noticed. The correlation times are reported in table AV1. The data are in very good agreement with those of ref. 34.

They have been fitted to both the Kawasaki eq. 30 and Peliti-Palatin formulas, using the value of ξ_o determined by turbidity measurements. The viscosity was determined in ref. 35. However a later check of the calibration of the viscosimeter revealed a 5% systematic error on the absolute values. The viscosity has therefore been calculated using :

$$\eta = \eta_o \exp\left(\frac{E}{1+t}\right) t^{-y_\eta}$$

with $\eta_o = 1.36\ 10^{-4}$ Po, E = 3.58 and $y_\eta = 0.043$. The only adjustable parameter was R. Since most of the data lie in the hydrodynamic region, the functions are very close to each other. Therefore the values obtained :

$$R_K = 0.99 \pm 0.05$$

$$R_{pp} = 0.98 \pm 0.05$$

are very close to each other. The uncertainty include that on ξ_o and q.

REFERENCES

[1] F.J. Wegner, Phys. Rev. B5, 4529 (1972)

[2] For review, see "Phase transitions, status of the experimental and theoretical situation", Cargèse 1980, ed. by M. Lévy S.C. le Guillou and J. Zinn-Justin (Plenuum Press 1981)

[3] J. Zinn-Justin, J. Physique 42, 783 (1981)

[4] P.R. Hohenberg, A. Ahorony, B.I. Halperin and E.D. Siggia, Phys. Rev. B13 2986 (1976)

[5] C. Bervillier, Phys. Rev. B14 73 (1976)

[6] E. Brézin, J.C. le Guillou and J. Zinn-Justin, in phase transitions and critical phenomena, C. Domb and M.S. Green editors (Academic, New-York) Vol 6 (1976)

[7] H.B. Tarko and M.E. Fisher, Phys. Rev. B11 1217 (1975)

[8] H.B. Tarko and M.E. Fisher, Phys. Rev. B5 2668 (1972)

[9] E. Brézin, J.C. le Guillou and J. Zinn-Justin, Phys. Lett. A47 285 (1974)

[10] A. Aharony and P.C. Hohenberg, Phys. Rev. B13 3081 (1976)

[11] D. Beysens, J. Chem. Phys. 64 2579 (1976)

[12] Y. Garrabos, G. Zalczer, D. Beysens, Phys. Rev. A25 1147 (1982)

[13] D. Beysens, A. Bourgou, Phys. Rev. A19 2407 (1979)

[14] J.V. Sengers, D. Bedeaux, P. Mazur and S.C. Greer, Physica (Utrecht) 104A, 573 (1980) and references therein

[15] D. Beysens, M. Gbadamassi, Phys. Rev. Lett. 47 846 (1981)

[16] P. Calmettes, I. Lagues, C. Laj, Phys. Rev. Lett. 28 478 (1972)

[17] A.J. Bray, Phys. Rev. B14 1248 (1976)

[18] K. Kawasaki, Annals of Physics 61 1 (1970)

[19] R.A. Ferrell, Phys. Rev. Lett. 24, 1169 (1970)

[20] E.D. Siggia, B.I. Halperin and P.C. Hohenberg, Phys. Rev. B13 2110 (1976)

[21] H.C. Burstyn and J.V. Sengers, Phys. Rev. A25

[22] D. Beysens, in ref (1)

[23] C. Paladin, L. Peliti, Journal de Physique Lett. 43 L15 (1982)

[24] S.H. Chen and N. Polonski, Opt. Comm. 1, 64 (1969)

[25] J. Timmermans, in "Physico chemical constants of pure organic" compounds, Elsevier, Amsterdam, 1965

[26] D. Beysens, A. Bourgou and P. Calmettes, to be published Saclay, preprint ref DPhG/PSRM/1538/81

[27] D. Beysens and G. Zalczer, Phys. Rev. A18 2280 (1980)

[28] D. Beysens and G. Zalczer, Opt. Commun. 23, 142 (1977)

[29] D. Beysens, Rev. Sci. Instrum. 50 509 (1979)

[30] D. Beysens and P. Calmettes, J. Chem. Phys. 66 766 (1977)

[31] Landolt-Boïnstein in "Eigenshaften der materie...8-Teil Optische Konstanten". Berlin, Springer Verlag (1962)

[32] J. Timmermans, The physico-chemical constants of binary systems in concentrated solutions. Interscience N.Y. (1959)

[33] D. Beysens, M. Bouanz and M. Gbadamassi, to be published Saclay

[34] D. Beysens and G. Zalczer, Phys. Rev. A15 765 (1977)

[35] D. Beysens, S.H. Chen, J.P. Chabrat, L. Letamendia, J. Rouch and C. Vaucamps, Journal de Physique Lettres 38 203 (1977)

TABLE CAPTIONS

I The expected universal amplitude combinations, their theoretical values and the experimental values determined for the nitrobenzene-n-hexane mixture

AI1 Difference of refractive indices of the two phases below T_c

AI2 Refractive index data above T_c versus the volume fraction of nitrobenzene. They can be represented by the function $n = 1.3741 + 0.1989\varphi - 0.0214\varphi$

AIII1 Values of the parameters determined by refractive index and volume measurements (see text). Fits were performed to

$$\Delta n = T_c\left(\frac{\partial n}{\partial T}\right)^{reg}_{p,M} t + R_n\, t^{0.890} \quad \text{and} \quad \Delta\rho = \rho T_c\left[\frac{1}{\rho}\left(\frac{\partial P}{\partial T}\right)^{reg}_{p,M}\right] t + Rp\, t^{0.890}$$

AIII2 Refractive index variations along the critical isochore

AIII3 Dilatation of the nitrobenzene n-hexane system near T_c. $T_c = 19.522°C$ (add + 0.5°C to obtain absolute values)

AIV1 Coefficients of the approximation to Bray's structure factor (eq.AIV1)

AIV2 Turbidity along the critical isochore

AIV3 Turbidity along the coexistence curve

AIV4 Turbidity along the critical isotherm

AV1 Correlation time of the concentration fluctuations along the critical isochore

Universal combination	R.G. value	HTS value	Experimental value (this work)
$\frac{C^+}{C^-}$	$4.5^{[5]}$	$5.03^{[6]}$	4.3 ± 0.3
$\frac{\xi_o^+}{\xi_o^-}$	$1.91^{[7]}$	$1.96^{[8]}$	1.9 ± 0.2
$R_C^+ = \frac{A^+ C^+}{B^2}$	$0.066^{[9]}$	$0.059^{[9]}$	0.050 ± 0.015
$R_\xi^+ = \xi_o^+ A^{+1/3}$	$0.27^{[3]}$	$0.25^{[4]}$	0.27 ± 0.03
$R_\xi^+ R_c^{+-\frac{1}{3}} = \xi_o^+ \left(\frac{B^2}{C^+}\right)^{1/3}$	0.67	0.67	0.73 ± 0.05
$R_\chi^+ = C^+ D\, B^{\delta-1}$	$1.7^{[3]}$		1.75 ± 0.30
$Q_2 = \frac{C^+}{C_C} \left(\frac{\xi_o^C}{\xi_o^+}\right)^{2-\eta}$		$1.21^{[6]}$	1.1 ± 0.30

Table I

$\|t\|$	$10^4 \times \Delta\eta$
$1.1\ 10^{-4}$	156
$2.0\ 10^{-4}$	194
2.8	215
4.5	245
4.85	243
7.0	271
$1.1\ 10^{-3}$	316
1.62	351
2.02	380
2.82	416
3.82	472
3.89	477
4.66	495
6.17	546
8.16	610
$1.11\ 10^{-2}$	680
1.47	745
1.84	802

Table AI.1

Difference of refractive indices of the two phases below T_c.

$n\begin{pmatrix}5890\ \mathring{A}\\ 22°C\end{pmatrix} \pm 5.10^{-4}$	$\varphi_{(NBZ)}$
1.3741	0
1.4213	25
1.4326	30
1.4427	35
1.4488	40
1.4593	45
1.4682	50
1.5516	100

TABLE A.I.2

Refractive index data above T_c versus the vol. fraction of Nitrobenzene. They can be represented by the function $n = 1.3741 + 0.1989\ \varphi - 0.0214\ \varphi^2$.

System	$n^{6328\ \text{Å}}_{20°C}$	$(\partial n/\partial T)^{reg}_{P,M}$ ($\times 10^{-4}$ K^{-1})	$\alpha=0.110$ R_n ($\times 10^{-2}$)	$\rho^{20°C}$ ($\times 10^{3}$ $Kg.m^{-3}$)	$\left(\frac{1}{\rho}\frac{\partial P}{\partial T}\right)^{reg}_{P,M}$ ($\times 10^{-4}$ C^{-1})	$\alpha=0.110$ R_ρ ($\times 10^{-2}$)
Nitrobenzene	1.5480 a)b)	-4.827 ± 0.005 c)	-	1,2037 d)	- 8.07 ± 0.02 e)	-
n-Hexane	1.3737 e)	-5.376 ± 0.007 c)	-	0.6603 d)	-12.60 ± 0.06 f)	-
Nitrobenzene + n-Hexane	1.444 g)	-5.58 ± 0.04	1,16 ± 0,09	0,8753 h) 0.8635 d)		
					(-11,82) i)	2.79 ± 0.08

TABLE A.III.1

Values of the parameters determined by refractive index and volume measurements (see text). Fits were performed to $\Delta n = T_c\left(\frac{\partial n}{\partial T}\right)^{reg}_{P,M} . t + R_n\, t^{0.890}$ and $\Delta\rho = \rho T_c\left[\frac{1}{\rho}\left(\frac{\partial P}{\partial T}\right)^{reg}_{P,M}\right] t + R_\rho t^{0.890}$.

a) Ref. 30

b) Cited in Ref. 31

c) This work. In order to obtain absolute values, add $+2.5\times10^{-7}$ K^{-1}, i.e. the correction due to the cell expansion.

d) Cited in Ref. 24

e) This work. For absolute values, add 1% uncertainty and compare with $-(8.16\pm0.04)\times10^{-4}$ K^{-1} reported in d).

f) This work. For absolute values, add 1% uncertainty and compare with $-(12.85\pm0.05)\times10^{-4}$ K^{-1} reported in d).

g) This work.

h) Ideal value

i) Value imposed to 1.08 times the ideal value. See text.

1st series		2nd series	
t	Δn	t	Δn
$6,06\ 10^{-2}$	0	$2,665\ 10^{-3}$	0,004
5,31	$1,111\ 10^{-3}$	1,087	0,242
4,51	1,710	$8,06\ 10^{-4}$	0,272
4,908	1,714	5,54	0,307
3,988	3,081	4,19	0,326
3,173	4,250	2,85	0,342
3,174	4,292	2,09	0,351
2,445	5,368	1,27	0,361
1,902	6,171	0,73	0,367
1,384	6,938	0,63	0,376
1,086	7,377		
1,085	7,373		
$7,703\ 10^{-3}$	7,832		
6,323	8,035		
5,506	8,153		
4,609	8,283		
3,353	8,465		
2,749	8,552		
2,174	8,635		
1,599	8,715		
1,033	8,796		
$7,512\ 10^{-4}$	8,835		
4,71	8,875		
1,93	8,513		

TABLE A.III.2

Refractive index variations along the critical isochore

T(°C)	Δx(cm)	T(°C)	Δx(cm)
SET.1		SET.4	
29.7125	4.575	19.7605	5.750
29.4330	3.780	19.6802	5.510
29.5660	4.160	19.5993	5.300
29.6998	4.530	19.5599	5.195
29.8340	4.895	19.5530	5.170
29.9693	5.275		
30.1079	5.645	SET.5	
30.2445	6.015	19.6304	5.330
30.3845	6.395	19.5484	5.130
30.5239	6.770	19.5330	5.085
30.6700	7.165	19.5514	5.125
30.8098	7.545	19.5690	5.155
30.9530	7.935	19.5845	5.205
		19.6102	5.260
SET.2		19.6434	5.335
23.0515	3.845	19.6824	5.445
23.1498	4.120	19.7153	5.525
23.2487	4.385	19.7575	5.630
23.3487	4.645	19.8413	5.820
23.4495	4.505	19.9260	6.050
23.5505	5.175	19.8271	5.805
23.6515	5.450	19.7429	5.590
23.8036	5.855	19.6601	5.395
23.9590	6.265	19.5786	5.180
24.1039	6.650	19.5465	5.100
24.2589	7.060	19.5306	5.060
24.4050	7.445	19.5443	5.080
24.5625	7.860		
SET.3			
20.3215	3.820		
20.4059	4.030		
20.5015	4.265		
20.6298	4.580		
20.7625	4.930		
20.8966	5.265		
21.0288	5.605		
21.1635	5.945		
21.2987	6.295		
21.4342	6.645		
21.5696	6.985		

TABLE A III-3

Dilatation of the Nitrobenzene-n-Hexane system near T_c. T_c = 19.522°C (add +0.5°C to obtain absolute values).

	a	b=1−μ	c
1	1.040056	$1-\frac{\eta}{2}=0.98425$	1
2	1.058947	1.554213	1
3	1.053932	1.627419	−1

Table A.IV.1

Coefficients of the approximation to Bray's structure factor (eq.A.IV.1)

$t_{\ell=2cm}$	τ (cm^{-1})	t	τ
$9.74.10^{-3}$	$8.7.10^{-3}$	2.93	5.26
5.88	$1.91.10^{-2}$	2.92	5.26
2.90	4.61	2.67	5.46
2.17	6.60	2.67	5.46
1.44	$1.08.10^{-1}$	2.45	5.64
$7.54.10^{-4}$	2.09	2.45	5.84
4.81	3.40	2.20	6.05
4.16	3.93	2.20	6.05
3.75	4.04	1.89	6.88
3.45	4.39	1.88	6.88
2.49	5.69	1.52	8.41
2.15	6.37	1.52	8.64
1.81	7.24	1.52	8.64
1.60	7.88	1.32	9.58
1.90	8.62	1.09	$1.03.10^{\circ}$
1.19	9.59	1.08	1.06
1.06	$1.04.10^{\circ}$	$8.91.10^{-5}$	1.16
$\ell=0.5cm$		8.84	1.16
$4.22.10^{-4}$	$3.41.10^{-1}$	7.20	1.30
4.21	3.59	7.10	1.30
3.53	4.31	5.36	1.54
3.52	4.31	5.29	1.54
3.23	4.88	3.24	1.33
3.22	4.68	3.17	1.86

Table A.IV.2

Turbidity along the critical isochore

t	τ (cm^{-1})
2.87	1.97
2.80	1.97
2.53	2.10
2.08	2.18
2.05	2.22
1.43	2.52
$9.90.10^{-6}$	2.74
9.56	2.74
8.53	2.93
8.19	2.99
4.78	3.36
4.44	3.36
1.71	4.38

Table A.IV.2 (continued)

$\|t\|$	$\tau(cm^{-1})$		
	ℓ = 2cm		
$9.27\ 10^{-3}$	$2.54\ 10^{-3}$	$1.32\ 10^{-5}$	$1.07\ 10^{0}$
3.12	$1.29\ 10^{-2}$	$5.46\ 10^{-6}$	2.15
2.33	1.55	$3.86\ 10^{-6}$	1.93
1.86	2.07	1.82	3.01
1.15	3.30	1.52	3.21
$8.70\ 10^{-4}$	4.96	$8.23\ 10^{-7}$	3.51
6.69	6.96		
5.36	8.26		
4.03	$1.15\ 10^{-1}$		
2.90	1.64		
2.08	2.36		
1.60	2.90		
1.16	3.86		
	ℓ = 0,5cm		
$1.40\ 10^{-4}$	$3.92\ 10^{-1}$		
1.33	3.52		
$7.40\ 10^{-5}$	4.52		
5.95	5.71		
5.51	8.10		
4.38	8.91		
2.50	$1.01\ 10^{0}$		
2.26	1.15		
1.38	1.27		

Table AIV-3

Turbidity along the coexistence curve

$\lvert\phi-\phi_c\rvert$	$\tau(cm^{-1})$
$4.22\ 10^{-2}$	0.39
4.03	0.33
3.50	0.31
3.28	0.45
3.18	0.73
2.96	0.65
2.46	0.85
2.38	0.93
2.03	1.39
2.00	1.43
1.50	2.11
1.34	1.91
1.05	2.7
0.99	2.95
0.81	3.3

Table AIV4

Turbidity along the critical isotherm

t	$\tau(\mu s)$		
$5.52.10^{-3}$	48.1	1.003	30.9
5.91	47.1	$9.22 .10^{-3}$	35.2
6.31	44.8	9.22	28.7
6.71	42.2	8.40	36
7.12	37.7	7.59	36.6
8.02	35.8	6.47	40.3
9.46	31.8	6.47	46.2
$1.081.10^{-2}$	31.9	$1.202.10^{-2}$	26.0
1.2	27.9	1.008	32.5
1.2	27.9	$8.38 .10^{-3}$	36
1.588	22.7	6.83	42.4
1.614	19.8	6.02	43.2
1.540	25.9	6.02	43.2
1.467	25.1	5.70	45.3
1.409	25.6	5.06	51.2
1.328	24.3	4.73	49.8
1.247	28.4	4.42	51.2
1.165	30.4	4.09	59.2
1.165	32	3.77	58.4
1.165	27.5	3.44	67.5
1.084	30.7	3.36	61.0
1.084	27.6	3.12	68.3
1.084	27.5	2.87	66.7
1.003	35.2	2.62	80.3
1.003	32	2.38	75.5

Table A.V.1

Correlation time of the concentration fluctuations along the critical isochore

$2.372.10^{-3}$	81.6	$1.355.10^{-3}$	113.6
2.120	84	1.492	110.8
2.120	87.2	1.672	104
2.120	91.2	1.857	97.6
1.864	96	2.041	90
1.604	107.6	2.044	88
1.413	112	2.041	88.3
1.413	115.2	3.672	60
1.215	118.4	2.041	88
1.215	128	1.501	93.2
1.027	136	1.727	102.4
1.027	128	1.553	101.2
$8.43\ .10^{-4}$	137.6	1.553	106
6.59	156.8	1.345	114.4
6.55	157.4	1.164	122
3.69	192.8	$9.50\ .10^{-4}$	129.1
3.69	193.3	8.09	153
3.69	196	6.28	173.2
5.80	176.7	3.58	199.6
3.99	203.4		
7.61	173.5		
9.42	141.4		
$1.120.10^{-3}$	128.5		
$9.45\ .10^{-4}$	144.5		
$1.304.10^{-3}$	121.6		

Table A.V.1 (continued)

FIGURE CAPTIONS

AI-1 : Schematic representation of the set-up used for measuring the refractive index of the mixture. The cell can be moved vertically in order to investigate both phases.

AI-2 : Residuals of the fit of the refractive index difference data with the function $n_1-n_2 = B_n(t)^{0.325}(1+a(t)^{0.5})$ with $B_n = 0.140$ and $a = 3.3$.

AII-1 : Rayleigh Brillouin spectrum recorded with a free spectral range of 78 GHz

AII-2: Rayleigh Brillouin ratio measured from spectra reduced with a FSR of 78 GHz, showing the pure power law behaviour. The square denotes the spectrum recorded with a FSR of 5.92 GHz.

AII-3: Rayleigh Brillouin spectrum recorded at 41.1°C with a FSR of 5.92 GHz.

AIII-1: Residuals of the fit of the refractive index along the critical isochore.

AIII-2: Dilatation of the mixture at different temperatures observed by a volumetric method.

AIV-1: Turbidity along the three principal trajectories.
Critical isochore : ■ 5mm cell □ 2cm cell
Coexistence curve : ● 5mm cell o 2cm cell
critical isotherm : × 5mm cell (inner scales)
The $|\phi|$ and $|t|$ scales are related by $|\phi| = B|t|^{\beta}$.

AV-1 : Residuals of the fit of the linewidth data to the Kawasaki function with R = 0.99.

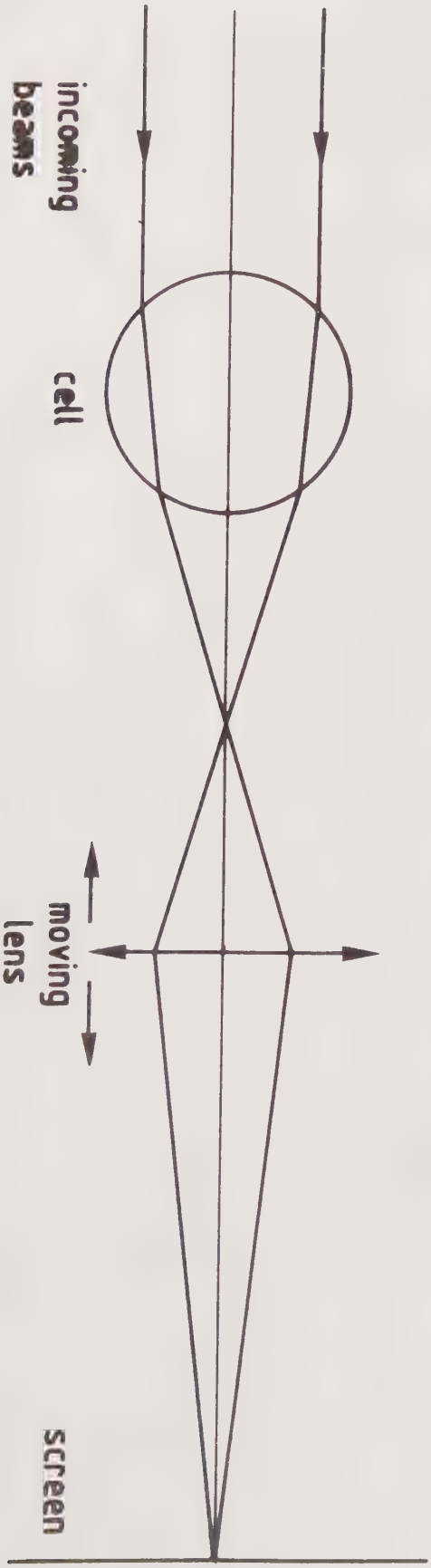
incoming
beams
cell
moving
lens
screen

Δ%
4
2
0
-2
10-4
10-3
10-2
1

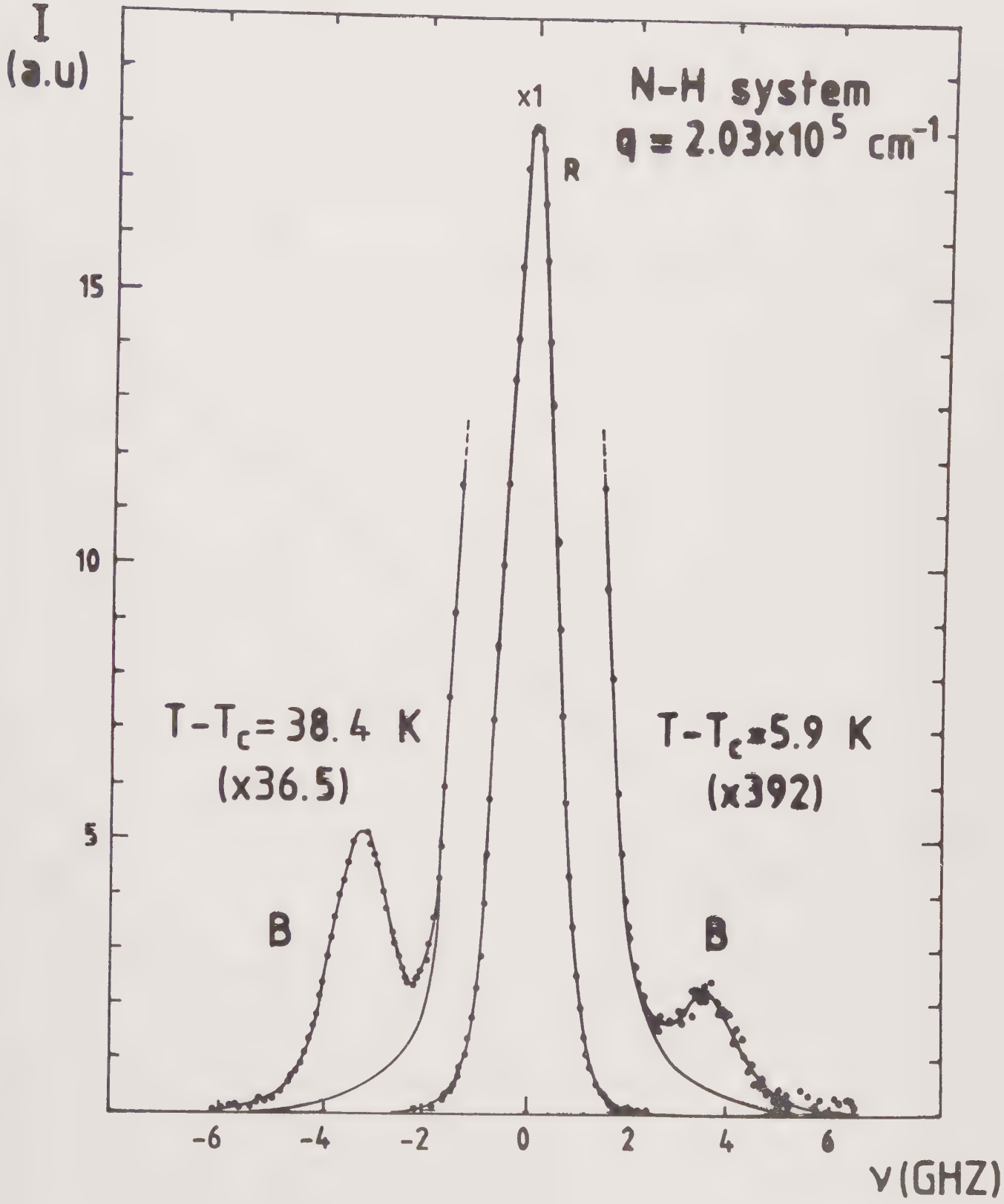
I
(a.u)
x1
N-H system
q = 2.03x10^5 cm^-1
R
15
10
5
T-T_c= 38.4 K
(x36.5)
T-T_c=5.9 K
(x392)
B
B
-6
-4
-2
0
2
4
6
ν(GHZ)

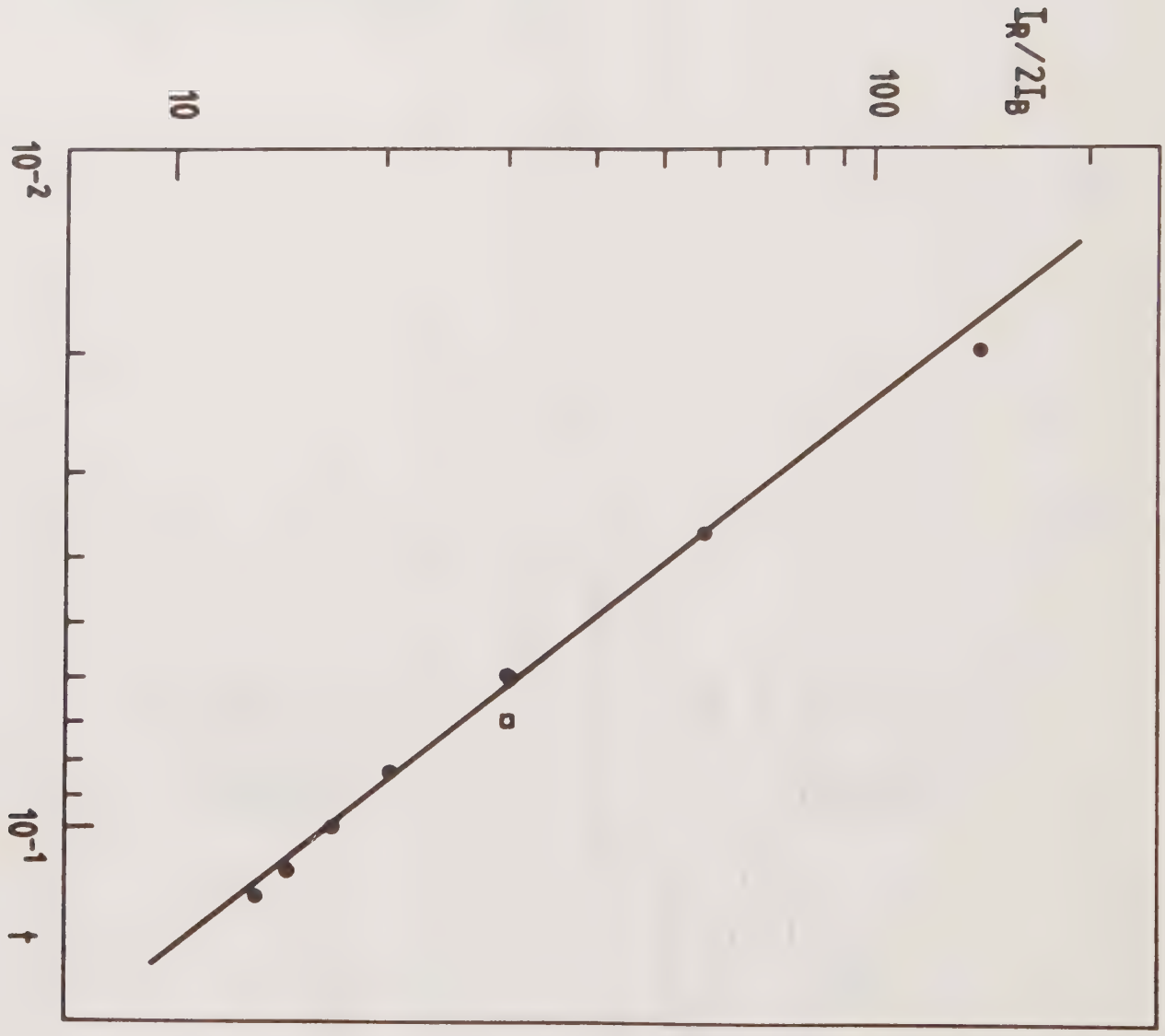
$I_R/2I_B$
100
10
10^{-2}
10^{-1}
t

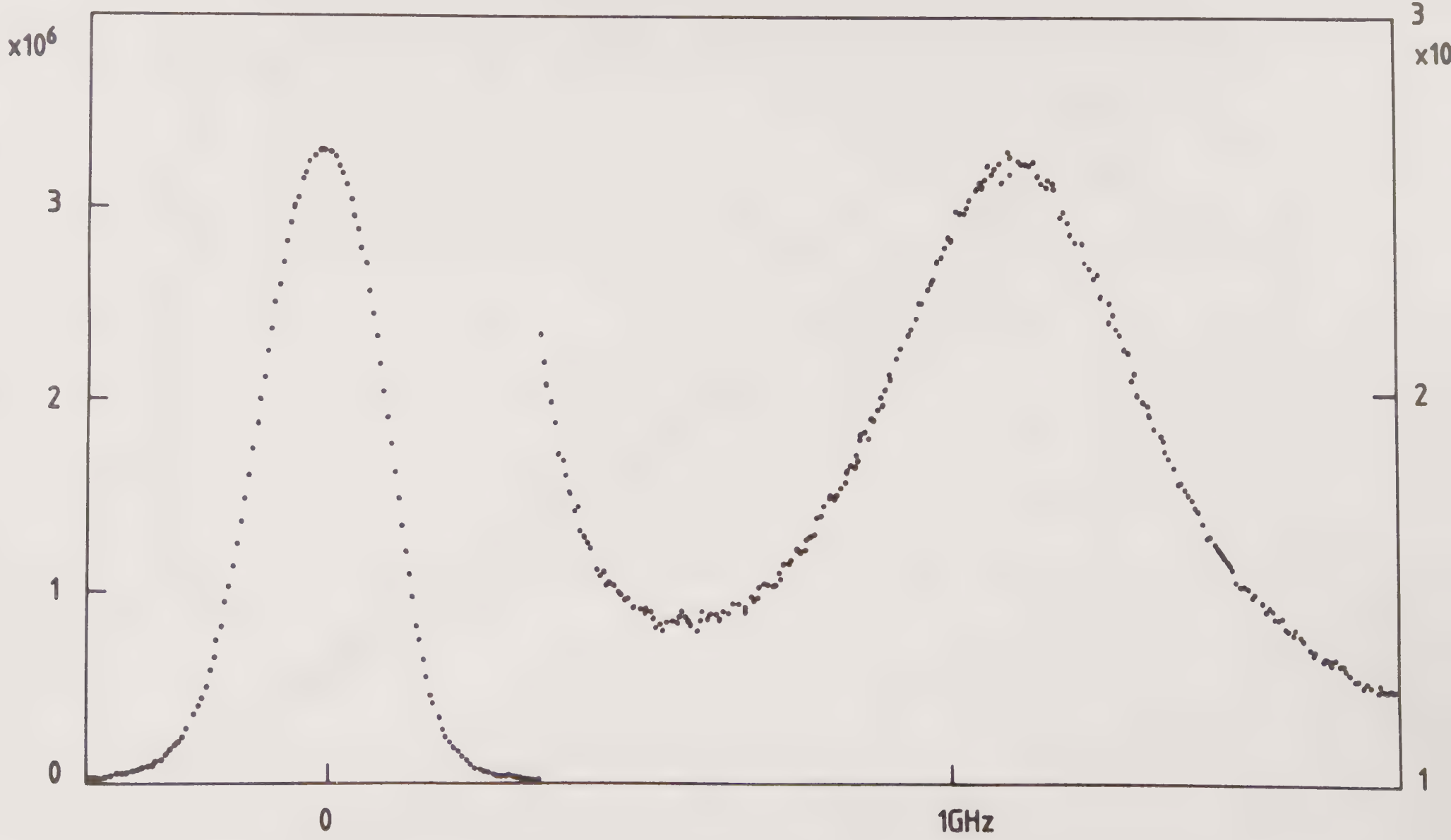
x10^6
3
2
1
0
0
1GHz
3
x10
2
1

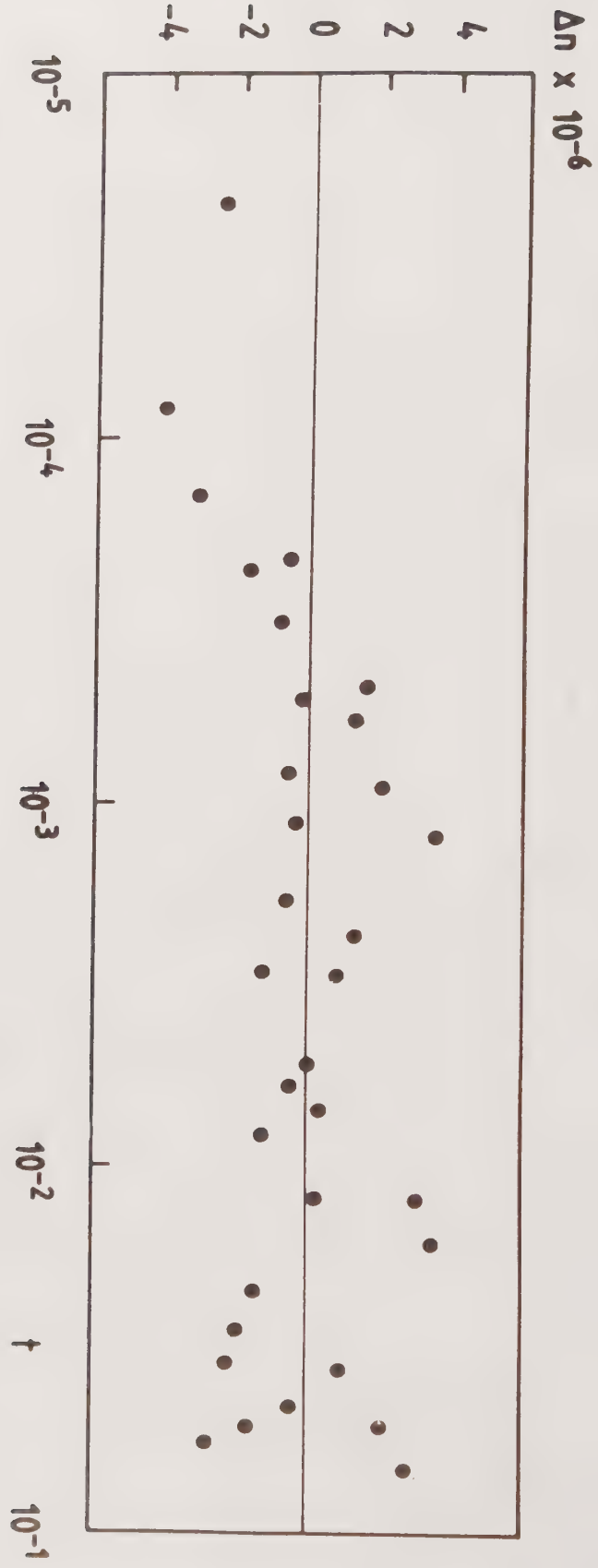
Δn x 10⁻⁶
4
2
0
-2
-4
10⁻⁵
10⁻⁴
10⁻³
10⁻²
t
10⁻¹

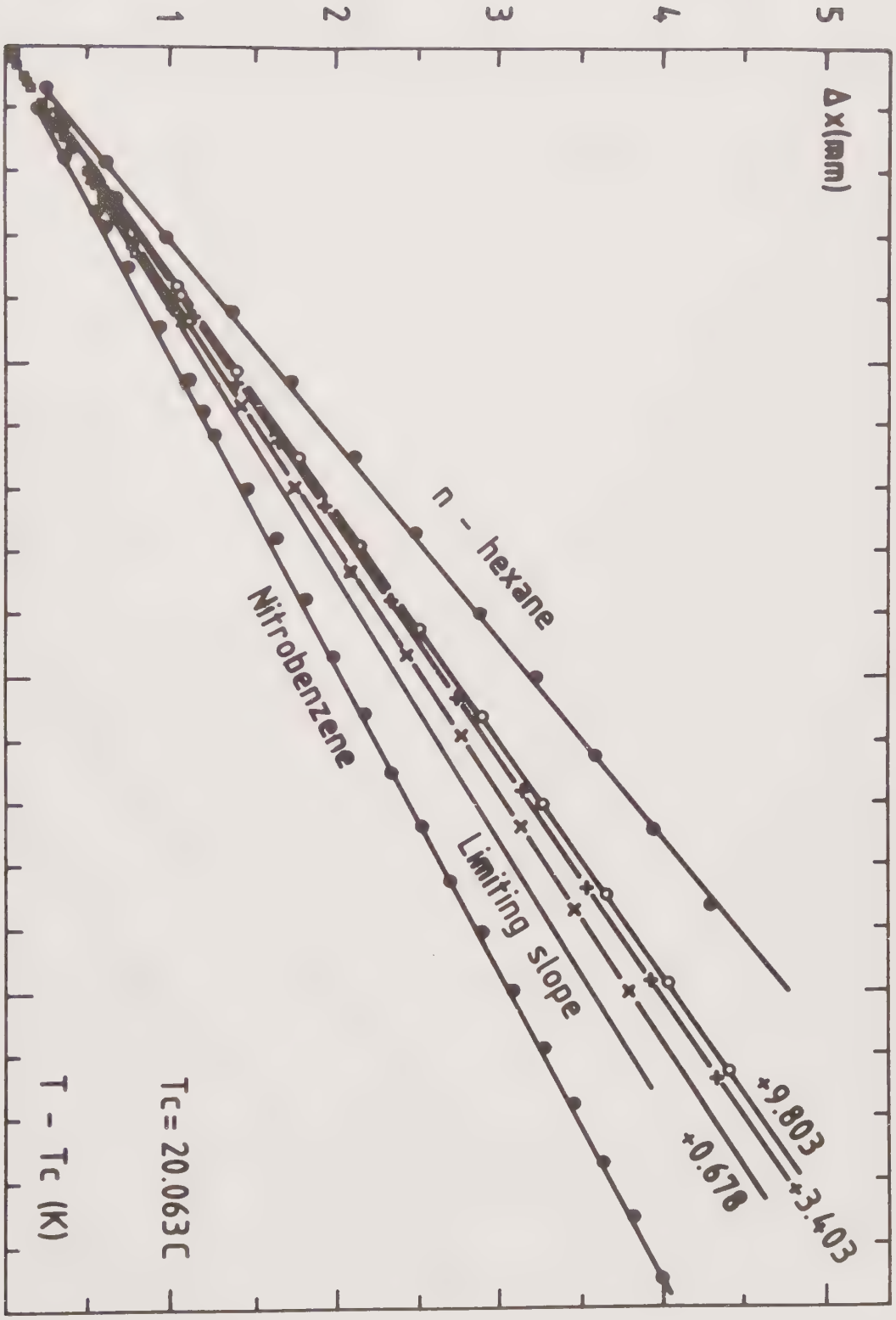
Δx(mm)
5
4
3
2
1
0.5
1
1.5
T - Tc (K)
Tc= 20.063C
n - hexane
Nitrobenzene
Limiting slope
+9.803
+3.403
+0.678

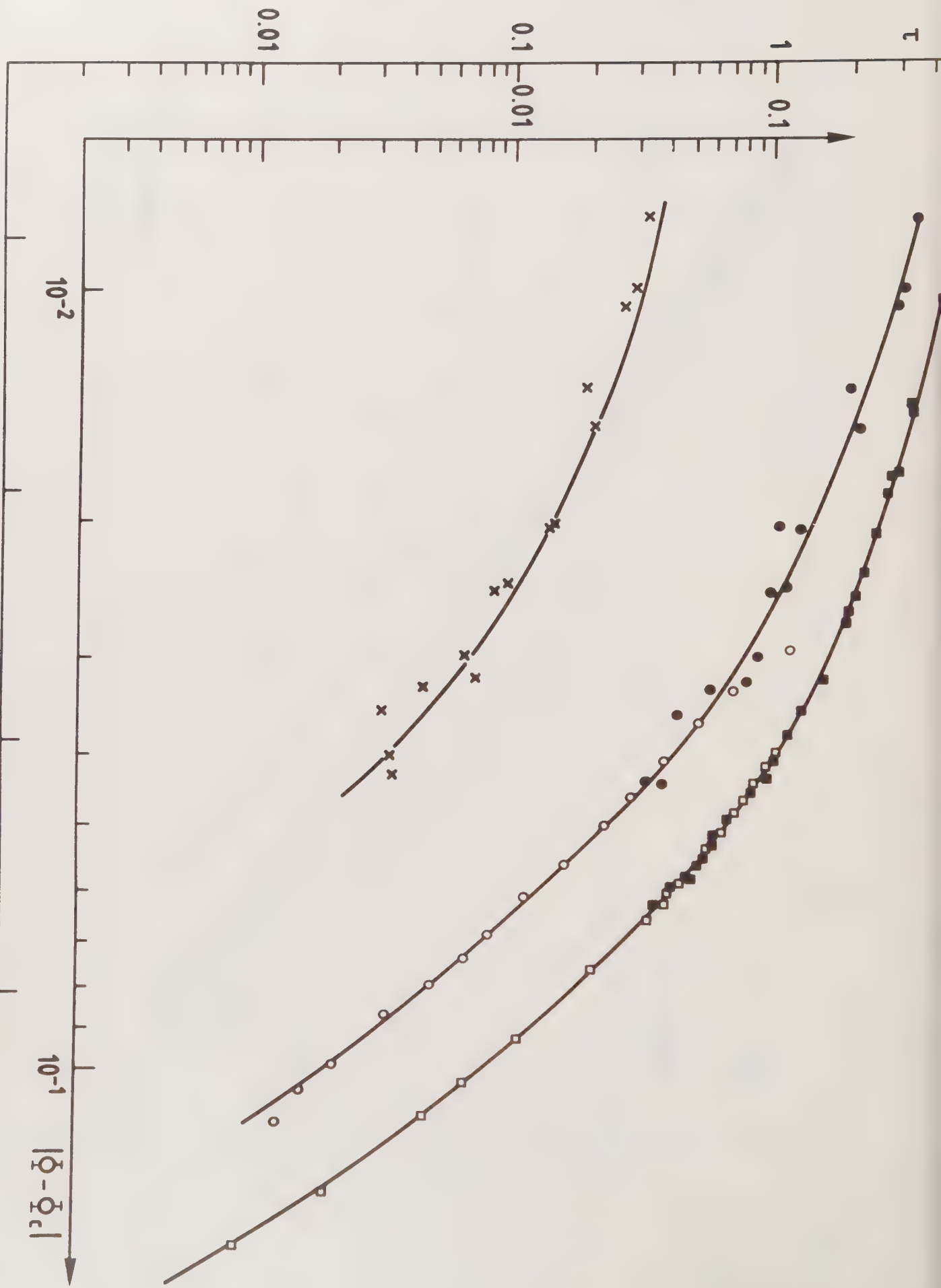
0.01
0.1
0.01
1
0.1
τ
10⁻⁶
10⁻⁵
10⁻⁴
10⁻³
10⁻²
10⁻¹
|t|
|δ - δc|

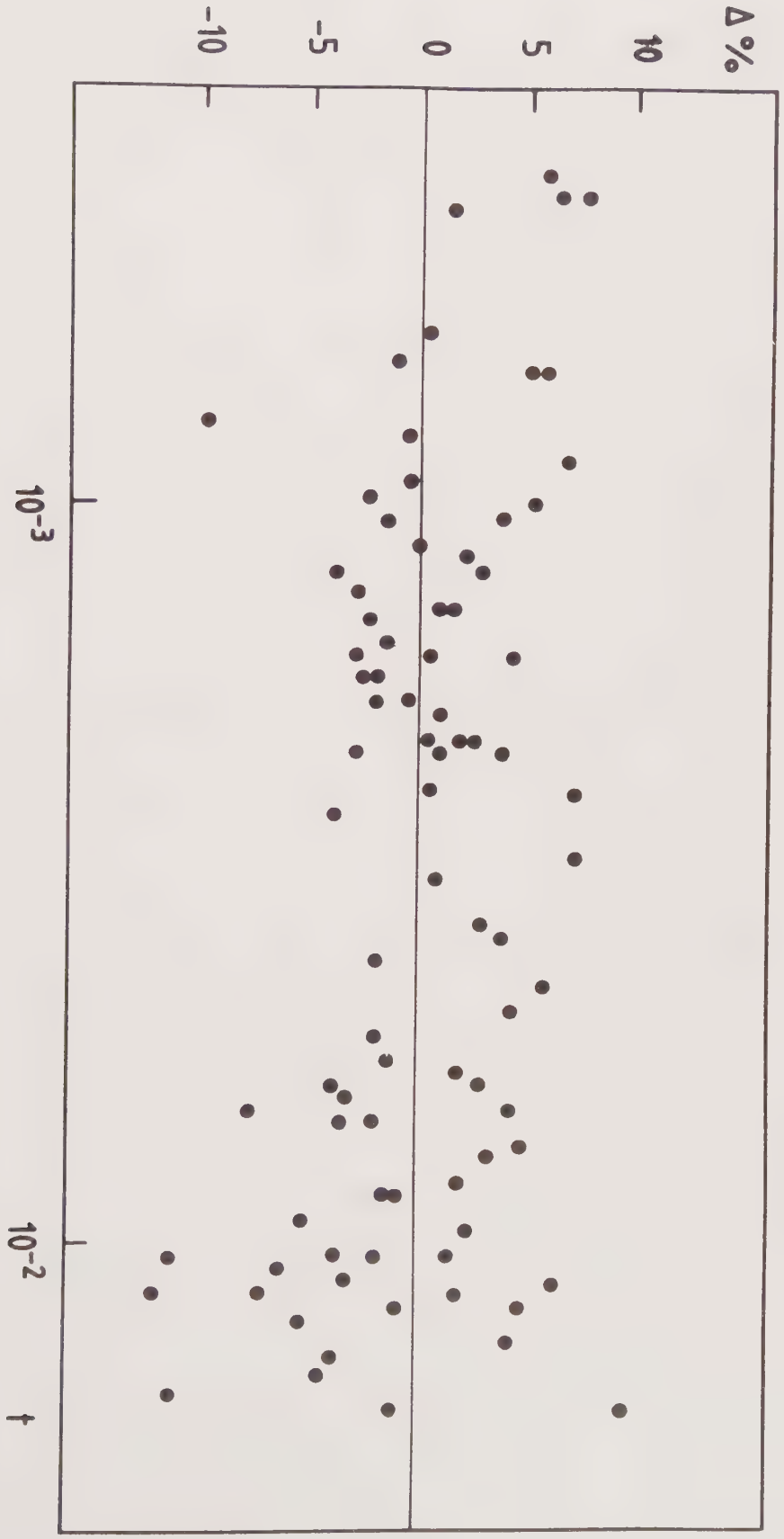
Δ%
10
5
0
-5
-10
10-3
10-2
t

C H A P I T R E V I I

Dissymétrie du doublet Brillouin induite par un gradient de température

VII.1 - Introduction

Les développements récents de la mécanique statistique ont conduit à s'intéresser au-delà des situations d'équilibre, aux problèmes posés par les systèmes soumis à des flux de diverses grandeurs, en particulier à des gradients stationnaires. C'est ainsi que récemment sont apparus plusieurs travaux théoriques étudiant l'effet d'un gradient de température stationnaire de température sur un fluide homogène. Bien que les méthodes employées par les différents auteurs soient très diverses (moléculaires ou hydrodynamiques) un accord général a été obtenu, après quelques rectifications. Dans un fluide où la vitesse du son est v et son absorption Γq^2, soumis à un gradient de température stationnaire $\vec{\nabla}T$, le doublet Brillouin observé au vecteur de diffusion $\vec{q}$ est dissymétrique, la dissymétrie étant donnée par :

$$\varepsilon = \frac{I^+ - I^-}{I^+ + I^-} = \frac{v}{2\Gamma q^2} \quad \frac{\hat{q}.\vec{\nabla}T}{T}$$

I^+ et I^- étant les intensités des deux raies.

VII.2 - Modèle simplifié

Ce comportement peut se comprendre par le modèle simple suivant (voir figure a) ; au point d'observation M, l'une des raies Brillouin est composée d'excitations ("phonons") issues de la partie supérieure chaude, l'autre d'excitations issues de la partie froide, respectivement n^+ et n^-. Cette différence peut se développer au 1er ordre de la différence de température entre ces régions. Cette différence est elle-même égale au produit du gradient de température par une distance moyenne à l'origine du "phonon" qui n'est autre que le libre parcours moyen]

$$n^+ - n^-\alpha\ T^+ - T^- = \ ].\vec{\nabla}T = \frac{v}{\Gamma q^2}\ \vec{\nabla}T\ .\ \tilde{q}$$

Un effet similaire avait déjà été prédit dans les solides [6].

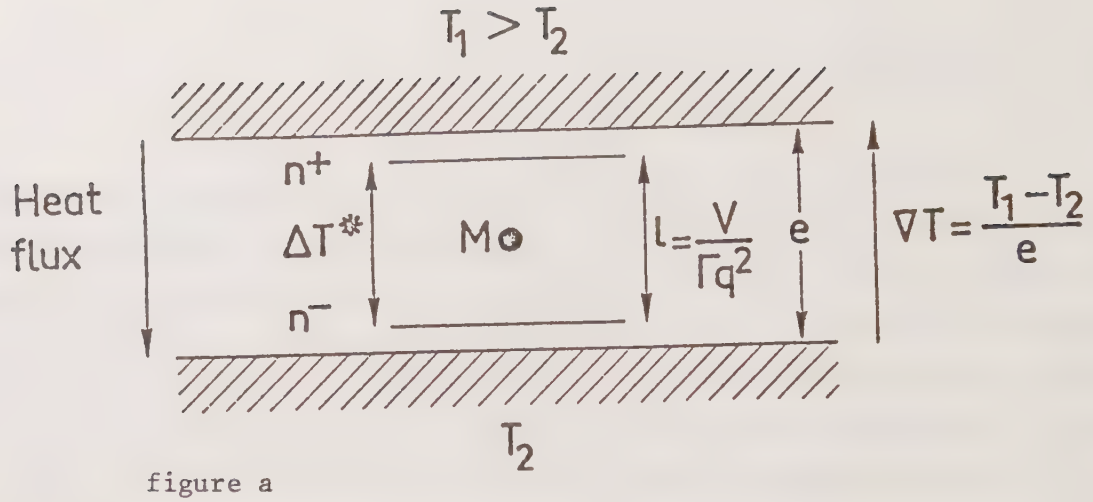

figure a

Si cependant on essaye d'appliquer directement ce modèle au cas expérimental, on constate que 1 > e c'est-à-dire qu'il faudrait tenir compte de "phonons" venant de l'extérieur. La différence observée sera donc vraisemblablement plus faible que celle prédite par la théorie linéaire. Une analyse quantitative de cet effet a été effectuée [a] mais elle nécessite de nombreuses hypothèses sur l'influence des parois.

De plus, selon certains travaux récents [b] la théorie linéaire cesserait d'être valable pour les gradients utilisés lors des expériences et cela conduirait également à une diminution de l'effet.

VII.3 - Montage expérimental

Les premiers travaux théoriques prenaient comme exemple l'argon à basse température et sous haute pression. Les problèmes technologiques liés à ces conditions nous ont conduit à rechercher un autre fluide, exploitable au voisinage de la température ambiante et sous pression atmosphérique. Les tables de vitesse et d'absorption du son montrent que dans ces conditions l'eau est le fluide pour lequel on peut espérer le plus grand effet, et nous l'avons donc choisie. Cependant ce fluide présente deux inconvénients : d'abord il diffuse relativement peu de lumière et d'autre part il a tendance à se polluer rapidement, donnant naissance à une diffusion Rayleigh parasite intense. Il a donc été nécessaire de monter un système de filtration près de la cellule utilisé entre deux mesures.

La cellule elle-même était composée d'un cadre de plexiglass confiné entre deux plaques de cuivre. La couche fluide était longue de 10 cm et

épaisse de 0,515 cm. Du fait de la courbure du faisceau la différence de température maximale possible était de l'ordre de 50 K.

Cette différence de température aurait été plus faible dans tout autre fluide du fait du très faible $\partial n/\partial T$ de l'eau. La lumière diffusée à très petit angle était recueillie au travers d'une fente mobile permettant de sélectionner $\vec{q}.\vec{\nabla T}$ positif,négatif ou nul avec q nul ou non nul. Cette lumière était ensuite analysée par l'interféromètre confocal dont la description a été donnée au chapitre III. Le schéma complet est donné par la figure 1.

VII.2 - Résultats

Un spectre typique est représenté figure 2. Si la dissymétrie est clairement visible, on voit également que son évaluation quantitative est sujette à une forte incertitude. L'ensemble des résultats, montré par la figure 3, montre en effet une forte dispersion. Il est toutefois clair que les dissymétries mesurées sont plus faibles que celles prédites par la théorie linéaire, la meilleure droite ayant une pente environ 3 fois plus faible que la prédiction théorique.

Les résultats sont comparés à la théorie non linéaire (fig.b) et à celle tenant compte des conditions aux parois (table a). Dans les deux cas, on obtient un accord convenable mais l'imprécision des expériences ne permet pas de conclusion plus tranchée.

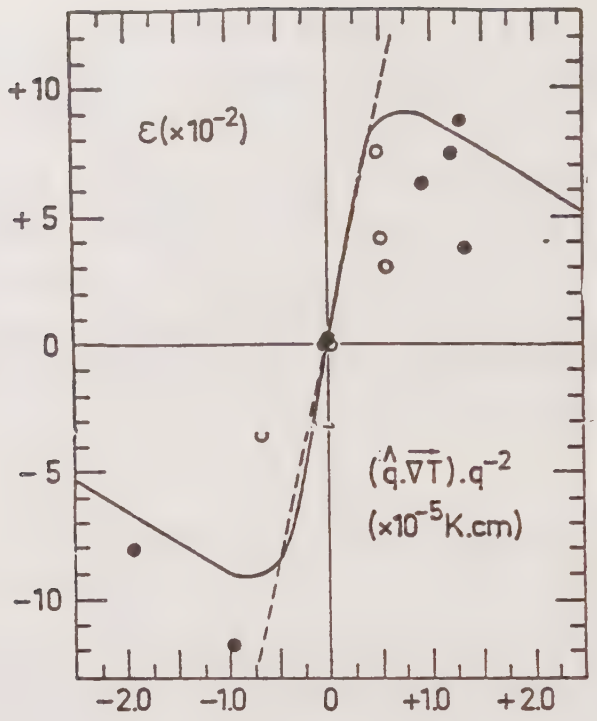

Figure b

Comparaison des résultats expérimentaux avec la théorie non-linéaire de la réf. (b)

q	VT	$\varepsilon(\beta=0) \times 10^2$	$\varepsilon(\beta=.5)\times 10^2$	$\varepsilon(\beta=1)\times 10^2$	$\varepsilon(\text{expt})\times 10^2$	$\varepsilon\times 10^2$ (linear theory, Eq. (1))
3420	59	1.08	3.38	3.77	7.5	9.4
3360	59	1.05	3.40	3.80	4.3	9.8
3220	59	.98	3.44	3.87	3.5	10.6
3130	59	.93	3.47	3.92	3	11.2
2380	59	.56	3.65	4.27	11.74	19.4
2110	59	.44	3.70	4.38	8.84	24.7
3060	83	1.26	4.91	5.57	6.25	16.7
2100	84	.62	5.27	6.25	7.92	35.8
2720	92	1.13	5.58	6.43	7.38	23.4
2590	93	1.04	5.69	6.59	3.93	26.1

Table a

Comparaison des résultats expérimentaux avec les valeurs de la réf.(a)

VII.5 - Conclusion

Nous avons prouvé expérimentalement l'existence d'un effet prédit par des développements récents de la mécanique statistique des fluides. L'accord qualitatif observé est une confirmation de la validité de ces théories, beaucoup plus profondes que ne le laisse croire notre modèle simpliste, et qui peuvent s'appliquer à d'autres problèmes("long time tails", par exemple) dont l'approche expérimentale est parfois impossible. Par ailleurs le désaccord quantitatif observé a nécessité de nouveaux développements théoriques qui donnent maintenant une image compatible avec les données expérimentales.

Références

[a] G.SATTEN and D. RONIS

[b] T.KIRKPATRICK and E.G.D. COHEN
Phys. Lett. 78A, 350 (1980)

PHYSICAL REVIEW
LETTERS

VOLUME 45 | 11 AUGUST 1980 | NUMBER 6

Experimental Evidence for Brillouin Asymmetry Induced by a Temperature Gradient

D. Beysens, Y. Garrabos,[a] and G. Zalczer
Département de Physique du Solide et de Résonance Magnétique, Centre d'Etudes Nucléaires de Saclay, F-91190 Gif-sur-Yvette, France
(Received 15 April 1980)

Very-low-angle Brillouin light-scattering experiments have been performed in liquid water subjected to a temperature gradient. The line intensities are unequal, and both the sign and the order of magnitude of this effect agree with recent theoretical calculations for nonequilibrium systems.

PACS numbers: 05.70.Ln, 78.35.+c

Recently a number of theoretical predictions have been made concerning fluids out of equilibrium.[1-5] Although they start from different basic assumptions, all the theories give the same general result, i.e., when a fluid is brought out of equilibrium by a steady temperature gradient ∇T, long-range correlations should appear, leading chiefly to a modification of the structure factor $S(\vec{q},\omega)$ which would exhibit an extra $1/q^2$ term. This can be tested by a light-scattering experiment, more precisely in the Brillouin spectrum, whose lines are expected to show different intensities:

$$S(\vec{q},\omega) = [1 \pm \epsilon(\vec{q},\omega)]\,\Gamma q^2/[(\omega \pm vq)^2 + (\Gamma q^2)^2]\,.$$

Here $\vec{q}$ is the transfer wave vector, v is the sound velocity, and ω is the angular frequency. Γq^2 corresponds to the sound damping and is the half-width at midheight of the Brillouin lines at equilibrium. $\epsilon(\vec{q},\omega)$ is in general a complex—and debated—function of $\vec{q}$ and ω. Here we will be concerned only with the *static* (integrated) intensities of the Brillouin lines, and in this case ϵ reduces to

$$\epsilon = \frac{v}{2\Gamma}\,\frac{\hat{q}\cdot\nabla T}{T}\,\frac{1}{q^2}\,,$$

with $\hat{q} = \vec{q}/q$. This formulation corresponds, in fact, to the similar situation in crystals[6] where heat is carried only by phonons. To a temperature gradient corresponds a heat flux, and therefore an increase of the phonon density at a given $\vec{q}$ vector, varying as $1/q^2$. This increases the intensity of the Brillouin line which corresponds to fluctuations propagating in the direction of the heat flux (i.e., $-\nabla T$), and lowers the intensity of the other line.

It is of prime importance to verify this prediction experimentally. Indeed, if the statistical methods have been well verified to apply for systems at equilibrium, up to the present time no experimental verification has been given of the methods used in physics out of equilibrium.

The long-range contribution $1/q^2$ implies that experiments had to be performed at very low scattering angles. (See Fig. 1.) As a fluid, we used water near room temperature and atmospheric pressure, despite the fact that it is a poor light scatterer and that it is difficult to remove the dust, which scatters chiefly at small angles. However, the small variation of the refractive index with temperature allows high-temperature gradients to be applied without giving rise to spurious effects due to the beam bending and to defocusing (thermal lens). The experiments were carried out with the temperature kept near 40 °C.

© 1980 The American Physical Society

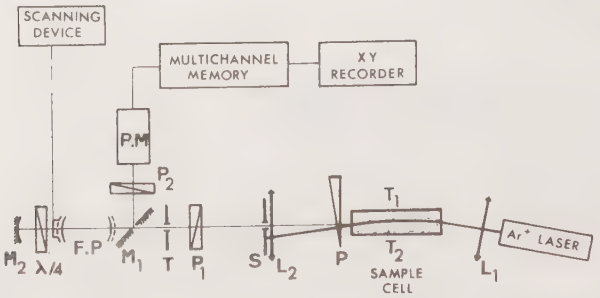

FIG. 1. Experimental setup: L_1 and L_2, lenses; P, prism; P_1 and P_2, polarizers; M_1 and M_2, mirrors; S, slit; T, pinhole.

At this temperature, $v = 1.53\times10^5$ cm/sec and $\Gamma = 1.30\times10^{-2}$ cm^2/sec.[7] The smallest scattering angle attainable was 0.7° ($q \simeq 2000$ cm^{-1}). The Brillouin shift is thus 3×10^8 rad/sec (50 MHz), the half width is 5.2×10^4 rad/sec (0.008 MHz), corresponding to a mean free path of fluctuations $l = v/\Gamma q^2 \simeq 3$ cm. With a gradient $|\nabla T| \simeq 100$ K/cm, the expected asymmetry in the Brillouin intensity is about 50%.

The cell was composed of two copper plates (12 cm×5 cm) maintained at constant temperatures within 0.1 K by circulating water from thermostatic baths. The upper plate was at a temperature higher than that of the lower plate in order to prevent convection phenomena. The water was confined between the plates by means of a transparent Plexiglass frame. The spacing between the copper plates was $e = 0.515$ cm, allowing temperature gradients of about 100 °C/cm to be obtained. The temperature difference was measured and controlled by thermocouple junctions placed inside the two copper plates. During an experiment (recording time: 1 or 2 days) the gradient was maintained constant within 1%. Deionized water was used. Between runs the water was filtered through 0.2-μm Teflon filters.

The scattering wave vector was selected by means of a slit whose larger dimension was always maintained perpendicular to $\vec{q}$. The uncertainty on $\vec{q}$ is typically 10%, due to the finite dimensions of both the slit and the beam. We used a 213.545-MHz free-spectral-range confocal Fabry-Pérot spectrometer which was piezoscanned and could be used either in a single-pass or a double-pass arrangement, the latter providing a much better contrast. The light source is a monomode argon-ion laser of 200 mW power whose beam (diameter, 0.02 cm) is slightly focused in the sample. The frequency drifts of both the laser and the Fabry-Pérot spectrometer are compensated by a triggering technique associated to a multichannel memory.[8] Because of the vibrations of the laser tube ("jitter"), the resolution corresponding to the half-width at midheight of the apparatus function (5.7 MHz) was about 4 times the resolution expected from the reflection factor (1.3 MHz), but this spurious effect had no influence on the contrast, which was found to be larger than 5×10^5 in the double-pass arrangement. When compared to the natural Brillouin linewidth (0.008 MHz), this resolution prevents any attempt being made to resolve the spectrum. In any case, some other limitations occur (see below), which prevent improvement of the resolution. Finally, the *sign* of the frequency shift with respect to the incident laser frequency was determined by using, in place of the sample, an electro-optic modulator working at 40 MHz.

In such a low-angle and strongly temperature-dependent experiment, we have to carefully consider the following points:

(i) The sound velocity variation in the observed volume, $\Delta v = (\partial v/\partial T)_p |\nabla T| \Delta Z$, where ΔZ is the full height difference of the illuminating beam in the same direction as ∇T. ΔZ is partly due to the beam diameter and partly due to the bending of the beam in the temperature gradient. Typically $\Delta Z \lesssim 0.1$ cm, and with $(\partial v/\partial T)_p \simeq 200$ cm sec^{-1} K^{-1},[7] $|\nabla T| \lesssim 100$ K cm^{-1}, the uncertainty is $\Delta v \lesssim 2\times10^3$ cm/sec, leading to an apparent linewidth broadening, $\Delta\omega = \vec{q}\cdot\Delta\vec{v} \simeq 4\times10^6$ rad/sec (0.6 MHz) at $q = 2000$ cm^{-1}. This is negligible with respect to the Brillouin shift and the Fabry-Pérot spectrometer resolution, but it is 100 times the true linewidth.

(ii) The linewidth variation, $\Delta\Gamma = (\partial\Gamma/\partial T)_p |\nabla T| \times \Delta Z$. With the data of Ref. 7, $\Delta\Gamma/\Gamma \simeq 15\%$, which is negligible when the linewidth broadening from (i) is considered, and remains weak when the value of ϵ has to be estimated.

(iii) The influence of the finite aperture angle, of the finite beam diameter, and of the defocusing effects due to the gradient. Indeed, in water the second-order derivative of the refractive index $(\partial^2 n/\partial T^2)_p$ is not negligible at high temperature gradient, leading to a cylindrical-lens effect. Typically, the uncertainty Δq varies from 5% ($|\nabla T| = 0$), to 10% ($|\nabla T| \simeq 100$ K/cm). At $q \simeq 2000$ cm^{-1}, the broadening varies from 1.5×10^7 rad/sec (2.5 MHz, $|\nabla T| = 0$), to 3×10^7 rad/sec (5 MHz, $|\nabla T| \simeq 100$ K/cm). This effect is weak enough to not very much alter the detection of the Brillouin lines but it is sufficiently high to be measured

TABLE I. The measured Brillouin intensity asymmetries and half-widths at midheight of the Brillouin lines, with corresponding wave vectors and thermal gradients.

q [a] (cm^{-1})	$\lvert\nabla T\rvert$ (K/cm)	sign of $\vec{q}\cdot\nabla T$	$10^{2}\epsilon_{expt}$ [b]	$10^{-6}\Gamma_B$ [c] (rad/sec)
3360	59	+	+4.3[d]	4
3420	59	+	+7.5[d]	4
3130	59	+	+3[d]	8.2
2760	0	0	0[d]	3.5
3220	59	−	-3.5[d]	7.8
2110	59	+	+8.84	9.7
2380	59	−	-11.74	11.9
2080	0	0	0	3.5
2120	59	0[e]	0	6.6
3060	83	+	+6.25	17.3
2720	92	+	+7.38	24.5
2590	93	+	+3.93	24.8
2100	84	−	-7.92	16.6

[a] q is deduced from the measured Brillouin shift.

[b] $\epsilon_{expt} = [I(\omega<0) - I(\omega>0)]/[I(\omega<0) + I(\omega>0)]$, where I is the integrated Brillouin intensity. The accuracy of $10^2\epsilon_{expt}$ is about 1.

[c] Half-width at midheight of the Brillouin lines, obtained by subtracting the apparatus function half-width (35.8×10^6 rad/sec) from the experimental half-width.

[d] The Fabry-Pérot spectrometer was used in single-pass arrangement.

[e] $\vec{q}$ is perpendicular to ∇T.

(see Table I).

(iv) The mean free path l of the sound waves compared to the dimension e of the cell in the gradient direction: $l/e \simeq 6$ at $q \sim 2000$ cm^{-1}. It is not easy to estimate the influence of this on ϵ_{expt}. Moreover, l varies strongly with T: At the top of the cell, $l \sim 8.5$ cm, and at the bottom, $l \sim 1.5$ cm.[7] Nevertheless, we can state that a wave which "feels" the gradient in a direction cannot be efficiently reflected so as to feel the gradient in the opposite direction, which, in principle, could cancel the effect of the gradient. The sound wavelength is indeed small ($\simeq 30$ μm) compared to the surface roughness of the copper plates ($\simeq 100$ μm), and the efficiency of the reflection can be expected to be weak.

The various results are given in Figs. 2, 3, and Table I. The check of the asymmetry was performed by changing the sign of $\vec{q}\cdot\nabla T$ under nearly the same experimental conditions, and verifying that the asymmetry in the Brillouin intensities is reversed. The lines remained symmetrical in intensity whenever $\vec{q}\cdot\nabla T = 0$, that is for $\nabla T = 0$ or $\vec{q}\perp\nabla T$. The measurement of this

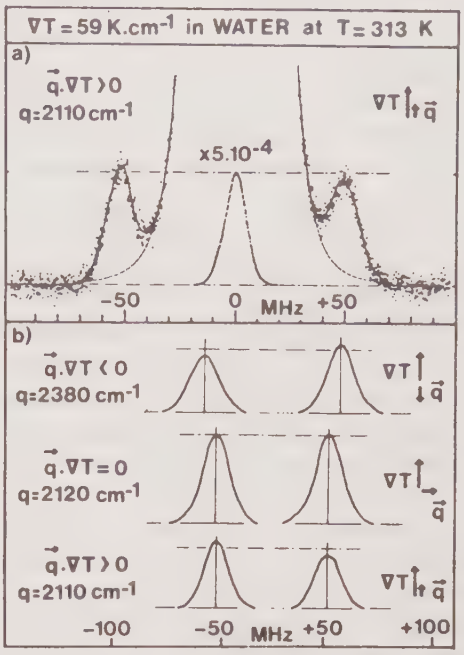

FIG. 2. (a) Experimental spectrum. The solid line is the best fit. The strong central peak (dotted line) corresponds to an elastic scattering by dust and windows. (b) Brillouin lines: Best fit for different orientations of $\vec{q}$ vs ∇T, showing that the intensities asymmetry varies as $\vec{q}\cdot\nabla T$.

asymmetry was performed by integrating the lines after having subtracted the base line. The accuracy of ϵ_{expt} is typically 10^{-2}. In order to check the variation of the experimental value of

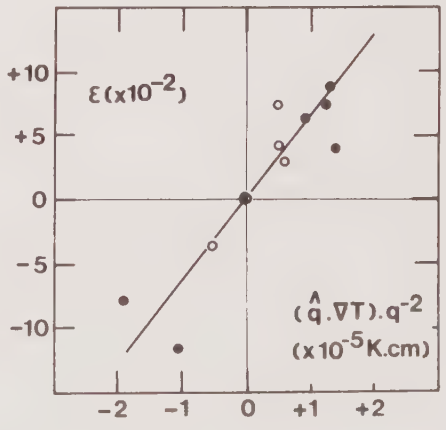

FIG. 3. Intensity asymmetry. $\epsilon_{expt} = [I(\omega<0) - I(\omega>0)]/[I(\omega<0) + I(\omega>0)]$ vs $\hat{q}\cdot\nabla T/q^2$. The expected variation is linear with slope $\simeq 19\,000$ cm^{-1} K^{-1}. The experimental slope is $\simeq 6700$ $cm^{-1}K^{-1}$ (straight line). Full points, with double-pass Fabry-Pérot spectrometer arrangement; open circles, with single-pass Fabry-Pérot spectrometer arrangement.

ϵ, $\epsilon_{expt} = [I(\omega<0) - I(\omega>0)]/[I(\omega<0) + I(\omega>0)]$, with the reduced variable $\hat{q}\cdot\nabla T/q^2$, we determined the actual q vector by the experimental Brillouin shift $\omega_B = \vec{v}\cdot\vec{q}$. The accuracy was better than 0.5%. As shown in Fig. 3, the linear dependence of ϵ_{expt} with $\vec{q}\cdot\nabla T/q^2$ is well verified, but the experimental slope $\epsilon_{expt}[(\vec{q}\cdot\nabla T)/q^2]^{-1} \simeq 6700$ K^{-1} cm^{-1} is about 3 times weaker than the expected value $v/2\Gamma T \simeq 19000$ K^{-1} cm^{-1}. This may be due to the finite-size effect of the sample ($l/e \sim 6$).

We have experimentally shown that when a fluid is brought out of equilibrium by a temperature gradient, the structure factor determined by light scattering is changed by a long-range contribution, following $\hat{q}\cdot\nabla T/q^2$, which makes the Brillouin line intensities asymmetric. Both the sign and the order of magnitude of the effect have been found to be in agreement with the theoretical expectations, and thus provide a direct check of the statistical methods used in nonequilibrium physics. Spurious effects, due to the gradient itself, or to the geometry of the experiment, prevent any further investigation of the spectral shape being made. Finally, other systems, including solids, should exhibit an analogous behavior under a thermal gradient. This kind of experiment is in progress.

---

[a]On leave from Laboratoire des Interactions Moléculaires et des Hautes Pressions, Université Paris-Nord, Avenue J.-B. Clément, F-93430 Villetaneuse, France.

[1]I. Procaccia, D. Ronis, and I. Oppenheim, Phys. Rev. Lett. 42, 287, 614(E) (1979).

[2]T. Kirkpatrick, E. G. D. Cohen, and J. R. Dorfman, Phys. Rev. Lett. 42, 862 (1979), and 44, 472 (1980).

[3]G. Van der Zwan and P. Mazur, Phys. Lett. 75A, 370 (1980).

[4]D. Ronis and S. Putterman, to be published.

[5]A. M. S. Tremblay, E. D. Siggia, and M. S. Arai, Phys. Lett. 76A, 57 (1980).

[6]A. Griffin, Can. J. Phys. 46, 2843 (1968).

[7]J. Rouch, C. C. Lai, and S. H. Chen, J. Chem. Phys. 65, 4016 (1976).

[8]D. Beysens, Rev. Phys. Appl. 8, 175 (1973), and J. Chem. Phys. 64, 2579 (1976).